

University of Texas at Arlington

MavMatrix

Civil Engineering Dissertations

Civil Engineering Department

2023

TESTING AND EVALUATION OF POLYMERIC SPRAY APPLIED PIPE LINING IN PRESSURE PIPE APPLICATIONS

Kawalpreet Kaur

Follow this and additional works at: https://mavmatrix.uta.edu/civilengineering_dissertations



Part of the [Civil Engineering Commons](#)

Recommended Citation

Kaur, Kawalpreet, "TESTING AND EVALUATION OF POLYMERIC SPRAY APPLIED PIPE LINING IN PRESSURE PIPE APPLICATIONS" (2023). *Civil Engineering Dissertations*. 393.
https://mavmatrix.uta.edu/civilengineering_dissertations/393

This Dissertation is brought to you for free and open access by the Civil Engineering Department at MavMatrix. It has been accepted for inclusion in Civil Engineering Dissertations by an authorized administrator of MavMatrix. For more information, please contact leah.mccurdy@uta.edu, erica.rousseau@uta.edu, vanessa.garrett@uta.edu.

**TESTING AND EVALUATION OF POLYMERIC SPRAY
APPLIED PIPE LINING IN PRESSURE PIPE APPLICATIONS**

By

KAWALPREET KAUR



DISSERTATION

Presented to the Faculty of the Graduate School of

The University of Texas at Arlington

In Partial Fulfillment of the Requirements

for the Degree of

DOCTOR OF PHILOSOPHY

THE UNIVERSITY OF TEXAS AT ARLINGTON

August 2023

Copyright © by Kawalpreet Kaur 2023

All Rights Reserved



Dedication

I dedicate this thesis to my mother, father, mother-in-law, father-in-law and
my beloved husband for their wishes, love, and
endless support.

Acknowledgements

I would like to thank my supervisor, Dr. Mohammad Najafi, for his guidance and endless support throughout the study. Dr. Najafi contributed countless hours to support this work, which would not have been possible without his encouragement and patience. I will always appreciate his motivation, support, and advice for introducing me to trenchless technology and making me a proficient professional.

I would like to thank my thesis committee, Dr. Mohsen Shahandashti, Dr. Jay Michael Rosenberger, Dr. Vinayak Kaushal, and Dr. Karthikeyan Loganathan, for their valuable time, support, and advice for this work.

I sincerely thank the industry professionals, Ms. Sanaz Ghalambor, Mr. Brandon Caldwell, and Mr. Broncheny Pascal, for their support. Without their support, this work would not be possible. I would also like to thank Mr. Brandon Hightower, Mr. Chris Mcgaughy, Mr. Robert Chapman, Mr. John Peters, and Mr. Stephen Johnson for providing their valuable inputs and knowledge during the test setup and testing.

I would also like to thank Mr. Mark Garrison and Mr. Darryl Peterson from MicroMeasurements for their support in instrumentation work. I sincerely thank Mr. Majid Tavakoli, Mr. Zachary Reeves, Mr. Vignesh Santhanagopalan, Mr. Kaveh Mahdvar, and Mr. Mohammad Jasim from United Rentals for their support.

My special thanks to my parents for their love, support and relentless efforts to help me achieve my goals. I will always be indebted to them. I am also thankful to my father-in-law and mother-in-law for always supporting me for my Ph.D. studies, their saying good luck to me every day while leaving the home was a support and motivation that was much required to achieve this goal. My beloved husband is the backbone to me and his support throughout this journey is the

key to achieve this success. I would also like to thank my sisters-in-law, cousin sisters and cousin brothers, and my whole family for their continuous support for this study.

I would like to thank my friend Ms. Malu Deav for the motivation and support that helped me to be determined to put my best efforts into this study. I would also like to thank Dr. Ahmad Jibreen for his help in setting up the instrumentation for the test setup. Many thanks to Diego Calderon for his contribution to tensile material testing. I would like to thank Dr. Zaid Momani for his invaluable support of this work. My special thanks to all CUIRE past and current graduate students Suhas Patil, Venkata Varshneya, Kashif Mohammed, Akshay Surana, Nupur Patel, Shubham Patil, Rajvardhan Desai, Shreyas Varma, Niraj Bhoir, Pratik Poojari, Charbel Salloum, Rojasadat Sharifian, Roz Javadi, Venkat Rao, Anoop Podduturi, Jayesh Magar, Prashik Gangawane, Rajvardhan Patil, Ukendran Gopi, Chirag Gudhka, Shayan Sharifzad, Zahra Borhani, and Parth Patel for helping me in the test setups preparations.

August 29, 2023

Abstract

TESTING AND EVALUATION OF POLYMERIC SPRAY APPLIED PIPE LINING IN PRESSURE PIPE APPLICATIONS

Kawalpreet Kaur, Ph.D.

The University of Texas at Arlington, 2023

Supervising Professor: Dr. Mohammad Najafi

Pressure pipes are an important component of pipe infrastructure for water mains, distribution lines, fuel and gas piping, process piping, building services piping, and many more. Various material types are available to be used in the pressure pipes, in which metal pipes are ubiquitous for high pressure applications, plastic pipes are also commonly used, and sometimes concrete pressure pipes are used in large diameter pipes for its economic factors. Most of these pipes currently in service are 50 to 60 years old, and some are 100 years old. Furthermost pipelines have exceeded their design life and are continuously deteriorating to the catastrophic situations; thus, there is an urgent need to develop a method or technology to restore the existing underground pipeline and infrastructure.

Spray applied pipe lining (SAPL) is a trenchless pipe renewal technology that can combat the issue of pipe aging and failure. SAPL is applied inside a pipe for either corrosion prevention or load-bearing capacity enhancement of the existing pipe by creating a new stand-alone pipe within the host pipe. Adding to the structural capabilities of SAPL, in some cases, its application also improves the hydraulic flow capacity of the pipelines by providing a smooth internal surface profile, even considering the application decreases the internal diameter.

This dissertation presents the detailed testing and evaluation of structural and hydraulic properties of the polymeric liner material in pressure pipes. The testing plan includes full-scale laboratory tests of short-term hole-spanning, vacuum pressure, pressure integrity, and hydraulic flow. The short-term hole spanning test results on 30-inch pipe diameter samples determined the hole-spanning capacity of the SAPL when designed as semi-structural. The lining system was tested for a pressure resistance of up to 500 psi. The vacuum pressure test determined the vacuum load resistance of the lining system. The pressure integrity test on 8-inch pipe diameter samples determined the pressure resistance of the liner at extreme temperature conditions when designed as fully structural, i.e., with no support from the host pipe.

Lastly, the hydraulic flow test was critical to determine the effect of liner installation on improving the flow characteristics of a 6-inch lined pipe sample, though the liner decreases the internal diameter. The head loss of the lined pipe was compared with a moderately corroded pipe in a turbulent flow regime, and the results showed a reduction in the head loss of the lined pipe when compared with a moderately corroded pipe. Furthermore, the experimental results provided the design methodologies and validated the design equations for applying SAPL in pressure pipes.

The recommendations for future research studies are provided to test the lining system when designed as semi-structural and fully structural at different pipe diameters, with different thicknesses, and at varied temperatures. These test results will help evaluate the material's performance under different conditions of host pipes, environment, and loading.

List of Acronyms

AASHTO	The American Association of State Highway and Transportation Officials
ABS	Acrylonitrile Butadiene Styrene
ACP	Asbestos-cement pipes
ANN	Artificial Neural Network
ANOVA	Analysis of Variance
ASTM	American Society for Testing and Materials
AWWA	American Water Works Association
CCTV	Closed-circuit television
CI	Cast Iron
CIPP	Cured-in-Place-Pipe
CMP	Corrugated Metal Pipe
DAQ	Data Acquisition
DM	Mean diameter of the host pipe
DP-3	Triple Diaphragm
E	Modulus of Elasticity, psi
EECW	Emergency Equipment Cooling Water
EPA	United States Environmental Protection Agency
Es	Short-term Modulus of Elasticity (psi)
ε	Equivalent Roughness
f	Friction Factor (Unitless)
F	Fahrenheit
FEM	Finite Element Modeling
fps	Feet per second
ft	Feet
ft/min	Feet per minute
g	Gravitational acceleration (32.174 ft/s ²)
GMP	Gallon per minute
GRP	Glass Reinforced Polyester
HDB	Hydrostatic Design Basis
HDPE	High-Density Polyethylene
Hg	Mercury
ID	Internal diameter
K	Enhancement factor (dimensionless)
kN	kilonewtons
kPa	kilopascals
kW	kilowatts
lbs	Pounds
mA	Milliamperes
MAOP	Maximum allowable operating pressure
mm	millimeters
MPa	Megapascals
mph	miles per hour

N	Design factor of safety
n	Manning's coefficient of roughness, dimensionless
NPT	National Pipe Thread
NSF	National Sanitation Foundation
OD	outer diameter
PCCP	Prestressed concrete cylinder pipe
PCP	Polymer concrete pipe
PE	Polyethylene
PUU	Polyureaurethane
PVC	Polyvinyl chloride
q	Ovality of host pipe (%)
RCP	Reinforced concrete pipe
Re	Reynolds number
rpm	Rate per minute
SAPL	Spray Applied Pipe Lining
SIPP	Spray-in-Place Pipe
SL	Sliplining
SOL	Spray-on Lining
TNM	Three Network Model
UC&L	Underground Coatings and Linings
WL	surface live load at pipe burial depth (psi)
WRF	Water Research Foundation
WTM	Water transmission mains
ε/D	relative roughness
μm	Micro-meter
$\mu\varepsilon$	Micro-strain

Table of Contents

Acknowledgements	iv
Abstract	vi
List of Acronyms	viii
Table of Contents	x
1. Chapter 1 Introduction and Background.....	1
1.1 Introduction	1
1.2 Pressure Pipes.....	3
1.3 Pressure Pipe Material.....	5
1.3.1 Asbestos-Cement Pipes	5
1.3.2 Concrete Pipes.....	5
1.3.3 Plastic Pipes.....	5
1.3.4 Ductile Iron Pipes.....	6
1.3.5 Cast Iron Pipe	6
1.3.6 Steel Pipe.....	7
1.4 Pipe Deterioration and Failure	7
1.4.1 Structural Pipe Failure.....	10
1.4.2 Hydraulic Pipe Failure	11
1.5 Pipe Rehabilitation Methods	12
1.6 Selection of Trenchless Renewal Methods	16

1.6.1	Spray Applied Pipe Lining	17
1.6.2	Liners.....	18
1.7	Problem Statement	19
1.8	Goal and Objectives	21
1.9	Scope of Work.....	22
1.10	Hypothesis.....	22
1.11	Methodology	23
1.12	Expected Outcomes.....	25
1.13	Overview of Chapters.....	25
1.14	Chapter Summary.....	26
2.	Chapter 2 Literature Review	27
2.1	Introduction	27
2.2	Causes of Pipe Deterioration and Failure.....	27
2.2.1	Physical Indicators	27
2.2.2	Environmental Indicators	30
2.2.3	Operational Indicators	32
2.3	Classification of Pipe Failures.....	32
2.4	Pipe Rehabilitation	34
2.5	Spray Applied Pipe Linings	35
2.5.1	Cementitious Spray Applied Pipe Lining.....	36

2.5.2	Polymeric Spray Applied Pipe Lining	37
2.6	Structural Design Considerations of SAPL Renewal Method	40
2.6.1	Partially Deteriorated Condition of Gravity Pipes	41
2.6.2	Fully Deteriorated Condition of Gravity Pipes	41
2.6.3	Partially Deteriorated Condition for Pressure Pipes	41
2.6.4	Fully Deteriorated Condition for Pressure Pipes.....	42
2.6.5	SAPL Application Design Standards	42
2.7	Hydraulic Design Consideration of SAPL Renewal Method.....	50
2.7.1	Gravity Flow Design by Manning’s Equation	50
2.7.2	Pressure Flow Design by Hazen-Williams Equation	51
2.7.3	Pressure Flow Design by Darcy-Weisbach Equation	52
2.8	Research Studies on the Application of SAPL as a Renewal Method	55
2.8.1	Structural Analysis of SAPL lining system.....	55
2.8.2	Hydraulic Flow Analysis of Pipe Linings	65
2.9	SAPL Application as an Effective Renewal Method	67
2.10	Chapter Summary	69
3.	Chapter 3 Structural Evaluation of Spray Applied Pipe Lining	71
3.1	Introduction	71
3.2	Testing Methodology	71
3.3	Material Testing	72

3.3.1	Material Testing Hybrid Polyurea.....	73
3.3.2	Material Testing Pure Polyurea.....	77
3.4	Structural Evaluation of SAPL.....	78
3.4.1	Short-term Hole Spanning Testing.....	78
3.4.2	Vacuum Pressure Testing 2-inch Hole Spanning Sample.....	97
3.4.3	Pressure Integrity Test.....	99
3.4.4	Pressure Integrity Test Methodology	100
3.4.5	Pressure Integrity Testing.....	115
3.5	Chapter Summary.....	125
4.	Chapter 4 Hydraulic Evaluation of Spray Applied Pipe Lining	126
4.1	Introduction	126
4.2	Hydraulic Flow Testing Methodology	127
4.3	Equipment Details.....	128
4.3.1	Variable Flow Rate Pump	129
4.3.2	Water Tank.....	130
4.3.3	Heat Enclosure Unit	131
4.3.4	Entrance Section and Thermocouples	131
4.3.5	Pipe Test Section.....	132
4.3.6	Exit Section	134
4.3.7	PVC Pipe Return Section	135

4.3.8	Data Acquisition System (DAQ).....	137
4.4	Bare Pipe Test	137
4.5	Lined Pipe Test.....	138
4.5.1	Liner Installation	138
4.5.2	Sand Blasting.....	139
4.5.3	Primer and Liner Application.....	141
4.5.4	Lined Pipe Test.....	146
4.6	Chapter Summary.....	147
5.	Chapter 5 Results and Discussion.....	148
5.1	Introduction	148
5.2	Material Testing Results.....	148
5.2.1	Hybrid Polyurea Flexural Strength and Modulus	148
5.2.2	Hybrid Polyurea Tensile Strength and Modulus	149
5.2.3	Pure Polyurea Tensile Strength	150
5.2.4	Hybrid Polyurea Punch Shear Strength.....	151
5.3	Short-term Hole Spanning Hydrostatic Pressure Test Results.....	152
5.4	Vacuum Pressure Testing Results	157
5.5	Pressure Integrity Test Results	158
5.5.1	Pressure Integrity Test Results at 73° F Temperature.....	159
5.5.2	Pressure Integrity Test Results at 120° F Temperature.....	167

5.5.3	Pressure Integrity Test Results at 150° F Temperature.....	175
5.5.4	Pressure Integrity Test Results at 41° F Temperature.....	184
5.5.5	Pipe Failure Mode Analysis	192
5.5.6	Hoop Stress Calculations	195
5.5.7	Effect of Temperature on Burst Pressure and Hoop Stress.....	200
5.5.8	Validation of AWWA Structural Design Equation.....	204
5.6	Hydraulic Properties of Liner.....	212
5.6.1	Bare Pipe Test Results.....	212
5.6.2	Lined Pipe Test Results.....	221
5.6.3	Field Measured Roughness of Lined Pipes.....	227
5.6.4	Laboratory Measured Roughness of Lined Sample with Optical Profilometer 229	
5.6.5	Comparison of Equivalent Estimated Roughness	231
5.6.6	Comparison of Lined Pipe Test Results with Bare and Corroded Pipes.....	232
5.7	Contribution to Body of Knowledge.....	237
5.8	Practical Applications	237
5.9	Chapter Summary.....	237
6.	Chapter 6 Conclusions and Recommendations for Future Research Studies	239
6.1	Conclusions	239
6.1.1	Short-term Hole Spanning Test.....	239

6.1.2	Vacuum Pressure Test.....	240
6.1.3	Pressure Integrity Test.....	241
6.1.4	Hydraulic Properties Test.....	245
6.2	Recommendations	247
6.2.1	Short-term Hole Spanning Test.....	247
6.2.2	Vacuum Pressure Test.....	248
6.2.3	Pressure Integrity Test.....	248
6.2.4	Hydraulic Flow Test.....	249
	References.....	250

List of Tables

Table 1.1 Differences Between Pressure and Gravity Pipes.....	4
Table 1.2 Open Cut and Trenchless Methods.....	13
Table 1.3 Factors for Pipe Renewal Selection Method.....	16
Table 1.4. Main Characteristics of SAPL (Source: Najafi and Gokhale, 2022).....	17
Table 1.5 Scope of Work	22
Table 2.1 Water Main Deterioration Indicator (Adapted from Yan, (2006)).....	28
Table 2.2 Pipe Failure and Factors	33
Table 2.3 AWWA Structural Classification of Lining Systems (2019)	43
Table 2.4 Structural Classification and Rehabilitation Purposes (Kaur et al., 2023a).....	43
Table 2.5 Recommended Tests to Evaluate SAPL Application in Pressure Pipes	54
Table 3.1 Designed Thickness of Elastomeric Polyurea SAPL.....	85
Table 3.2 Test Data 0.5-inch Hole Spanning.....	88
Table 3.3 Test Data 1-inch Hole Spanning.....	92
Table 3.4 Test Data 2-inch Hole Spanning.....	95
Table 3.5 Pipe Sample Dimensions for Testing at 73° F.....	120
Table 3.6 Pipe Sample Dimensions for Testing at 120° F.....	121
Table 3.7 Pipe Sample Dimensions for Testing at 150° F.....	122
Table 3.8 Pipe Sample Dimensions for Testing at 41° F.....	123
Table 4.1 Measured Internal Pipe Diameter with a Digital Caliper	145
Table 5.1. Test Results Short-term Hole Spanning Testing.....	152
Table 5.2. Pressure Integrity Test Results at 73° F.....	159
Table 5.3 Summary of Burst Pressure at 73° F.....	163

Table 5.4 Data Set at 73° F Excluding Outliers.....	166
Table 5.5 Pressure Integrity Test Results at 120° F Temperature	167
Table 5.6 Summary of Pressure Integrity Test Results at 120° F.....	171
Table 5.7 Data Set Excluding Outliers at 120° F.....	173
Table 5.8 Pressure Integrity Test Results at 150° F Temperature	176
Table 5.9 Summary of Pressure Integrity Test Results at 150° F.....	180
Table 5.10 Data Set Excluding Time-to-Failure Less than 60 seconds at 150 °F	182
Table 5.11 Pressure Integrity Test Results at 41° F Temperature	184
Table 5.12 Summary of Pressure Integrity Test Results at 41° F.....	189
Table 5.13 Data Set Excluding the Outliers at 41° F.....	191
Table 5.14 Pipe Failure Modes	192
Table 5.15 Calculated Hoop Stress at 73° F Temperature.....	197
Table 5.16 Calculated Hoop Stress at 120° F Temperature.....	197
Table 5.17 Calculated Hoop Stress at 150° F Temperature.....	198
Table 5.18 Calculated Hoop Stress at 41° F Temperature.....	199
Table 5.19 Average Hoop Stress at Different Temperatures	202
Table 5.20 Experimental Results vs. AWWA Analytical Design Calculations at 73° F.205	
Table 5.21 Experimental Results vs. AWWA Analytical Design Calculations at 120° F.207	
Table 5.22 Experimental Results vs. AWWA Analytical Design Calculations at 150 °F.208	
Table 5.23 ME and SD for Test Dataset at 73° F	210
Table 5.24 ME and SD for Test Dataset at 120° F	210
Table 5.25 ME and SD for Test Dataset at 150° F	210
Table 5.26 Measured Roughness Readings with Portable Surface Roughness Tester ...	228

Table 5.27 Measures Liner Roughness with Optical Profilometer.....	230
Table 5.28 Comparison of Equivalent Estimated Roughness (ϵ)	231

List of Figures

Figure 1.1 ASCE Report Card 2017 (left) and ASCE Report Card 2021 (Right)	2
Figure 1.2. Pipe Failure Development (Adapted from Misiunas, 2005)	8
Figure 1.3. Bathtub Curve of Pipe Performance.....	8
Figure 1.4 Pipe Failure.....	11
Figure 1.5. Pipe with Corrosion Deposit Affected Hydraulic Flow Capacity	12
Figure 1.6 Open Cut Method	14
Figure 1.7 Larger Diameter Pipe Rehabilitation (Left) Source: CUIRE,	14
Figure 1.8 Renewal Solutions in Trenchless Technology	15
Figure 1.9 SAPL Manual Application	18
Figure 1.10 SAPL Robotic Application.....	18
Figure 1.11 Research Methodology	24
Figure 2.1 Failure Mode of Underground Pipe Due to Direct Tension	33
Figure 2.2 Failure Mode of Underground Pipe Due to Bending and Flexure	34
Figure 2.3 Failure Modes of Underground Pipes Due to Hoop Stress (Adapted from Rajani & Kleiner, 2001)	34
Figure 2.4 Hydrostatic Test Apparatus (Harries and Sweriduk, 2013).....	58
Figure 2.5 Corrosion Damaged Pipes Repaired with Epoxy	59
Figure 2.6 Pressurized Cast Iron Pipes Lined with Polymeric Liners	61
Figure 3.1 Structural Evaluation of SAPL.....	72
Figure 3.2 Three-Point Flexural Bending Test	73
Figure 3.3 Tensile Test (left) and Specimen Rupture (Right)	75
Figure 3.4 Specimen before Testing (left)	75

Figure 3.5 Punch Shear Test	76
Figure 3.6. Specimen after Shear Failure.....	76
Figure 3.7 Tensile Test Pure Polyurea Material	77
Figure 3.8 (a)Pipe Sample with Hole Spanning.....	79
Figure 3.9 Inside View of Test Section with Pure Polyurea Liner	80
Figure 3.10 Spigot End Grinding before Welding	80
Figure 3.11 (a) Welding Spigot End to Test Section	81
Figure 3.12 Spigot Ends Welded on Both Ends of the Test Section	81
Figure 3.13 (a) Pressure Transducer (b) Strain Gauge	82
Figure 3.14 Air Release Value.....	82
Figure 3.15 Hydrostatic Pressure Pump.....	83
Figure 3.16 Pipe Sample with 0.5 in. Hole Spanning.....	86
Figure 3.17 (a) Pump Hose Connection to Test Setup (b) Transducer Connected to Test Setup	87
Figure 3.18 Complete Test Setup.....	87
Figure 3.19 (a) Pressure Dial Gauge Initial Reading (b) Pressure Dial Gauge Reading at the End of the Test (c) Pressure Dial Gauge Reading of the Pump.....	89
Figure 3.20 Cutting the Welding Joints from Spigot Ends to Separate Out the Middle Test Section.....	90
Figure 3.21 (a) Cutting of Test Section from Spigot Ends	90
Figure 3.22 1-inch Hole Spanning Pipe Sample.....	91
Figure 3.23 (a) Pressure Dial Gauge Initial Reading at the Start of the Test	92
Figure 3.24 (a) Pressure Dial Gauge Reading at the End of the Test	93

Figure 3.25 Pipe Sample 2 in. Hole Spanning	94
Figure 3.26 Strain Gauge Installed on 2 in. Hole Spanning	95
Figure 3.27 (a) Pressure Dial Gauge Reading on Test Setup (b) Pressure Dial Gauge Reading on Pump.....	96
Figure 3.28 Vacuum Pressure Test Setup for 2 in. Hole Spanning Pipe Sample	98
Figure 3.29 Vacuum Pressure Dial Gauge Reading	98
Figure 3.30 Vacuum Pressure Dial Gauge Reading	99
Figure 3.31 Test Setup	100
Figure 3.32 Chiller Unit.....	101
Figure 3.33 Water Bath.....	101
Figure 3.34 Pressure Hose in Water Bath.....	102
Figure 3.35 Pressure Generating Unit.....	103
Figure 3.36 Chiller Unit.....	103
Figure 3.37 Control Panel Unit.....	104
Figure 3.38 Pipe Cutting at Lathe Machine	105
Figure 3.39 Uneven Parts Cut from Pipe Sample	105
Figure 3.40 Marked Pipe Sample.....	106
Figure 3.41 Pipe Sample Marking System	107
Figure 3.42 Visual Inspection of Pipe Samples	108
Figure 3.43 Top End Cap.....	109
Figure 3.44 Bottom End Cap	109
Figure 3.45 O-ring/Rubber Gasket	110
Figure 3.46 Snap Ring	110

Figure 3.47 Clamping System.....	110
Figure 3.48 Rods and Holding Plates	111
Figure 3.49 Pipe Sample with Snap Ring	112
Figure 3.50 Pipe Pipe Sample with Snap Ring and O-ring.....	112
Figure 3.51 Bottom End Cap Installation in Process	113
Figure 3.52 Pipe Sample with Top End Cap Installed.....	113
Figure 3.53 Pipe Sample with Restrained End	114
Figure 3.54 Top End Cap Installed on Pipe Sample.....	114
Figure 3.55 Pipe Sample with Both End Caps.....	115
Figure 3.56 End Caps Installation in Progress.....	116
Figure 3.57 Pipe Sample Connected with Pressure Hose	116
Figure 3.58 Bleed Value Opened (Left) and Closed (Right)	117
Figure 3.59 Pipe Sample with Safety Cage	117
Figure 3.60 Pipe Sample Lifting with Crane	118
Figure 3.61 Pipe Sample Placed in Water Bath.....	118
Figure 3.62 (a) Sample #6 Oval in Shape (b) Sample #9 Oval in Shape.....	124
Figure 3.63 Sample #42 Visual Cracks and Bulging Areas.....	124
Figure 4.1 Hydraulic Flow Test Equipment Setup	127
Figure 4.2 Centrifugal Variable Flow Rate Pump	130
Figure 4.3 Water Tank	130
Figure 4.4 (a) Frame Tent for Water Tank (b) AC Duct Connected to Tent.....	131
Figure 4.5 (a) Thermocouple (b) Entrance Section with Thermocouple Installed	132
Figure 4.6 Carbon Steel Pipe Test section	133

Figure 4.7 (a) Transducer #1 (Entrance Section) (b) Transducer #2 (Exit Section).....	134
Figure 4.8 Thermocouple Installed at Exit Section	134
Figure 4.9 PVC Pipe Return Loop	135
Figure 4.10 (a) Air Release Valve (b) Magnetic Flow Meter.....	136
Figure 4.11 Test Setup End Loop Connection to Water Tank.....	136
Figure 4.12 Inside View of Carbon Steel Pipe before Sand Blasting	139
Figure 4.13 Sand Blasting Machine.....	140
Figure 4.14 Sand Blasting Before Liner Application	140
Figure 4.15 Sand Blasting in Progress	141
Figure 4.16 Inside View of Pipe After Sand Blasting	141
Figure 4.17 Spin Cast for Liner Application	142
Figure 4.18 Primer Application in Progress	142
Figure 4.19 Inside View of Pipe After Primer Application	143
Figure 4.20 Inside View of Pipe After Liner Application	143
Figure 4.21 Measured Internal Pipe Diameter with a Digital Caliper	144
Figure 4.22 Measurements at Different Distances from Flange Connection.....	146
Figure 4.23 Pipe Internal Diameter Readings at Different Distance	146
Figure 5.1 Flexural Stress vs. Strain	148
Figure 5.2 Tensile Load vs. Strain	150
Figure 5.3 Average Tensile Stress vs. Strain	151
Figure 5.4 Punch Shear Load vs. Displacement	151
Figure 5.5 Pressure Transducer Measurements (1 in. Hole Spanning Pipe Sample)	153
Figure 5.6 Pressure Transducer Measurements (2 in. Hole Spanning Pipe Sample)	154

Figure 5.7 Strain Measurements at 2 in. Hole Spanning	154
Figure 5.8. Stress vs. Strain (Obtained from Strain Gauge Data).....	155
Figure 5.9 Stress vs. Strain (Obtained from Tensile Coupon Test).....	156
Figure 5.10 Burst Pressure vs. Pipe Thickness at 73 °F	164
Figure 5.11 Burst Pressure vs. Pipe Thickness (after Data Curation)	166
Figure 5.12 Burst Pressure vs. Pipe Thickness at 120° F	172
Figure 5.13 Burst Pressure vs. Pipe Thickness (After Data Curation)	174
Figure 5.14 (a) Bulging of Pipe Samples (b) Measurement of Increase of OD.....	175
Figure 5.15 Burst Pressure vs. Pipe Thickness at 150° F	181
Figure 5.16 Burst Pressure vs. Pipe Thickness (After Data Curation)	183
Figure 5.17 Burst Pressure vs. Pipe Thickness at 41° F	189
Figure 5.18 Burst Pressure vs. Pipe Thickness (After Data Curation)	191
Figure 5.19 Pipe Failure Analysis.....	195
Figure 5.20 Burst Pressure vs. Pipe Sample Thickness	201
Figure 5.21 Hoop Stress vs. Temperature.....	203
Figure 5.22 Experimental Test Results and AWWA Analytical Calculation at 73 °F...	206
Figure 5.23 Experimental Test Results and AWWA Analytical Calculation at 120° F.	207
Figure 5.24 Experimental Test Results and AWWA Analytical Calculation at 150° F.	208
Figure 5.25 Mean Error and Standard Deviation of Predicted AWWA Burst Pressure.	210
Figure 5.26 Bare Pipe Measured Head Loss vs. Flow Rate.....	215
Figure 5.27 Bare Pipe Calculated Friction Factor vs. Reynolds number.....	216
Figure 5.28 Bare Pipe Multiple Linear Regression Predicted Friction Factor vs. Calculated Friction Factor.....	217

Figure 5.29 Bare Steel Pipe Friction Factor vs. Relative Roughness	219
Figure 5.30 Bare Pipe Friction Factor vs. Relative Roughness	220
Figure 5.31 Lined Pipe Head Loss vs. Flow Rate.....	221
Figure 5.32 Lined Pipe Friction Factor vs. Reynolds number	222
Figure 5.33 Lined Pipe Multi Regression.....	223
Figure 5.34 Friction Factor vs. Lined Pipe Relative Roughness	225
Figure 5.35 Friction Factor vs. Lined Pipe Relative Roughness	226
Figure 5.36 Roughness Measurement with Portable Surface Roughness Tester.....	227
Figure 5.37 KLA Tencor Profilometer	229
Figure 5.38 Sample 6 3D Roughness Profile.....	230
Figure 5.39 Sample 6 3D Image Roughness Characteristics	230
Figure 5.40 Nuclear Service Water System Piping Tubercles Increased Pipe Roughness and Reduce Pipe Internal Diameter (Adapted from Onat et al., (2016))	233
Figure 5.41 Head Loss Comparison for Bare, Lined and Corroded Pipes	234
Figure 5.42 Friction Factor Comparison for Lined Pipe with Bare Pipe, and PVC Pipe	236

Chapter 1 Introduction and Background

1.1 Introduction

The underground water and wastewater infrastructure is one of the utmost essential components of urban infrastructure. The United States drinking water infrastructure includes an underground pipe network of approximately 2.2 million miles, providing safe and reliable water to millions of people (ASCE, 2021). These pipes were mainly installed between the early and mid-20th century.

The expected design life of these pipes was 75 to 100 years, and thus, many of these pipes are reaching the end of their design life. On the other hand, the wastewater system includes a pipe network of both public and private sewers, over 800,000 miles and 500,000 miles, respectively, connecting homes and businesses to public sewer lines (ASCE, 2021). Most of the U.S. wastewater underground infrastructure is more than 100 years old (EPA, 2004) and has surpassed its design life and deteriorating to its failure point.

According to American Society of Civil Engineers (ASCE) report card 2021, the U.S. had made some incremental progress towards rebuilding the nation's infrastructure for the first time in 20 years. America's infrastructure grade has been improved from D+ to C- (as shown in Figure 1.1, ASCE Report Cards 2017 and 2021). However, the stormwater and wastewater infrastructure have D and D+ grades, respectively, and urgently needs attention. As reported in the ASCE report card (2021), there is an average water main leaks of 10 to 37 per 100 miles and an estimated water main breaks of 250,000 to 300,000 per year, equivalent to breaking a water main every two minutes. Due to these water breaks and leaks, at least 6 billion gallons of water are lost every day, and this loss is equivalent to a minimum of 2.1 trillion gallons of non-revenue water lost every year. There was a loss of \$7.6 billion in revenue from treated water due to water leaks in 2019.

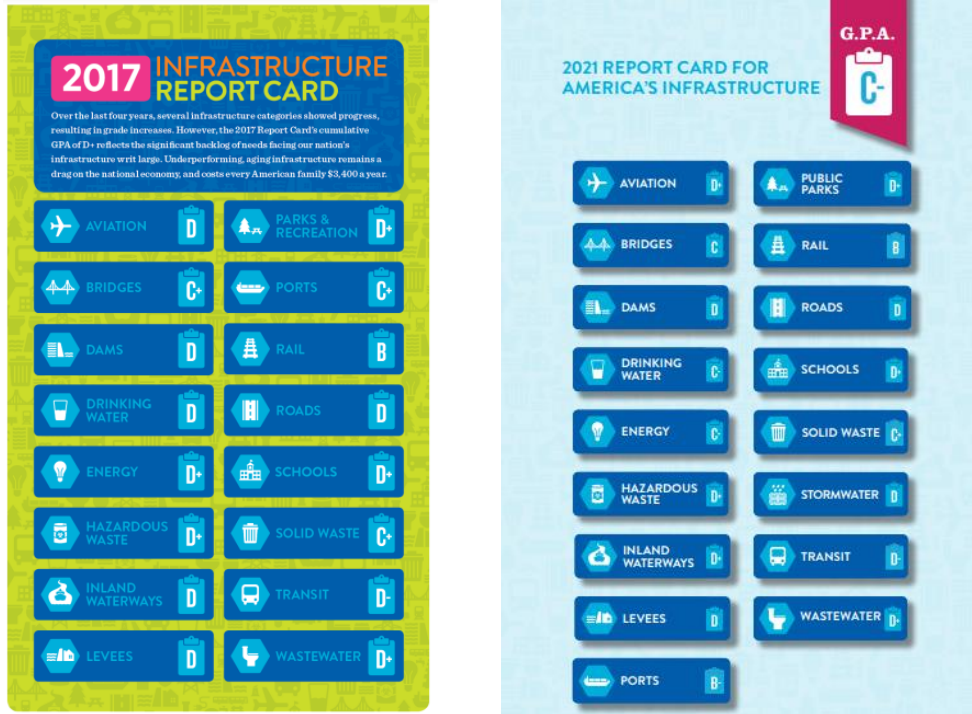


Figure 1.1 ASCE Report Card 2017 (left) and ASCE Report Card 2021 (Right)

In 2015, water utilities increased the rate of pipe replacement by an average of 0.5% of their total pipe network (ASCE, 2021). At this replacement rate, it would take nearly 200 years to replace the entire system. However, in 2019, the rate of replacement increased to a range of 1% to 4.8% per year, which matches with the lifecycle of the pipes. In 2020, drinking water utilities nationwide planned to replace over 12,000 miles of water pipes.

In addition to the challenge of aging the water and wastewater infrastructure, water demand is increasing due to population growth, yet, water resources are decreasing due to various environmental factors. Even though technology and science are working in the direction of recycling water and minimizing water usage, water conveyance is still a critical backbone of our infrastructure. The cumulative investment needs from the years 2020 to 2029 based on the current trends for drinking water, wastewater, and stormwater is \$1,045 billion; however, the provided funding is only \$611 billion (ASCE, 2021). Thus, this shows a funding gap of \$434 billion.

A Water Infrastructure Network report (2001) depicted that over the next 20 years, U.S. water and wastewater systems forecast an estimated funding gap of \$23 billion per year between the current infrastructure investment and the annual investments needed to replace aged and failed pipes. This funding is necessary to meet the objectives of the Clean Water Act and Safe Drinking Water Act. When comparing the forecasted funding with the current ASCE report card, it can conclude that the funding gap has been increasing over time. Therefore, investment in new underground infrastructure and maintaining the existing infrastructure is of critical need, despite having limited available funds to do so.

Therefore, there is a urgent need to address the issue of replacing and renewing our old and deteriorated underground water and wastewater infrastructure before its catastrophic failure impacts our economics and social life. To address this issue, more detailed investigation, advancement, investment, technology, and research are needed in the field of water and wastewater infrastructure, especially in renewal and rehabilitation processes to improve underground infrastructure without the costly option of open cut removal and replacement. It is critical to maintain the condition and integrity of our water and wastewater infrastructure as well the pipeline infrastructure of other industrial usage.

1.2 Pressure Pipes

Pressure pipes are most commonly used for water mains and distribution lines, process piping, building services piping, fuel and gas piping, and many more. Pressure pipes are circular, tubular designed structure made of different types of materials to convey fluids and gases under significant pressure. The fluid conveyed through the pipelines is pressurized for the required flow rate. Pressure pipes are used in water distribution systems to supply water for various purposes, such as households and agriculture. Some of the pressure pipes are specifically designed for high-

pressure industrial applications. The pressure requirement for the pipes is the most significant factor in designing the pipe diameter and thickness. In contrast, gravity pipes in the underground pipeline and infrastructure are commonly used for sewer systems, drainage systems, and culverts. The flow in the gravity pipes is with gravity energy, and no pressure is needed for the flow.

The pipe material used for the pressure pipes should have enough strength and capability to withstand the designed pressure. The most commonly used materials for pressure pipes are steel, cast iron, ductile iron, carbon steel, copper, polyvinyl chloride (PVC), High-Density Polyethylene (HDPE), and concrete. The common materials used for gravity and sewer pipes are concrete, clay, PVC, HDPE, and Acrylonitrile Butadiene Styrene (ABS). Table 1.1 shows the difference between pressure and gravity pipes.

Table 1.1 Differences Between Pressure and Gravity Pipes

Pressure Pipes	Gravity Pipes
Pressurized pipelines are designed to facilitate the required flow rate of a fluid.	Pipeline in which flow is with the gravity energy, no pressure is needed for the flow.
Pressure pipelines are designed as needed.	Gravity water flow designed to the site terrain.
For example, watermains and distribution lines, fuel gas piping, process piping, building services piping, etc.	For example, sewer system, drainage system, culverts and etc.
Pressure pipe materials: steel, cast iron, ductile iron, carbon steel, copper, polyvinyl chloride (PVC), High-Density Polyethylene (HDPE), and concrete pipes.	Gravity pipe materials: concrete, clay, PVC, HDPE, and Acrylonitrile Butadiene Styrene (ABS).

1.3 Pressure Pipe Material

Different types of materials are used for pressure pipes and depending upon physical, environmental, and operational factors, a material can be selected. The most commonly used material for the pressure pipes is described in this section.

1.3.1 Asbestos-Cement Pipes

Asbestos-cement pipes (ACP) are used for both gravity and pressure applications. These pipes are composed of Portland cement, silica, and are reinforced with asbestos fibers. These pipes were used for water distributions and sewer lines, but the manufacturing and installation of these pipes were banned in the late 1980s (Najafi & Gokhale, 2022). The expected service life of ACP is 70 years (Salman, 2018); however, it depends on the pipe usage and other environmental and physical factors.

1.3.2 Concrete Pipes

Concrete pipes for pressure application are engineered with different types of reinforcement, such as steel and wires, to enhance the pipe's capability to resist internal pressure and external loads. The common types of concrete pipes are reinforced concrete pipe (RCP), prestressed concrete cylinder pipe (PCCP), reinforced concrete cylinder pipe, bar-wrapped steel-cylinder concrete pipe, polymer concrete pipe (PCP) (Najafi & Gokhale, 2022 and Jibreen et. al., 2023). These are most commonly used for water distribution systems.

1.3.3 Plastic Pipes

Plastic pipes were introduced to North America in the late 1950s. The three commonly used plastic pipes are polyvinyl chloride (PVC), high-density polyethylene (HDPE), and glass reinforced pipe (GRP). PVC pipes for pressure application are made of solid walls of uniform

thickness (Najafi & Gokhale, 2022). HDPE and GRP pipes are also used for pressure applications. Plastic Pipes are lightweight and have better corrosion protection than other pipes such as metal, concrete, and asbestos cement pipes.

1.3.4 Ductile Iron Pipes

Ductile iron pipes have been used since the 18th century (AWWA Manual M41). These pipes can be used in high pressure application due to its high yield and tensile strengths. Adding an anti-corrosion protective coating such as cement mortar and polymeric lining increases the pipe resistance to corrosion (Najafi & Gokhale, 2022). The corrosion in these pipes occurs as a result of an electrochemical reaction, and leading to the formation of rust as the end product. This process is continuous and unavoidable and it affects the reliability of the pipes. According to Chukhin et al. (2014), the corrosion process is at its fastest rate during the first few years; however, this process slows down due to the formation of the corrosion deposit on the pipe surface, which resists the contact of the pipe surface with dissolved oxygen.

1.3.5 Cast Iron Pipe

Cast iron (CI) pipe was introduced to the United States in the early 1800s (Najafi & Gokhale, 2022). CI pipes in water utilities started in the late 19th century and were extensively used until the 1960s (Rajani & Kleiner, 2001; Mazumder et al., 2019). According to Kirmeyer et al. (1994), approximately 48% of the water distribution pipelines in the United States are made of grey cast iron pipes. Due to its high material strength, CI pipes are also used in high pressure industrial applications. The corrosion resistance of cast iron pipes is meager; thus, these pipes need different corrosion protective coatings such as cement lining and epoxy before installation.

1.3.6 Steel Pipe

The steel pipes have been in use since the 1850s (Elliot, 1992) and have more resistance to corrosion than other metal pipes. The material strength of steel pipes is the highest among metal pipes, and thus, due to its high strength, it can be used for transporting fluids such as oil, gas, and petroleum at high pressure and longer distances. Steel pressure pipes are used by municipalities for large diameter drinking water transmission applications (Najafi & Gokhale, 2022). Different manufacturing processes are used to produce steel pipes such as rolled and welded pipe, electric resistance welded pipe, and spiral welded pipe (Najafi & Gokhale, 2022).

1.4 Pipe Deterioration and Failure

Pipe deterioration and failure is a complex process and it is not a typical process. Pipe deterioration is a progressive process of degradation due to physical, operational, and environmental factors which impacts the structural and hydraulic capabilities of pipe. Misiunas (2005) explained pipe deterioration as a multi-step process over the service period of time; however, the process illustrated by Misiunas (2005) may not be applicable to all pipes. Misiunas (2005) divide the pipe deterioration into five steps, as given below.

- 1) Installation.
- 2) Initiation of corrosion.
- 3) Crack before leak.
- 4) Partial failure.
- 5) Complete failure

As illustrated in Figure 1.2, each step's service reliability depends upon the pipe's service life. The pipe deterioration is a gradual process with a decreasing efficiency and structural capability. Thus, a gradual declining curve of pipe service reliability is shown in Figure 1.2.

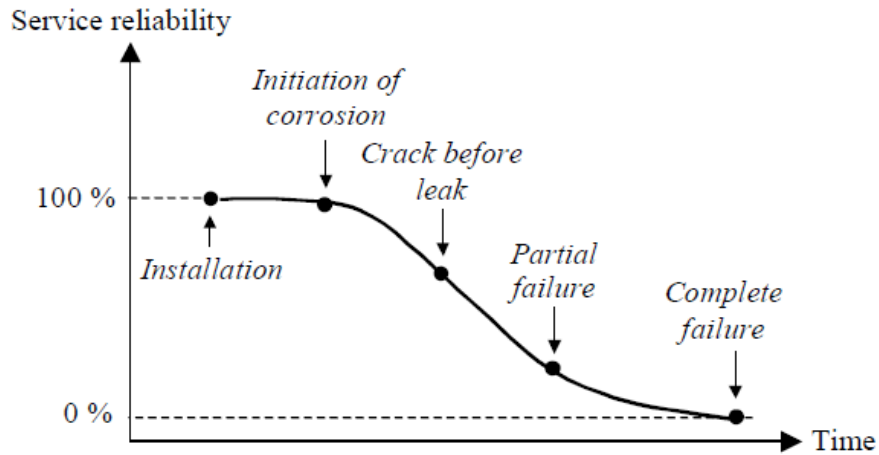


Figure 1.2. Pipe Failure Development (Adapted from Misiunas, 2005)

Other studies by Najafi and Gokhale (2022) & Singh and Adachi (2011) represented pipe failure in the shape of the “bathtub curve.” The bathtub curve was derived from the pipe failure rate versus time, as shown in Figure 1.3. The first stage is the “Early stage,” which shows a steep downward curve. This downward curve indicates that a greater number of pipe failures were recorded just after the installation due to defective installation procedures and/or faulty pipe material.

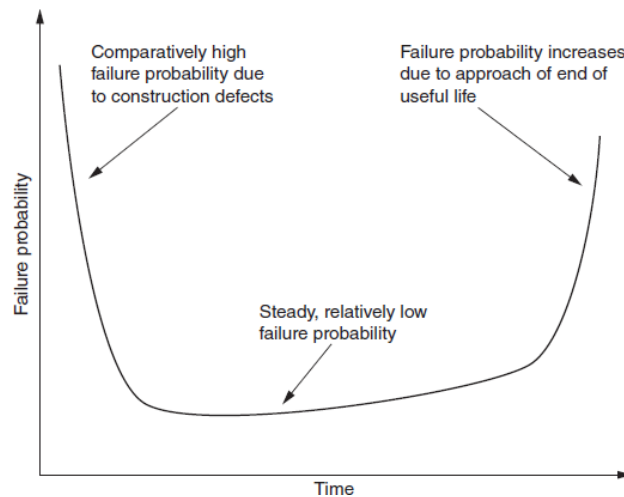


Figure 1.3. Bathtub Curve of Pipe Performance (Najafi & Gokhale, 2022)

The second stage is the “Useful life” period, which shows a lower failure rate. Failure in this stage generally happens due to some incidents, such as heavy traffic loading, ground movement, or interference by a third party. The third stage is the “Wear-out” stage which again shows a higher number of pipe failures. This higher rate could be due to the end of the design life; during this time, the pipe entirely deteriorates.

Other researchers have also studied pipe deterioration process, such as Saegrov et al. (1999) concluded that pipe material influences the development of failure, Atkinson et al. (2022) showed that the time interval can differ between different steps of pipe deterioration and Zhou, Y. (2018) concluded that the failure development process is not a typical process for the pipes, and it is expected to be explicit for a specific pipe.

The rate at which a pressure pipe deteriorates is less likely determined by its age, but in fact influenced by the combined effect of external forces acting on it (Najafi & Gokhale, 2022). In addition, internal forces also play a critical role in the pipe deterioration for pressure pipes. Jun et al. (2020) specifically worked on the pipe failure mechanism of the water transmission mains (WTM). According to their study, many factors cause the pipe failure mechanism, and the influence of these factors may vary with the location and operational condition of the pipes. The factors are as follows:

- 1) **Physical factors** are influenced by pipe geometry, pipe characteristics, and loading impact. For example, pipe material, pipe geometry (pipe diameter and thickness), pipe age, joint types, lining or coating if provided internally and externally to the pipe, traffic loading, and pipe manufacturing and installation procedure.
- 2) **Environmental factors** include soil type, soil load, soil moisture, groundwater, water quality and its chemical reaction with the pipe material.

- 3) **Operational factors** are mostly related to the operational condition of the pipe. For example, internal working pressure, surge pressure (if any), flow velocity, and operational and maintenance practices are the operational factors influencing the piping system.

Najafi and Gokhale (2022) described the mechanism of pipe failure as **structural**, which is due to cracks, fractures, and breaks; **hydraulic**, caused due to insufficient capacity, overflows, infiltration, and sharp bends of the pipe network (if any), affecting the hydraulic flow; **material degradation** occurs due to chemical corrosion, external and internal corrosion, and erosion; **operational problems** cause due to ingrown roots, blockage, grease, and deposit.

The deterioration process starts as soon as the pipe is installed underground. There are continuous and discontinuous stresses that act on the pipe caused by physical, environmental, and operational factors and contributing to pipe aging and degradation. The pipe's structural integrity plays an important role to resist the effect of these factors and retaining its strength. However, when the residual strength of the pipe cannot resist the applied stresses, then pipe failure will occur. There are typically two types of pipe failure, such as structural failure and hydraulic failure.

1.4.1 Structural Pipe Failure

Structural pipe failure can be caused by longitudinal pipe cracks, circumferential pipe cracks, pipe deformation, fractures, rupture of the pipe wall, or joint failure. Sometimes pipe failure can occur due to water hammer, in which the pipe experiences a sudden and excessive increase in pressure, leading to extreme stresses. Figure 1.4 (a) shows the pipe failure due to cracks. Figure 1.4 (b) shows the pipe failure due to corrosion holes and pipe joint failure. Figure 1.4 (c) shows the pipe failure due to a corrosion pinhole. Figure 1.4 (d) shows the pipe failure due to a circumferential break.

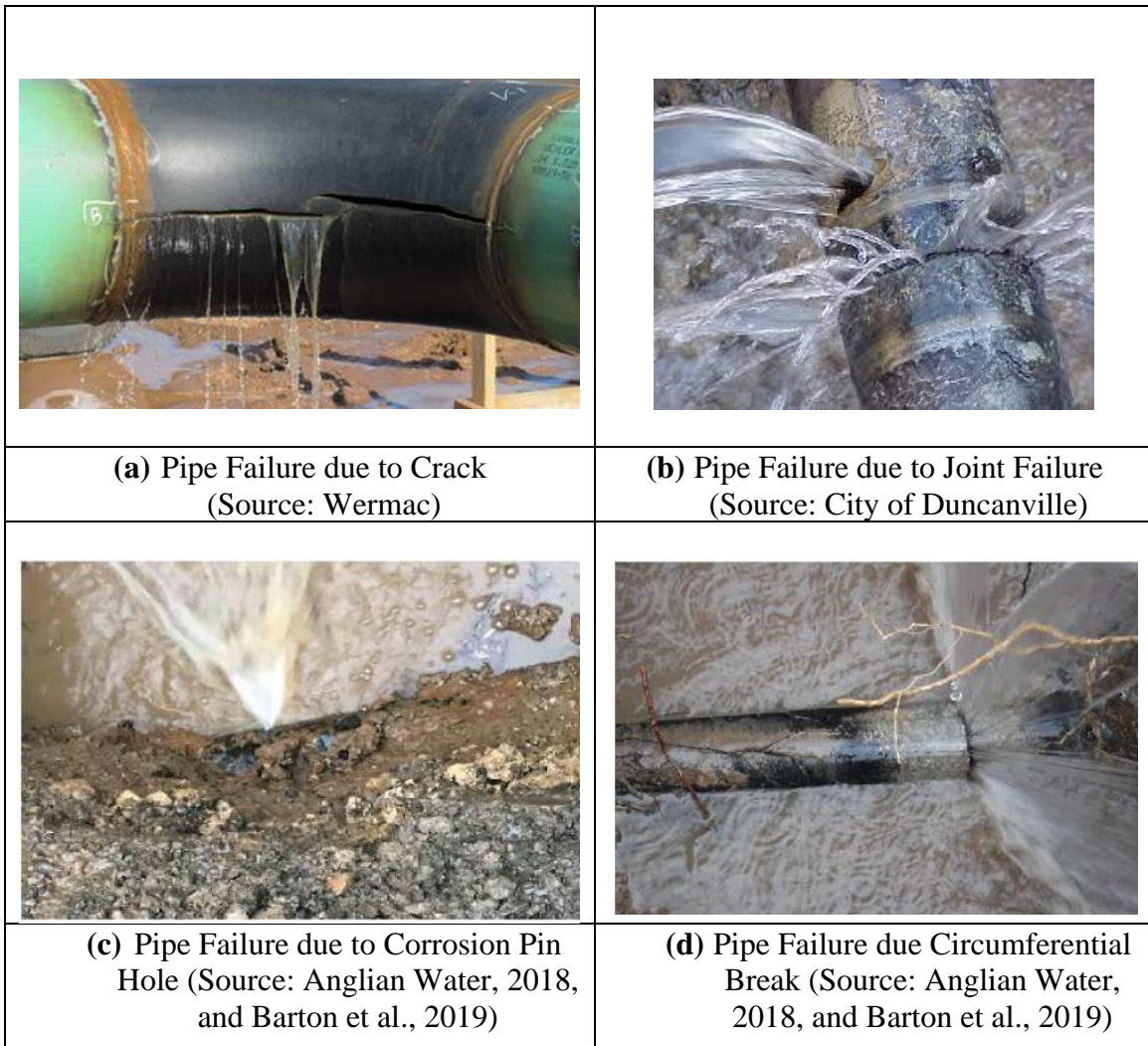


Figure 1.4 Pipe Failure

1.4.2 Hydraulic Pipe Failure

The second most common type of pipe failure is hydraulic failure. A hydraulic pipe failure occurs when the pipelines fail to supply the fluid at the required pressure (Zhou, 2018). The hydraulic failure can be due to irregularities on the internal pipe surface, and deposits created due to corrosion. These irregularities and deposits reduce the internal diameter and subsequently, affect the flow capacity of the pipe. In addition, these corrosion-deposited irregularities also affect the pipes' internal smoothness, which increases the friction factor and decreases the flow capacity.



Figure 1.5. Pipe with Corrosion Deposit Affected Hydraulic Flow Capacity
(Source: APP Manufacturing)

Rajani and Kleiner (2002) described the hydraulic failure of the pipe when the system cannot fulfill the demand, which may be due to heavy leaks in the supply system, pipe burst, pump shutdown, or a failed system. Also, if the pipes are heavily deteriorated, that will affect the carrying capacity of the pipe, as shown in Figure 1.5.

Therefore, pipe deterioration and failure mechanism are a complicated process to predict since many factors influenced it; additionally, the influence of these factors may differ based on the location and operational conditions. Hence, our aged and deteriorated underground infrastructure is in a critical need of improvement. Depending upon the host pipe condition and the type of defects on the pipe, a trenchless renewal method can be adapted to renew and rehabilitate the deteriorated pipe systems. For designing the trenchless pipe renewal method, selecting the most appropriate, cost-effective, and reliable method is one of the most critical steps in this process (Najafi & Gokhale, 2022). In addition, the adapted renewal method should be suitable to the individual project conditions.

1.5 Pipe Rehabilitation Methods

There are two main types of pipe rehabilitation methods, such as open cut and trenchless, which are commonly used to replace or renew old pipelines. Open-cut is a traditional method used

for the construction, replacement, and renewal of underground pipe infrastructure, which includes digging the trench for the proposed pipeline, providing support to the trench walls, preparing pipe bedding, placing and embedding the pipe sections in the trench, backfilling and compacting the trench and surrounding areas (Najafi, 2010; Najafi & Gokhale, 2022). This method is also called dig-and-install, dig-and-replace, dig-and-repair (Najafi & Gokhale, 2022).

On the other side, trenchless pipe renewal and rehabilitation method is an advanced construction technology used for construction, replacement, and renewal of underground pipe infrastructure with minimal surface and subsurface disruptions, and thus, minimize the social and environmental cost (Najafi, 2010; Najafi & Gokhale, 2022). This method is also known as trenchless renewal method (TRM). The main differences between these two methods are shown in Table 1.2.

Table 1.2 Open Cut and Trenchless Methods

Open Cut	Trenchless
More excavation and backfilling	Less excavation, minimal ground disturbance
Time consuming, increased time and labor cost, and thus, increased project cost	Faster and more reliable project cost
Carbon footprint is greater	Social and environmental cost benefit
Unsafe and less productive	Safer and more productive
Suitable for heavily clogged pipes and collapsed pipes	Not suitable for clogged pipes

Najafi and Gokhale (2022) explained that the open cut renewal method is more expensive and time-consuming than the trenchless techniques; about 70 percent of the extra cost is due to site restoration. Figure 1.6 shows the open cut method of replacing the pipe. In contrast, Figure 1.7 shows the trenchless method of rehabilitating the larger diameter pipe (left side) and smaller diameter pipe (right side).



Figure 1.6 Open Cut Method



Figure 1.7 Larger Diameter Pipe Rehabilitation (Left) Source: CUIRE, and Smaller Diameter Pipe Rehabilitation (Right) Source: DrainsAid

There are different trenchless renewal methods currently in practice to renew old and deteriorated pipes which includes both gravity and pressure pipes. The range of application include sanitary and storm sewers, culverts and drainage structures, drinking water pipes, oil and gas pipelines, and so on. Trenchless pipe renewal methods are applied to address structural defects, infiltration/ inflow problems, hydraulic capacity problems, corrosion problems, and many more (Najafi & Gokhale, 2022).

For selecting the trenchless renewal method, the knowledge of the pipe geometry, pipe depth, interior pipeline condition, such as the severity of corrosion and deposits, cracks characteristics, misalignments, deformation, and any joint issues, etc., is required as well as the information on the ground conditions around the pipe are important. In addition, selection of pipe renewal method should consider the construction cost, and availability of space for installation,

project specific conditions and constraints, availability of trenchless technology contractors and providers, and plans for future pipe applications (Najafi, 2010). Figure 1.8 shows the different renewal solutions based on renewal methods and the material used.

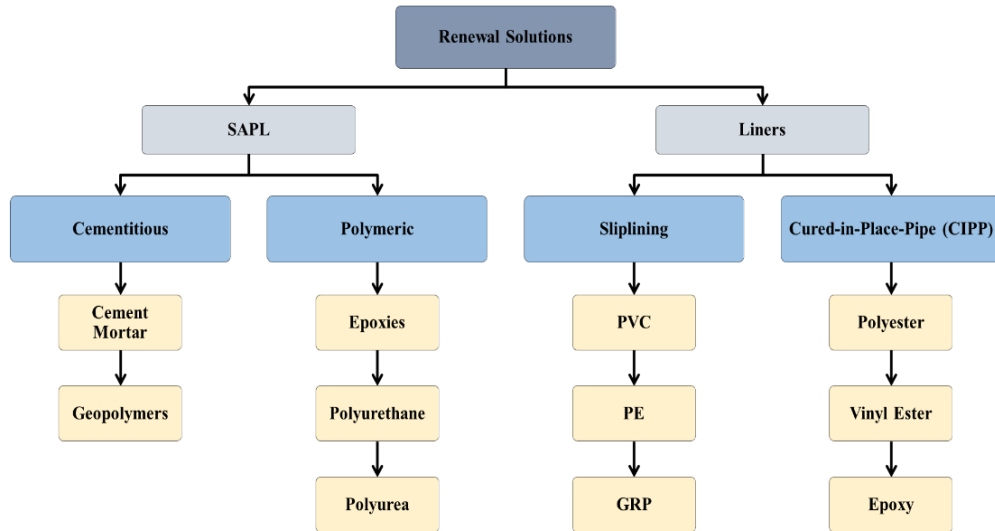


Figure 1.8 Renewal Solutions in Trenchless Technology
(Adapted from Najafi & Gokhale, 2022)

As shown in Figure 1.8, the renewal solution is categorized into two main types.

- 1) **Spray applied pipe lining (SAPL)**, which is also known as Underground Coatings and Linings (UC&L), Spray-on Lining (SOL), and Spray-in-Place Pipe (SIPP) (Najafi and Gokhale, 2022). SAPL is a trenchless technology of spraying a material (such as cementitious or polymeric) on the host pipe to rehabilitate or renew it. The installation of SAPL can be either manual or robotic, depending upon the site conditions or space constraints.
- 2) **Liners** are installed into the existing/host pipe, and then different curing methods are used to cure them depending upon the type of liner used. For example, Cured-in-Place-Pipe (CIPP) is installed on the existing pipe and cured with steam or hot water. On the other

hand, slipping involves the insertion of a pipe inside the existing host pipe, and the annular space between the host pipe and the new pipe is filled with grout.

1.6 Selection of Trenchless Renewal Methods

Selecting the pipe renewal method is complicated, and many factors are involved in its selection process. The selected method should be best suited to renew old and deteriorated pipes. A condition assessment of pipes can give an idea about the stage of the pipe deterioration. Various condition assessment tools are available to assess the pipe condition and predict the failure stage. In addition, other important factors such as ground conditions, new pipe service requirements, project site constructability, and limitations affect the selection of renewal methods, as described in Table 1.3.

Table 1.3 Factors for Pipe Renewal Selection Method
(Adapted from Najafi, 2010; Najafi & Gokhale, 2022)

Pipe Renewal Method Selection			
Pipe Conditions	Site Conditions	New Service Pipe Requirements	Constructability and Limitations
-External and internal condition of pipe. -Failure stage such as corrosion extent, corrosion holes, cracks, circumferential cracks. -Hydraulic failure -Presence of bends, fittings, service connections, valves.	- Existing utilities located. -Location of proposed pipeline such as under road, lake or river. -Accessibility issues, and site constraints. -Soil corrosion potential. -Soil settlement potential.	-Structural requirements. -Flow capacity. -Corrosion potentials. -Anticipated service life. -Length of pipe for renewal.	-Availability of contractors for selected renewal methods. -Technology availability -Initial and long-term cost -Access required for existing pipe -Other utilities hindrance to site activities. -Quality control and assurance.

As represented in Table 1.3, the existing pipe condition and other factors can provide guidance in selecting a renewal method to renew the deteriorated pipes.

1.6.1 Spray Applied Pipe Lining

The trenchless technology renewal method of SAPL is one of the most cost-effective and sustainable methods, with minimum ground disturbance. This method provides an effective solution for improving the deteriorated condition of the culverts and pipelines to enhance their design life (Kaur et al., 2022a). In addition, SAPL provides a monolithic layer that prevents further deterioration of pipes (Najafi & Gokhale, 2022). The materials used for SAPL fall within two broad categories: cementitious and polymeric. Cementitious products are categorized as rigid, and polymeric materials, including polyurea, polyurethane, and epoxy, are categorized as flexible. The polymeric liner has a thermoset material characteristic, i.e., it is in a liquid form prior to curing and can be molded into various shapes after appropriate curing. Table 1.4 depicts the main characteristics of SAPL.

Table 1.4. Main Characteristics of SAPL (Source: Najafi and Gokhale, 2022)

Method	Diameter Range (in.)	Maximum Installation (ft)	Liner Material	Applications
Spray Applied Pipe Lining	3-180	1,000	Epoxy, polyurea, polyurethane, cementitious	Gravity and pressure pipelines

Polymeric SAPL is a new renewal application that can be used to structurally renew deteriorated gravity and pressure pipelines. It can be applied to a varied range of concrete, masonry, corrugated metal, and steel pipelines. Furthermore, the polymeric lining is approved for water mains by the National Sanitation Foundation (NSF) (Najafi & Gokhale, 2022). The polymeric SAPL can be applied manually or with a robotic application, depending on the pipe diameter and space constraints. Figure 1.9 below shows a manual application of the polymeric SAPL liner and Figure 1.10 shows a robotic application. Polymeric SAPL has material

characteristics that can be applied for corrosion protection and/or to increase the load bearing capacity of the host pipe.



Figure 1.9 SAPL Manual Application



Figure 1.10 SAPL Robotic Application

1.6.2 Liners

Sliplining (SL) and Cured-in-place (CIPP) are the oldest trenchless renewal methods used to renew old pipes structurally and non-structurally. In the SL method, a new pipe of a smaller diameter is inserted into the existing old or deteriorated pipe. The annular space between the existing pipe and the new pipe is grouted (Najafi & Gokhale, 2022). The commonly used pipe

material for the SL method is PVC, polyethylene (PE), and glass reinforced polyester (GRP). However, other types of insertion pipe materials can also be used for the SL.

Cured-in-place (CIPP) is the most commonly used trenchless method to repair old and deteriorated pipes. In the CIPP process, a pipe sleeve covered with a liquid thermoset resin-saturated material is inserted into the existing pipeline by hydrostatic force, air inversion, or mechanical pulling with the help of a winch and a cable. Then, hot water or steam is used to cure the resin by heating it, as a result, it attaches to the host pipe. Once the material is fully cured, it acts as a new pipe inside the existing pipe.

Therefore, various rehabilitation methods are available to rehabilitate or renew the old and deteriorated pipes based on the material used and the installation methods.

1.7 Problem Statement

The research and development for underground water and wastewater infrastructure rehabilitation has been continuously making progress in technology and application methods (Kaur et al., 2022a). Many researchers are working in pipeline asset management to develop various decision-making support tools using advanced algorithmic models to prioritize the condition assessment of water and wastewater infrastructure and save tons of money by prioritizing the inspection of underground infrastructures (Loganathan, 2021; Loganathan et al., 2022; Loganathan et al., 2023; Grigg, 2006). These models can be helpful in planning the rehabilitation processes well in advance to enhance the useful life of pipelines and avoid catastrophic failures.

Researchers have been working closely to test different products such as epoxy, polyurea, and polyurethane to classify their potential structural capability and recommending their use in the application of SAPL for pipe renewal and rehabilitation (Kaur et al., 2022b). The potential application of SAPL as a fully structural renewal process has been approved for culverts and

drainage structures (Kohankar Kouchesfehni, 2020; Darabnoush Tehrani, 2020), but it is still underway for pressure pipeline rehabilitation. SAPL as a Class IV (fully structural liner) has been proposed for non-pressure pipes; however, it is still in the developmental phase for pressure pipes (Shannon & Azroor, 2020). Several researchers are actively engaged in developing testing methodologies for evaluating the application of polymeric SAPL in pressure pipes. Numerous research studies have reported successful experimental results for testing polymeric SAPL as a semi-structural solution. However, limited data is available on the testing of polymeric SAPL as a fully structural lining system.

Currently, manufacturers and contractors are implementing design methodologies for SAPL applications from other available methods, such as “*ASTM F1216- Standard Practice for rehabilitation of existing pipelines and conduits by the inversion and curing of a resin-impregnated tube*” and “*ASTM F1743 Standard Practice for rehabilitation of existing pipelines and conduits by pulled-in-place installation of cured-in-place thermosetting resin pipe (CIPP)*.” There is no design standard available that can be used for the design methodology and application of SAPL (Kouchesfehni et al., 2021). Currently, methodologies and analytical design equations developed for other purposes are used for SAPL application (Darabnoush Tehrani, 2020).

Most municipalities, contractors, and researchers use ASTM F1216 (2016) and American Water Works Association Structural Classification (2019) for designing lining in pressure pipes applications. However, no documented and well-developed test methodologies or standards exist to test the emerging new lining products for pressure pipes. Not enough design equations information was collected on the SAPL application in pressure pipes. Limited research on the design equations validation and design parameters was found for polymeric SAPL in the pressure application.

Further testing for SAPL is required for creep, and whether a liner can survive the fracture of a pipe under pressure is needed (Ellison et al., 2010). The ability of a liner to function in the long-term run is crucial, and thus, more testing is required (Ellison et al., 2010). Limited data are available on the hydraulic properties of the polymeric liner, and a lack of evidence was found to see the improvement in the hydraulic flow properties when the liner is used to reduce the corrosion and defects of pressure pipes.

The lack of comprehensive available standards, design guidelines, testing, and evaluation of SAPL is limiting its acceptance and use by DOTs and private entities to renew old pipes. Thus, sufficient information is not available to confirm SAPL as a structural and durable renewal technology to enhance the expected lifespan of the pressure pipeline. Because of the necessity for sufficient information on this technology, more research is needed to test and evaluate the structural properties of Polymeric SAPL in pressure pipes application. Thus, conducting a comprehensive testing and evaluation analysis of SAPL can contribute to the potential recommendation of its use as a structural application in pressure pipes.

1.8 Goal and Objectives

This study focuses on testing and evaluating polymeric SAPL for its application in pressure pipes. The objectives of this study are as follows:

- 1) To develop the testing and evaluation procedure for the application of polymeric SAPL to structurally renew and rehabilitate the pressure pipes. To accomplish this, the evaluation of SAPL was conducted through a series of full-scale laboratory tests, as listed below.
 - a. Short-term Hole Spanning Internal Pressure Testing.
 - b. Vacuum Pressure Testing
 - c. Short-term Pressure Integrity Testing.

- 2) To validate the adopted design equations for the application of SAPL.
- 3) To determine the mechanical properties of liner material and utilize these properties to design the liner thickness in the full-scale laboratory testing.
- 4) To conduct testing and evaluation to assess the hydraulic flow characteristics of SAPL lined pipe and compare it with the corroded pipes.

1.9 Scope of Work

The scope of this research is showed in Table 1.5.

Table 1.5 Scope of Work

Attribute	Description	Included	Not Included
Structural Evaluation of SAPL	Testing of SAPL liner material	Pressure Pipes	Gravity Pipes
SAPL Material	Different Renewal Materials	Polymeric SAPL	Composite materials
Material Testing	Mechanical Properties	Short-term mechanical properties such as flexural, tensile, and punch shear	Other mechanical and long-term creep properties
Design and Structural Classification Testing	Class I, II, III and IV Design Classification	Class II, and Class IV design (AWWA Standards)	Class I and III (AWWA Standards)
Full Scale Laboratory Testing	Designed laboratory testing for structural evaluation	Short-term hole-spanning internal hydrostatic pressure testing, Vacuum test, and Short-term pressure integrity testing	External Buckling Test, Long-term pressure integrity testing
Flow Characteristics	Evaluation of flow characteristic of lined pressure pipes	Darcy-Weisbach's friction factor	Hazen-Willian and Manning's constant

1.10 Hypothesis

The hypothesis of this dissertation is illustrated as follows:

Hypothesis 1:

Null Hypothesis: Polymeric SAPL material can structurally renew corrosion holes in pressure pipes application when designed as Class II.

Alternative Hypothesis: Polymeric SAPL material cannot structurally renew corrosion holes in pressure pipes application when designed as Class II.

Hypothesis 2:

Null Hypothesis: Polymeric SAPL material can structurally renew a fully deteriorated pipe in pressure application when designed as Class IV.

Alternative Hypothesis: Polymeric SAPL material cannot structurally renew a fully deteriorated pipe in pressure application when designed as Class IV.

Hypothesis 3:

Null Hypothesis: Polymeric SAPL application can reduce the head loss of deteriorated and corroded pressure pipes by more than 20%.

Alternative Hypothesis: Polymeric SAPL application cannot reduce the head loss of deteriorated and corroded pressure pipes by more than 20%.

1.11 Methodology

The study includes the research methodology as illustrated in Figure 1.11. A comprehensive literature review was performed to explore the application of SAPL in both gravity and pressure pipes. A study was conducted to understand the design methodologies that are applied in both gravity and pressure application. The literature review identified the potential problems and knowledge gaps in the application of SAPL. Based on these knowledge gaps, the research objectives of this study were outlined.

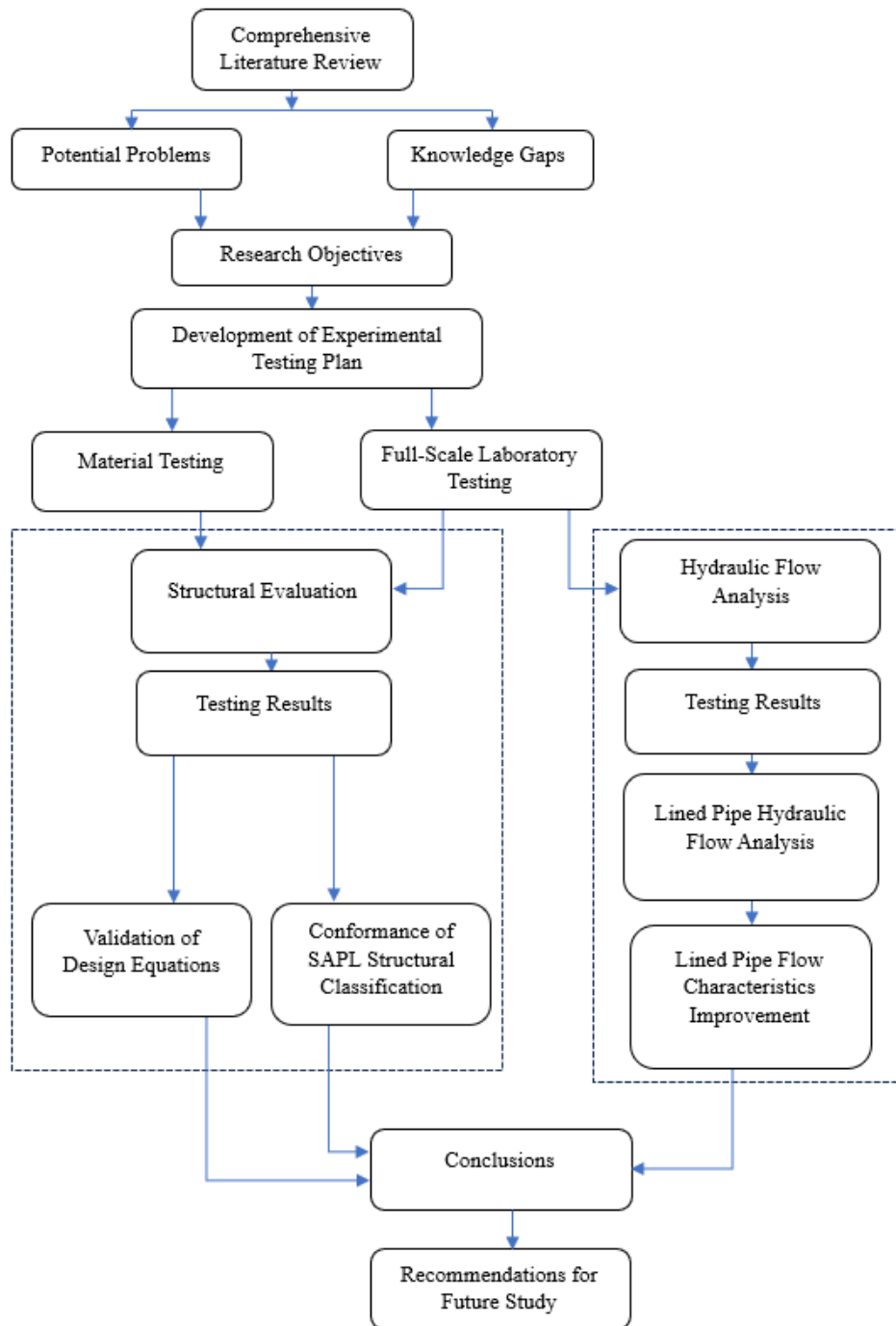


Figure 1.11 Research Methodology

To achieve the objectives, a series of full-scale laboratory testing were designed and executed to evaluate the structural characteristic and performance of SAPL when used for renewing and rehabilitating pressure pipes. In addition, a flow test was performed to determine the

hydraulic properties of the liner material. Material testing was executed to determine the mechanical properties of the material, which were used in designing the liner thickness for full-scale laboratory testing.

Analytical design equation calculations were conducted to validate the design equations with experimental results. If necessary, any required modifications to the design equations were suggested based on the analysis. The conformance of the structural application of polymeric SAPL lined pipes was evaluated when designed as both semi-structural and fully structural solutions. Additionally, the hydraulic performance of the lined pipes was compared with both bare pipes and corroded pipes. The friction factor and roughness were calculated for the SAPL lining system.

1.12 Expected Outcomes

The expected outcome of this dissertation is listed as follows:

- Validation and verification of design equations for the application of polymeric SAPL in renewal of pressure pipes.
- Structural Classification of polymeric SAPL as per AWWA structural Classification II, and IV.
- Determine the friction factor and roughness of SAPL material based on the experimental data, and equations for the relative roughness using regression modeling.
- Comparison of flow characteristics of SAPL lined pipe with bare and corroded pipes.

1.13 Overview of Chapters

The summary of the chapters in this dissertation is given as below:

Chapter 1: Introduction

Chapter 2: Literature Review

Chapter 3: Structural Evaluation of Spray Applied Pipe Lining

Chapter 4: Hydraulic Evaluation of Spray Applied Pipe Lining

Chapter 6: Results and Discussion

Chapter 7: Conclusions and Future Research Recommendations

1.14 Chapter Summary

This chapter provided an introduction and background to water and wastewater infrastructure, along with an overview of the condition of our underground infrastructure. Additionally, the chapter provided a concise introduction to pressure pipes and their various applications.

This chapter presented the pipe deterioration mechanism and the factors influencing this process. Furthermore, it provides insights into the consequences of deterioration and pipe failure, including both structural and hydraulic effects.

In this chapter, the trenchless renewal methods, such as SAPL and Liners for deteriorated and old pipes, were discussed. At the end of the chapter, the problem statement, goals and objectives, scope of work, hypothesis, research methodology, and expected outcomes were discussed.

Chapter 2 Literature Review

2.1 Introduction

Chapter 1 presented an overview of trenchless renewal methods that are commonly used to rehabilitate and renew deteriorated pipes. In Chapter 2, an extensive literature review was performed on the application of SAPL for rehabilitating deteriorated pipes. The literature review encompasses studies conducted on both gravity and pressure pipes, highlighting different research works in the field, and design methodologies adopted for applying SAPL in pressure pipes. Furthermore, the literature review identifies potential problems and knowledge gaps associated with the application of SAPL. In addition, the literature review identified various design methodologies that have been adopted for the application of SAPL.

2.2 Causes of Pipe Deterioration and Failure

There are various factors that initiate and influence the pipe deterioration process; however, Zhou (2018) suggested the key factors of pipe deterioration can be the environmental characteristics and material properties. Yan (2006) specifically illustrated the pipe deterioration indicator for the water mains, as given in Table 2.1. However, pipe deterioration is a complex process, and identifying the influence factors of each indicator is non-exhaustive.

As represented in Table 2.1, there are three types of deterioration indicators such as 1) physical indicators, 2) environmental indicators, and 3) operational indicators.

2.2.1 Physical Indicators

Pipe material: Pipe material is an essential factor for pipe service life, and the rate of deterioration is affected by the type of material. The material's chemical property governs the capability of the pipe against corrosion. The interaction between the pipe material and fluids

flowing through it governs the corrosion rate. Pipe material also determines the pipe’s strength and performance against loading and the impact strength required to protect it from damage during material handling and installation.

Table 2.1 Water Main Deterioration Indicator (Adapted from Yan, (2006))

Physical indicators	Environmental indicators	Operational indicators
Material	Bedding condition	Frequency of supplies
Year of installation	Traffic load	Duration of water supplies
Diameter	Surface permeability	Number of valves
Length	External protection	Number of connections
Joint method	Soil condition	Leakage record
Internal protection	Groundwater table	Complaint frequency
Workmanship	Buried depth	Breakage history

Pipe age: The age of a pipe is determined by the year of installation, which provides information about the duration the pipe has been in operation. Pipe age can be the first indicator of pipe deterioration, considering the internal and external surrounding environmental conditions, regardless of accounting for the pipe operation and loading conditions. Some studies have shown that pipe age alone may not be a sufficient indicator of pipe strength. Because there are instances that the pipe is not at its full capacity after installation, or the fluid running through the pipe may not significantly deteriorate the pipe. Additionally, Wang et al. (2010) suggested that pipe age should not be considered a decisive indicator for pipe replacement and rehabilitation.

Pipe diameter: Many studies have concluded that the pipe diameter is an influential factor in pipe deterioration. Several research studies have stated that small diameter mains (diameter less than 300 mm) have higher breakage numbers than larger diameter mains (Boxall et al., 2007; Lubini & Fuamba, 2011; Loganathan, 2021a; Najafi & Gokhale, 2022). These studies have found

that larger diameter pipes, being buried at greater depths, tend to have higher structural integrity and experience fewer instances of breakage.

However, other studies have identified an inverse relationship between pipe diameter and breakage. According to these studies, larger diameter pipes had a higher breakage rate and failed more frequently than small diameter pipes (Walski & Pelliccia, 1982). The increased deterioration of larger pipes is attributed to their larger surface area, which is exposed to internal and external environmental factors (Jeong et al., 2005).

Pipe length: Some of the studies have concluded that shorter pipes deteriorate faster than longer pipes. One reason could be that shorter pipes often have more severe bends, which can result in the accumulation of debris and blockages, leading to pipe deterioration (Davies et al., 2001; Najafi & Gokhale, 2005; Loganathan, 2021a). In contrast, Malek Mohammadi (2019) concluded that the rate of deterioration of longer pipes is higher as compared to shorter pipes. This is because the long run of the pipes required pipe joints, which could be the common source of infiltration of the soil and groundwater in the case of gravity pipes or sewers (Jeong et al., 2005).

Pipe Joint Method: The pipe joint method depends upon the pipe material and the anticipated water pressure within the pipeline. Pipe joints can be Classified into rigid and flexible joints (Zhou, 2018). Flexible joints are designed to be adaptable and can accommodate soil movement or variations in the connected pipe sections (Zhou, 2018). On the other hand, rigid joints are stiff and unable to accommodate misalignments. This lack of flexibility can result in an increase of stresses at certain points and leading to a greater vulnerability of deterioration. In addition, improper and faulty joints can lead to water leakage and increase the pipe deterioration.

Pipe Internal Protection: The internal protection of a pipe depends upon the pipe material. Typically, pipes are provided with the lining or coating before installation, especially the

cast iron pipe. However, pipe manufacturing companies are using advanced technologies to protect the pipes with an anti-corrosive coating, which slows down the process of corrosion of metal pipes and increases the useful life of the pipes. This coating reduces or slows down the corrosion and also improves the hydraulic flow condition.

Workmanship: Workmanship also plays a vital role in the pipe deterioration process. The workmanship is responsible for ensuring quality control and quality assurance during the installation and pipe maintenance. Poor workmanship can have adverse effects on pipe condition and increase the risk of deterioration, regardless of factors such as pipe age, material, and other influences. Although, there is no explicit evaluation of the impact of workmanship on the pipe deterioration.

2.2.2 Environmental Indicators

Bedding Condition: Bedding is the material laid below the pipe to support it from the top and adjacent soil load. The type of bedding depends on the pipe material, pipe diameter, external load, and working pressure. A proper and well-compacted bedding material around the pipe is crucial to distribute the load evenly and prevent pipe failure. The load carrying capacity of the pipe depends on the support provided by the bedding. Improper bedding may create breaks in the joints, which can lead to pipe leakages. Therefore, bedding conditions play an important role in pipe deterioration.

Loads: Loading on the pipe can be internal and external. Internal loads are caused by live load or fluid pressure, and these loads influence the structural integrity and performance of the pipe. The external loads are due to the traffic load and soil backfill. Other types of loads that may occur during pipe's service life, for example, thermal expansion loads resulting from changes in the temperature of the fluid flowing through the pipe or variations in environmental factors.

The intensity and nature of the loading impact depend on factors such as pipe material, pipe dimensions, burial depth, installation of pipe joints, etc. Therefore, if the pipe loading increases more than the design load, then, the pipe may suffer cracks, deflection, and joint failure. In addition, surge events occur occasionally that can have an immediate and vicious impact from the internal pressure. This sudden impact can cause excessive load on some of the vulnerable parts of the pipe network, resulting in pipe failure (Skipworth et al., 2002). It is imperative to consider all the expected loading factors during the design and installation of the pipe system. Hence, the loads on the pipe play a critical role in its deterioration and service life.

Surface Permeability: Surface permeability of the pipe refers to the pipe's ability to allow liquids, gases, and moisture to pass through its surface. The permeability of the pipe surface depends on the pipe material and surface characteristics. Some of the pipe materials are prone to be more permeable such as concrete and porous ceramic pipes. In contrast, certain types of material, such as plastic and metal pipes, have low permeability. The higher the permeability, the greater the risk of corrosion and leaks. The coatings or linings are recommended to reduce the surface permeability based on the type of material. Surface permeability has not been studied well and recorded in area of the water utilities (Zhou, 2018).

Groundwater Table: The deterioration of pipes, particularly those that are underground, is significantly influenced by groundwater. Groundwater frequently contains minerals and chemicals that speed up corrosion and cause pipe degradation, indentation, and, occasionally, pipe wall perforation (Zhou, 2018). Additionally, when there is a high groundwater table, it can result in an external hydrostatic pressure on the pipe walls that leads to stresses in the pipe. The frequent stresses can create recurrent strains and weaken the pipe walls, and this can impact pipe

deterioration. Additionally, changes in the groundwater table may cause soil movement, which may affect the stability and alignment of the pipes.

Buried Depth: The depth of the pipe influences its resistance to failure. A sufficient depth is required so that overhead traffic loads do not affect the pipe's structural integrity. Davies et al. (2001) suggested that as the depth of the pipe increases, the defect rate decreases. However, this depth should be within the design standards because the deeper installation of the pipe increases the soil, backfill, and earth pressure loads (Zhou, 2018). These additional loads may impact pipe deterioration and failure.

2.2.3 Operational Indicators

The operational indicators, such as the number of connections and valves, can impact the pipe deterioration rate. Because as the number of connections increases, the flow turbulence, which can impact the pipe deterioration and pipe failure. Similarly, operational indicators like the frequency and duration of water supplies can indicate greater usage of a particular water supply line, thus accelerating pipe deterioration. Thus, operational indicators impact pipe deterioration; some are direct indicators, and some are indirect indicators.

2.3 Classification of Pipe Failures

The traditional design of pipes has been based on physical behavior of the pipe that attempts to provide pipe resistance capacity against expected loads (operational and environmental) with a sufficient margin of safety (Rajani & Kleiner, 2001). Pipe failure occurs when the performance strength of the pipe has reached its material limit. Pipe failure can be categorized as given in Table 2.2.

Table 2.2 Pipe Failure and Factors

Pipe Defects and Failure	Factors
Longitudinal cracks and fractures results into longitudinal break (Najafi & Gokhale, 2022)	<ul style="list-style-type: none"> Excessive crushing and ring stress. Radial tension due to excessive hoop stress or pressure surge. Pipe wall thinning due to corrosion.
Circumferential cracks and fractures results into circumferential break or splitting (Najafi & Gokhale, 2022)	<ul style="list-style-type: none"> Excessive shear and bending stresses (most likely near joints). Longitudinal Stresses (due to thermal contraction, bending stresses, inadequate bedding support).
Stress rupture (Brittle or ductile failure depends upon pipe material)	<ul style="list-style-type: none"> Pipe's material stress reaches the ultimate stress of material.
Fatigue failure	<ul style="list-style-type: none"> Repetitive cyclic stresses induce fatigue stresses in the pipe material.
Creep failure	<ul style="list-style-type: none"> Continuous pipe deformation due to sustained pressure, and pipe failed due to long-term effect of creep.
Corrosion failure	<ul style="list-style-type: none"> Corrosion deposits and tubercules on internal pipe diameter. Corrosion holes and pits. Wall thinning.

Figure 2.1 represents the graphical representation of pipe defects and failure mode of an underground pipe due to direct tension. Figure 2.2 illustrates the pipe failure mode due to bending and Flexure. Figure 2.3 exemplifies the pipe failure due to hoop stress.

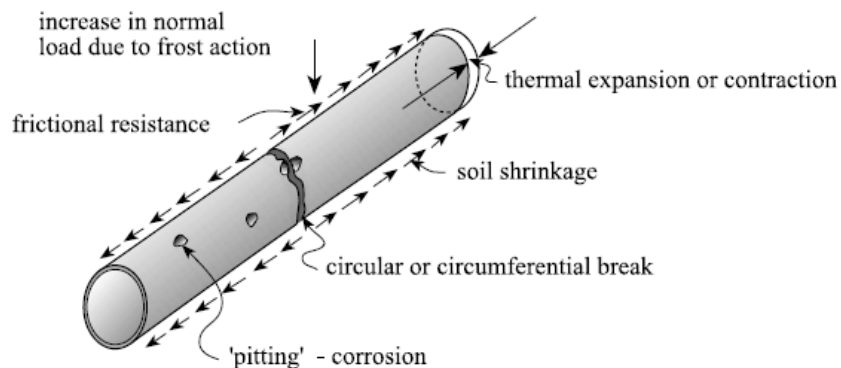


Figure 2.1 Failure Mode of Underground Pipe Due to Direct Tension
(Adapted from Rajani & Kleiner, 2001)

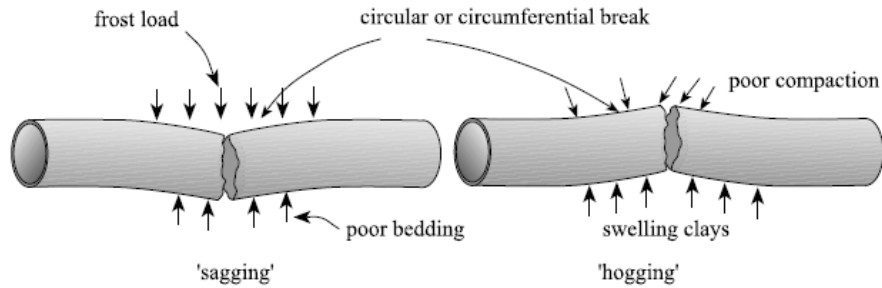


Figure 2.2 Failure Mode of Underground Pipe Due to Bending and Flexure (Adapted from Rajani & Kleiner, 2001)

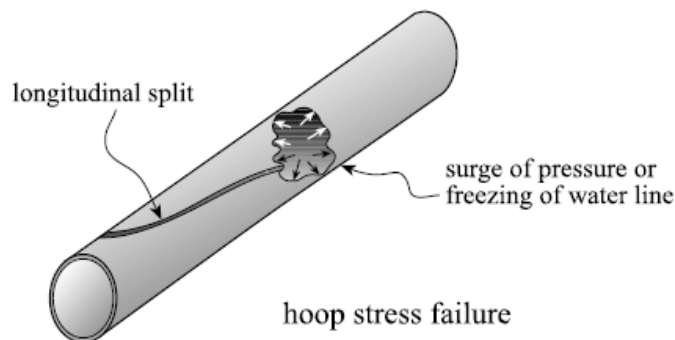


Figure 2.3 Failure Modes of Underground Pipes Due to Hoop Stress (Adapted from Rajani & Kleiner, 2001)

Table 2.2 represents different types of defects and failures and their associated factors. Some of these pipe defects can cause the pipe condition to partially deteriorate, and some can lead to severe failure, and thus leading to a fully deteriorated pipe condition. Therefore, depending on the condition of the host pipe and the intensity of the defects, a pipe rehabilitation method can be adapted to renew and rehabilitate the pipe.

2.4 Pipe Rehabilitation

As described in the previous sections, pipe deterioration and failure are critical components of underground infrastructure. Both water and wastewater infrastructure are severely affected by pipe deterioration and aging. Deteriorated water pipes are significantly affecting the water quality,

and these must be renewed and repaired to provide clean and safe drinking to everyone (USEPA, 2005). Depending upon the host pipe condition and the type of defects on the pipe, a trenchless renewal method can be adapted to renew and rehabilitate the deteriorated pipe systems. It is obvious that the renewal solution depends on the host pipe condition and is necessarily suitable to the individual project conditions. Selecting the most appropriate, cost-effective, and reliable method is one of the most critical steps in designing the trenchless pipe renewal method (Najafi & Gokhale, 2022).

Many available rehabilitation methods are being used worldwide. The differences between these methods are the installation procedure, the material used and its structural strength, and the design requirements. In addition, these methods are differentiated based on their purpose, such as structural, semi-structural, and non-structural (basically applied as corrosion protection). The trenchless methods such as spray in place lining (cementitious and polymeric) and cure-in-place liner are applied on varied types of host pipe such as cast iron, steel, concrete, and PVC. These methods have been practiced since the 1900s (Alloche et al., 2005; Ampiah et al., 2010). This study evaluates the application of spray applied pipe lining (SAPL) material for rehabilitation of pressure pipes with particular emphasis on the polymeric material.

2.5 Spray Applied Pipe Linings

Spray applied pipe lining (SAPL), also known as spray-in-place pipe (SIPP), has been used to protect and renew water and wastewater infrastructure above and underground. SAPL is applied as a monolithic layer that prevents deterioration, and it can be designed as a structural replacement for the host pipe. The following are three categories of SAPL design applications for host pipe (Najafi & Gokhale, 2022).

(1) **Non-structural:** Non-structural is provided for corrosion protection. For this purpose, the host pipe should have full structural integrity, and the SAPL can only fulfill the purpose of preventing any further pipe corrosion.

(2) **Semi-structural:** Semi-structural lining system is completely bonded to the host pipe; thus, the lining and host pipe act as a composite structural system, enhancing the system's load-bearing capacity.

(3) **Structural:** Structural lining system is not bonded to the host pipe. Thus, the lining acts as a standalone pipe inside the existing pipe, and the lining system should act as a structural composite to sustain the desired loading or pressure.

The two main categories of SAPL are cementitious and polymeric. At the beginning of the 20th century, shotcrete, a cementitious SAPL liner, was developed, and later in 1910, it was accepted as a construction renewal method (Najafi & Gokhale, 2022). There are mainly two types of materials, geopolymers, and cement mortar, that are commonly used in cementitious liners. On the other, polymeric liners have three main types of material, such as epoxy, polyurethane, and polyurea, that are commonly used in renewal methods (Najafi & Gokhale, 2022). Depending on site conditions and constraints, SAPLs can be applied manually, spin caster, and robotic application.

2.5.1 Cementitious Spray Applied Pipe Lining

The cement mortar lining was introduced in 1930s (Ellison et al., 2010). The first successful trial of cement mortar lining underwent in the early 1930s (Motlagh et al., 2013). The cementitious lining is more popular because of its cost-effectiveness and it can be applied to both water and sewer applications. The cementitious lining needs more curing time as compared to polymeric liners. The cementitious lining is used for corrosion protection, but it is not appropriate

for pipes that have leaks and where the wall thickness is reduced significantly due to corrosion (Najafi & Gokhale, 2022). Cementitious material is also used as a primer before the polymeric lining application (Najafi & Gokhale, 2022).

There are two types of cementitious SAPL such as cement mortar and geopolymer. The tensile and compressive strengths of the geopolymer are more and it requires less setting time as compared to conventional cement mortar SAPL (Davidovits, 2015). In addition, the geopolymer liner has high chemical and fire resistance, and the shrinkage and creep factors are lower when compared to cement mortar (Park et al., 2016). The cementitious SAPL has brittle behavior, and cracks are generated generally due to shrinkage, lower tensile strength, and stress concentration (Darabnoush Tehrani, 2020; Kohankar Kouchesfehane et al., 2019). Typically, the cementitious SAPL application starts with pipe diameter of 36 in., a manual entry pipe size (Darabnoush Tehrani, 2020). The minimum thickness needed for cementitious SAPL is 1 and 1.5 in., depending upon the design engineer or pipe owner (Royer & Iseley, 2017).

2.5.2 Polymeric Spray Applied Pipe Lining

Polymeric SAPL material possesses the advantage of quick return-to-service and is considered more efficient compared to cementitious liners. It is also more flexible than cementitious lining material. SAPL performs as a plastic-type material when cured; thus, it has inherent properties to resist environmental corrosion element (Najafi & Gokhale, 2022). The application of SAPL is safe to use in confined spaces when proper safety procedures are followed. The liner thickness of polymeric is less than cementitious, thus, having less effect on the internal pipe diameter reduction. Three most commonly used polymeric materials for SPAL applications are: 1) Epoxy, 2) Polyurethane, and 3) Polyurea. However, some applications have included hybrid polyurea in SAPL these days.

2.5.2.1 Epoxies

Epoxy resins are generally two-part materials. When these materials are mixed, they either co-polymerize or go through a catalytic reaction activated by one part upon another. These are thermoset polymers that are applied as liquids, and the material is self-catalyzing and become hardened and holds the shape as firm solids (Xometry, 2023). During the late 1970s, the United Kingdom was the first country to introduce the use of epoxy lining, and in the early 1990s, it was introduced to North America (Motlagh et al., 2013).

The drawbacks of cementitious lining were overcome by introducing epoxy lining in the underground infrastructure. Epoxies are most commonly used for corrosion protection for metals since it has excellent adhesion property to the metals. In addition, epoxies provide high moisture, chemical, and impact resistance to the substrate. Epoxies are also used as a primer, as a base coating for other polymers, such as silicones, polyurethanes, and polyureas (Curran & Cain, 2016).

Epoxies are the best solution for corrosion control; however, alternative corrosion protection control systems are being used because of the limitation of epoxy material. Epoxies are not very flexible, and tend to crack in the application when the substrate has movement and heavy impacts. Their performance is generally lower due to the increased brittleness of the material (Curran & Cain, 2016). Epoxy lining is classified as a non-structural since it needs to be completely adhesive to the host pipe. However, the use of epoxy lining is commonly used to prevent corrosion of the host pipe. The lining also provides a smooth finish to the host pipe, which improves the flow capacity.

2.5.2.2 Polyurethanes

Polyurethane is a plastic material that can be formulated either as a rigid or flexible. Polyurethane is formed when two components, i.e., diisocyanates (or polyisocyanates), react with

polyols. In the chemical reaction of Polyurethane, a catalyst is required for the rapid reaction of isocyanate and polyol components, except for moisture-cured systems (Curran & Cain, 2016). During the mid-1970s, North America was the first country to introduce Polyurethane to seal the underground tanks to prevent corrosion. During the same time, Europe used Polyurethane as a lining to protect the oil and gas pipelines (Motlagh et al., 2013).

During the 1980s, with technological advancement, polyurethane lining was installed in the water industry (AWWA C22, 2008). The elastomeric Polyurethane is flexible with elongation properties and it has good impact and abrasion resistance. Polyurethane is known for its good adhesive properties to the host substrate. However, the polyurethane lining is moisture sensitive and has a higher permeability rating. During the mid-1990s, technological advancement led to the development of 100% solid rigid polyurethane lining. The rigid Polyurethane formed a three-dimensional cross-linked structure, making the material more superior in providing resistance to chemicals, water penetration, and elevated temperatures (Kouchesfehani, 2020). Polyurethane also exhibits strong long-term properties (NASSCO, 2023). Polyurethane has quick curing capabilities, and the service can be returned quickly.

2.5.2.3 Polyurea

Polyurea is also a plastic material that can be formulated either rigid or flexible. Polyurea is formed when two components, i.e., diisocyanates (or polyisocyanates), react with amines. However, in the hybrid system, the isocyanates reacted with a mixture of amines and polyols, producing an attractive combination of flexibility and hardness. In the chemical reaction system of polyurea, isocyanate rapidly reacts with amines without a catalyst. Polyurea coating is 100% solids, zero-volatile organic compounds formulations that can be cured without a catalyst, heat or at low temperatures up to -20 °C. In addition, the curing time of polyurea is less than 30 seconds.

The urea links in the polyurea make it moisture-resistant, and helps prevent blistering and also contributes to better chemical resistance. The polyurea exhibits excellent mechanical properties of hardness, tear, and abrasion resistance compared to polyurethane. In addition, polyurea coating has good resistance against thermal shock and impact resistance (Curran & Cain, 2016).

Since polyurea has less curing time, it can be applied as a thicker layer, which can act as a protective coating and provide structural integrity to the substrate. Proper mixing of components is essential for the right film formation and adhesion (Curran & Cain, 2016). In addition, the preparation and conditions of the host substrate are essential for the proper installation of polyurea. Polyurea provides a smooth surface which helps in the improvement of the flow capacity of the pipe.

2.6 Structural Design Considerations of SAPL Renewal Method

A buried pipe is designed to resist or transmit all service loads, including the weight of the soil, hydrostatic pressures, vacuum, internal working pressures, and loads applied by the traffic at the ground surface (Najafi & Gokhale, 2022). Since there is currently no single design equation that can be used for the proper design of SAPL for different conditions, thus, it is necessary to divide these conditions into different categories. The design equations have been divided into categories such as “partially deteriorated” and “fully deteriorated” conditions of the existing pipe to be rehabilitated for both gravity and pressure pipes (Najafi & Gokhale, 2022). However, AWWA (2019) further divided the design equations into different structural classifications depending on the host pipe conditions. The pipe conditions “partially deteriorated” and “fully deteriorated” are defined as follows:

2.6.1 Partially Deteriorated Condition of Gravity Pipes

A pipe with partial deterioration may have displaced joints, cracks, or corrosion but is still structurally sound to carry all soil and surface loads acting on it. This type of pipe is intended to provide full support around the SAPL. Assuming a pipe is partially deteriorated, the SAPL is designed to withstand uniform hydrostatic pressure throughout its entire circumference. For a conservative SAPL design, it should be assumed that the SAPL is not connected or bonded to the existing pipe in any way. Therefore, there is no support to the SAPL system from the host pipe (Najafi & Gokhale, 2022).

2.6.2 Fully Deteriorated Condition of Gravity Pipes

A fully deteriorated pipe is one that does not have enough strength to support the weight of the soil and other surface live loads. This type of pipe is characterized by extreme corrosion, missing sections, long cracks, and a severely deformed or distorted shape. When designing the SAPL for a completely deteriorated pipe, the designed SAPL should act as standalone pipe within the host pipe and must withstand all hydrostatic, soil, and live loads that may be present in the SAPL-soil system, with the necessary soil support (Najafi & Gokhale, 2022).

In some circumstances where there are isolated sections of missing or severely misaligned pipes, an alternative design approach was discussed by Najafi and Gokhale (2022). In these cases, it may be possible to perform localized repairs and restore the pipe considering it as a partially deteriorated condition. However, each situation should be evaluated by a qualified professional engineer.

2.6.3 Partially Deteriorated Condition for Pressure Pipes

Najafi and Gokhale (2022) discussed that the partially deteriorated pressure pipe may have minor corrosion, leaking joints, and/or small holes, but free from any longitudinal cracks. The

existing host pipe is assumed to be capable of withstanding the designated internal design pressure for the expected duration of its life. If the pressure pipe is partially deteriorated, it is assumed that the SAPL will fit tightly against the host pipe in all areas including bends or changes in diameter and use the strength of the existing pipe to bear the stresses. In this case, the designed SAPL thickness is not enough to resist pressures, but it can cover small holes or leaking joints. If the pressure pipe is assumed to be leaking, the designer must take into account external hydrostatic pressure to make sure that the SAPL's minimum designed thickness is enough to withstand these forces over the product's design life and not collapse.

2.6.4 Fully Deteriorated Condition for Pressure Pipes

Najafi and Gokhale (2022) described a pressure pipe as fully deteriorated when it has failed or does not have the strength to work at the intended working pressures. Additionally, a pipe can be considered fully deteriorated if it is predicted that it will not be able to handle the design pressures over its expected lifespan. A fully deteriorated pressure pipe is identified by a considerable decrease in wall thickness due to extreme corrosion, large holes, missing parts of the pipe, and leaking longitudinal cracks. Assuming a pipe is completely deteriorated, the SAPL is designed to be a single pipe that can handle all internal pressure without any bonding between the liner and the original pipe. Furthermore, the designer must be aware that a completely deteriorated SAPL pressure pipe must be able to withstand external hydrostatic pressure.

2.6.5 SAPL Application Design Standards

Polymeric SAPL is a new technology with limited design methodology or standards for its application. As a result, manufacturers and contractors are using design guides developed for the Cured-In-Place Pipe (CIPP), such as ASTM F1216, when applying SAPL. Recently, the American Water Works Association (AWWA) developed a Structural Classifications of Pressure Pipe

Linings, which categorizes structural lining systems into Classes I, II, III, and IV, and provides corresponding design equations. These design equations are derived from ASTM F1216, which itself is based on CIPP application. However, there is a lack of sufficient testing and experimental data to fully validate the suitability and accuracy of these equations for SAPL application.

As per AWWA Structural Classification of Lining Systems (2019), the SAPL lining system is categorized into Class I, II, III, and IV as shown in Table 2.3.

Table 2.3 AWWA Structural Classification of Lining Systems (2019)

System Class	Non Structural I	Semi-Structural		Structural IV
		II	III	
Corrosion Protection	Yes	Yes	Yes	Yes
Gap Spanning Capability	No	Yes	Yes	Yes
Inherent Ring Stiffness	No (Depends on Adhesion)	No (Depends on Adhesion)	Yes (Self Support)	Yes (Self Support)
Survives Burst failure of old pipe	No	No	No	Yes

Table 2.4 below shows a general and broad spectrum for the host pipe condition and the suggested liner Classification design as per AWWA structural Classification.

Table 2.4 Structural Classification and Rehabilitation Purposes (Kaur et al., 2023a)

Structural Classification	Pipe condition	Structural or Non-structural	Interactive to Host Pipe	Rehabilitation Purposes
Class I	Structurally good with minimum corrosion or new pipe	Non-structural	Satisfactorily bonded to host pipe, and transfers load to the host pipe	Corrosion protection, flow and water quality improvement
Class II	Deterioration due to corrosion holes, cracks or pits	Semi-structural	Completely bonded and interactive to the host pipe with minimum essential ring stiffness to intact the liner in	Corrosion holes or pits or minor pipe gaps at the joints

Structural Classification	Pipe condition	Structural or Non-structural	Interactive to Host Pipe	Rehabilitation Purposes
			place during vacuum loading	
Class III	Deterioration more than as mentioned in Class II, with major leaks, joints failures	Semi-structural	May or may not be completely bonded. Interactive to the host pipe with sufficient ring stiffness to prevent collapse due to negative pressure	Corrosion holes, cracks or joint gaps or major leaks. Protection against external buckling effect due to ground water table seeping through holes or cracks.
Class IV	Fully deteriorated with minimal or zero structural support by the host pipe	Fully structural	Non-bonded to the host pipe. Lining is completely independent within a host pipe, assuming no load is transferred to host pipe.	External buckling and longitudinal bending failures. Burst failure assuming that host pipe is completely gone. Long-term creep failure.

The AWWA (2019) structural Classification of the lining system and the design equation adopted in the AWWA standard are based on the formulas provided in ASTM F1216. ASTM F1216 is specifically designed for CIPP (Cured-in-Place Pipe) materials. The AWWA structural design equations are presented below.

2.6.5.1 Structural Design Class I

In this Classification system, **Class I** is non-structural, with zero intention to provide any structural support. Thus, the lining material will only provide corrosion protection to the host pipe, assuming the host pipe will take all the internal and external loads. The lining system is bonded to the host pipe and assumes that the lining should resist vacuum loading when experiencing negative pressure during service.

When designing the SAPL as Class I, the SAPL liner should satisfy Equation 2.1. The designed SAPL system should have enough strength to resist the negative pressure generated in the pipe during routine pipe maintenance and normal or cyclical events.

$$\sigma_{adh} \geq P_N \times N \quad \text{AWWA (2019) 2.1}$$

Where σ_{adh} = adhesion strength of the lining to host pipe substrate (psi)

P_N = negative pressure from groundwater and vacuum (psi)

$$= \frac{\gamma_w(H_w + \frac{D_M}{12})}{144} + P_v$$

P_v = vacuum pressure (psi)

γ_w = unit weight of water = 62.4 lb/ft³

H_w = height of groundwater above pipe, measured from crown/top of pipe (ft)

D_M = mean diameter of the host pipe (in.) = $D + \frac{(D_o - D)}{2}$

D = Inside diameter of host pipe (in.)

D_o = Outside diameter of host pipe (in.)

N = design factor of safety

2.6.5.2 Structural Design Class II

Class II is a semi-structural lining system. When considering the bond between the host pipe and lining system, Class II is bonded to the host pipe and has minimum essential ring stiffness. Thus, during negative pressure, the adhesive property of the lining system helps the liner not to collapse. The lining system in Class II is interactive with the host and transfers some of the load to the host pipe. Thus, Class II lining systems should be capable of resisting the internal pressure at the corrosion holes, cracks, or joint gaps of deteriorated pipes.

When designing the SAPL lining system as Class II, the designed liner thickness at the spanning across holes or cracks (presented or expected to be form due to external corrosion) should withstand internal hydrostatic pressure. Thus, the condition of the pipe for Class II design is

assumed as partially deteriorated. The design equation for Class II is given in Equation 2.2. This equation is derived on the assumption that lining system at the hole will act as a uniformly pressurized round flat plate with fixed edges (Najafi & Gokhale, 2022).

$$t = \frac{D}{\left[\left(\frac{D}{d} \right)^2 \left(\frac{5.33 \cdot \sigma_{FL}}{P_W \cdot N} \right) \right]^{\frac{1}{2}} + 1} \quad \text{AWWA (2019) 2.2}$$

Where t = minimum lining thickness to span holes in the existing pipe wall (in.)

d = diameter of hole in the existing pipe wall (in.)

σ_{FL} = long-term flexural strength of the lining system (psi)

P_W = internal working pressure (psi)

N = design factor of safety

The liner thickness determined by Equation 2.2 should be checked if the design condition of circular plate is valid (Najafi & Gokhale, 2022 and AWWA, 2019) by using Equation 2.3.

$$\frac{d}{D} \leq 1.83 \times \left(\frac{t}{D} \right)^{1/2} \quad \text{AWWA (2019) 2.3}$$

If this condition does not meet, then, the liner will experience ring tension or hoop stress.

Thus, the liner thickness needed to be designed as Class IV.

2.6.5.3 Structural Design Class III

Class III is also a semi-structural lining system. When considering the bond between the host pipe and lining system, Class III may or may not be bonded to the host pipe, assuming that the lining is keeping the hydrostatic integrity and has sufficient ring stiffness and self-support due to the liner adhesion when negative pressure is generated in the pipeline during service. When the lining system is interactive with the host and it transfers some of the load to the host pipe. Class III lining system should be capable of resisting the internal pressure at the corrosion holes, cracks,

or joint gaps of deteriorated pipes. In addition, Class III lining, compared to Class II, should be able to resist the external hydrostatic pressure caused by groundwater seeping through cracks or holes.

When designing the lining system as Class III, adhesion is not required for the ring stiffness of the installed SAPL inside the host pipe. However, the SAPL should be watertight to the host pipe. Adhesion is not required for the above ground applications where the liner might experience wide-ranging temperature changes. AWWA (2019) provides the design equation for Class III, further dividing into two scenarios: external buckling conditions experienced by pressure pipelines as short-term or long-term.

Short-term External Buckling

Short-term external buckling condition is applied when depressurizing the pipelines periodically due to routine maintenance or cyclic events. The loading condition in this design is analyzed as instantaneous or dynamic loads. Furthermore, the design equations are divided based on the host pipe condition as rigid or flexible. The equation for a rigid host for external buckling resistance is given in Equation 2.4.

$$t = \frac{D}{\left(\frac{2KE_s C}{(1-\nu^2)NP_N}\right)^{\frac{1}{3}} + 1} \quad \text{AWWA (2019) } 2.4$$

In the design consideration of the flexible host pipes, the live loads are also considered and assumed that 50% of the surface live loads are transferred to the lining system. Considering the live loads transferred to the host is a conservative design, where it implied that the host pipe is not taking all the loads and transferring to the lining system.

$$t = \frac{D}{\left(\frac{2KE_S C}{(1-\nu^2)N(P_N + \frac{W_L}{2})}\right)^{\frac{1}{3}} + 1} \quad \text{AWWA (2019) } 2.5$$

Where t = minimum lining thickness to resist short-term buckling pressures (in.)

K = enhancement factor; a minimum value of 7.0 is recommended (dimensionless)

C = ovality reduction factor (dimensionless)

$$= \left(\frac{1 - \frac{q}{100}}{\left[1 + \frac{q}{100}\right]^2}\right)^3$$

q = ovality of host pipe (%)

ν = Poisson's ratio of the lining system (dimensionless)

W_L = surface live load at pipe burial depth (psi)

E_S = short-term modulus of elasticity (psi)

N = design factor of safety

P_N = negative pressure from groundwater and vacuum (psi)

For pressure design, ovality is not considered, this parameter is only considered when pipe experience external pressure during service or maintenance. Ovality measurements can be assumed based on the host pipe condition in case of unavailable measurements.

Long-term External Buckling

Long-term external buckling condition is applied when depressurizing the pipelines for a longer period of time due to out of service, or the pipelines build is redundant. The equation for long-term external buckling resistance is given in Equation 2.6.

$$t = \frac{D}{\left(\frac{2KE_L C}{(1-\nu^2)NP_N}\right)^{\frac{1}{3}} + 1} \quad \text{AWWA (2019) } 2.6$$

Where t = minimum lining thickness to resist long-term buckling pressures (in.)

E_L = long-term modulus of elasticity (psi)

2.6.5.4 Structural Design Class IV

Class IV is defined as fully structural and designed as non-bonded to the host pipe; thus, there is no support from the host pipe, and the lining is performing independently within a host pipe. In Class IV, the lining should be independently tested for short-term and long-term hoop strength and should be able to resist the maximum allowable operating pressure on short-term or long-term bases. In addition, the lining system should be able to resist the external buckling and longitudinal bending stresses as resisted by the original host pipe.

When designing the SAPL lining system as a Class IV, the SAPL should not be required to have a reliable adhesion to the host pipe to develop the ring stiffness. However, the installed SAPL should be water tight to the host pipe. The condition of the host pipe for Class IV design is assumed as fully deteriorated, and thus, there is no support from the host pipe. The design equation for Class IV is given in Equation 2.7. This equation is derived based on the Barlow's formula.

$$t = \frac{D}{\left(\frac{2\sigma_{THL}}{PN}\right) + 1} \quad 2.7$$

Where D = inside diameter of host pipe, i.e., outer diameter of bare liner pipe (in.)

σ_{THL} = long-term tensile strength of the lining system (psi)

P = internal working pressure (psi)

N = design factor of safety

t = minimum recommended lining thickness at maximum allowable operating pressure (MAOP) (in.)

The essential characteristics of designing the SAPL for pressure pipe include operating pressure, test pressure, surge pressure, and water hammer pressure which can be much higher than operating or test pressures. It is very important to carefully identify the host pipe condition, such as partially deteriorated or fully deteriorated, before designing the appropriate SAPL design thickness. The existing pipe condition can be changed from partially deteriorated to fully deteriorated after thoroughly cleaning of the pipe (Najafi & Gokhale, 2022). Therefore, all conditions must be carefully analyzed and considered for the SAPL application.

2.7 Hydraulic Design Consideration of SAPL Renewal Method

2.7.1 Gravity Flow Design by Manning’s Equation

SAPL installation provides a smooth and continuous surface to the existing pipe, which reduces the friction to the flow and typically improves the flow characteristics. Manning’s equation used to determine the flow rates in gravity and open channel conditions is given in Equation 2.8 (Najafi & Gokhale, 2022).

$$Q = \frac{1.486AR^{2/3}S^{1/2}}{n} \quad 2.8$$

For a circular pipe with full flow conditions, the modified Manning’s equation as given in Equation 2.9 (Najafi & Gokhale, 2022).

$$Q = \frac{0.463D^{8/3}S^{1/2}}{n} \quad 2.9$$

Where Q = flow rate, cfs

n = Manning’s coefficient of roughness, dimensionless (interior pipe roughness, depends upon pipe material/condition)

R = A/P = hydraulic radius, ft

A = flow area, ft²

P = wetted perimeter of the flow, ft

D = Pipe internal diameter, ft

S = h/L, slope of the grade line, generally expressed in percentage (dimensionless)

h = vertical drop (ft),

L = horizontal distance over which vertical drop occurs (ft)

To compare the flow capacity between existing pipe and SAPL lined pipe, the simplified Manning's Equation 2.10 can be used for full flowing circular pipes (Najafi & Gokhale, 2022).

$$\begin{aligned} \% \text{ Flow Capacity} &= \frac{Q_{\text{SAPL Lined Pipe}}}{Q_{\text{Existing pipe}}} \times 100 && 2.10 \\ &= \frac{n_{\text{SAPL material}}}{n_{\text{existing Pipe}}} \left(\frac{D_{\text{SAPL Lined Pipe}}}{D_{\text{Existing Pipe}}} \right)^{8/3} \times 100 \end{aligned}$$

2.7.2 Pressure Flow Design by Hazen-Williams Equation

The Hazen-Williams equation is commonly used for determining the flow rate of pressure pipes. The application of SAPL as a corrosion protection or to the corroded host pipe can provide a smooth surface to the host pipe, and subsequently, the application can improve the flow capacity. The Hazen-Williams equation is given in Equation 2.11 (Najafi & Gokhale, 2022).

$$Q = 1.318 C \times R^{0.63} \times S^{0.54} \times A \quad 2.11$$

Where Q = flow rate, cfs

C= Hazen-Williams Coefficient, dimensionless (interior pipe roughness, depends upon pipe material/condition)

R = A/P = hydraulic radius, ft

A = flow area, ft²

P = wetted perimeter of the flow, ft

$S = h/L$, slope of the grade line, generally expressed in percentage (dimensionless)

h = vertical drop

L = horizontal distance over which vertical drop occurs

To compare the flow capacity between existing pipe and SAPL lined pipe, the simplified Hazen-Williams Equation 2.12 can be used (Najafi & Gokhale, 2022).

$$\begin{aligned} \% \text{ Flow Capacity} &= \frac{Q_{\text{SAPL Lined Pipe}}}{Q_{\text{Existing pipe}}} \times 100 \\ &= \frac{C_{\text{SAPL material}}}{C_{\text{existing Pipe}}} \left(\frac{D_{\text{SAPL Lined Pipe}}}{D_{\text{Existing Pipe}}} \right)^{8/3} \times 100 \end{aligned} \quad 2.12$$

There are some limitations to using the Hazen-Williams equation for hydraulic flow design analysis. The equation is more suitable for water pipes and irrigation systems, where the pressure loss due to friction is moderate, i.e., the pressure in the pipeline is not as high as of industrial high-pressure pipelines. In addition, the equation does not consider the viscosity of water that depends upon temperature.

2.7.3 Pressure Flow Design by Darcy-Weisbach Equation

The Darcy–Weisbach equation is an empirical formula that relates head loss, or pressure loss, caused by friction along a certain length of the pipe to the average speed of fluid flow. Moody’s chart provides a graphical representation and relates the friction factor calculated using the Darcy-Weisbach equation, the Reynolds number, and relative roughness calculated using the Colebrook-White equation. Having the known roughness value of the pipe material and the calculated Reynold’s number at a given flow rate, the Darcy-Weisbach friction factor can be calculated by using the Colebrook-White equation (Colebrook, 1939) as given in Equation 2.13. The friction factor calculated can be used to calculate the head loss by using the Darcy-Weisbach equation given in Equation 2.15.

Colebrook-White Equation

$$\frac{1}{\sqrt{f}} = -2 \log \left(\frac{\epsilon}{3.7D} + \frac{2.51}{Re\sqrt{f}} \right) \quad 2.13$$

$$\text{Reynolds number (Re) for turbulent flow, } Re = \frac{VD}{\nu} \quad 2.14$$

$$\text{Darcy – Weisbach friction factor, } f = h_L \frac{D}{L} \frac{2g}{V^2} \quad 2.15$$

Where, h_L is the head loss between two points at distance, L (ft)

L is the length of test section between two points of pressure measurement (ft.)

Q is flow rate (ft³/s)

A is pipe cross-sectional area (ft²)

V is the fluid mean velocity (ft/s)

D is the pipe diameter (ft)

ν is the kinematic viscosity of water (ft²/s)

(Note: The kinematic viscosity (ν) changes with the observed water temperature during each test run).

g is the gravitational acceleration (32.174 ft/s²)

f is the friction factor

By using the Darcy-Weisbach equation, the head loss can be compared between the host pipe and the SAPL lined pipe at any flow rate to determine the improvement in head loss as given in Equation 2.16. In Equation 2.16, the percentage head loss calculated will be at any given flow rate.

$$\% \text{ Head Loss} = \frac{h_{L \text{ SAPL Lined Pipe}}}{h_{L \text{ Existing pipe}}} \times 100 \quad 2.16$$

Thus, after discussing the structural and hydraulic design considerations in Sections 2.6 and 2.7, it is concluded that currently, the researchers and industry users are utilizing both ASTM F1216 and AWWA (2019) guidelines for the structural design of SAPL in pressure pipes. Hazen-William’s equation is useful for the hydraulic flow analysis for the SAPL lined pipe from low to medium pressure range. However, the Darcy-Weisbach equation is useful for the hydraulic flow analysis of SAPL lined pipe for high pressure applications.

There are several short-term and long-term full-scale laboratory testing methods to test and evaluate the structural design capabilities of SAPL for pressure pipes application as listed in Table 2.5. These testing methods are designed based on the host pipe conditions.

Table 2.5 Recommended Tests to Evaluate SAPL Application in Pressure Pipes

Test Method	Significance
Short-Term Testing	
Hole Spanning Internal Hydrostatic Pressure	Determine hole spanning capacity of liner in pressure application.
Pressure Integrity Test	Determine the burst pressure of liner pipe samples. Useful in calculating the short-term hoop strength of liner material.
Vacuum Pressure Test	Determine liner resistance and adhesion strength to negative pressure and maintain the liner integrity to host pipe in case of negative pressure.
Hydraulic Flow Test	Evaluate the hydraulic flow characteristics of the liner material in comparison with the host pipe without liner, considering diameter reduction and surface smoothness under high flow.
External Hydrostatic Pressure	Determine liner resistance to external hydrostatic pressure.
Long-Term Testing	
Fatigue Full-scale Test	Determine if liner can withstand cyclic loads that are 1.5 or 2 times higher than its pressure Class for two million or more cycles and to predict design service life.
Hole Spanning Internal Hydrostatic Pressure	Determine resistance of liner for long-term hole spanning.
Pipe Burst- Hydrostatic Design Basis (HDB) (ASTM D2837)	Determine effects of temperature and pressure on the life span of liner material and long-term hoop tensile strength.

Test Method	Significance
Fatigue Full-scale Laboratory Test	Determine if liner can withstand cyclic loads that are 1.5 or 2 times higher than its pressure Class for two million or more cycles and predict design service life.

For the structural evaluation of polymeric SAPL, the short-term tests mentioned above were conducted in this study except the external hydrostatic pressure test. The long-term tests were out of scope and were not included in the study. These selected tests in this study provided the information on the structural capabilities of the polymeric SAPL when designed based on the host pipe conditions. These tests provided information both for the semi-structural and fully structural applications of the SAPL in pressure pipes. In addition, in the deteriorate condition of pipes, the water quality problems could be an issue due to high deposits of pipe internal tubercules. This can also impact the flow capacity of the pipe. Therefore, the hydraulic flow test will determine the flow characteristics of the liner material. These tests are described in the following chapters. In addition to testing methods, the SAPL installed must satisfied the project and site conditions.

2.8 Research Studies on the Application of SAPL as a Renewal Method

2.8.1 Structural Analysis of SAPL lining system

SAPL application for both gravity and pressure is continuously studied by various researchers all over the world. These research studies evaluate the SAPL technologies by implementing numerous test methodologies, and valuable results have been observed for implementing this technology for renewing the old and deteriorated pipeline and underground infrastructure. For this dissertation, a literature review was performed on the application of SAPL in gravity and pressure pipes and represented in the following sections.

2.8.1.1 Structural Analysis of SAPL in Gravity Pipes

Many researchers are working on testing and evaluating the use of SAPL as a pipe renewal and rehabilitation method. Darabnoush Tehrani (2020) worked on the development of a structural design methodology for cementitious SAPL in gravity stormwater conveyance conduits. In this study, Darabnoush Tehrani (2020) investigated the structural capacity of cementitious SAPL to renew deteriorated arch and circular corrugated metal pipe (CMP) culverts. The researcher developed a full-scale soil box testing to test the structural capability of three circular (60 in. diameter) and three arch pipes (span 71 in. and rise 47 in.) with and without cementitious liner. In addition, in this study, three control tests on the bare pipes were conducted. The feasibility of design equations for application to fully deteriorated culverts was investigated.

Darabnoush Tehrani (2020) concluded that the renewed pipe was able to withstand the equivalent AASHTO H20 service truck load. However, the cementitious SAPL's structural integrity was dependent on the host pipe. Thus, the cementitious liners are not fully structural. The Watkins equation and partially and fully CIPP design equations were used to design the liner thickness for the CMPs. However, the result showed that none of these equations truly represented SAPL-CMP behavior under applied vertical load. In contrast, the modified AASHTO equation with two enhancement factors was developed, which complied with the laboratory test results. This study considered the effect of load on the SAPL thickness but did not include the depth of cover, different soil material, and different pipe diameters.

Similar to Darabnoush Tehrani's (2020) study, Kohankar Kouchesfehiani (2020) worked on the development of a structural design methodology for polymeric SAPL. In this study, the structural capacity of the fully deteriorated invert of large circular and arch CMPs renewed with polymeric SAPL was investigated. A full-scale soil box testing on three circular pipes (60 in.

diameter) and three arch pipes (span 71 in. and rise 47 in.), as well as three control tests on bare pipe samples were performed. The structural capacity of these pipes was tested with and without polymeric liner. The comparison was made for the load-carrying capacity of circular and arch pipes.

Kohankar Kouchesfehni (2020) applied the ASTM F1216 CIPP design equations applied to the SAPL polymeric design. As a result, the CIPP design equation was modified with an enhancement factor of 2.738, which can be used for the polymeric liner design for fully deteriorated culverts. In addition, it was concluded that the adapted AWWA C950 design equation is applicable for polymeric SAPLs, but the moment of inertia in this equation is required to be calculated depending on the corrugations of CMP. The study showed that the polymeric SAPL is fully structural in the renewal process.

2.8.1.2 Structural Analysis of SAPL for Hydrostatic Pressure

Awe (2017) investigated the lining material of polyurea and epoxy polyurethane as non-structural and semi-structural systems to renew portable water mains in the field. The design specifications of the pipe linings were verified in the field. A series of experimental tests, such as pipe surface preparation, bond strength, thickness, material properties, chemical resistance, and hole spanning capabilities, were performed in this study. It was found that the liner did not have enough flexibility, resulting in the formation of cracks shortly after liner installation. Therefore, the liner could not withstand the occasional pressure surges in pressure pipes. The adhesion of the liner to the host pipe was minimal, and gaps were visible between the host and liner materials. The experimental results were used to develop the performance quality control and assurance requirements for applying SAPL. The limitations of this study include that only preliminary tests were conducted, such as examining material properties, CCTV liner thickness, performing pull-

out tests, and conducting manual inspections of the surface preparation before and after installation. No full-scale laboratory testing was conducted to determine the structural Classification of the liner according to AWWA standards.

Harries and Sweriduk (2013) performed the hydrostatic pressure tests on Spray-Applied Epoxy Lining System. The experimental setup was designed to evaluate the ability of spray-applied epoxy liner to resist internal hydrostatic pressure, as shown in Figure 2.4. The experimental program replicated the ‘blow out’ of any enclosed structure under hydrostatic pressure. Defects ranging from 0.5 to 6 inches were created in the concrete structure, and then, these defects were lined with an epoxy liner. Hydrostatic pressure was applied to the test setup and the pressure values resisted by the liner were determined.

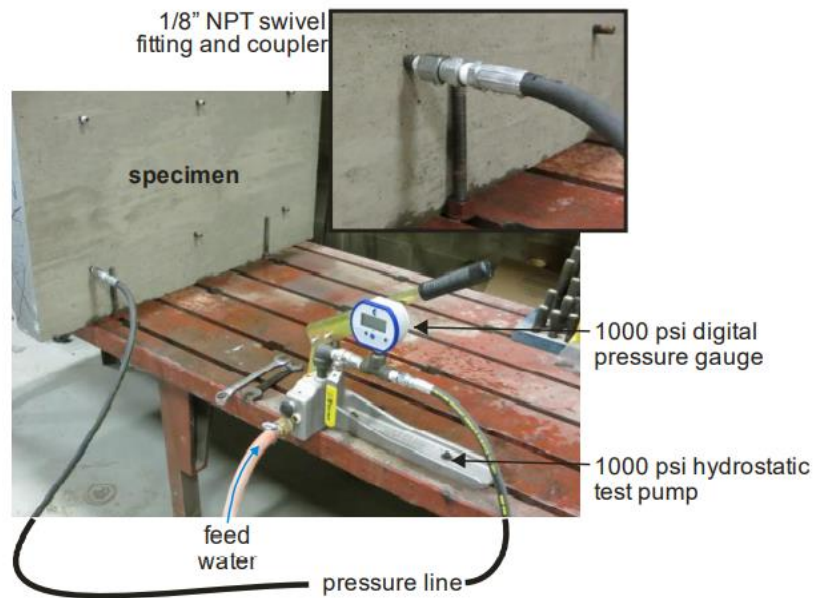


Figure 2.4 Hydrostatic Test Apparatus (Harries and Sweriduk, 2013)

The pressure resistance and the epoxy liner thickness were compared for different specimens. The average ultimate capacity of all the specimens exceeds 400 psi. The failure modes were observed for the liner system applied at the defects. However, the experiment was performed

on the concrete substrate and did not perform on other substrates which are commonly used as pipe materials. In addition, the test was formed on the rectangular structure formed with concrete slabs; thus, it did not simulate the actual pipe conditions, considering hoops and axial stresses.

Costa Mattos et al. (2012) also performed research on hydrostatic burst test on water pipelines similar to the research work done by Harries and Sweriduk (2013), but this study also included the long-term hydrostatic test. The study evaluated the strength of epoxy lining for repairing the corrosion damaged water pipelines (approx. 3.5 in. diameter) that were used in offshore oil and gas platforms. Burst tests and long-term hydrostatic tests were performed at constant pressure levels and at temperature between 175 °F and 195 °F. In these tests, the structural integrity of the epoxy lined pipelines was assessed. An average burst pressure of 3600 psi was applied to the test setup, whereas 1500 psi constant internal pressure was applied in a long-term test at 175 °F. A system failure was observed at a peak pressure of 2,490 psi after 6 days. Figure 2.5 shows the corrosion damaged pipes repaired with epoxy.



Figure 2.5 Corrosion Damaged Pipes Repaired with Epoxy
(Costa Mattos et al., 2012)

Costa Mattos et al. (2012) concluded that the burst pressure of the liner can be correlated with the ultimate tensile stress obtained from coupon tensile test. The prediction of burst pressure for samples using the developed elastic-plastic model was in good agreement with the experimental results. The model will be helpful in determining the burst pressure values by using the tensile test values instead of investing in expensive full-scale burst tests. One of the limitations of this study was that it only considered small diameter pipes, so it is difficult to accept the developed model for large diameter pipes.

Moore (2021) performed a study on polymeric liners installed within pressure pipes subjected to axial extension at the joints or ring fractures, the developed stresses at these joints were quantified. A numerical analysis was conducted to derive the stresses at the gaps due to axial extension. Finite element analysis was also used to calculate how axial stress in the liner develops as a gap opens up between pipe segments. It was concluded from the numerical analysis that the maximum axial liner stress depends on the gap that opens across the joint, liner modulus, internal fluid pressure, and coefficient of friction between the liner and host pipe. However, it is inversely proportional to liner thickness.

Fu et al. (2022) conducted research work on polymeric lined cast iron pipes with circumferential defects to numerically analyze the mechanical performance of polymer under internal hydrostatic pressure and ground movements. The research focused on designing gap spanning equations for thermosetting polymeric lined pipes. In this study, three failure modes were studied with numerical models created by FEM: 1) lining through existing gaps, 2) formation of gaps in the pressurized piped when subjected to axial movements, and 3) ring fracture in the pressurized pipes under bending. Three failure modes are illustrated in Figure 2.6. The equations derived for these three failure modes were based on the numerical results using non-linear

regression. Different pipe properties, liner properties, loading conditions, and interface properties were considered while developing the equations. This study was based on numerical analysis, in which the available models and results from the literature were used. The study did not perform the experimental data for validating the developed models.

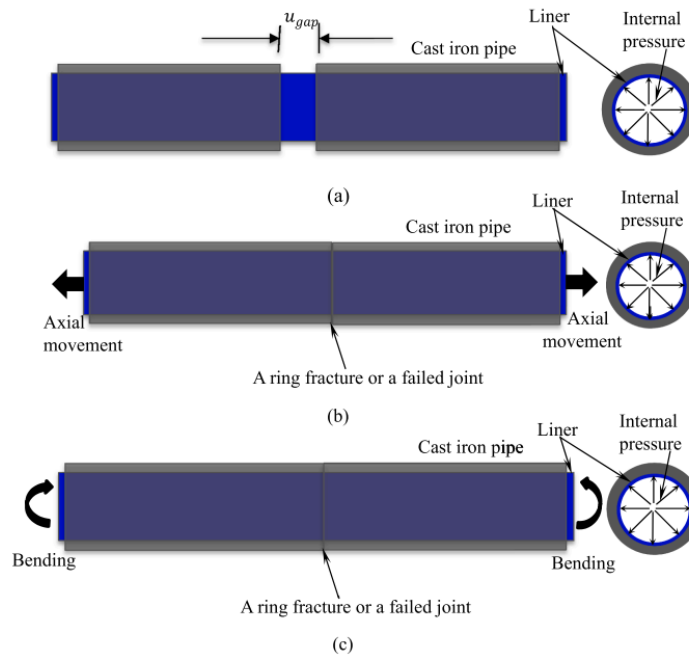


Figure 2.6 Pressurized Cast Iron Pipes Lined with Polymeric Liners
(Adapted from Fu et al. 2022)

Ha et al. (2015) studied the structural behavior and performance of a fast-setting polyurea–urethane (PUU) lining to rehabilitate water pipes. To test the structural properties of the liner, a sequence of experimental tests was carried out to evaluate: (1) bond strength; (2) hole spanning capability; (3) gap spanning capability; (4) angular displacement ability; (5) transverse shear resistance; and (6) fatigue cyclic loading resistance. The first test performed was pull-off bond tests to determine the bond characteristics of the lining system with the steel substrate prepared by three methods, and the corresponding results were: 1) dried surface with shot-blasting resulted in a bond strength of 764.35 psi (5.27 MPa), 2) dried surface treated with sandblasting yielded a bond

strength of 646.868 psi (4.46 MPa), and 3) dried surface treated with the grinding method exhibited a bond strength of 781.753 psi (5.39 MPa).

The second test performed was the hole spanning test in which a pipe sample of 5.9 in. (150 mm) diameter, 39.37 in. (1000 mm) long, with a hole of 0.197 in. (5 mm), was used. The pipe sample with a hole lined with PUU was able to withstand water pressure of 1595.415 psi (11 Mpa). However, in this study, only one hole size was tested in the hole spanning testing; thus, the liner material should be tested against different sizes of the holes. Third test conducted was the gap spanning test in which two pipe samples of 5.9 in. (150mm) diameter and 19.685 in. (500 mm) length was set up with a gap of 0.433 in. (11 mm) before lining them. The gap spanning samples failed due to a sudden blowout, and the data was not recorded, and this failure may be due to the stress concentration in the lining system exposed at the gap spanning part.

The fourth test performed on PUU by Ha et al. (2015) was angular displacement and transverse shear tests to measure the performance of the lining system under bending and shear. Two pipes of 5.90 in. (150 mm) in diameter and 39.37 in. (1000 mm) in length with a gap of 0.433 in. (11 mm) between them were sprayed with 0.1181 in. (3 mm) thickness of PUU. During the test, the material experienced a failure load of 971.17 lbs. (4.32 kN). The average displacement until peel-off failure occurred was measured at 2.327 in. (59.11 mm), and this failure was observed to happen at an angle of 6.74°. In the transverse shear deformation test, two pipe samples 5.905 in. (150 mm) diameter x 19.685 in. (500 mm)) was laterally placed, and lining material was applied to them. A pressure of 2.32 psi (0.016 MPa) was applied to the test assembly with no shear deformation. A lateral displacement was subsequently applied to the samples until the displacement reached 1.496 in. (38 mm), which corresponds to 25% of the pipe diameter. In the transverse shear test, no water leakage or peel-off failure of lining at the joint was observed.

The fifth test conducted by Ha et al. (2015) was the fatigue test to determine the lining capacity under cyclic loading. In this test, a fatigue resistance was tested for 100,000 cycles at 1 Hz level. The displacement control of 0.001456 in./s (0.037 mm/s) was used until a maximum displacement of 0.240 in. (6.10 mm) reached. The maximum displacement of 0.240 in. (6.10 mm) was then decreased at a rate of 0.01456 in./s (0.37mm/s) until it reached zero. The initial load for the first cycle was 517.06 lbs. (2.3 kN), which gradually decreased to 337.213 lbs. (1.5 kN) over the course of 100,000 cycles. No water leakage or failure of the lining system was observed in the fatigue testing.

2.8.1.3 Structural Analysis of SAPL Lining for External Buckling

Li et al. (2018) performed a research study on the elastic buckling behavior of thin-walled polyhedral pipe liners, which were close-fit in a circular pipe under uniform external pressure. This work determined the performance of a thin-walled polyhedral polymeric liner for the interior rehabilitation of a damaged/cracked pipe. The pipe's liner was externally confined and subjected to the external hydrostatic pressure of water. The critical buckling pressure was derived analytically. Additionally, the post-buckling behavior and the stability of the liner under severe deformation were determined three-dimensionally using the FEM model. The analytically calculated critical buckling pressure values were verified with numerical values obtained from FEM. In this study, the test was performed on polymeric liner, but the elastoplastic behavior and time-dependent property of polymers were neglected in the FEM.

Another study was performed by Rueda et al. (2016) on the buckling collapse of HDPE liners which includes both experimental and Finite Element Modelling (FEM). This study was focused on the oil and gas pipelines. The objective of the study was to develop a short-term thermoplastic model to improve the design of high-density polyethylene (HDPE) liner when

subjected to external pressure. When there is a sudden loss of internal pressure, the liner can collapse because of the external hydrostatic pressure build-up due to confined gases in the annular region between the host pipe and the liner. This collapse generally occurs when the liner design thickness and mechanical properties are insufficient to resist this external hydrostatic pressure. The external hydrostatic pressure generates a stress state in the liner material and causes radial buckling failure.

A test setup was developed by Rueda et al. (2016) to perform the short-term physical collapse of HDPE liners to emulate in-service behavior under controlled conditions. Temperature conditions ranging from 0 to 60 °C were considered to evaluate the behavior of the liner and its response to temperature effects. The 3D FEM simulations of collapse buckling tests were conducted, and these models were validated against the experimental data. In addition, a three Network Model (TNM) was developed to determine the response of HDPE liner at different loading rates. A performance model was assessed by comparing experimental data and predicted failure pressure of the liner by FEM. It was found that the material strain rate dependency significantly impacted collapse pressure. An equation was proposed to predict the critical collapse pressure considering the effect of temperature, strain rate, and aspect ratio.

Another study was performed by Zhao (1999) on the creep buckling behavior of CIPP liners under external pressure. The study investigated the long-term structural behavior of CIPP liners under external hydrostatic pressure. The FEM analysis with a focus on the structural behavior and mechanism of buckling and the influence of inelastic material (yield strength and creep rates) properties were analyzed. Also, the geometric parameters such as the dimension ratio of the liner, the gap between the liner and the host pipe, and the ovality of the host pipe were considered to determine the liner's buckling resistance. The numerical simulations were verified

with experimental data and then, used to derive the CIPP liner design methodology. It was determined that the buckling resistance of the CIPP liner depends on the geometric parameters. In addition, a 50-year design life was predicted using the FEM.

2.8.2 Hydraulic Flow Analysis of Pipe Linings

In the process of rehabilitating the old and deteriorated pipes with SAPL, there is a potential reduction in the pipe's internal diameter. It is essential to conduct a study to assess the impact of this diameter reduction on the flow capacity of the pipes. Guo et al. 2019 investigated the equivalent sand grain roughness for ductile iron pipes coated with different anti-corrosion materials. Fluid flow experiments were performed on three different pipes that were coated with epoxy, cement mortar, and polyurethane. The experimental data and the Moody chart were employed to determine the friction factor and head loss. The pipe samples used in this study had a diameter of 0.302 meters and a length of 6 meters. The obtained roughness values were calibrated by considering the uncertainties in the experimental data. In this experiment, only one diameter pipe size was considered. Therefore, additional data points are required to comprehensively understand the impact of the liner friction factor and the reduction in the internal diameter of the pipe.

Barber et al. (2005) investigated the flow characteristics of a new steel pipe before and after the installation of a high-density polyethylene (HDPE) liner through sliplining. They conducted a flow test on both the unlined steel pipe and the steel pipe with the HDPE liner. The friction factor was compared between the lined and unlined pipes, and the improvement in flow performance of the lined pipe was evaluated. Installation of the 6.35 mm (1/4 in.) thick liner in the 152.4 mm (6 in.) pipe reduced its cross-sectional flow area by 16% and would decrease the flow by 20% under the same head loss. The results concluded that surface roughness coefficient values

obtained in the new and lined pipe are similar. It was concluded that a deteriorated pipe with significant roughness could be restored to its original condition using close-fit sliplining. The test was limited to only one pipe diameter and one type of liner material.

Adams and Grant (2008) performed a study to develop an algorithm to determine the sand grain roughness of the pipe by using the optical profilometer data because performing a full-scale flow test is cost-prohibitive. A simple algorithm with Matlab was developed, which can be used to convert surface roughness parameters measured with an optical profilometer to equivalent sand-grain roughness. Experimental data were also used to validate this algorithm. In this experiment, different pipe diameters were tested. The results indicated that every surface roughness value converted to equivalent sand-grain roughness by using the algorithm, showed improved agreement with fluid flow experiments. Thus, conversion factors were established to convert the optical profilometer data to equivalent sand-grain roughness. One limitation of this study was the lack of sufficient validation provided for the developed algorithm.

Cetinel (2012) conducted a study to develop an artificial neural network (ANN) based prediction model to determine the friction properties of a thermal coating on carbon steel pipe. First, the experiment was performed using PLINT TE88 multi-station friction and wear test machine at room temperature to determine the wear loss values. Different loads and environmental conditions were used in this experiment. Based on this experiment data, an ANN model was calibrated to determine the wear loss and friction coefficient values. This study predicted the variation of wear loss and friction as a function of time. The prediction of friction coefficient with the ANN model reduced the experimental work.

EPA (2012) evaluated the performance of CIPP rehabilitated water main in Cleveland, Ohio. This study provided the overall information on the CIPP technology, the site selection and

preparation for the CIPP installation, and post-demonstration field verification. They also conducted different technology performance tests during the study, such as tensile, flexural, hardness, negative pressure, and burst pressure testing. In addition, the study also examined the friction factor analysis after rehabilitating the water main line. The Hazen-Williams flow test was conducted to determine the friction factor analysis and evaluate the improvement in the flow. The average C-factor of the rehabilitated test pipe was 112.1, which was less than 120, however, the rehabilitation of the pipe was significantly greater than the pre-rehabilitation C-value of 78.5, resulting in an improvement of nearly 43%.

2.9 SAPL Application as an Effective Renewal Method

The pipes in the U.S. buried are 6 feet to 8 feet deep (WRF Report 4326, 2018). Considering the depth of the pipes, an open cut method would require heavy excavation to replace the old and deteriorated pipes. Using the SAPL renewal method can effectively reduce the excavation cost and hence it can be adopted as a cost-effective renewal method. SAPL renewal method presents a minimal social and environmental cost because it requires minimum surface and subsurface ground disturbance. Kohankar Kouchesfehni (2020) conducted research on the application of polymeric SAPL on culverts and drainage structures to evaluate the structural capacity of the polymeric liner as a fully structural component. Whereas Darabnoush Tehrani (2020) performed research on the application of cementitious liners on the culverts system to test its structural capabilities.

Awe (2017) investigated the lining system (polyurea and epoxy polyurethane) for non-structural and semi-structural to renew portable water mains in the field and then, verified the design specifications for the lining system. Harries and Sweriduk (2013) performed the hydrostatic pressure tests on Spray-Applied Epoxy Lining System and confirmed the pressure resistance of

the SAPL lined concrete specimen up to 400 psi. Costa Mattos et al. (2012) also performed research work on hydrostatic burst test on water pipelines, similar to the research work done by Harries and Sweriduk (2013), but Costa Mattos et al. (2012) study also included the long-term hydrostatic test. The epoxy lined pipes were able to withstand a pressure of 2,490 psi, and the system failed after 6 days.

Ha et al. (2015) studied the structural behavior and performance of a fast-setting polyurea–urethane (PUU) lining to rehabilitate water pipes. For this research, a comprehensive evaluation of SAPL was conducted to assess its various structural capabilities. These included the assessment of bond strength, hole and gap spanning capabilities, angular displacement ability, transverse shear resistance, and resistance to fatigue under cyclic loading. Li et al. (2018) performed a research study on the elastic buckling behavior of a thin-walled polyhedral pipe liners, which were installed close-fit in a circular pipe. The liner was tested under uniform external pressure to evaluate its buckling behavior, which is another important structural property to consider. Another study was performed by Rueda et al. (2016) on the buckling collapse of HDPE liners which includes both experimental and Finite Element Modelling (FEM). It was found that the material strain rate significantly impacted collapse pressure. Zhao (1999) investigated the long-term creep buckling behavior of the CIPP liners under external hydrostatic pressure.

Moore (2021) performed a study on polymeric liners installed in pressure pipes subjected to axial extension at the joints or ring fractures, and then, the developed stresses at these joints were quantified. Fu et al. (2022) conducted research to numerically analyze the mechanical performance of polymer lined cast iron pipes with circumferential defects under internal hydrostatic pressure and ground movements.

Barber et al. (2005) examined the flow conditions through a new steel pipe before and after sliplining with high-density polyethylene (HDPE) liner. Adams and Watson (2008) performed research to develop an algorithm to determine the sand grain roughness by using the optical profilometer data. Cetinel (2012) performed a study to develop an artificial neural network (ANN) prediction model to determine the friction properties of a thermal coated carbon steel pipe. EPA (2012) evaluated the C-value for the CIPP rehabilitated water main in Cleveland, Ohio, there was an improvement of the C-value by 43% compared to a deteriorated pipe.

The studies presented above provide evidence that the SAPL renewal method is a highly effective and efficient solution for rehabilitating old and deteriorated pipes. These studies demonstrate through various tests and their corresponding results that SAPL can serve as both a semi-structural and structural lining system. In addition to its effectiveness, SAPL is also cost-effective and offers a quick return to service time. Considering the associated social and environmental benefits, SAPL is one of the most prominent methods to solve the problem of aging and old underground infrastructure.

2.10 Chapter Summary

This chapter presented a comprehensive literature review on SAPL renewal research studies performed for different structural parameters. Various SAPL structural integrity aspects including, hole-spanning, gap spanning, external buckling pressure, internal pressure resistance, bond strength, angular displacement ability, transverse shear resistance, vacuum pressure, and fatigue cyclic loading resistance, etc. were discussed.

Many researchers suggested that analyzing the structural capabilities of SAPL liner material is important to accept its use in the renewal methods. Because of the absence of specifically designed specifications and standards for SAPL renewal methods, various

methodologies and analytical design equations which were originally developed for other purposes can potentially be implemented in the SAPL applications. However, there is limited experimental test data available to validate these adopted design equations. In addition, the number of research studies that have been conducted to confirm the accuracy of the design equations used is limited.

Furthermore, there is limited available data to evaluate the hydraulic properties of polymeric liners. Additionally, there is a lack of evidence to thoroughly measure the extent of improvement in hydraulic flow properties resulting from the use of liners to mitigate corrosion and defects in pressure pipes. Based on the findings and gaps identified in the literature review, test design methodologies were developed to perform the full-scale laboratory testing to evaluate and determine the structural and hydraulic properties of the liner.

Chapter 3 Structural Evaluation of Spray Applied Pipe Lining

3.1 Introduction

Chapter 2 indicated that there is lack of comprehensive study and experimental testing data available on development and evaluation of SAPL to confidentially implement as a renewal process in underground water and wastewater infrastructure. In addition, there is lack of available design standards and guidelines to adopt in the design application of SAPL. The equation which was developed for the other trenchless methods such as CIPP has been using in the SAPL application. However, these equations have not been adequately tested and analyzed with the experimental testing. This chapter presents the testing design methodologies to determine the structural properties and material properties of polymeric.

3.2 Testing Methodology

The testing methodology for this study is divided into three main categories such as structural properties, and material properties. Figure 3.1 shows the SAPL designed testing for this study.

As presented in Figure 3.1, for the material testing, three material tests were performed to determine the flexural, tensile and punch shear strength. These material properties were important to determine mechanical behavior of the material, and these properties were used in designing the liner thickness for the full-scale laboratory testing developed for determining the structural properties of the liner material. The test designed for the structural properties are short-term hole spanning internal hydrostatic pressure testing, which is evaluating the structural properties of the material as semi-structural and determining the hole-spanning capacity of the polymeric SAPL lined pipe with corrosion holes.

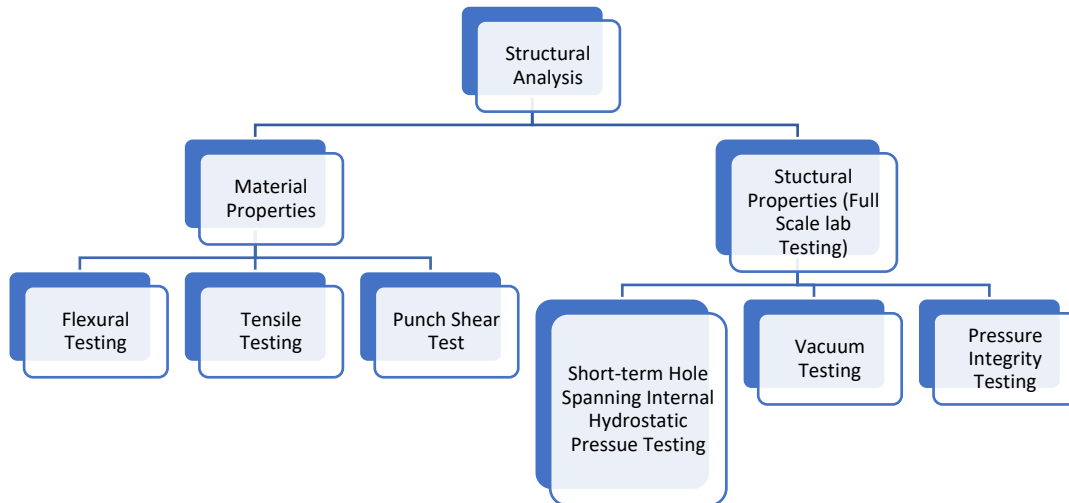


Figure 3.1 Structural Evaluation of SAPL

The second test designed was the vacuum pressure to determine the ring stiffness of the pipe, which is required for evaluating the SAPL material under vacuum loads. The third test designed was the pressure integrity test, which is designed to determine the fully structural strength of the liner.

3.3 Material Testing

Two types of polymeric material were tested for the SAPL application.

- 1) **Hybrid Polyurea:** It is a two component, 100% solid, and a specialized high performance polyurea coating which is developed to protect buried and exposed structures. This material has excellent adhesion to most substrates with and without primer.
- 2) **Pure Polyurea:** The liner material is a fast gel pure polyurea and suited best for metal, non-metal and concrete structures. This liner material exhibits excellent adhesion to the substrate with or without primer material.

3.3.1 Material Testing Hybrid Polyurea

3.3.1.1 Three Point Bending Test

The flexural strength is an essential property of the material, which determines the material's resistance to deformation under loads. Flexural strength is also known as bend strength. Therefore, the flexural strength is a stress in a material at yield point, i.e., the material bends but does not break under load. In addition, the flexural modulus measures material stiffness or rigidity. Thus, the material with higher flexural modulus is difficult to bend, and on the other side, the material with lower flexural modulus is easier to bend. Henceforth, when you increase the stress to the material, the change in the length, i.e., strain is less for the stiffer material. Since the polymer is a viscoelastic material, and to better understand the material properties of the polymer, flexural modulus is important to measure in addition to the flexural strength. Understanding these properties and its response under load is critical when liner is used in the pipe renewal.



Figure 3.2 Three-Point Flexural Bending Test

The three-point bending flexural test is conducted to investigate the flexural (bending) properties of the Polymeric SAPL according to the ASTM D790. Method A is used to perform the

testing. Figure 3.2 shows the MTS machine used to conduct the three-point bending test along with one of the specimens.

Five specimens are tested for bending strength. Sections for five samples are identical and as follows: width = 1.874 in. (47.6 mm), and thickness = 1.146 in. (29.1 mm). The specimens are subjected to a test speed of 0.454 in./min (11.53 mm /min), and the support span is 17.047 in. (433 mm). During the three-point bend test, a solid rectangular cross-section liner specimen acts as a simply supported beam, and a point load through the nose is applied to it at the midpoint of the span. The deflection of the specimen is measured until rupture happens at the outer surface or until a maximum strain of 5% is reached, whichever occurs first.

3.3.1.2 Tensile Test

The tensile test evaluates the strength of material in tension. When a pulling load is applied, the material elongates, and the elongation is directly proportional to load applied. Thus, the tensile strength is the maximum stress a material can handle before fracture. Tensile strength measures the material stiffness.

The tensile test was conducted to investigate the tensile performance and to determine the tensile properties of the Polymeric SAPL according to the ASTM D638. The test was performed in the displacement control mode. Figure 3.3 (left picture) shows the MTS machine used to conduct the tensile test on one of the specimens. Five dog bone specimens were tested for tensile strength. The specimen thickness and width were 0.118 in. (3.0 mm) and 0.512 in. (13.0) mm respectively. The specimen was placed and tightened in the grips of the testing machine. The specimens were subjected to a test speed of 0.197 in./min (5.0 mm /min), and were pulled against opposite end at this speed. As a result, tension was generated in the specimen. Failure occurred when the strain or elongation exceeded the material's limits. The tensile strength represents the maximum load a

material can experience under tension divided by the cross-sectional area. Figure 3.3 (right) represents the broken specimen due to tensile failure. The test were performed at different temperatures of 73° F, 120° F, 150° F, and 32° F.



Figure 3.3 Tensile Test (left) and Specimen Rupture (Right)

3.3.1.3 Punch Shear Test

Shear strength testing is used to determine the load at which a plastic will yield when sheared between two metal edges. This test method covered the procedure for determining the shear strength of polymeric material according to the ASTM D732-17. Six plastic specimens were tested for shear strength. All specimens were 2-inch squared plates and 0.50 in. thick, as shown in Figure 3.4 (left). Specimens were installed in the punch shear fixture as shown in Figure 3.4 (right).



Figure 3.4 Specimen before Testing (left)
Specimen Installed in Punch Shear Fixture (right)



Figure 3.5 Punch Shear Test

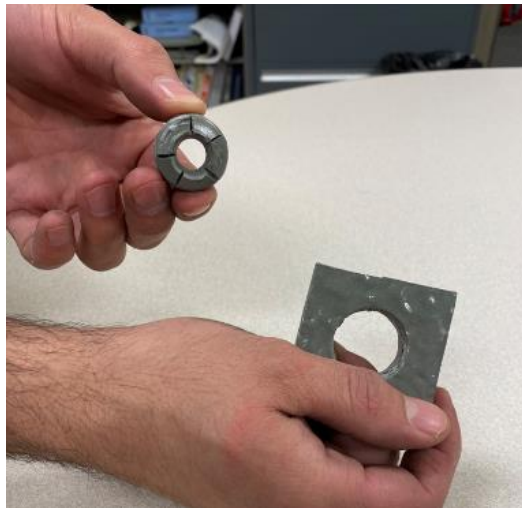


Figure 3.6. Specimen after Shear Failure

Figure 3.5 shows the MTS testing machine and the punch shear fixture that are used to conduct the Shear strength test as per the ASTM D732-17. The specimens were subjected to a test speed of 0.050 in./min. During the Shear strength test, the male punch is forced through the hole in the metal fixture causing shear along the edge of the hole. An MTS testing machine equipped with Data Acquisition (DAQ) system is used to provide the vertical load on the punch shear fixture

until shear failure of the specimen occurs. DAQ recorded the load vs displacement data at a periodic interval of 0.10 seconds. Figure 3.6 shows the specimen after the shear failure.

3.3.2 Material Testing Pure Polyurea

3.3.2.1 Tensile Test

A similar procedure as described in section 3.3.1.2 was applied to test the tensile strength of the pure polyurea material. This material was elastomeric in nature and was more flexible. Five dog bone specimens were tested for tensile strength. The specimen thickness and width were 0.071 in. (1.790 mm) and 0.242 in. (6.134 mm) respectively as per ASTM D638 Class IV. The specimen was placed and tightened in the grips of the testing machine. The specimens were subjected to a test speed of 0.197 in./min (5.0 mm /min), and were pulled against opposite end at this speed. DAQ recorded the load vs displacement data at a periodic interval of 0.10 seconds.



Figure 3.7 Tensile Test Pure Polyurea Material

3.4 Structural Evaluation of SAPL

The structural evaluation of the liner material was conducted in two categories: semi-structural and fully structural. For the semi-structural evaluation, pure polyurea material was utilized in the short-term hole spanning testing. Pure polyurea demonstrates excellent adhesive properties and can be employed as a rehabilitation material when the host pipe exhibits corrosion holes and cracks while still retaining some of its strength.

In contrast, for the fully structural evaluation, a hybrid polyurea liner material was employed. Hybrid polyurea is a more rigid material compared to pure polyurea. And it was selected for the pressure integrity test to assess the liner's capability to withstand and maintain structural integrity under pressure conditions when there is no support from the host pipe.

3.4.1 Short-term Hole Spanning Testing

The objective of the short-term hole spanning test was to evaluate the hole spanning capacity of SAPL lined pipes in industrial applications with pressures of up to 500 psi. Carbon steel pipe samples were lined with a pure polyurea polymeric liner, known for its elastomeric properties. The experimental testing consisted of three pipe samples with hole spanning sizes of 0.5, 1, and 2 in. These samples were subjected to internal hydrostatic pressure. The objectives of this testing were as follows:

1. Design the appropriate liner thickness needed to withstand internal pressures up to 500 psi during hole spanning.
2. Determine the effectiveness of the liner in renewing old pipelines with corrosion holes and cracks under high-pressure conditions.
3. Analyze the failure modes of the liner when subjected to hole spanning conditions.

3.4.1.1 Test Methodology

In this experimental setup, three carbon steel pipe samples of 30 in. diameter with a thickness of 0.375 in. and 3 ft long were tested. To simulate actual field conditions of corrosion holes, circular holes of ½, 1-, and 2-inch diameters were created, respectively, in three pipe samples at the center of the pipes using drilling or torching techniques. The pipe hole is as shown in Figure 3.8 (a), and each hole was grinded for smoothness. The 3-foot pipe samples (as shown in Figure 3.8 (a)) were connected to 6 ft long spigot end (as shown in Figure 3.8 (b)) on both sides and fabricating an overall length of the test setup as 15 ft long. The pipe samples and spigot ends were in conformance with all applicable American Water Works Association (AWWA) standards. The pipe material used to fabricate these pipes was AWWA C200 Grade 42 or higher. The thickness of the pipes was designed to resist 500 psi pressure. For welding the spigot ends to the dish heads, a high-quality weld with a pressure rating of up to 500 psi was used.

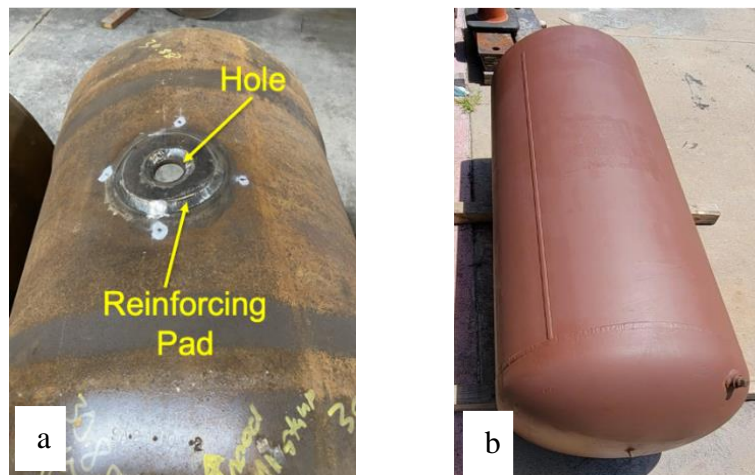


Figure 3.8 (a) Pipe Sample with Hole Spanning and (b) Spigot Ends with Dish Heads

The 3-ft test section with hole was solely lined with SAPL and connected to the spigot ends. The inside view of the test section with pure polyurea polymeric liner is shown in Figure 3.9.



Figure 3.9 Inside View of Test Section with Pure Polyurea Liner

The test section with different sized holes was changed in the 3 consecutive tests, and the two spigot ends were reused for each test. The certified high-quality arc welding was used to avoid any leakage and weld failure due to high pressure expected during the testing. Prior to welding, grinding was performed on both the spigot ends and the middle section to achieve a smooth surface. The grinding process for the spigot end is depicted in Figure 3.10.



Figure 3.10 Spigot End Grinding before Welding

The welding procedure involved approximately six passes to ensure a secure bond. Figures 3.11 (a) show the welding of the spigot end to the test section. Figure 3.11 (b) shows the welded test section with one of the spigot ends.

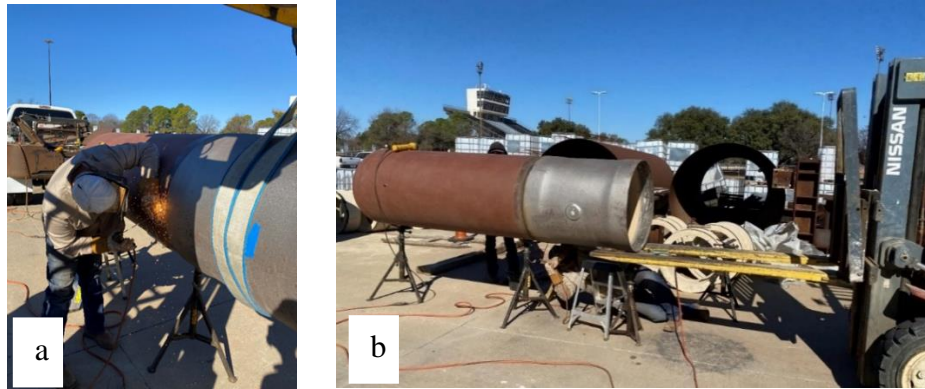


Figure 3.11 (a) Welding Spigot End to Test Section
(b) Welded Test Section to Spigot Ends

Figure 3.12 below shows the complete test setup of 15 ft long when both the spigot ends were successfully welded to the test section.



Figure 3.12 Spigot Ends Welded on Both Ends of the Test Section

The spigot end was equipped with dish heads that incorporated threaded coupling connections, facilitating the installation of water inlet and outlet connections, a transducer, and a pressure dial gauge.



Figure 3.13 (a) Pressure Transducer (b) Strain Gauge

As shown in Figure 3.13 (a), the Omega Engineering, model PX409-1.0KGI transducer was installed on the spigot end to accurately measure and monitor the pressure. The accuracy of the transducer is $\pm 0.08\%$, and the pressure range was from 0 to 600 psi. Its output is in the range of 4-20 mA and was connected to the Micro Measurement system 8000, a data acquisition (DAQ) system, for real-time monitoring and recording of pressure data in psi throughout the test.

Due to space constraints for installation on the 0.5-inch, the strain gauge was only installed on the liner exposed through the 1-inch and 2-inch diameter holes. The purpose of the strain gauges was to monitor the strain experienced by the liner material (exposed through hole) when subjected to internal hydraulic pressure. The strain gauge is represented in Figure 3.13 (b).



Figure 3.14 Air Release Valve

Figure 3.14 shows a 1-inch air release valve installed at the top of the spigot end to release any entrapped air before pressurizing the test section. The air release valve could handle the pressure of test setup up to 600 psi.

A Rice Hydro Inc hydrostatic pump, shown in Figure 3.15, was used to pressurize the test setup to a maximum pressure of 500 psi. The pump model was DPV-3B, a diesel-operated pump, and powered by the Briggs and Stratton Vanguard 200 engine. The DP-3 was a triple diaphragm pump. The pump outlet hose had a 0.5-inch quick connect coupling to provide an easy and quick connection to the test setup. The pressure regulator on the pump enabled adjustment of the pressure, with an operating range of up to 550 psi. A pressure dial gauge mounted on the pump continuously monitored the pressure output of the pump. The pump was connected to the test setup, incrementally pressurizing it in 50 psi increments until reaching a maximum pressure of 600 psi.



Figure 3.15 Hydrostatic Pressure Pump

3.4.1.2 Liner Thickness Design

The liner material is a fast gel pure polyurea and suited best for metal, non-metal and concrete structures. This liner material exhibits excellent adhesion to the substrate with or without primer material. The liner thicknesses for the pipe samples were designed as per Class II linings given by AWWA “Structural Classifications of Pressure Pipe Linings” (AWWA, 2019). In designing the lining system as per Class II, the lining shall adhere to the host with complete bonding and possess a characteristic of semi-structural integrity.

3.4.1.3 Liner Thickness Design AWWA Class II (Semi-Structural)

The minimum liner thickness required for hole spanning with 0.5, 1, and 2 in. to resist the internal pressure was designed with Equation 3.1 , but with modification, as given in Equation 3.2 (Kaur et al., 2023b). In Equation 3.2, the long-term tensile strength of the material was used instead of the long-term flexural strength.

Eq 1: AWWA Class II Structural Classification of Pressure Pipe Linings

$$t = \frac{D}{\left[\left(\frac{D}{d} \right)^2 \left(\frac{5.33 \cdot \sigma_{FAL}}{P_w \cdot N} \right) \right]^{1/2} + 1} \quad 3.1$$

Eq 2: Modified AWWA Class II Structural Classification of Pressure Pipe Linings

$$t = \frac{D}{\left[\left(\frac{D}{d} \right)^2 \left(\frac{5.33 \cdot \sigma_{THL}}{P_w \cdot N} \right) \right]^{1/2} + 1} \quad 3.2$$

Where: t = minimum lining thickness to span holes in the existing pipe wall (in.)

d = diameter of hole in the existing pipe wall (in.)

σ_{FAL} = long-term flexural strength of the lining system (psi)

σ_{THL} = long-term tensile strength of the lining system (psi)

P_w = internal working pressure (psi)

N = design factor of safety

In the design considerations, it was assumed that the lining system not only experienced transverse stress but also hoop stress. Thus, the long-term tensile strength of the material was considered instead of the long-term flexural strength of the lining system. This will also make the design more conservative.

The liner thickness determined from Equation 3.2 was also checked against the ring tension or hoop stress by using Equation 3.3 below. If Equation 3.3 did not satisfy the determined thickness by Equation 3.2, then the liner thickness needed to be designed as Class IV.

$$\frac{d}{D} \leq 1.83 \cdot \left(\frac{t}{D}\right)^{1/2} \quad 3.3$$

Thus, the liner thicknesses for hole sizes 0.5, 1, and 2 in. were determined by using Equation 3.2. The designed thicknesses were satisfied with Equation 3.3. The designed liner thicknesses for holes 0.5, 1, and 2 in. is given in Table 3.1.

Table 3.1 Designed Thickness of Elastomeric Polyurea SAPL

Pipe Sample #	d: Hole Diameter (in.)	D: Pipe Diameter (in.)	t: Considered Liner Thickness (in.)
1	0.5	30	0.25
2	1	30	0.50
3	2	30	0.75

As shown in Table 3.1, the diameter of the hole spanning impacts the liner thickness. The calculated SAPL liner thickness for pipe samples of 30 in. diameter with hole spanning 0.5, 1, and 2 in. to resist the desired internal pressure of 500 psi were 0.25, 0.50, and 0.75 in., respectively. The liner thickness calculated also considered that the liner is completely bonded to the host pipe.

3.4.1.4 Testing 0.5-inch Hole Spanning

The first pipe sample tested was with a 0.5-inch hole spanning. The liner thickness for the pipe sample was designed as per AWWA Class II, and the liner thickness calculated for the 0.5-inch hole spanning was 0.25-inch. The liner exposed through a 0.5-inch hole spanning is shown in Figure 3.16. Prior to the application of the liner, the pipe sample was abrasive blasted and primed with "Metal Prime" at a thickness of 4-5 mils. A pure polyurea liner was then sprayed onto the surface, achieving a thickness of 0.25 inches.



Figure 3.16 Pipe Sample with 0.5 in. Hole Spanning

The polymeric lined pipe sample was welded to the spigot at both ends, creating a test setup with a total length of 15 feet, as described in the test methodology section. This 15-foot test setup was then placed inside a 72-inch diameter carbon steel pipe and securely fastened to steel hooks available within the pipe. Figures 3.17 (a) and 3.17 (b) illustrate this setup. The purpose of the strapping was to provide an added safety measure in case of liner failure and to prevent any movement of the test setup during the application of high pressure, up to 500 psi. The test setup was connected to the pump at the water inlet connection provided at the spigot end, as shown in Figure 3.18.

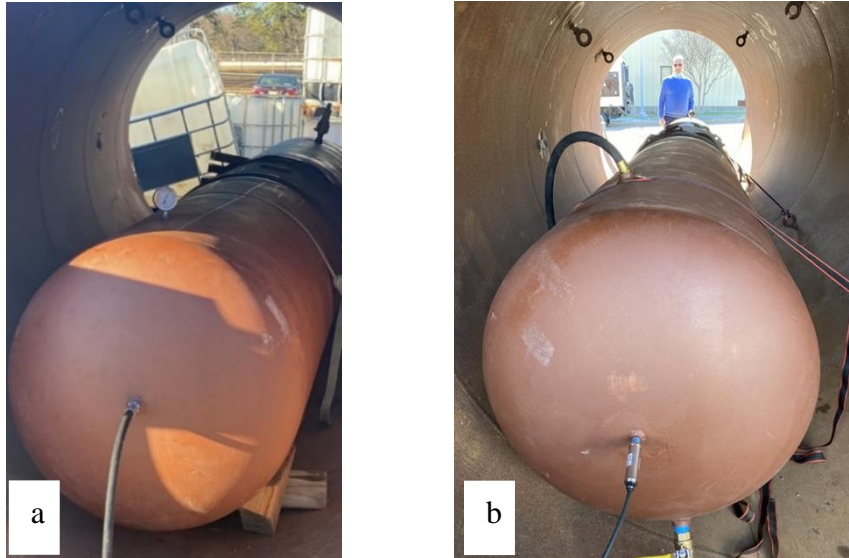


Figure 3.17 (a) Pump Hose Connection to Test Setup (b) Transducer Connected to Test Setup



Figure 3.18 Complete Test Setup

The pressure in the test setup was gradually increased at 50 psi increments until it reached 500 psi. The pressure was monitored by two pressure monitoring devices, such as a pressure dial gauge mounted on the spigot end (as shown in Figure 3.17 (a)) and a pressure transducer installed

on the dish head (as shown in Figure 3.17 (b)). The air release valve was installed at the highest point of the test setup to remove any entrapped air before pressuring the test setup.

Figure 3.18 shows the complete assembly of the test setup. During the test procedure, four test runs were performed. The weather and environmental conditions were recorded on the test day, as shown in Table 3.2.

Table 3.2 Test Data 0.5-inch Hole Spanning

Description	Test Conditions
Test sample	0.5 in. hole spanning
Number of trials	Four
Ambient temperature during the test run	47° F
Water temperature	42° F
Wind speed	6 mph
Maximum pressure holds by the test sample	500 psi
Duration of pressure hold by the test setup	2 hours at 500 psi

Table 3.2 shows that the temperature recorded on the test day was 47° F, and the wind speed was six mph. The water temperature during the test was noted at 42° F. Prior to pressurizing the test setup at a desired pressure of 500 psi, the setup was tested for any leak detection. The test setup was pressurized to 100 psi and held for 15 minutes to check any water leakage from weld joints or the coupling joints of the instrumentation provided. In addition, the proper functioning of the instrumentation was checked during this leak detection test.

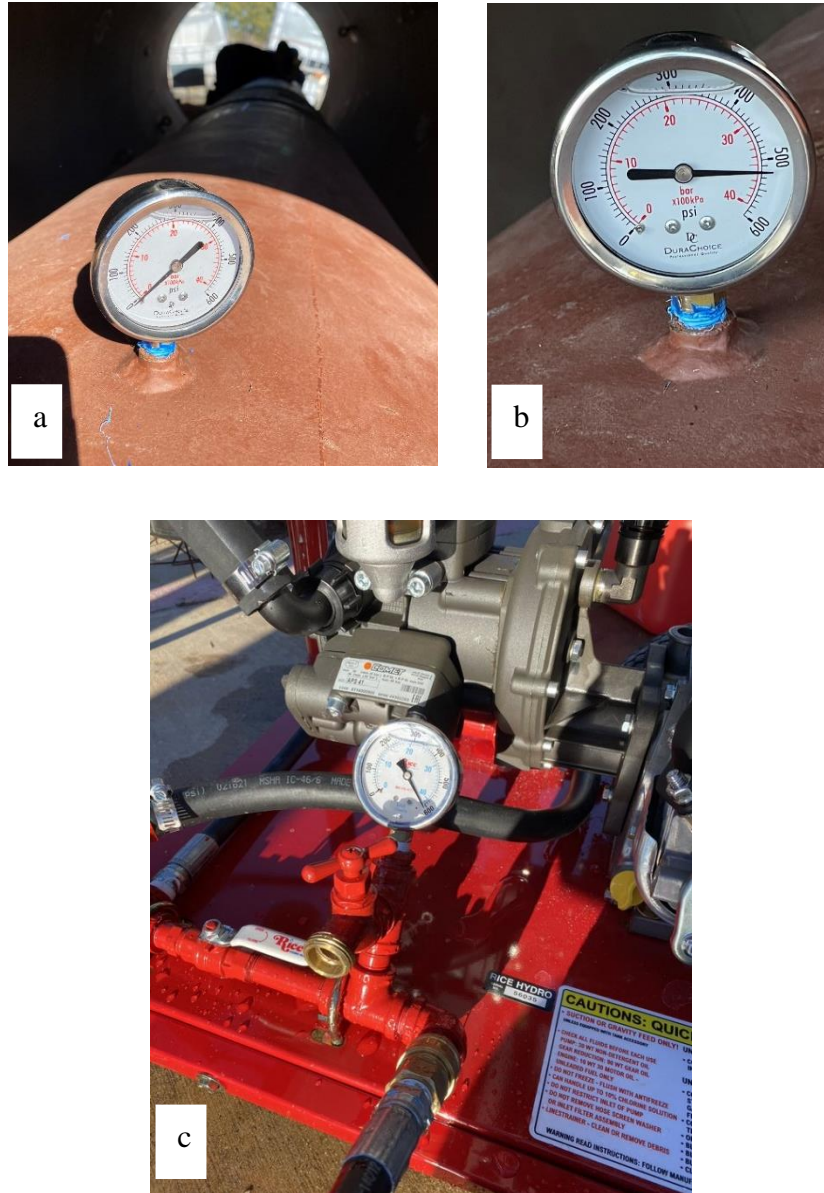


Figure 3.19 (a) Pressure Dial Gauge Initial Reading (b) Pressure Dial Gauge Reading at the End of the Test (c) Pressure Dial Gauge Reading of the Pump

The proposed pressure to test the liner capacity for the hole spanning was 500 psi. The test setup was successfully pressured to more than 500 psi and held for 10 to 15 minutes. Figures 3.19 (a) show the increase in pressure on the dial gauge, and the maximum pressure achieved was more than 500 psi as shows in Figure 3.19 (b). Figure 3.19 (c) shows the pressure recorded in the dial gauge mounted on the pump.

No failure of the liner was detected during the test. The test setup was pressurized four times, and each time the test run passed the pressurizing capacity of more than 500 psi. Thus, the elastomeric liner successfully showed the capacity to rehabilitate the corrosion holes up to 0.5 inches.

After successfully achieving more than 500 psi in the test setup without any liner failure at hole spanning, the test setup was held at 500 psi pressure for up to two hours, and further, any leaks were tested at certain intervals of time. After 2 hours, no failure points were noted for the test setup. Therefore, the liner at the hole spanning still showed positive results without failure after holding the pressure for two hours. The pressure was released after the completion of the test, and the water was drained through the drain outlet at the lowest point of the test assembly.



Figure 3.20 Cutting the Welding Joints from Spigot Ends to Separate Out the Middle Test Section

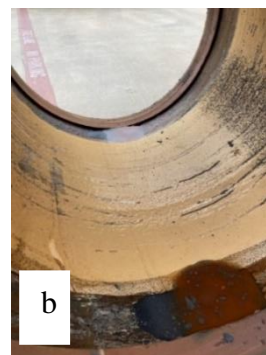
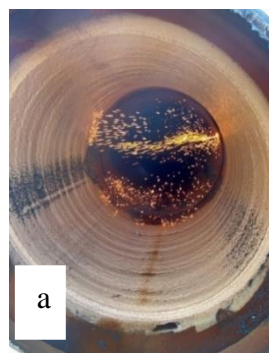


Figure 3.21 (a) Cutting of Test Section from Spigot Ends
(b) Inside View of Test Section after Cutting

After conducting the test on the 0.5-inch hole spanning pipe sample, the spigot ends were cut with the torch and detached from the pipe sample, as shown in Figure 3.20. These spigot ends were reused for the second pipe sample with a hole spanning 1 in. The cut section of the pipe sample from the spigot ends is shown in Figure 3.21 (a). Figure 3.21 (b) shows the inside view of the first tested pipe sample after it detached from the spigot ends.

3.4.1.5 Testing 1-inch Hole Spanning

The first pipe sample tested was with a 1-inch hole spanning. The liner thickness for the pipe sample was designed as per AWWA Class II, and the liner thickness calculated for the 1-inch hole spanning was 0.5-inch. The liner exposed through a 1-inch hole spanning is shown in Figure 3.22. Similar to 0.5-inch hole spanning liner installation, prior to the application of the liner, the pipe sample was abrasive blasted and primed with "Metal Prime" at a thickness of 4-5 mils. A pure polyurea liner was then sprayed onto the surface, achieving a thickness of 0.5 inches. The installation procedure of the liner was entirely similar to first pipe sample.



Figure 3.22 1-inch Hole Spanning Pipe Sample

Similar to the test setup of the first pipe sample, the test setup of the second pipe sample was fabricated and securely placed in the 72-inch diameter pipe section. The pump was connected to the test setup. A leak detection and instrumentation functioning check were performed before

the start of test. The pressure in the test setup gradually increased at 50 psi increments until it reached 500 psi. The pressure dial gauge and pressure transducer continuously monitored and recorded the test setup's pressure. The weather and environmental conditions were recorded on the test day, as shown in Table 3.3.

Table 3.3 Test Data 1-inch Hole Spanning

Description	Test Conditions
Test sample	1-inch hole spanning
Number of trials	Four
Ambient temperature during the test run	76° F
Water temperature	60° F
Wind speed	8 mph
Maximum pressure holds by the test sample	More than 500 psi
Duration of pressure hold by the test setup	24 hours at 500 psi

Table 3.3 shows that the temperature recorded on the test day was 76 °F, and the wind speed was 8 mph. The water temperature during the test was noted at 60 °F. Prior to pressurizing the test setup at a desired pressure of 500 psi, the setup was tested for any leak detection. Then the test setup was pressurized to 100 psi and held for 15 minutes to check any water leakage from welding joints or the coupling joints of the instrumentation provided, and to check for the proper functioning of the instrumentation.

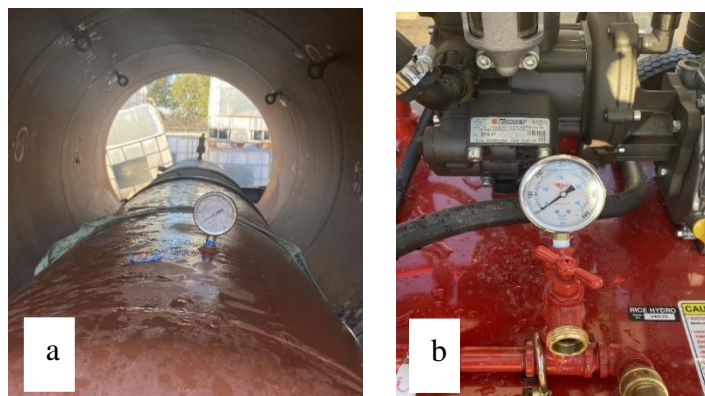


Figure 3.23 (a) Pressure Dial Gauge Initial Reading at the Start of the Test
 (b) Pressure Dial Gauge (on pump) During the Start of Test

Figures 3.23 (a) and (b) shows the zero readings at pressure dial gauge on the test setup and on the pump at the start of the test.

Similar pressure requirement of 500 psi was applied to second pipe sample. The test setup was successfully pressured to more than 500 psi pressure and held for 10 to 15 minutes. Figures 3.24 (a) and (b) show the test setup achieved the maximum pressure more than 500 psi.

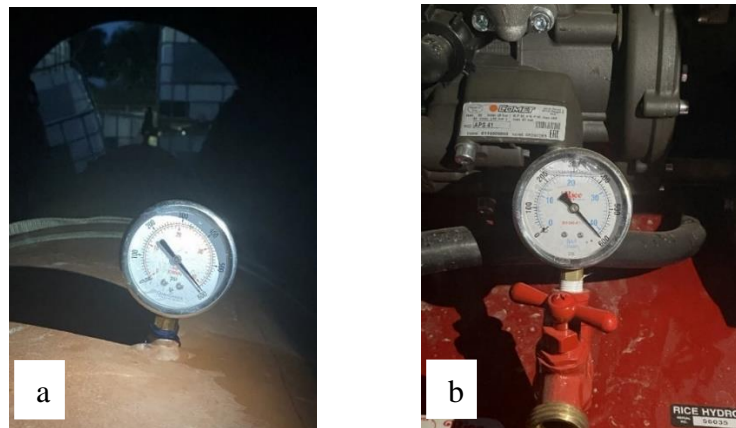


Figure 3.24 (a) Pressure Dial Gauge Reading at the End of the Test
(b) Pump Pressure Dial Gauge Reading at the End of the Test

No failure of the liner was detected during the test, indicating that the elastomeric liner was successful in rehabilitating the corrosion holes up to 1 inch in size. After successfully achieving more than 500 psi without any liner failure at hole spanning, the test setup was held at 500 psi pressure for up to 24 hours, and further, any leaks were monitored at certain intervals of time to ensure the integrity of the liner.

After 24 hours, no failure points were observed in the test setup, implied that the liner at the hole spanning endured intact without any signs of failure during 24 hours of pressure hold. The pressure was released after the completion of the test, and the water was drained through the drain outlet at the lowest point of the test assembly.

After completing the testing of the 1-inch hole spanning test section, the spigot ends were cut with the torch and detached from the test section, as explained in the 0.5 in. hole spanning test setup. These spigot ends were reused for the third pipe sample with a hole spanning 2.0 in.

3.4.1.6 Testing 2-inch Hole Spanning

The third sample tested was with a 2-inch hole spanning. The spigot ends cut from the 1-inch hole spanning test were reused for the 2-inch hole spanning pipe sample. The liner thickness for 2 in hole spanning sample was also designed as per AWWA Class II, and the calculated thickness is 0.75-inch.



Figure 3.25 Pipe Sample 2 in. Hole Spanning

The liner exposed through 2 in. hole spanning is shown in Figure 3.25. Similar to first and second pipe samples, the third pipe sample was also abrasive blasted and primed with the Metal Prime at 4-5 mils. A pure polyurea liner was then sprayed onto the surface, achieving a thickness of 1 in. The installation procedure of the liner was entirely similar to first and second pipe samples.

The test setup assembly and testing procedure were similar to 0.5 and 1 in. hole spanning testing. The strain gauge installed on the 2 in. hole spanning is shown in Figure 3.26. The strain

at the liner exposed through a 2 in. hole was measured continuously during the testing using the data acquisition system.



Figure 3.26 Strain Gauge Installed on 2 in. Hole Spanning

The pump connected to the test setup gradually increasing the pressure at 50 psi increments until it reached 500 psi. The dial gauge installed at one dish head, and the pressure transducer on other dish head were continuously monitoring the pressure of the test setup. The air release valve installed at the highest point of the test setup, removed any entrapped air before pressuring the test setup. The weather and environmental conditions were recorded on the test day, as shown in Table 3.4.

Table 3.4 Test Data 2-inch Hole Spanning

Description	Test Conditions
Test sample	2-inch hole spanning
Number of trials	Four
Ambient temperature during the test run	54° F
Water temperature	59° F
Wind speed	4 mph
Maximum pressure holds by the test sample	More than 500 psi
Duration of pressure hold by the test setup	10 days at 500 psi

Table 3.4 shows that the temperature recorded on the test day was 54° F, and the wind speed was 4 mph. The water temperature during the test was noted at 59° F.

Similar to previous testing of 0.5 and 1 in. hole spanning pipe samples, the water leak test was performed to detect any water leaks from the welding joints, and coupling connections of the instrumentations. The proper functioning of the instrumentations was performed before pressurizing the test setup to a desired pressure. The test setup was successfully pressured to more than 500 psi pressure and held for more than 10 days.

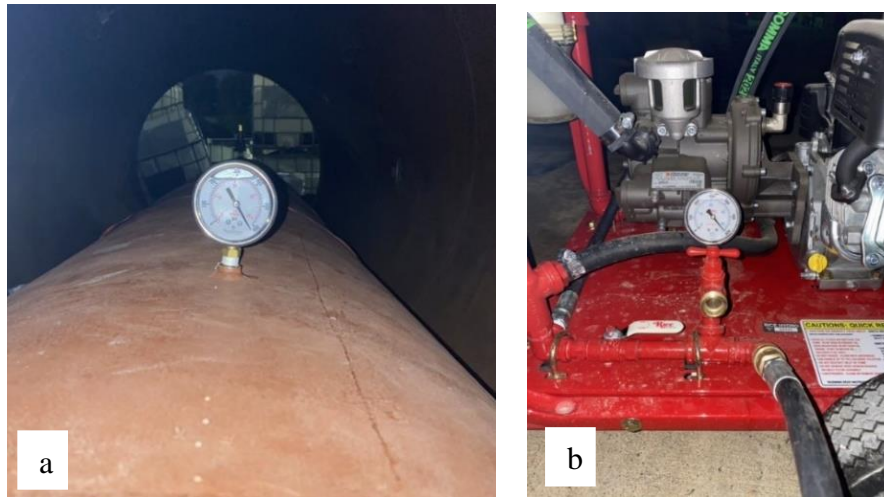


Figure 3.27 (a) Pressure Dial Gauge Reading on Test Setup (b) Pressure Dial Gauge Reading on Pump

Figures 3.27 (a) and (b) show the dial gauge readings installed on the third pipe sample and the pump, respectively, indicating the achieved pressure of 500 psi during the test. No failure of the liner was detected during the test, indicating that the elastomeric liner was successful in rehabilitating the corrosion holes up to 2 inch in size. After successfully achieving more than 500 psi without any liner failure at hole spanning, the test setup was held at 500 psi pressure for up to 10 days, and further, any leaks were monitored at certain intervals of time to ensure the integrity of the liner.

After 10 days, no failure points were observed in the test setup, implied that the liner at the hole spanning endured intact without any signs of failure during 10 days of pressure hold. The

pressure was released after the completion of the test, and the water was drained through the drain outlet at the lowest point of the test assembly.

3.4.2 Vacuum Pressure Testing 2-inch Hole Spanning Sample

After conducting the hole-spanning test on the 2-in. hole spanning pipe sample, a vacuum test was performed on the same test assembly. The purpose of the vacuum test was to determine the strength and integrity of the installed SAPL material to the host pipe under vacuum pressure. Applying vacuum pressure to the pipe lined with the liner material may cause the lining material to detach from the host pipe if the liner's adhesion strength is insufficient to withstand the vacuum pressure.

3.4.2.1 Test Methodology

The test assembly for the 2-inch hole spanning, which was previously lined with pure polyurea liner material, was utilized for conducting the vacuum pressure test. The test setup consisted of a single enclosed unit comprising the pipe sample and two spigot ends. To conduct the vacuum pressure test, a vacuum pump was connected to the test assembly through the coupling connection on the spigot end.

The vacuum pressure test was conducted using a rotary vane oil lubricated vacuum pump with a power rating of 0.75 hp. A vacuum water separator was used in between the test assembly and the vacuum pump. This vacuum water separator collected any moisture entrapped in the test setup before it reached to the vacuum pump during the generation of vacuum pressure in the test setup. The vacuum water separator had a vacuum pressure capability ranging from -100 kPa to 1000 kPa. Figure 3.28 shows the vacuum pump connected to the test setup of 2-in. hole spanning test setup.



Figure 3.28 Vacuum Pressure Test Setup for 2 in. Hole Spanning Pipe Sample

3.4.2.2 Vacuum Pressure Testing

The vacuum pump connected to the test setup first evacuated the air entrapped, and a zero atmospheric pressure was reached in the closed chamber, as represented in Figure 3.29.



Figure 3.29 Vacuum Pressure Dial Gauge Reading
(Pressure Achieved Zero in. of Hg in Test Assembly)

After achieving zero atmospheric pressure, the test setup was subjected to further vacuum pressure, as shown in Figure 3.30.



Figure 3.30 Vacuum Pressure Dial Gauge Reading
(Pressure achieved 24.6-in. of Hg in Test Assembly)

3.4.3 Pressure Integrity Test

The previous tests determined the liner's capability to bridge the corrosion holes and cracks on the host pipe as a semi-structural liner. The experimental test described in this section is the pressure integrity test which determined the resistance of the liner material to internal hydraulic pressure when the liner was designed as a fully structural. A fully structural liner design assumes no support from the host pipe, i.e., the host pipe completely deteriorates. Thus, pipe samples were cast from the liner material and tested without host pipe support. The pressure integrity test determined the burst pressure of bare liner pipe samples. Subsequently, this pressure was used to calculate the hoop stress in the material due to internal pressure.

The following objectives were defined for this test:

1. Bare liner pipe samples with different thicknesses were tested to understand the relationship between the pipe thickness and internal pressure. In addition, the applicability of AWWA Class IV design equations was checked by comparing the analytical results with the experimental test results.

2. Samples were tested at room temperature, elevated temperature, and slightly above freezing temperature to understand the material performance and failure mode at different temperatures.

3.4.4 Pressure Integrity Test Methodology

3.4.4.1 Test Equipment

A hydrostatic pressure testing equipment, specifically designed as per ASTM D1599, was used to perform the test. The equipment was designed to apply constant pressure to the pipe samples at a required temperature. Throughout the test, the pressure and temperature were continuously monitored and recorded. Figure 3.31 shows the pressure integrity test setup, which included the water bath/thermal tank, pressure generating unit, and control panel. Figure 3.32 shows the chiller unit attached to the water bath.



Figure 3.31 Test Setup



Figure 3.32 Chiller Unit

3.4.4.2 Water Bath/ Thermal Tank

The water bath was made of high-quality stainless steel with internal dimensions of 74.80 in x 27.56 in. x 31.50 in. (1900 mm x 700 mm x 800 mm), as shown in Figure 3.33. The tank has an inbuilt heating system with a power of 13.5 kW, which was used to heat the water to achieve the required temperature for the test. A continuous water loop was running in the water bath tank to circulate the heated water to maintain temperature uniformity throughout the water bath tank. The water temperature can be heated from room temperature to 203° F with a temperature control accuracy of $\pm 0.9^\circ$ F.



Figure 3.33 Water Bath

The water bath tank had an excellent thermal insulation system to maintain the required water temperature. When the water was fully heated, the insulation kept the outer surface of the bath tank at room temperature. Thus, the insulation system provided an optimal energy-saving and safety feature to the water tank. In addition, the tank had an automatic water filling floating valve. The lid of the water bath tank was operated with a hydraulic system. As shown in Figure 3.34, the water bath was provided with a quick connect pressure valve to supply the pressure to the pipe sample.



Figure 3.34 Pressure Hose in Water Bath

3.4.4.3 Pressure Generating Unit

One end of the pressure generating unit was connected to the control panel from where the pressure was controlled. The other end was connected internally to the quick connect pressure valve in the water bath to pressurize the pipe sample. A continuous water supply was provided to the pressure-generating unit for generating and supplying the pressure to the pipe sample. The pressure range of the unit was from 0 to 1450 psi. The unit had an emergency stop as a safety feature. Pressure generating unit is shown in Figure 3.35.



Figure 3.35 Pressure Generating Unit

3.4.4.4 Chiller Unit

Chiller was used when the test water temperature needed to be below room temperature.

The Chiller unit is shown in Figure 3.36.



Figure 3.36 Chiller Unit

During this operation, the water connection to the heater was closed through the gate valve, whereas the water connection between the chiller unit and the water bath tank was opened. Thus, the water was continuously circulated through a loop connection between the chiller and the tank. In this way, the water was cool down to the required temperature. The lowest temperature achieved

with the chiller unit was 41° F. The cooling process of water took more time than the heating process.

3.4.4.5 Pressure and Temperature Control Unit

The pressure and temperature control unit had an inbuilt software to input the test parameters such as pipe diameter, thickness, length, and pipe material. The control panel was controlling and monitoring the pressure and water temperature. The target pressure was entered into the control unit, and the unit then communicated to the pressure generating unit to pressurize the pipe sample at this pressure uniformly within 72 seconds. During the test, if the pipe sample failed before the target pressure, the unit automatically stopped and recorded the burst pressure and time-to-failure. The time vs. pressure graph was recorded for each pipe sample. The Control unit panel is shown in Figure 3.37.



Figure 3.37 Control Panel Unit

3.4.4.6 Pipe Samples Preparation

Making Even Ends of Pipe Samples

The pipe samples were machined to cut the pipe's improper, uneven, or rough ends. Figure 3.38 shows that the pipe sample was cut on the lathe machine with the automatic saw cutter blade to remove the uneven ends. The pipe samples were cut at 90 degrees for the proper bedding of the end caps on the pipe sample. Removing the uneven ends was as minimum as possible so that the overall length of the pipe samples was not reduced.



Figure 3.38 Pipe Cutting at Lathe Machine

Figure 3.39 shows the uneven part cut from the pipe sample.

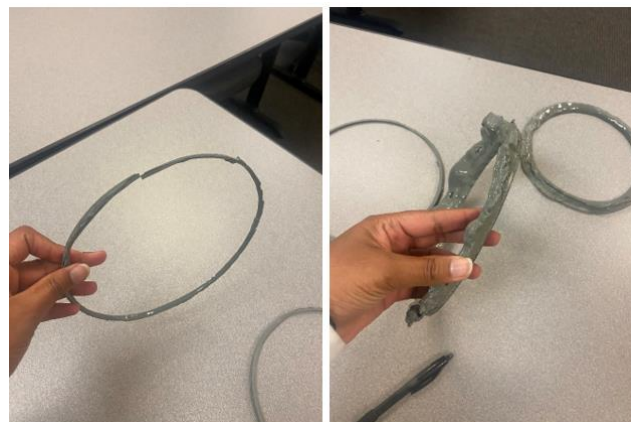


Figure 3.39 Uneven Parts Cut from Pipe Sample

Sample Measurements

Each pipe sample's dimensions such as outer diameter (OD), thickness and length were measure and the procedure for these measurements is explained in the following sections.

1. All the pipe samples were marked at four points circumferentially (as shown in Figure 3.40) on both ends of the pipe, such as 1,2,3,4 on top end and 1',2',3',4' on bottom end.



Figure 3.40 Marked Pipe Sample

2. Vernier caliper was used to measure the thickness at these four marked points on both ends of the pipe, and the average thickness was calculated.
3. The outer diameter (OD) was measured between the pair of each odd numbered points (1 and 3) and even numbered points (2 and 4) at one end and similarly on the other end of pipe using vernier caliper. The average OD of pipe sample was calculated.
4. The pipe length was measured at these four marked points, and the average length was calculated.
5. Samples were marked with sample number, orientation (used for end caps installation) and temperature. The example of the marking system is represented in Figure 3.41 below.

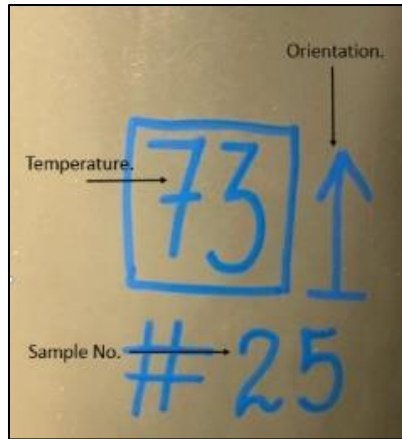


Figure 3.41 Pipe Sample Marking System

Visual Inspection of Pipe Samples

All the pipe samples were carefully inspected, and pictures were recorded for each sample.

Visual inspection observations are listed below.

1. Seam line joints formed due to jigs molding was a main concern and thus, it was thoroughly inspected for any irregularities or narrow gaps. Some of the samples showed gap intrusion which were minor or negligible, whereas some of them were major, but not throughout the pipe thickness. Major gap intrusions were reducing the effective pipe thickness. Some examples of gap intrusion are shown in Figure 3.42. These samples were able to be tested, but the defects were recorded for each sample.
2. The pipe interior and exterior were checked for any cracks, air pockets, bubbles, or bulging over the surface. Some of the samples had bulging on the inside of the pipe, which were captured during the inspection, as represented in Figure 3.42.
3. Three samples were found to be oval shaped on both ends, and due to this ovality, the installation of end caps was difficult. Thus, these samples were rejected from the test.




Visual Inspection of Pipe Samples		
		
Seam line defects	Gap intrusion of 0.2875 in.	Interior Pipe Bulging along Seam line

Figure 3.42 Visual Inspection of Pipe Samples

After visual inspection of the pipe samples, the seam line near the end caps was smoothed using suitable sandpaper (preferably 50-80 Grit) to ensure the perfect fit of clamps and rubber gasket/O-ring.

Pipe Sample Conditioning

The conditioning was an important procedure to prepare the pipe samples for testing at a specific temperature. Since the polymer material properties depend on the temperature, achieving a uniform temperature throughout the samples was essential to determine the specific behavior of the material in the different temperature ranges. All the pipe samples were conditioned at a minimum of 16 hours in the environmental chamber room and one-hour conditioning in the water bath for 41 °F, 120 °F, and 150 °F temperatures testing, whereas the 73 °F temperature samples were conditioned at the room temperature only.

3.4.4.7 End Closures/ End Caps

End caps of 8 in. diameter were designed with anti-corrosive material. The material of the end caps could withstand the maximum pressure required for the test without failure. Figure 3.43 shows the top-end cap with pressure inlet valve and bleed valve. Figure 3.44 shows the bottom end cap.

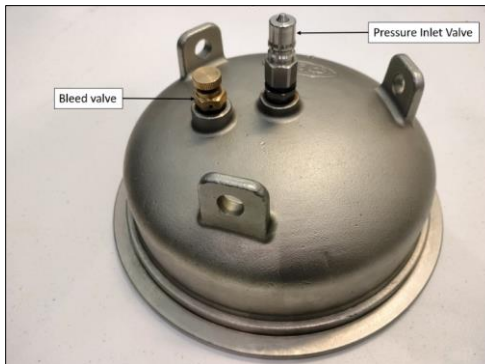


Figure 3.43 Top End Cap



Figure 3.44 Bottom End Cap

These end caps were specifically designed for polymeric material to be tested at different temperatures. The polymeric material exhibits greater elasticity at higher temperatures, which can present challenges when installing end caps to achieve leak-proof joints. In addition, the end caps were designed to fit the pipe samples with different thicknesses with constant outer diameter. To

prevent leakage, a leak-proof rubber gasket or O-ring was employed to seal any gaps between the pipe sample and the end cap. The O-ring/rubber gasket is shown in Figure 3.45.



Figure 3.45 O-ring/Rubber Gasket

The snap ring/retaining ring as shown in Figure 3.46, was designed to push the O-ring inside the end cap. The snap ring held the O-ring in place and made a close-fit connection. More detailed information of using the O-ring and snap ring is provided in end caps installation steps (steps 2 and step 3).

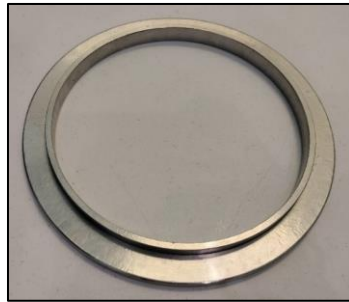


Figure 3.46 Snap Ring

The clamping system as shown in Figure 3.47, was used to hold the end caps.



Figure 3.47 Clamping System

The clamping system was designed with the intention of avoiding excessive stress on the pipe ends. However, to ensure that the end caps remained in place during the high-temperature test, they were restrained using rods and holding plates (as illustrated in Figure 3.48). The rods were of the same length as the pipe and were bolted together with the holding plates, effectively securing the end caps in a fixed position.



Figure 3.48 Rods and Holding Plates

Restrained end caps were necessary at elevated temperatures due to the elastic nature of the material, which prevented the end caps from slipping off. However, at room temperature and lower temperatures, restraining the end caps was not required. Nonetheless, in order to ensure comparable results across different temperatures, the rods were used during testing for all temperature conditions. The following steps were followed to install the end caps on the pipe samples.

Step 1: The sample was placed vertically, and the snap ring slid through the top end with its raised ridge facing up, as shown in Figure 3.49.



Figure 3.49 Pipe Sample with Snap Ring

Step 2: The rubber O-ring was cleaned with oil lubricant and placed above the snap ring, as represented in Figure 3.50.



Figure 3.50 Pipe Pipe Sample with Snap Ring and O-ring

Step 3: The bottom end cap was placed over the pipe and tapped gently with the rubber mallet to place it uniformly on the pipe sample. The O-ring was pushed inside the groove between the end cap and the pipe sample (as shown in Figure 3.51). Once the O-ring was perfectly pushed inside the groove, the snap ring was pulled upward towards the end cap to further push the O-ring

inside the end cap. The O-ring sealed any gap between the outer diameter of the pipe and the end cap to prevent any leaks.



Figure 3.51 Bottom End Cap Installation in Process

Step 4: The ridges of the end cap and the snap ring were fitted into the groove of the clamping system, which held the assembly together.



Figure 3.52 Pipe Sample with Top End Cap Installed

Then the clamps were tightened with two horizontal bolts on its two ends and eight vertical screws circumferentially (as shown in Figure 3.52). *(Note: Two horizontal bolts were tightened first but simultaneously to each other, and later tightened the eight vertical screws circumferentially).*

Step 5: The sample was flipped upside down and placed it on the restrained enclosure system specifically designed for these end caps (as shown in Figure 3.53). The pipe sample was filled with water with bottom end cap installed. *(Note: The water used to fill the sample was of the same temperature that was intended for the testing)*



Figure 3.53 Pipe Sample with Restrained End

Step 6: The other end cap was installed following a similar procedure as described in steps 1 through step 4. Both end caps installed on the pipe sample are shown in Figure 3.54.



Figure 3.54 Top End Cap Installed on Pipe Sample

Step 7: After the end caps were installed, the vertical rods with holding plates were tightened with the bolts simultaneously on both sides. The nuts were fastened but without putting

any pressure on the end caps. The rods were only holding the end caps; they did not push the end caps toward the inner side. The complete assembly of restrained end caps installed on the pipe sample is shown in Figure 3.55.



Figure 3.55 Pipe Sample with Both End Caps

Following the installation of the end caps on the pipe samples, a pressure integrity test was conducted at different temperatures, as described in the subsequent sections.

3.4.5 Pressure Integrity Testing

The test was designed to perform at temperatures of 73° F, 120° F, 150° F, and 41° F. The planned thicknesses for the test were 0.25 in., 0.35 in., 0.45 in., 0.55 in., and 0.65 in.; however, the actual thicknesses tested were close but not exactly these numbers. The pipe sample thickness details are given in the following sections. In total, 60 samples were tested, with three pipe samples tested at each of the five different thicknesses for each temperature.

The water bath tank was filled with water to the required level. The heating system of the water bath/ thermal tank was used to heat the water up to 73° F, 120° F, and 150° F temperatures, whereas the chiller unit was used to lower the water temperature to 41° F. The water from the

water bath was utilized to fill the pipe sample at a required testing temperature. Figure 3.56 shows the installation of end caps.



Figure 3.56 End Caps Installation in Progress

After installing both end caps, the pressure hose in the water bath tank, which was internally connected to the pressure generating unit as illustrated in Figure 3.57, was connected to the pressure inlet valve on the top end cap. This pressure hose allowed water to be introduced into the pipe sample, filling any empty space.



Figure 3.57 Pipe Sample Connected with Pressure Hose

The bleed value on the top end cap was used to release any entrapped air from the pipe sample, as shown in Figure 3.58 (left). The bleed value was opened, and a slight pressure was applied to the sample to let the water come out from the bleed value to remove any entrapped air. The bleed valve was closed after water came out from it, as shown in Figure 3.58 (Right).

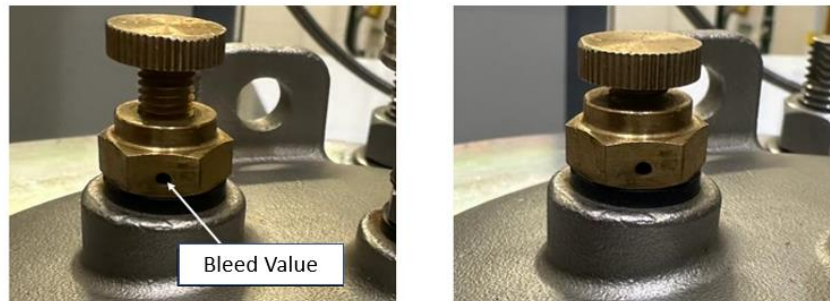


Figure 3.58 Bleed Value Opened (Left) and Closed (Right)

The seam lines and the end caps were checked for any water leakage. The pipe sample with end caps was placed in the safety cage, as shown in Figures 3.59. The pressure hose was connected to the pipe sample before placing the sample in the water bath.

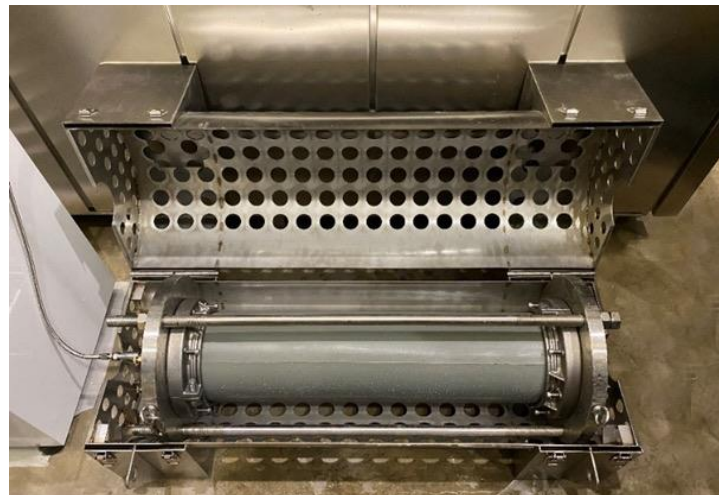


Figure 3.59 Pipe Sample with Safety Cage

The pipe sample with the safety cage was lifted with the help of chains and a crane as in Figure 3.60.



Figure 3.60 Pipe Sample Lifting with Crane

The pipe sample with the cage placed in the water bath is shown in Figure 3.61.



Figure 3.61 Pipe Sample Placed in Water Bath

Pressure was applied to the pipe samples after conditioning them. The time to failure for all pipe samples shall be between 60 and 70 seconds as per ASTM D 1599, Procedure A. Bursting

the pipe sample between 60 to 70 seconds determined the mode of failure. The target pressure for the test was set from the control panel unit, and the pressure generating unit uniformly applied the target pressure to the pipe sample within 72 seconds (as explained in test setup section). During the test, if the pipe sample failed, the unit automatically stopped and recorded the burst pressure and time-to-failure. If the time to failure is less than 60 seconds, the targeted pressure was reduced, and the test was repeated. During the testing, pressure and time-to-failure were recorded for each pipe sample.

Before the actual test started, some trial runs were performed to get an idea of the pressure resistance of the material so that target pressure could be predicted to fail the pipe samples between 60 to 70 seconds to determine the burst pressure. However, due to the limited trial samples data, it was a challenge to make a correlation between the thickness and the burst pressure. In addition, the predicted target pressure based on the trial sample thickness sometimes did not give uniform results. Some samples with the same thickness and target pressure gave different burst pressure results. The reason for this non-uniform behavior of the material at the same thickness could be the external and internal defects of pipe samples as mentioned below.

1. **Pipe Sample Internal Defects-** In some cases, the pipe samples had internal defects that were not detectable during visual inspection. However, it was assumed that these defects had an impact on the burst pressure values of pipe samples with similar thicknesses.
2. **Pipe Sample Seam Line Defects-** The presence of seam line defects potentially influenced the pressure resistance results and failure mode. In cases where pipe samples had these defects, the target pressure was determined based on the best judgment to determine the burst pressure.
3. **Major Gap Intrusion on Seam Line-** Gap intrusion at the seam line resulted in an

effective reduction of the pipe thickness. Consequently, pipes with gap intrusions could not be compared directly in terms of thickness.

Setting up the target pressure for the pipe samples to determine the burst pressure within 60 to 70 seconds was a challenge and thus, more than one test run was performed on some pipe samples. If the pipe sample failed before 60 seconds, the burst pressure of this pipe sample would not truly represent the actual burst pressure value. This is because the failure occurred at a higher-pressure rate compared to samples that failed between 60 and 70 seconds. Consequently, even if the desired time-to-failure range of 60 to 70 seconds was achieved through multiple test runs on the same pipe sample, the resulting recorded burst pressure represented a more conservative data point due to the material being subjected to stress in multiple test runs.

The target internal pressure, burst pressure and time-to-failure data were collected during the test. The burst pressure was used to calculate the hoop stress on the SAPL material due to internal pressure. The failure mode was observed during the testing of each pipe sample. The failure modes of pipe samples were ductile, elastic and catastrophic, and brittle catastrophic failure.

3.4.5.1 Pressure Integrity Testing at 73° F Temperature

A total of 15 samples were tested at 73° F temperature. The measured dimensions of pipe samples are given in Table 3.5 below.

Table 3.5 Pipe Sample Dimensions for Testing at 73° F

Sr. No.	Sample #	Average Thickness, t (in.)	Average Outer Diameter, D (in.)	Total Sample Length (L) (in.)
1	11	0.228	7.90	35.36
2	10	0.249	7.89	35.19
3	16	0.250	7.93	35.26
4	56	0.310	7.88	35.55
5	35	0.334	7.87	35.56
6	45	0.336	7.89	35.56
7	40	0.370	7.84	35.55
8	49	0.388	7.90	35.53

Sr. No.	Sample #	Average Thickness, t (in.)	Average Outer Diameter, D (in.)	Total Sample Length (L) (in.)
9	31	0.394	7.89	35.53
10	4	0.502	7.87	35.59
11	27	0.507	7.85	35.59
12	60	0.532	7.86	35.58
13	17	0.534	7.91	35.48
14	48	0.618	7.89	35.20
15	33	0.631	7.85	35.37

As given in Table 3.5, the minimum thickness tested was 0.228 in., and the maximum thickness tested was 0.631. The average diameter of these 15 pipe samples was 7.882 in., average total length of the pipe samples was 35.46 in.

3.4.5.2 Pressure Integrity Testing at 120° F Temperature

A total of 15 samples were tested at 120° F temperature. The measured dimensions of pipe samples are given in Table 3.6 below.

Table 3.6 Pipe Sample Dimensions for Testing at 120° F

Sr. No.	Sample #	Average Thickness, t (in.)	Average Outer Diameter, D (in.)	Total Sample Length (L) (in.)
1	8	0.241	7.93	35.36
2	2	0.241	7.88	35.33
3	44	0.267	7.91	35.56
5	55	0.304	7.86	35.58
4	62	0.316	7.91	35.55
6	37	0.323	7.89	35.53
7	32	0.382	7.84	35.56
8	46	0.39	7.89	35.55
9	20	0.456	7.88	35.52
10	39	0.539	7.85	35.55
12	26	0.539	7.85	35.39
11	14	0.542	7.86	35.4
13	59	0.574	7.89	35.28
14	47	0.595	7.88	35.47
15	57	0.614	7.89	35.25

As given in Table 3.6, the minimum thickness tested was 0.241 in., and the maximum thickness tested was 0.614. The average diameter of these 15 pipe samples was 7.881 in., average total length of the pipe samples was 35.46 in.

3.4.5.3 Pressure Integrity Testing at 150° F Temperature

A total of 15 samples were tested at 150° F temperature. The measured dimensions of pipe samples are given in Table 3.7 below.

Table 3.7 Pipe Sample Dimensions for Testing at 150° F

Sr. No.	Sample #	Average Thickness, t (in.)	Average Outer Diameter, D (in.)	Total Sample Length (L) (in.)
1	5	0.207	7.90	35.34
2	1	0.226	7.88	35.34
3	3	0.232	7.91	35.38
5	23	0.316	7.91	35.55
4	53	0.329	7.9	35.55
6	43	0.339	7.91	35.56
7	30	0.401	7.84	35.55
8	22	0.402	7.88	35.52
9	24	0.413	7.83	35.56
10	12	0.461	7.88	35.48
12	29	0.476	7.9	35.53
11	19	0.479	7.87	35.44
13	13	0.509	7.88	35.31
14	50	0.567	7.88	35.53
15	51	0.576	7.81	35.56

As given in Table 3.7, the minimum thickness tested was 0.207 in., and the maximum thickness tested was 0.576. The average diameter of these 15 pipe samples was 7.881 in., average total length of the pipe samples was 35.48 in.

3.4.5.4 Pressure Integrity Testing at 41 °F Temperature

Out of 15 samples, 12 were tested at 41° F temperature, and 3 were rejected from the test due to defects. The measured pipe sample dimensions are given in Table 3.8 below.

Table 3.8 Pipe Sample Dimensions for Testing at 41° F

Sr. No.	Sample #	Average Thickness, t (in.)	Average Outer Diameter, D (in.)	Total Sample Length (L) (in.)	Comments
1	25	0.248	7.91	35.34	Defective Sample
2	6	0.252	7.44	35.11	Defective Sample
3	9	0.285	7.87	34.94	Defective Sample
5	15	0.298	7.86	35.09	
4	54	0.33	7.91	35.55	
6	34	0.362	7.9	35.56	
7	52	0.385	7.89	35.58	
8	36	0.414	7.89	35.52	
9	18	0.425	7.87	35.55	
10	38	0.429	7.86	35.55	
12	7	0.508	7.84	35.47	
11	21	0.52	7.87	35.31	
13	61	0.568	7.89	35.14	
14	42	0.631	7.89	35.38	
15	58	0.642	7.91	35.47	

Table 3.8 shows that the minimum thickness tested was 0.248 in., and the maximum thickness tested was 0.642. The average diameter of tested 12 pipe samples was 7.88 in., the average total length was 35.43 in.

Rejected Pipe Samples from the Test

During the visual inspection, it was observed that samples #6 and #9 exhibited an oval shape at both ends. Figures 3.62 (a) and 3.62 (b) illustrate these samples. Due to the irregular shape, the end caps could not be properly installed on these pipe samples, and, thus, they were rejected from testing.

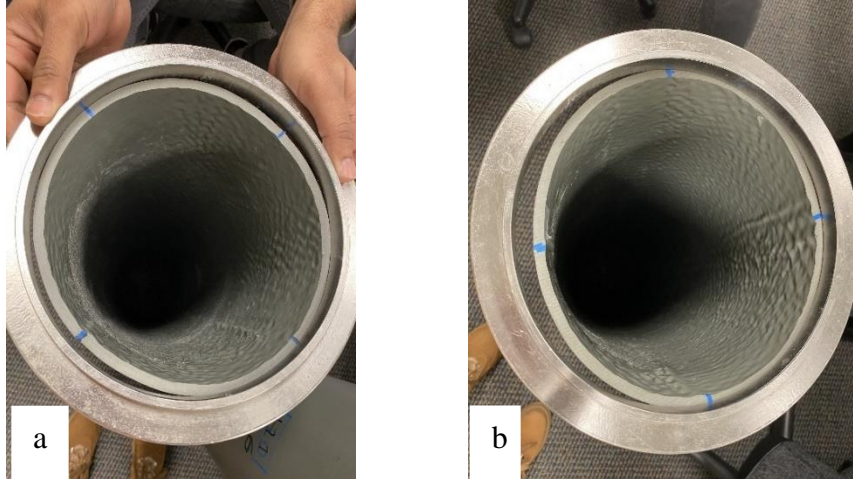


Figure 3.62 (a) Sample #6 Oval in Shape (b) Sample #9 Oval in Shape

Furthermore, pipe sample #42 displayed a significant bulging/bubble area along with an internal crack, as depicted in Figure 3.63. Despite these major defects, the sample was still subjected to testing. However, the sample was unable to withstand the applied pressure and subsequently failed.

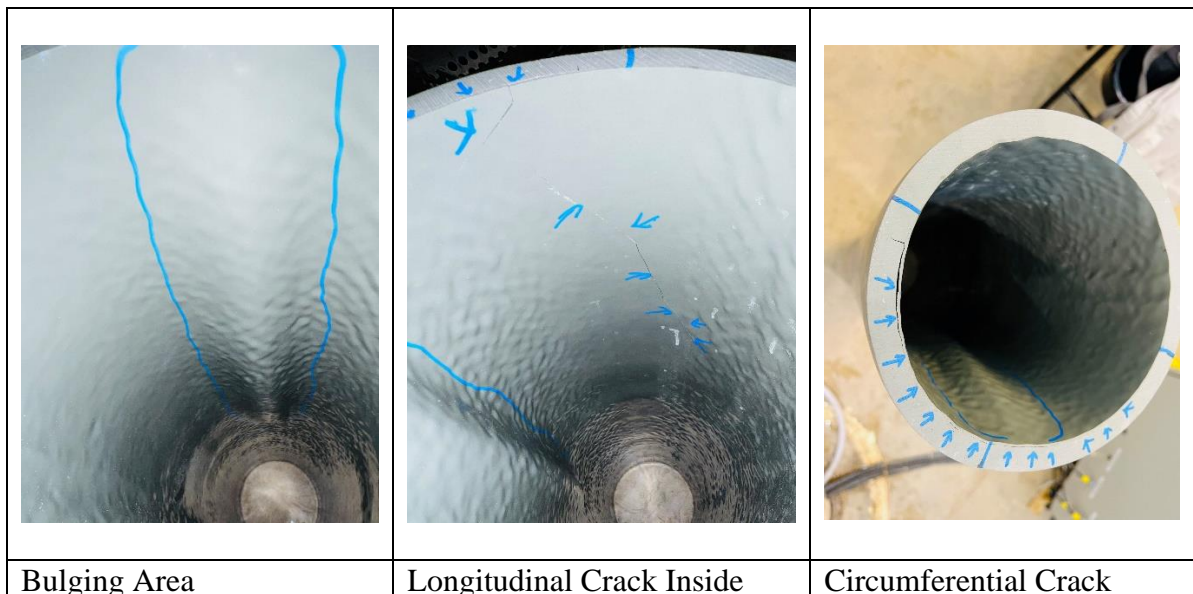


Figure 3.63 Sample #42 Visual Cracks and Bulging Areas

3.5 Chapter Summary

This chapter describes the material testing performed to determine the mechanical properties of the material. The chapter gave the comprehensive full-scale laboratory test methodology designed and performed for the structural evaluation of SAPL polymeric liner as per AWWA structural Classification of Class II and Class IV. The chapter provided information about the instrumentation and data collected techniques adopted for tests performed. In addition, the chapter also enlisted the test challenges for performing these tests. Thus, to evaluate and analyze the hydraulic properties of the liner, hydraulic flow test was designed and is represented in Chapter 4. Chapter 5 will provide the results and a detailed discussion of structural evaluation test results.

Chapter 4 Hydraulic Evaluation of Spray Applied Pipe Lining

4.1 Introduction

The inevitable aging of pipelines has become a challenge in the underground infrastructure industry. During the service life of the pipe, corrosion can have a detrimental effect on the material and life span of the pipe. The corrosion effect increases with time, and in the worst-case scenario, corrosion can considerably reduce the effective internal pipe diameter, subsequently increasing the pipe roughness. The pipe roughness affects the friction factor and, consequently, has a negative impact on the pipe flow and pumping requirements. Therefore, a liner installation can be a potential rehabilitation process to reduce the impact of corrosion and improve pipe roughness.

Lining the host pipe decreases the internal diameter (ID), which can affect the flow capacity of the pipe, especially in pressure pipes. Therefore, it is important to evaluate the flow characteristic of the lining system when applied to pressure pipes. Chapter 4 presents the testing methodology designed to perform hydraulic flow tests to assess the friction factor “ f ” of the lined pipe and compare it with the new carbon steel pipe. The magnitude of the “ f ” factor allows the engineer to measure the smoothness of a pipeline, which is an important factor in estimating head loss in the flow, a major contributor to pipe discharge and hydraulic performance.

The specific objectives of this test were as follows:

- 1) To determine the friction factor ‘ f ’ and hydraulic characteristics of circular pipe before and after applying the liner system.
 - a. Determine “ f ” by measuring the pressure head difference between two fixed points in a straight pipe with a circular cross-section under fully steady state flows.
 - b. Consider flow rates from 800 to 1800 gallon per minute (GPM).

- 2) To measure the roughness profile of the liner system by full-scale lab testing and by using laboratory profilometer.
- 3) To compare the effect of the “f” factor on water flow through a pipe with and without a liner.
- 4) To compare the head loss of SAPL lined pipe with a corroded pipe to determine the percentage reduction in head loss.

4.2 Hydraulic Flow Testing Methodology

The test setup was assembled to evaluate changes in the flow characteristics of lined and unlined carbon steel pipe section configured in a closed loop piping system as shown in Figure 4.1. The direction of water flow is illustrated in Figure 4.1.

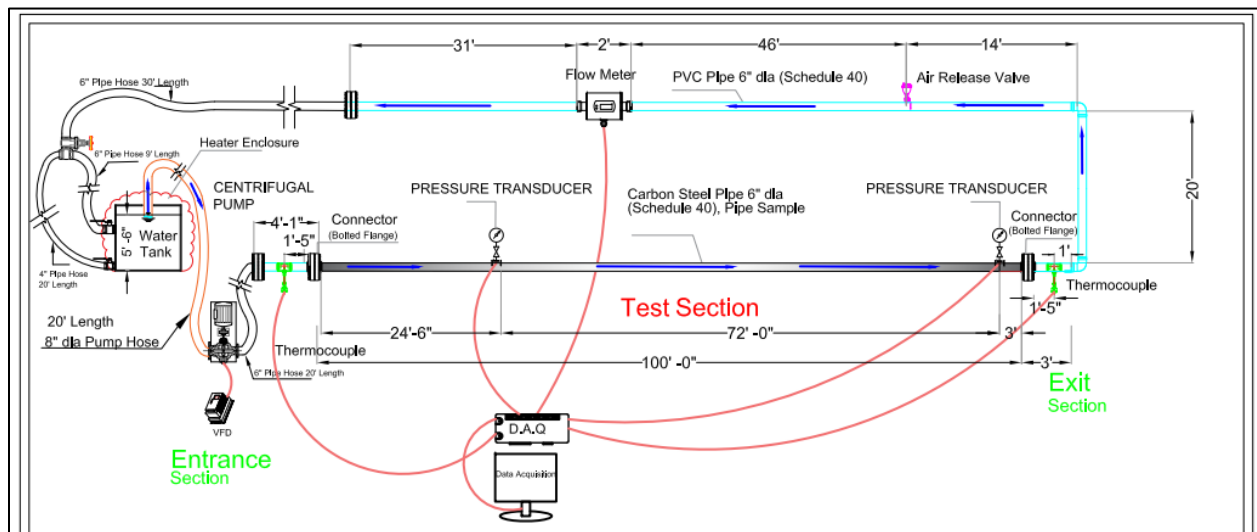


Figure 4.1 Hydraulic Flow Test Equipment Setup

A new 6-in. diameter schedule 40 carbon steel pipe with a length of 100 ft was used as a test pipe section. An additional 120-ft of 6-in. PVC pipe was used to create a closed-loop piping system returning flow to reservoir and the pump.

The test setup used various equipment such as a flow measurement device to measure flow rate, two pressure transducers to measure water pressure, two thermocouples to measure water temperature at two ends of the test section, one centrifugal pump with variable flow rate, one water tank with heat enclosure system as well as air conditioning unit, and other plumbing fittings, such as, gate valve, flanges, joints, and attachments. The variable flows were considered for the test setup; however, these variable flows were considered at a high Reynolds number to achieve the turbulent flow in the test setup. The “f” factor was obtained by measuring the head loss at the two ends of the test section.

The friction factor was determined by using Darcy-Weisbach formula, shown below:

$$h_L = f \frac{L}{D} \frac{v^2}{2g} \quad 4.1$$

Where, f = friction factor [unitless]

L/D = equivalent length of a resistance to flow [unitless]

V = mean flow velocity [fps]

g = gravitational acceleration [32.174 ft/s²]

h_L = pressure head loss [ft]

The pressure head difference (h_L) between two fixed points was determined under steady-state flow conditions.

4.3 Equipment Details

Figure 4.1 illustrated location of each component, which are described in the following sections. The test setup included the following components:

- 1) Centrifugal variable flow rate pump (1 unit)

- 2) Water tank with heat enclosure system (1 unit)
- 3) Air conditioning equipment (1 unit)
- 4) Carbon steel pipe section – new condition (100 ft)
- 5) PVC pipe (120 ft)
- 6) Thermocouple (2 units)
- 7) Transducers (2 units)
- 8) Flow meter (1 unit)
- 9) Air release valve (1 unit)
- 10) Gate valve (1 unit)
- 11) Data acquisition system (2 units)

4.3.1 Variable Flow Rate Pump

The test setup consisted of a centrifugal diesel pump with variable flow rate. The maximum flow capacity was 2,680 GPM with a maximum shutoff head of 164 ft (71 psi) at an operating speed of 1,800 rpm. The minimum flow capacity was 450 GPM with a minimum shutoff head of 74 ft (32 psi). The minimum and maximum speed of the pump was 1,200 rpm and 1,950 rpm. The pump was driven by 75 horsepower Duetz diesel engine. The pump was a single-stage single suction pump with suction and discharge sizes of 6-in. diameters.

The flow rate for the pump was controlled by varying the engine speed. The maximum and minimum flow rates selected were 1,800 and 800 GPM respectively, which allowed the pump to run at the best operating efficiency between 72% to 81%. The pump was equipped with a vacuum-assisted priming system that automatically drew out the air until the water filled in the pumping system. Figure 4.2 below shows the diesel operated centrifugal variable flow rate pump.



Figure 4.2 Centrifugal Variable Flow Rate Pump

4.3.2 Water Tank

A carbon steel mini frac tank of 8,400 gallons was used for water storage and supply to the test setup. The model of water tank was “MINIFRACL”, and the make was “Wichita Tanks.”

Figure 4.3 shows the water tank used in this project.



Figure 4.3 Water Tank

The interior of the tank was smooth and lined with chemical resistance “Phenoline 380” for easy cleaning and maintenance. The exterior of the tank was coated with high gloss polyurethane. The tank's length, width, and height were 23 ft- 6 in., 8 ft- 6 in., and 8 ft- 6 in.,

respectively. The tank had three 4 in. 150# threaded flange with butterfly valves, two on the front of the tank and one on the rear side. The front drain and rear flush consisted of 4 in. NPT male with cap and chain on both sides. The fill line was a 3 in. schedule 80 top fill with capped MPT extension at the front of the tank. The water tank was connected to the pump through an 8 in. diameter pipe hose. The length of the hose pipe between the water tank and pump was 20 ft.

4.3.3 Heat Enclosure Unit

The tank was protected by a heat enclosure unit to maintain the required temperature. A frame tent of 10 x 20 ft enclosed the water tank as shown in Figure 4.4 (a). An air condition unit (as shown in Figure 4.5 (b)) with capacity of 25 to 30 tons, supplied with a 480 V, maintained the required air temperature within the enclosure and hence helped maintained the water temperature. The heat enclosure unit operated with a generator unit was included to maintain the water viscosity during different test runs at different times.

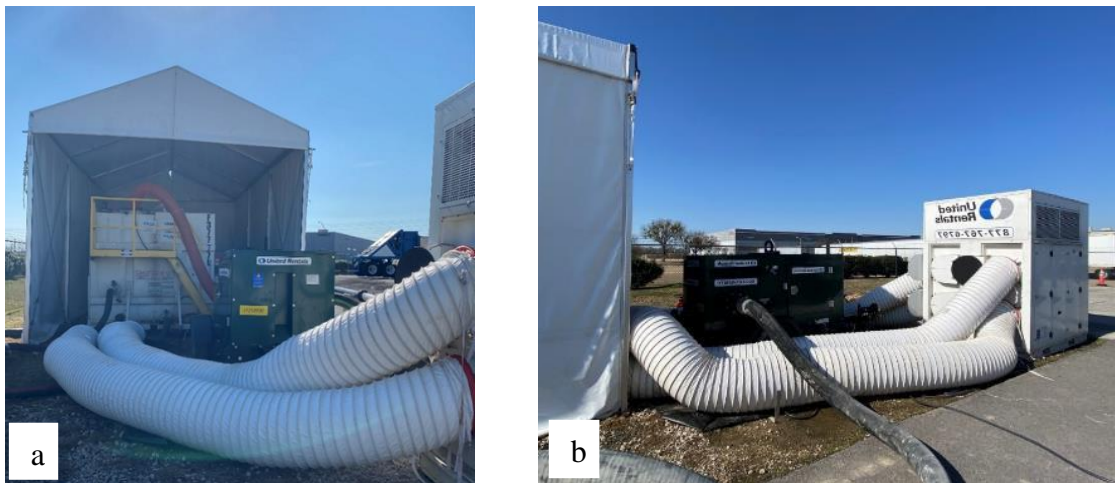


Figure 4.4 (a) Frame Tent for Water Tank (b) AC Duct Connected to Tent

4.3.4 Entrance Section and Thermocouples

The entrance section of the test setup included the connection between the water tank and pump, and from the pump to the carbon steel pipe test section. An 8 in. inlet hose was used to

supply water from the tank to the pump. A 6 in. outlet hose of length 20 ft supplied water from the pump to the test setup. The pump outlet hose and the carbon steel pipe were connected with a 3.5 ft length, 6 in. diameter schedule 40 PVC pipe. The entrance section pipe connections with installed thermocouple are shown in Figure 4.5 (a). Figure 4.5 (b) shows the detailed of the thermocouple.

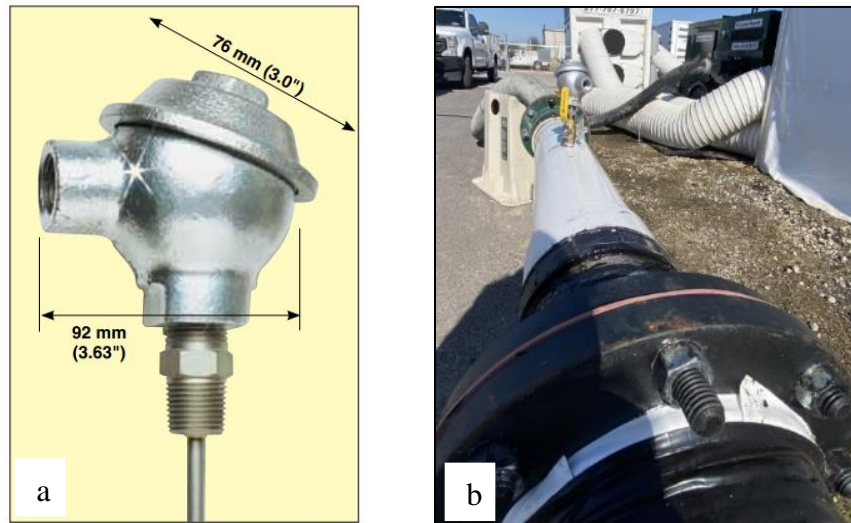


Figure 4.5 (a) Thermocouple (b) Entrance Section with Thermocouple Installed

The thermocouples were installed on the PVC pipe in the entrance and exit sections to measure and monitor the fluid temperature running through the test setup. Omega Engineering type “T” thermocouple probes with industrial protection heads, model NB1-CPSS-14U-4-CAL-3 were used in the test setup. The probe length of the thermocouples was 4 in., and the thread on the probe was 0.5 in. NPT. The temperature range was from -328 °F to 662 °F, with a temperature measuring accuracy of 1 °F.

4.3.5 Pipe Test Section

The pipe sample consists of new 6 in. carbon steel pipes, schedule 40, of an overall length of 100 ft. The internal diameter (ID) of the pipe was 6.065 in. Carbon steel pipes of 20-ft sections

were welded together to fabricate a 100-ft straightened test section, as represented in Figure 4.6. The cribbing was used throughout the test setup to elevate the pipe at same level, as shown in Figure 4.6.



Figure 4.6 Carbon Steel Pipe Test section

The entrance section of the PVC pipe was connected to the carbon steel pipe section with a 40 PVC coupling schedule. An epoxy adhesive was used at the coupling connection to ensure tightness. A steel socket bolt flange with thickness of 3/4 in. was installed at the start and end of the carbon steel pipe test section for easy installation and removal of the test section. Rubber gaskets were placed between opposing flanges to ensure a tight and leak-proof joint.

Fabricating a test section with flange connections was beneficial for easy removal of the test section and for preparing it for SPAL material for the next test run. The pipe section was straight with no defects and damages. The elevation of the test section was aligned at the same level to ensure a zero-elevation difference at the two ends of the test section. Two pressure transducers, PX209 and PX309, from Omega Engineering were installed at the two ends of the test section (as represented in Figures 4.7 (a) and 4.7 (b)) to measure the difference in pressure. The range of the pressure transducer #1 PX309 was from 0 to 300 psi for, and pressure transducer #2 PX209 from 0 to 200 psi.

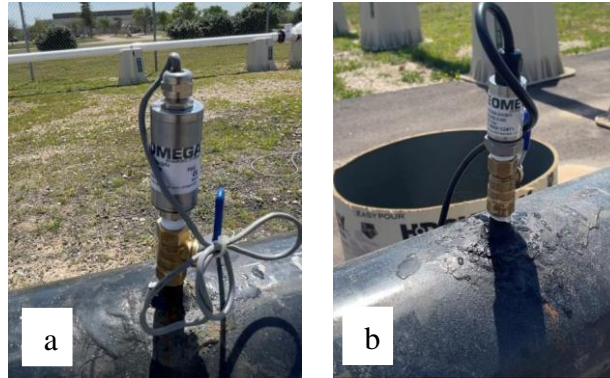


Figure 4.7 (a) Transducer #1 (Entrance Section) (b) Transducer #2 (Exit Section)

Taking into account the entrance and exit effect requirements for a fully developed flow, transducer #1 is positioned 25 feet downstream from the starting point of the carbon steel pipe test section. Transducer #2, on the other hand, is installed 3 feet upstream from the endpoint of the carbon steel pipe test section in the exit area. Thus, the pressure transducers at the inlet and outlet points were 72 ft apart from each other.

4.3.6 Exit Section

The exit section comprises a 6-inch PVC pipe with a length of 3 ft, connected to the carbon steel pipe section via a bolted flange connection, as illustrated in Figure 4.8. To monitor and record the water temperature and assessed any heat gain during water flow in the 100-ft carbon steel test section, a second thermocouple was installed on the PVC line at a distance of 1 ft 5 in. from the flange connection of the carbon steel pipe.



Figure 4.8 Thermocouple Installed at Exit Section

4.3.7 PVC Pipe Return Section

The PVC pipe return section was fabricated to create the closed loop of the test section. At the downstream of the exit section, a 90° PVC elbow was connected to turn the PVC line at 90°, as shown in Figure 4.9. The returning PVC section perpendicular to the carbon steel pipe was 20 ft in length.



Figure 4.9 PVC Pipe Return Loop

At the downstream of this 90° elbow turn, a 6-in. air release valve was installed at a distance of 14 ft, as represented in Figure 4.10 (a). The air release valve was installed to release any entrapped air bubbles from the test setup in order to record the accurate head/pressure measurement at the pressure transducers.

A 6 in. electromagnetic flow meter “iMAG 4700 series” as shown in Figure 4.10 (b), was installed at 46 ft from the air release valve to measure the water flow in the test setup. The flow meter could record the bi-directional flow of the fluid in the test setup. The pressure rating of the flow meter was 150 psi. The accuracy of the flow meter reading was +/- 1%. The maximum flow capacity of the flow meter was 2,891 GPM. The downstream PVC pipe was selected to install the flow meter so that enough straight length of pipeline was provided to get accurate measurement of the water flow.

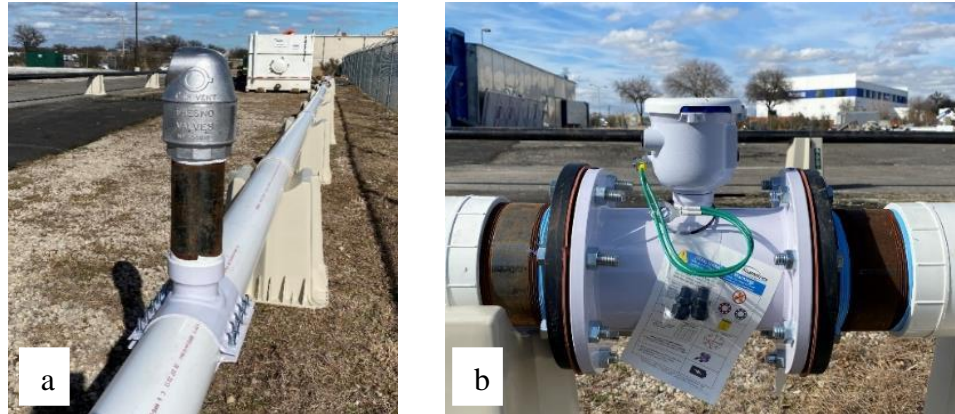


Figure 4.10 (a) Air Release Valve (b) Magnetic Flow Meter

A rubber pipe hose of 6 in. diameter, 30 ft was connected at the end of the PVC pipe to close the test loop. One end of the hosepipe was connected to the PVC return section, and another end was connected to the 6 in. gate valve, as shown in Figure 4.11. The gate value was connected to shut off the water supply from the test setup to the water tank.



Figure 4.11 Test Setup End Loop Connection to Water Tank

As shown in Figure 4.11, the gate valve had a two-way connection to the water tank to decrease water flow velocity while returning to the tank. One hose pipe 6 in. of 9 ft length connected the gate valve and water tank. Another hose pipe 4 in. of 20 ft length connected the gate

valve and water tank. The two-way connection helped to minimize the turbulence effect while returning the water supply to the tank.

4.3.8 Data Acquisition System (DAQ)

A Micro Measurement system 8000 was used to connect transducers and flow meter to monitor and to record data during each test run. The data was continuously monitored and recorded at the required frequency of time. The thermocouples were connected to the Omega Engineering thermocouple data logger to record the temperature at the entrance and exit point of the carbon steel pipe test section during the test run.

4.4 Bare Pipe Test

The bare pipe test was performed on a 6 in. new carbon steel pipe schedule 40 with the corresponding pipe internal diameter 6.065 in. The test was designed at a high Reynolds number, that is, the flow velocity of the water flowing through the pipe was high.

Five test runs were performed; however, the ambient temperature variation was considered as an essential factor in selecting the test time during the test run. Water temperature was considered an important factor when the test was performed. During these test runs, the ambient temperature was in the range from 55 °F to 61 °F, and the water temperature was between 61 °F to 65 °F. The air conditioning unit installed in the tank system was continuously running to reduce any increase in the temperature due to the heat produced by the water pump.

During the experiment, five test runs were conducted, and the variation in ambient temperature was considered a crucial factor in determining the appropriate start time for each test. During these tests, the ambient temperature was in the range of 55 ° F to 61 ° F, and the water temperature was between 61 ° F and 65 ° F. To mitigate any temperature rise caused by the water

pump's heat generation, the air conditioning unit installed in the tent system was operated continuously.

The duration for each test run was 55 minutes. The pump was operated from 800 GPM to 1,800 GPM, at an increment of 100 GPM. The readings were recorded starting from 800 GPM and then increased by 100 GPM until reaching 1,800 GPM. Each flow rate was operated for 5 minutes so that a turbulent flow at a steady-state regime was maintained, and the corresponding readings were collected. The pressure readings at the inlet and outlet points were recorded using the DAQ system at a frequency of 10 readings per second. The water temperature was continuously monitored so that the correct value of the kinematic viscosity based on the water temperature was considered in calculating the friction factor. After completing the bare pipe test, a similar test procedure was followed to test the lined pipe.

4.5 Lined Pipe Test

The purpose of this experiment was to evaluate the friction factor of the lined pipes that can be used in pressure pipes. The test quantified the expected magnitude of the improvement of the friction factor due to liner application. The study conducted on the carbon steel pipe lined with a liner system included two products, the liner, and the topcoat.

4.5.1 Liner Installation

The thickness of the liner system was 85-90 mils including the primer thickness. The purpose of installing the liner in this test was to mitigate the impact of corrosion-induced roughness. The experiment was carried out on the lined pipe under similar experimental conditions as the bare pipe testing.

4.5.2 Sand Blasting

Sand blasting was the first step for preparing a carbon steel pipe for the liner application. Sand blasting was also known as abrasive blasting, and it was a surface finishing process that involves the use of an air compressor and a sand blasting machine. Sand blasting machine sprays the sand particles with high pressure against the surface of the carbon steel pipe to smoothen it by removing rust and other contaminants on the surface of the pipe. Figure 4.12 shows the inside view of carbon steel pipe before sand blasting process. The primary purpose of the sand blasting was to create a clean and profiled surface so that the polymeric resin liner adhered to the 6 in. steel pipe.



Figure 4.12 Inside View of Carbon Steel Pipe before Sand Blasting

This process of cleaning the pipe using the sand blasting technique was carried out for two complete passes to ensure that the surface was free of irregularities and any contaminations. The total time taken for sand blasting was approximately 2 hours 30 minutes. Sand blasting was also performed to achieve 2 to 3 mils of anchor profile, which was required for a good bonding of the liner application to the host pipe. The sand blasting machine is shown in Figure 4.13.



Figure 4.13 Sand Blasting Machine

Figure 4.14 shows the sand blasting machine being sanding inside the pipe from one end.



Figure 4.14 Sand Blasting Before Liner Application

The sand blasting machine was connected to the sand blasting medium and air compressor on the truck. Figures 4.15 show the sand blasting of pipe in progress.



Figure 4.15 Sand Blasting in Progress

Figure 4.16 represented the inside view of the pipe after the sand blasting was completed. Sand blasting achieved the SP5 white blast with 2 to 3 mils of anchor profile.



Figure 4.16 Inside View of Pipe After Sand Blasting

4.5.3 Primer and Liner Application

The liner application started the day after the blasting was completed. One coat of 4-5 mils thickness of primer was applied inside the carbon steel pipe prior to the liner installation. Using a

spin-cast machine, the primer was sprayed uniformly on the inside circumference of the pipe. Figure 4.17 shows the spin-cast used both for the primer and liner installation.



Figure 4.17 Spin Cast for Liner Application

The spray head was positioned at the entrance of the pipe and begins its operation from one end of the pipe section at a speed of 24 ft/min with the spray head rotating until it travels to the other end of the pipe section. The speed of the spin cast machine was operated from a control station. The spin cast cone spins at approximately 10,000 rpm when it was dry, but it slows down to 8,500-9,000 rpm when polyurea material starts spraying. Figure 4.18 shows the spin cast applying the primer to the bare pipe.



Figure 4.18 Primer Application in Progress

Primer was touch dry in 3 to 4 hours. Figure 4.19 shows the inside view of the pipe with primer application.



Figure 4.19 Inside View of Pipe After Primer Application

After the primer was completely dry, the liner was sprayed inside the carbon steel pipe using a spin cast machine which sprays the resin material uniformly along the circumference of the pipe.



Figure 4.20 Inside View of Pipe After Liner Application

The spray head was positioned at the entrance of the pipe and began its operation from one end of the pipe section at a speed of 24 ft/min. The spin cast cone spined at approximately 10,000 rpm when it was dry, but it slowed down to 8,500-9,000 rpm when polyurea material started

spraying. The frequency of the spin cast machine was operated from a control station. The liner thickness of approximately 85 to 90 mils was achieved in one pass. After applying the polymeric resin to the surface of the pipe, it was allowed to dry out completely for 24 hours to ensure optimal bonding between the liner and the pipe's surface. The curing process was done at ambient temperature. Figure 4.20 shows the liner application on the pipe sample.

The test setup was reinstalled after 3 days of liner application. All the experimental conditions such as pump, instrumentation, loop length and the position of the instrumentation remained the same, so that comparable results can be achieved.

In the calculations, for the pipe diameter, the liner thickness was deducted to calculate the net effective diameter of the pipe. The internal diameter was measured manually with a digital caliper.

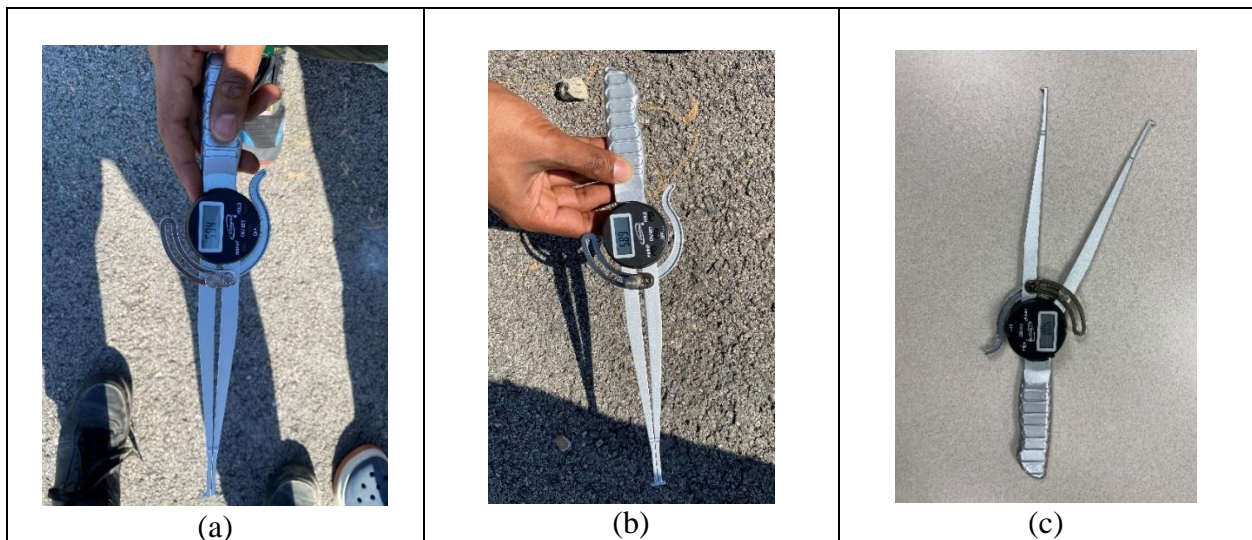


Figure 4.21 Measured Internal Pipe Diameter with a Digital Caliper

The digital caliper can measure the internal diameter of the pipe from 0.5 in. to 8 in. with an accuracy of 0.01 in. Figure 4.21 (a), (b), and (c) shows examples of the measured readings of the pipe diameter with digital caliper. The known internal diameter of the PVC pipe was measured

with the digital caliper to calibrate the device. The measured internal diameter of the PVC pipe with digital caliper was 6.04 in. as compared to the known pipe diameter of 6.03 in. Therefore, 0.01 in. was used as calibration parameter for all the measured values of the internal diameter of the carbon steel pipe with installed liner. Thus, all measurements for the internal diameter were subtracted by 0.01 in. Table 4.1 shows the average internal diameter of the pipe after liner application was 5.894 in.

Table 4.1 Measured Internal Pipe Diameter with a Digital Caliper

Measurement #	Measured Distance from Flange Connection at Entrance	Internal Diameter (in.)			
		Vertical	Horizontal	Left Diagonal	Right Diagonal
1	6 in.	5.940	5.970	6.020	6.030
2	1 ft 6 in.	5.620	5.970	5.930	5.950
3	2 ft.	5.970	5.820	5.750	5.760
4	2 ft 5 in.	5.880	5.900	5.920	5.880
	Average	5.853	5.915	5.905	5.905
Average Internal Pipe Diameter (in.)		5.984			

$$\begin{aligned} \text{Liner thickness} &= \text{Original pipe internal diameter (in.)} - \text{Measured internal diameter after liner application (in.)} \\ &= 6.065 \text{ (in.)} - 5.894 \text{ (in.)} = 0.170 \text{ in./2} = 0.0853 \text{ in.} = 85.3 \text{ mils} \approx 85 \text{ mils} \end{aligned}$$

$$\begin{aligned} \text{Net effective pipe diameter} &= \text{Original pipe diameter (in.)} - 2 \times \text{liner thickness (in.)} \\ &= 6.065 - 2 \times 0.08 = 5.895 \text{ in.} \end{aligned}$$

Figure 4.22 shows the graphical representation of the measured pipe internal diameter with a digital caliper represented in Table 4.1. Figure 4.23 shows the distance of these measurements from the flange connection.

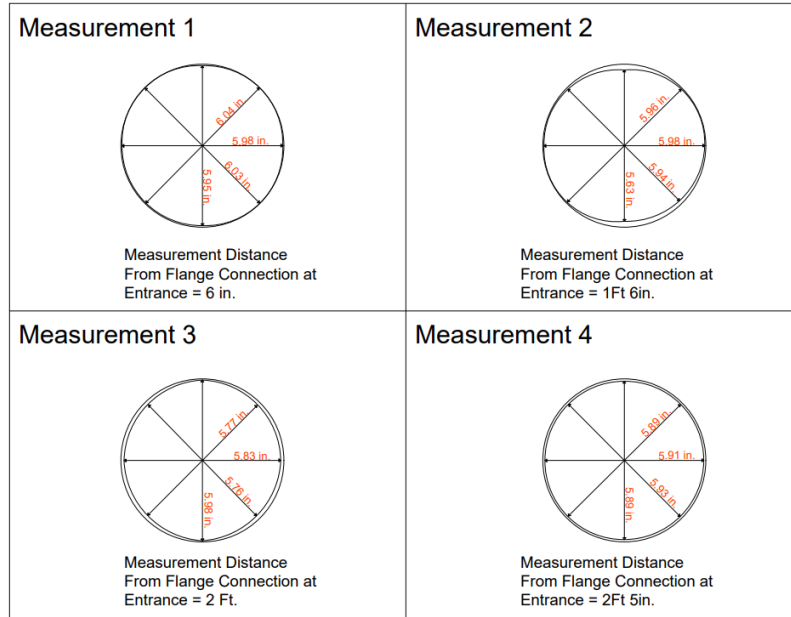


Figure 4.22 Measurements at Different Distances from Flange Connection

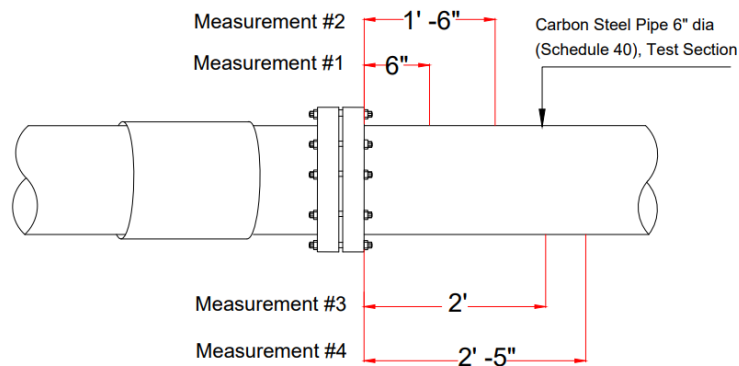


Figure 4.23 Pipe Internal Diameter Readings at Different Distance from Flange Connection at Entrance Section

4.5.4 Lined Pipe Test

The test setup was similar to the bare pipe test. The fluid used in the experimental setup was clean tap water. The test was designed at a high Reynolds number, that is, the flow velocity of the water flowing through the pipe was high.

Six test runs were performed; however, the temperature variation was considered as an important factor in scheduling determining the appropriate start time for each test. Water

temperature was continuously monitored to apply the correct value of kinematic viscosity of water for performing Reynolds number calculations. During these test runs, the water temperature was between 58 °F to 69 °F. The air conditioning unit installed in the tank system was continuously running to reduce any increase in the temperature due to the heat produced by the water pump.

The duration for each test run was 55 minutes. The pump was operated from 800 GPM to 1,800 GPM, at an increment of 100 GPM. The readings were recorded starting from 800 GPM and then increased by 100 GPM until reaching 1,800 GPM. Each flow rate was operated for 5 minutes so that a turbulent flow at a steady-state regime was maintained, and the corresponding readings were collected. The pressure readings at the inlet and outlet points were recorded using the DAQ system at a frequency of 10 readings per second. The water temperature was continuously monitored so that the correct value of the kinematic viscosity based on the water temperature was considered in calculating the friction factor. After completing the bare pipe test, a similar test procedure was followed to test the lined pipe.

After collecting the data, the head loss was calculated at each GPM between the entrance and exit point. The mean velocity (v), Reynolds number (Re), friction factor (f), relative roughness (ϵ/d) were calculated for each flow rate. These calculations were performed for each test run.

4.6 Chapter Summary

This chapter provided the detailed testing methodology adopted to determine the hydraulic flow properties of the lined pipe. The chapter provided detailed information on test design and the instrumentations installed for collecting various study parameters such as head loss, flow, and temperature. The data was collected to determine various parameters such as friction factor, Reynolds number, and roughness factor. The detailed results of the analysis are provided in Chapter 5.

Chapter 5 Results and Discussion

5.1 Introduction

This chapter presents the results and analysis of the experimental test conducted in Chapter 3 and Chapter 4. The results are presented in five sections such as 1) Material Testing, 2) Short-term hole spanning internal hydrostatic pressure test, 3) Vacuum pressure test, 4) Pressure integrity test, and 5) Hydraulic flow properties test.

5.2 Material Testing Results

5.2.1 Hybrid Polyurea Flexural Strength and Modulus

Failure will occur when the strain or elongation exceeds the material's limits. The flexural strength represents the highest stress experienced in the outer fiber of the test specimen before it breaks or yields. It is measured in terms of stress at the midpoint. Figure 5.1 illustrates the bending load versus displacement curves for all specimens. The sudden drops in these curves indicate failure (fracture) of specimen.

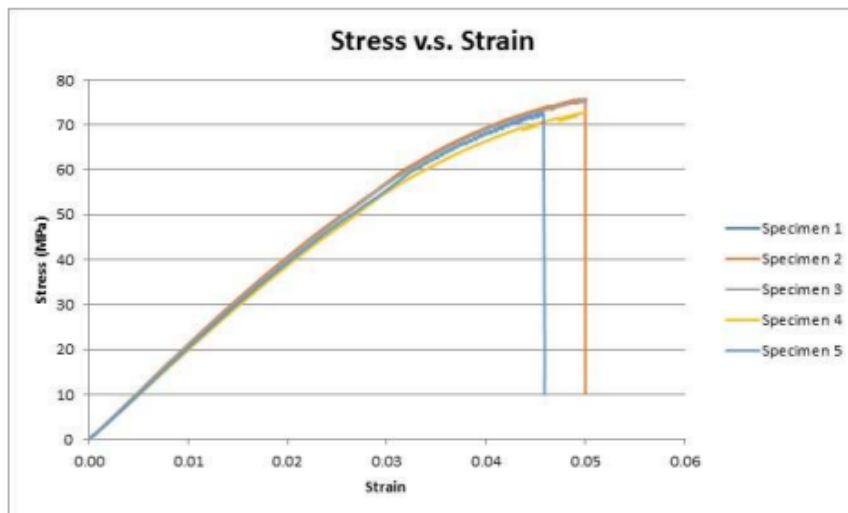


Figure 5.1 Flexural Stress vs. Strain

After removing the outlier's effects, the average calculated maximum flexural stress for hybrid polyurea was 10,730 psi. The flexural elastic modulus is the ratio of stress and corresponding strain, within the elastic limit. The flexural modulus is calculated by drawing a tangent line to the sharpest straight line of the load-deflection curve as shown in Figure 5.1 and using the following Equation 5.1 from ASTM D790.

$$E = \frac{L^3 m}{4bd^3} \quad 5.1$$

Where, E = Modulus of elasticity in bending, psi

L = Support span, in.

b = width of specimen tested, in.

d = depth of specimen tested, in.

m = slope of the tangent to the initial straight-line of the load-deflection curve, lbf/in. of deflection

Hence, the average calculated flexural elastic modulus for the hybrid polyurea Polymeric material was 303,000 psi.

5.2.2 Hybrid Polyurea Tensile Strength and Modulus

Figure 5.2 illustrates the load versus strain curves for specimens. The graph showed that during the initial loading, the stress vs strain curve is linear straight line, i.e., stress is directly proportional to strain. This is known as elastic region. After the elastic region, the material experiences the plastic behavior, where permanent deformation occurs. The final stage is the rupture stage where the increase in load breaks the material as illustrated in Figure 5.2.

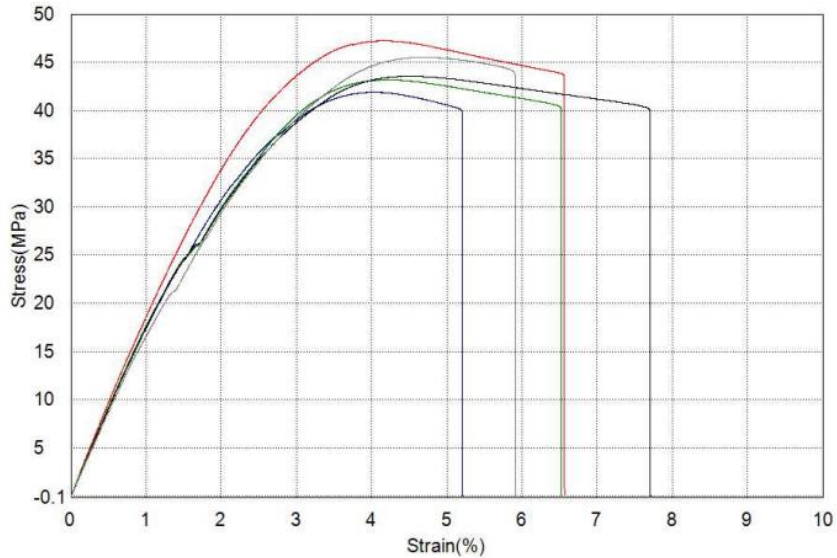


Figure 5.2 Tensile Load vs. Strain

The sudden drops in these curves indicated failure (fracture) of the material. The tensile modulus determines the material elasticity, and it is the ratio of load to corresponding strain within the linear elastic region. It was calculated by drawing a tangent or taking a slope to the steepest initial straight-line portion, which is the linear elastic region of the load-strain curve as shown in Figure 5.2. The average maximum tensile strength calculated for hybrid polyurea Polymeric material was 6,235 psi, and the tensile modulus was 280,600 psi.

5.2.3 Pure Polyurea Tensile Strength

The average tensile stress vs. strain graph for pure polyurea material is shown in Figure 5.3. Pure polyurea material was more elastic and showed more strain percentage. The calculated yield tensile strength of the material was 950 psi at 6% strain. The material elongates up to 300% at an ultimate tensile strength of approximately 3,300 psi, and the tensile modulus, E, calculated was approximately 25,900 psi.

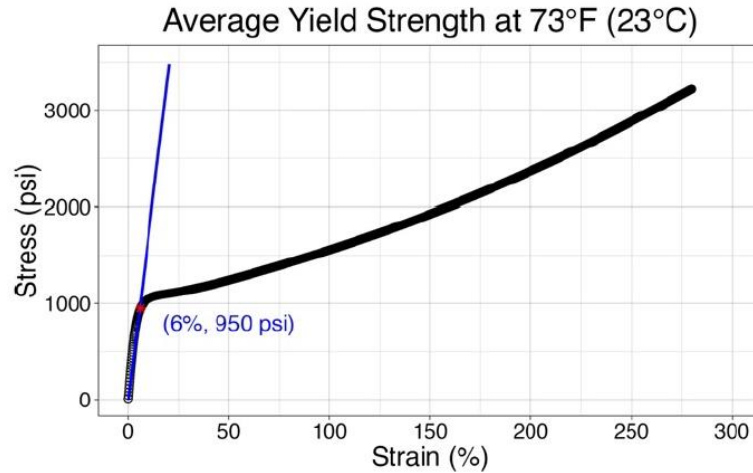


Figure 5.3 Average Tensile Stress vs. Strain

5.2.4 Hybrid Polyurea Punch Shear Strength

The load vs. strain graph for six specimens of hybrid polyurea material is shown in Figure 5.4. The shear strength is calculated by dividing the force required to shear the specimen by the area of the sheared edge. The area of the sheared edge is equal to the circumference of the punch multiplied by the thickness of the specimen. The calculated average shear strength of the polymeric material is $\tau = 4,800$ psi.

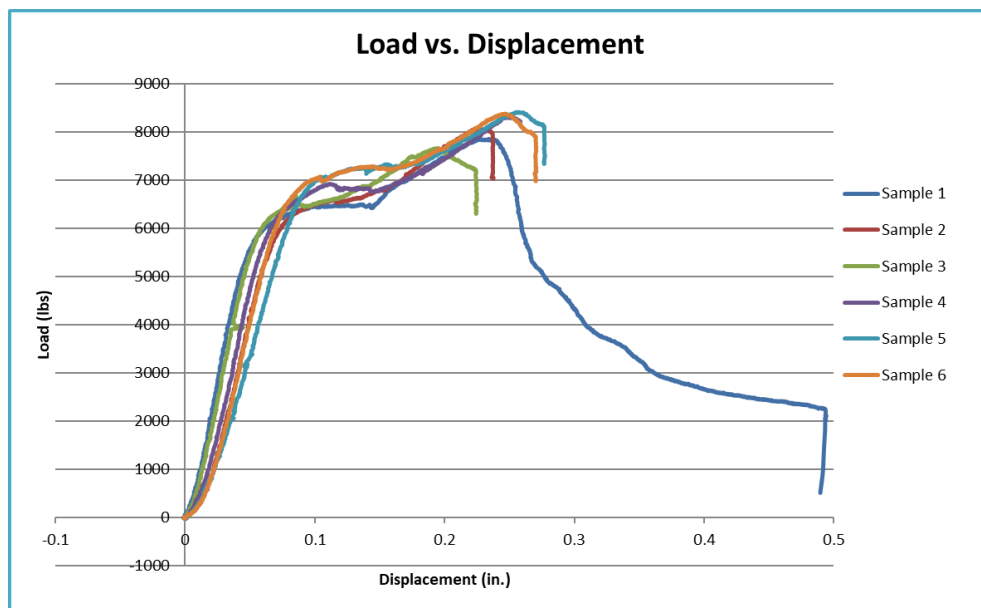


Figure 5.4 Punch Shear Load vs. Displacement

5.3 Short-term Hole Spanning Hydrostatic Pressure Test Results

Three full-scale laboratory tests were performed with hole sizes of 0.5, 1, and 2 in. The target pressure for these tests was 500 psi. The results of these tests are presented in Table 5.1.

Table 5.1. Test Results Short-term Hole Spanning Testing

Pipe Sample #	Pipe Sample Diameter (in.)	Hole Size (in.)	Liner Thickness (in.)	Internal Pressure Reached (psi)	Pressure Holding Time (hours)	Sample Failure	Liner Inspection after Test	Strain Value at Hole Spanning
1	30	0.5	0.25	490	2	No Failure	No Delamination, cracks, or bulging	Space constraint for installation of Strain Gauge.
2	30	1.0	0.75	495	24	No Failure	No Delamination, cracks, or bulging	Strain Gauge showed off scale during testing
3	30	2.0	0.75	485	240	No Failure	No Delamination, cracks, or bulging.	0.62 % of strain at hole spanning.

As represented in Table 5.1, the three pipe samples with holes spanning 0.25, 1, and 2 in. were able to resist the internal pressure of approximately 500 psi without any indication of liner failure, cracking, or bulging. After the short-term pressure test of these samples were completed, then, the internal pressure of the test setups was held for a few hours. The liner exhibited satisfactory performance at the hole spanning, showing no indications of liner failure or bulging.

Figure 5.5 shows the incremental and maximum pressure values recorded by a pressure transducer installed on a pipe sample with a 1-inch hole spanning.

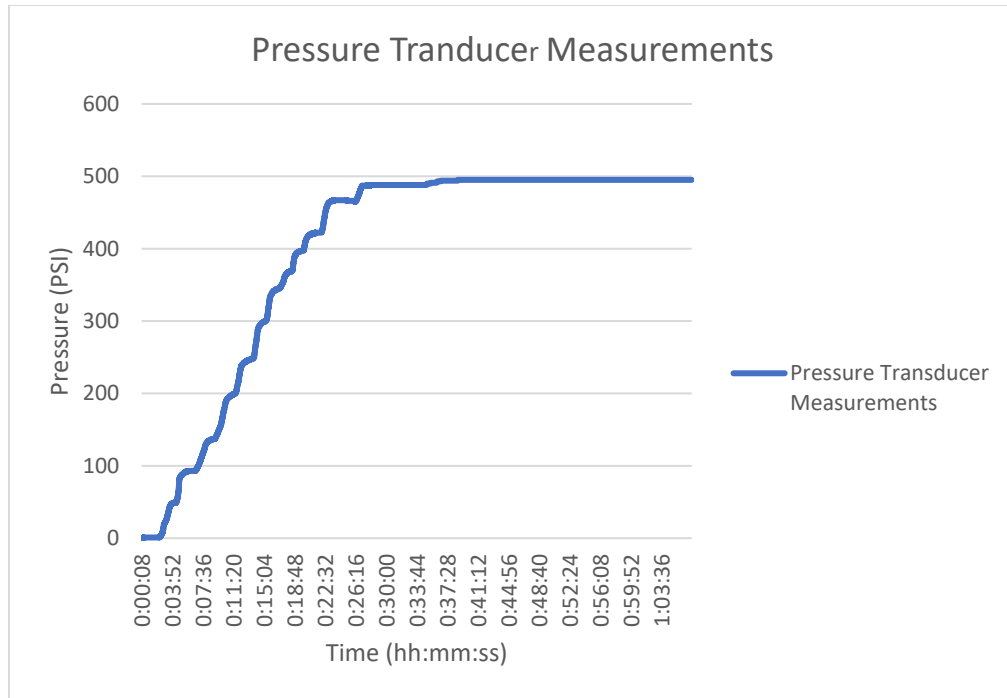


Figure 5.5 Pressure Transducer Measurements (1 in. Hole Spanning Pipe Sample)

The x-axis shows time, whereas the y-axis shows the pressure in psi. The pressure increment of approximately 50 psi was used to achieve the desired pressure in the test setup. The maximum pressure recorded was approximately 495 psi. During this test setup, a strain gauge was attached to the 1-inch hole spanning, but unfortunately, it showed off-scale readings throughout the test and the strain gauge data was lost. However, a visual inspection of the liner at the hole spanning indicated no signs of liner failure or any noticeable bulging. The liner demonstrated its ability to effectively rehabilitate corrosion cracks measuring up to 1 inch.

Figure 5.6 shows the incremental (approx. 50 psi) and maximum pressure (approx. 485 psi) recorded by a pressure transducer installed on a pipe 2-inch hole spanning sample. The x-axis shows time whereas y-axis shows pressure. Figure 5.7 shows the strain values obtained from the strain gauge that was installed on the liner exposed through 2 in. hole spanning. The x-axis shows the time, whereas the y-axis shows the strain values in the microstrain ($\mu\epsilon$).

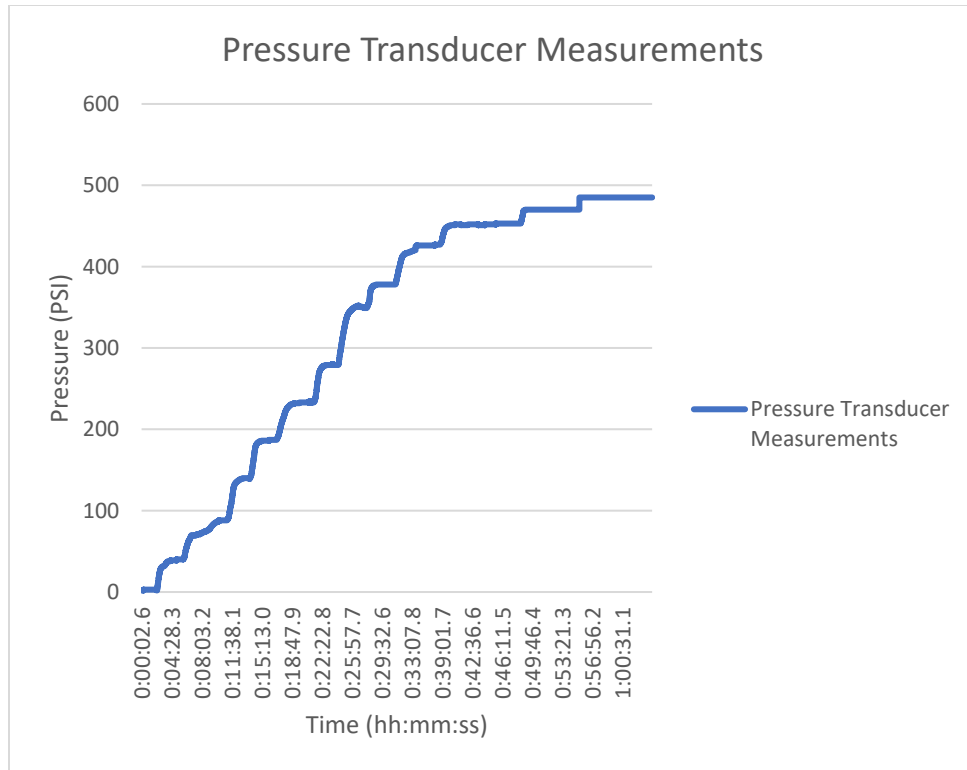


Figure 5.6 Pressure Transducer Measurements (2 in. Hole Spanning Pipe Sample)

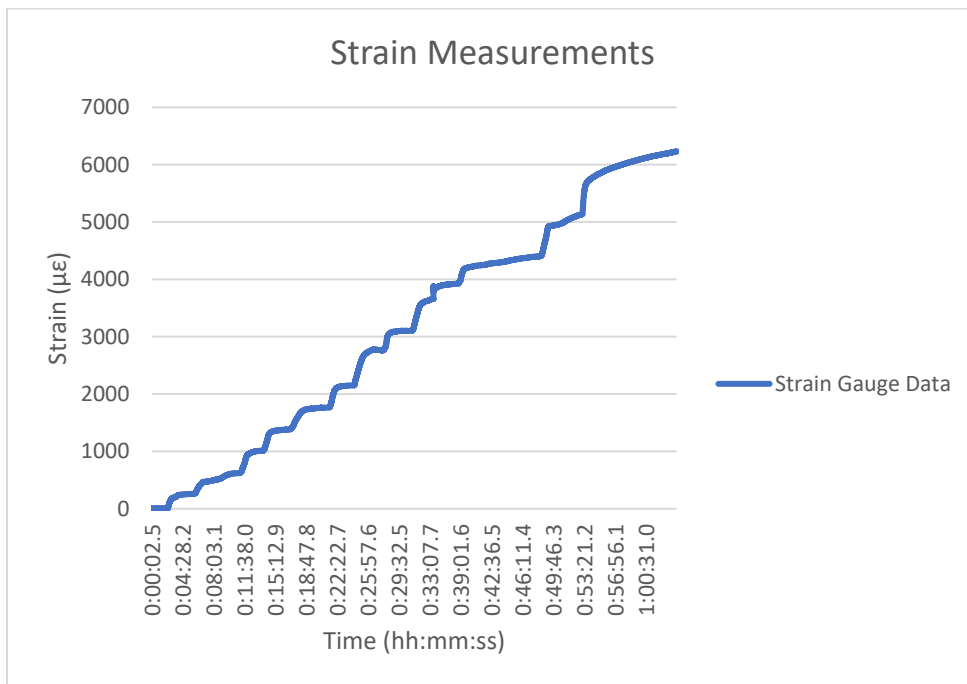


Figure 5.7 Strain Measurements at 2 in. Hole Spanning

The maximum strain value obtained at 485 psi pressure was approximately 6,200 $\mu\epsilon$, equal to 0.62% of strain. The percentage strain obtained was less than 5%, a recommended long-term performance strain of buried high density polyethylene pipes (HDPE) (Janson, 1981; Peggs et al., 2005). The material showed good resistance properties for high pressure values.

Figure 5.8 below represents the plotted stress vs. strain graph based on the strain data obtained from the strain gauge utilized in the experimental test. The stress was calculated from experimental strain values and using the modulus of elasticity (E) of the material obtained from tensile coupon test. The strain values obtained in the experiment was approximately recorded at 10 data point per second throughout the test duration of 1 hours. Consequently, a total of approximately 36,500 data points were utilized to plot the graph depicted in Figure 5.8.

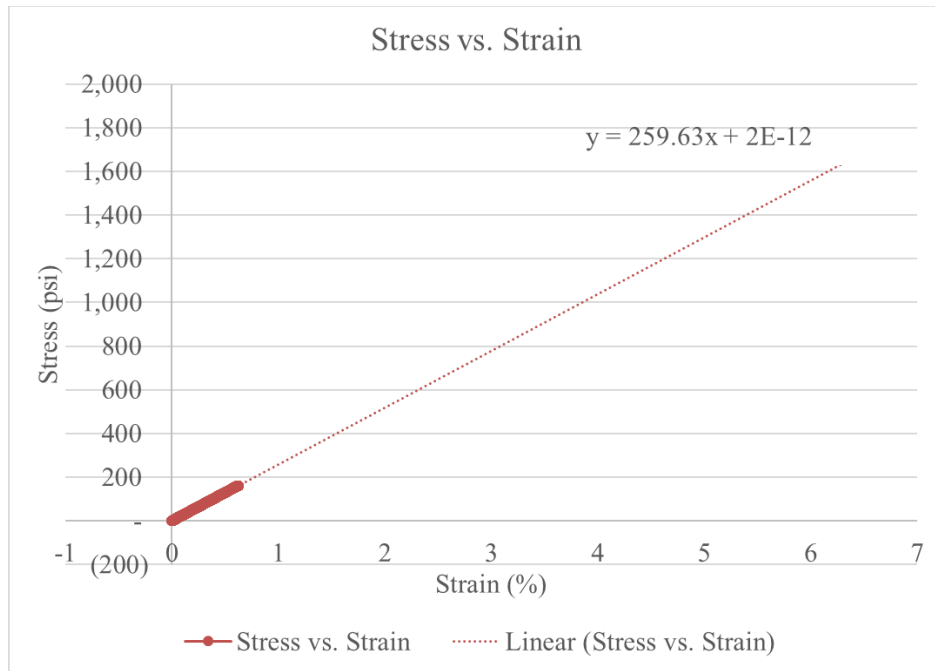


Figure 5.8. Stress vs. Strain (Obtained from Strain Gauge Data)

Figure 5.8 illustrates that the stress vs. strain values have a linear relationship. As the stress increases, the % strain increases. The linear relationship indicates that the material was experiencing stress and strain within the elastic stage of the material. The maximum strain %

obtained from the experimental results was 0.62%, and the stress generated in the material at this strain was approximately 162 psi. Based on the experimental results, the stress and strain values were extrapolated up to 6% of strain using linear regression, represented with a dotted line, as shown in Figure 5.8. The stress vs. strain data was extrapolated to compare the strain gauge data with the stress-strain graph obtained from the laboratory coupon tensile test. This analysis allowed for a comparison between the measured strain from the strain gauge and the corresponding stress values derived from the stress-strain graph of tensile coupon test.

Figure 5.9 shows the stress vs. strain graph obtained from the material tensile coupon test performed in the laboratory.

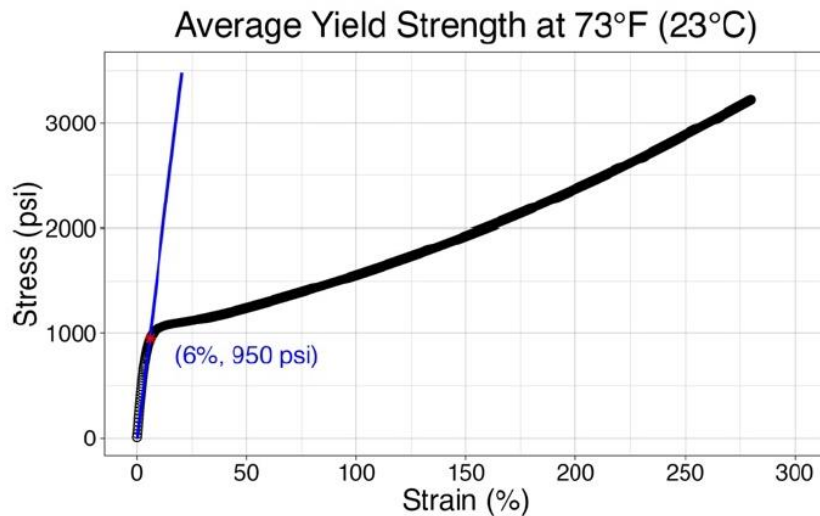


Figure 5.9 Stress vs. Strain (Obtained from Tensile Coupon Test)

Figure 5.9 shows the strain (%) on the x-axis and stress (psi) on the y-axis. These values of stress and strain were obtained during testing of the material at a temperature of 73° F. It was determined that the material has an average yield stress of 950 psi at a strain of 6%. Within the elastic limit, the material can sustain a stress of approximately 950 psi while experiencing a deformation of 6%.

The experimental stress calculated from a 2-inch hole spanning strain gauge was 162 psi at a deformation of 0.62%. Whereas interpolating the tensile coupon test stress vs. strain graph (Figure 5.9), at 162 psi stress, the strain is 1.02%, which is approximately double the 2-inch hole spanning strain gauge data. This indicates that the material deformation was less during the experiment as compared to the laboratory tensile testing. For this stress difference, there are two reasons identified. First, the material testing in the laboratory was conducted at 73° F, whereas the experiment was performed at an approximate ambient temperature of 54° F, and the water temperature of the test setup was 50° F. The elastomeric properties of liner material behave differently at different temperatures. The material behaves stiffer at lower temperatures as compared to higher temperatures. Thus, at a temperature of 50° F, the material showed better performance and experienced less deformation than the material properties tested at 73° F. Second, in the experimental conditions, the liner material exposed through the hole spanning was not experiencing pure tension. It experienced tension at the outer surface and compression at the inner surface.

Based on the comparison of stress and strain with the tensile coupon test graph, it can be observed that the material experienced stress and strain within the elastic range. Additionally, three pipe samples designed using modified AWWA Equation 3.2 demonstrated the ability to withstand the required pressure resistance of 500 psi. As a result, it was concluded that the experimental results indicated that modified AWWA design Equation 3.2 provided a suitable thickness to effectively bridge corrosion holes, as tested up to 2 inches in hole spanning.

5.4 Vacuum Pressure Testing Results

The vacuum pressure achieved was 24.6 in. of Hg in 28 minutes. The vacuum pump was continuously operated at 24.6 in of Hg for two hours. During the test, no cracks, failures, or

delamination of liner from the host pipe were observed. Thus, it was implied that the liner material successfully resisted the internal vacuum pressure of 24.6 in. of Hg without any delamination and cracks. The test results demonstrate a strong bonding strength between the liner and the host pipe. Therefore, it can be inferred that occasional negative pressure generated during the pipeline cleaning process will not affect the bonding strength of the liner when it is designed as Class II with adhesion to the host pipe.

5.5 Pressure Integrity Test Results

The pressure integrity test was designed to evaluate the resistance of the liner when applied as a fully structural. Bare liner pipe samples with varying thicknesses were tested under internal hydrostatic pressure at temperatures of 73° F, 120° F, 150° F and 41° F. The burst pressure values and time-to-failure were obtained during the test. It was observed that the failure modes of the pipe samples and the behavior of the material were different at different temperatures. The different failure modes were a result of the varying strength of the polymeric material when exposed to different temperatures. It was also observed that the strength of the pipe samples changed with test temperature. The following failure modes were identified during the testing.

Catastrophic failure: A catastrophic failure occurred when the pipe samples were shattered into pieces, which implied the brittle response of the pipe to pressure resistance. Failure was defined as bursting, cracking, splitting, weeping, or leaking fluid from the pipe samples during the test.



Elastic and catastrophic failure: An elastic and catastrophic failure was characterized when the pipe samples deformed and cracks were generated, consequently, the failure resulted in a few shattered pieces. Thus, this behavior showed both elasticity and a slight brittle characteristic of the pipe samples during pressure resistance.




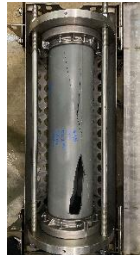

Ductile failure: A ductile failure was observed when the pipe responded more elastically and physically changed its shape before ultimately splitting to a much less extent. This type of failure was caused by pressure loss, ballooning, cracks, and pinhole leaks which were observed in pipe samples.

5.5.1 Pressure Integrity Test Results at 73° F Temperature





Table 5.2 below represents the results of the pressure integrity test conducted at a temperature of 73° F. The table includes the following information: sample number, sample thickness (in.), burst pressure (psi), failure time (seconds), failure mode of the pipe sample, any special material behavior observed, a picture of the pipe sample failure, and the pre-test visual inspection.

Table 5.2. Pressure Integrity Test Results at 73° F





Pressure Integrity Test Data @ 73 °F Temperature							
Sample #	Sample thk (in.)	Burst Pressure (psi)	Failure Time (S)	Failure Mode	Any Special Material Behavior	Pipe Sample Failure Picture	Pre-test Visual Inspection
11	0.228	306	72	Catastrophic failure on seam line	Sample showed good pressure resistance		No Defects
10	0.249	409	66	Catastrophic failure on seam line	Sample exhibited higher pressure resistance compared to sample #11, despite having approximately the same thickness.		No Defects

Pressure Integrity Test Data @ 73 °F Temperature							
Sample #	Sample thk (in.)	Burst Pressure (psi)	Failure Time (S)	Failure Mode	Any Special Material Behavior	Pipe Sample Failure Picture	Pre-test Visual Inspection
16	0.250	272	54	Catastrophic failure on seam line	Sample demonstrated lower pressure resistance compared to samples #11 and #10, despite having approximately the same thickness.		Minor defect on the seam line
56	0.310	534	69	Catastrophic failure other than seam line	Sample illustrated high pressure at this thickness. Shattered failure but didn't fail at the seam line.		No Defects
35	0.334	258	48	Crack and split failure on seam line	Sample exhibited less pressure as compared to the sample # 56 with approx. same thickness. Broken sample pieces showed the layers formation along the sample thickness.		No defects
45	0.336	100	30	Crack and split failure on seam line	Sample demonstrated less pressure as compared to sample # 56 with approx. same thickness.		Sample had irregularities or some weak joint at the seam line.
40	0.370	67	24	Crack failure	Material did not perform as expected, possibly due to the presence of joints or internal air bubbles. These factors may have contributed to the development of cracks failure during testing.		Sample might be internal defects. At one end, the gap intrusion was 0.184 in.

Pressure Integrity Test Data @ 73 °F Temperature

Sample #	Sample thk (in.)	Burst Pressure (psi)	Failure Time (S)	Failure Mode	Any Special Material Behavior	Pipe Sample Failure Picture	Pre-test Visual Inspection
49	0.388	550	72	Catastrophic failure on seam line	Material exhibited good pressure as compared to sample #31 with approx. similar thickness.		No defects
31	0.394	348	63	Crack and Split failure on seam line	Few pieces fell apart, but the primary cause of failure was attributed to cracks generated on the seam line.		Gap intrusion on one side of the pipe had a depth of 0.2875 inches and a thickness of 0.0205 inches.
4	0.502	660	54	Catastrophic failure on seam line	Shattered pieces showed the layers formation.		Minor defect on seam line
27	0.507	825	63	Catastrophic failure	Material not only shattered on the seam line, but also in other areas.		No defects

Pressure Integrity Test Data @ 73 °F Temperature

Sample #	Sample thk (in.)	Burst Pressure (psi)	Failure Time (S)	Failure Mode	Any Special Material Behavior	Pipe Sample Failure Picture	Pre-test Visual Inspection
60	0.532	810	60	Catastrophic failure on seam line	Material demonstrated good pressure resistance and good bonding between layers.		Very minor defects were seen on the seam line.
17	0.534	289	33	Crack failure but not on the seam line	Sample demonstrated less pressure as compared to sample # 27 with approx. same thickness. May be sample had internal defects.		No defects visual defects
48	0.618	925	60	Catastrophic failure other than seam line	Observed a good bonding between layers. When the sample was taken outside from water bath to tighten the bolts after the test run 5, small bulging areas were observed at different location due to pressurizing the pipe for couple of times.		No defects
33	0.631	1042	69	Catastrophic failure other than seam line	Sample demonstrated the highest pressure amongst 73 °F temperature tests.		No defects

As illustrated by the pipe sample failure pictures shown in Table 5.2, the pipe samples failed at 73° F, demonstrated a more catastrophic failure, and exhibited more resistance to pressure. These pipe samples had either no defects or minor defects, and they were shattered into pieces, implying brittle behavior of material during pressure resistance. Pipe samples #11, #10, #56, #49, #27, #60, #48, #33, #16 and #4 showed catastrophic failure and shattered into pieces at the burst point.

However, the pipe samples with the defects failed with less pressure resistance and demonstrated crack failure with leaks. Pipe samples #35, #45, #40, #31, and #17 showed crack failure. The failure mode of these pipe samples was cracking, splitting, weeping or leakage of fluid from the pipe during the test. The test results are summarized in Table 5.3 with burst pressure, time-to-failure, maximum pressure, and if the maximum pressure recorded was more than burst pressure. Multiple test runs were performed on some pipe samples so that the failure was achieved between 60 and 70 seconds as per ASTM D1599.

Table 5.3 Summary of Burst Pressure at 73° F

Sample #	Minimum Conditioning Time (hrs.)	Outer Diameter, OD (in.)	Total Number of Test Runs	Sample Thickness (in.)	Burst Pressure (psi)	Time-to-failure (s)	Max Pressure (psi)	Max Pressure > Burst Pressure
11	16	7.90	4	0.228	306	72**	306.2	No
10	16	7.89	4	0.249	409	66	409.0	No
16	16	7.93	2	0.250	272	54*	271.9	No
56	16	7.88	3	0.310	534	69	534.5	No
35	16	7.87	1	0.334	258	48*	258.5	No
45	16	7.89	1	0.336	100	30*	100.2	No
40	16	7.84	1	0.370	67	24*	67.4	No
49	16	7.90	3	0.388	550	72**	550.4	No
31	16	7.89	4	0.394	348	63	347.7	No

Sample #	Minimum Conditioning Time (hrs.)	Outer Diameter, OD (in.)	Total Number of Test Runs	Sample Thickness (in.)	Burst Pressure (psi)	Time-to-failure (s)	Max Pressure (psi)	Max Pressure > Burst Pressure
4	16	7.87	2	0.502	660	54*	659.9	No
27	16	7.85	4	0.507	825	63	824.9	No
60	16	7.86	4	0.532	810	60	909.0	Yes
17	16	7.91	1	0.534	289	33*	288.5	No
48	16	7.89	7	0.618	925	60	924.8	No
33	16	7.85	2	0.631	1042	69	1042.4	No

Note: *- if the time-to-failure < than 60 seconds and ** if the time-to-failure > than 70 seconds

Table 5.3 shows the burst pressure values of 15 samples. The time-to-failure of certain pipe samples was between 60 and 70 seconds, while others were less than 60 seconds or more than 70 seconds. Figure 5.10 shows the graphical representation of Table 5.3 and represents the correlation between the burst pressure and pipe sample thickness.

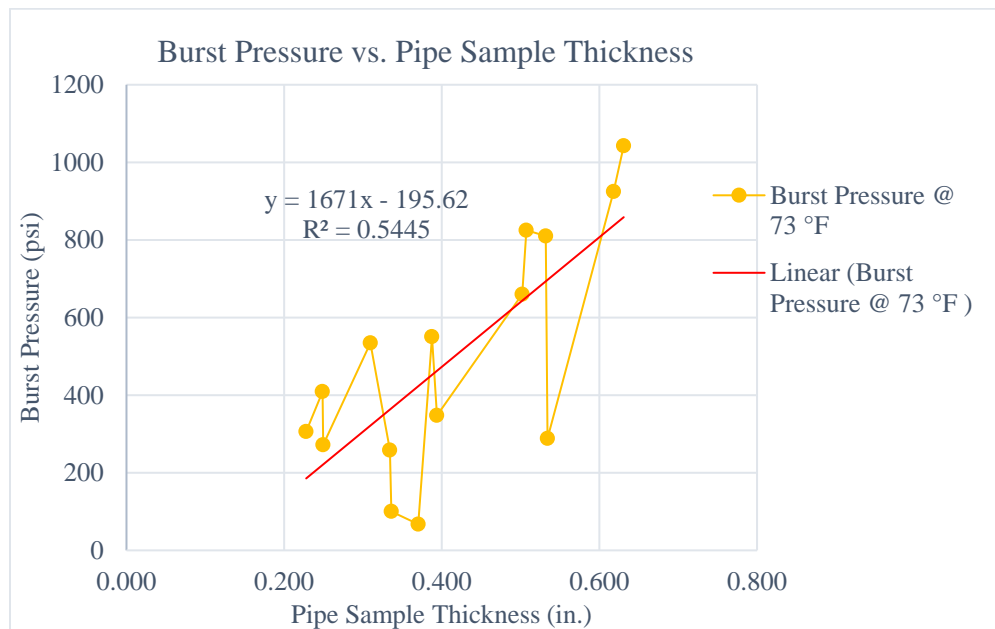


Figure 5.10 Burst Pressure vs. Pipe Thickness at 73 °F

As depicted in Table 5.3 and Figure 5.10, some pressure resistance values were abnormal compared to the rest. The dips in the graph showed pipe samples with less pressure resistance.

This can be attributed to the presence of defects, such as gap intrusions on the seam line. These defects created weak points in the pipe samples and resulted in a reduced effective thickness compared to other regions of the pipe.

Data Curation (excluding underperformed pipe samples with defects and excluding time-to-failure less than 60 seconds)

The pipes samples with abnormal pressure resistance values were identified and the pre-test visual inspection of these samples was checked. In the visual inspection column of Table 5.2, samples #45, #31 and #40 were found with seam line defects. In Table 5.3, it is depicted that samples #45, #31, #40, and #17 showed less resistance to pressure and failed with crack failure mode compared to other pipe samples. Sample #17 did not show defects in visual inspection but failed at a lower pressure resistance; therefore, it was implied that the sample could have internal defects. As a result, these samples were considered outliers and excluded from the data analysis.

Table 5.3 shows that for sample #60, the maximum pressure achieved in the previous test run was more than the burst pressure. But for the data analysis, the burst pressure of sample #60 was considered instead of maximum pressure, even though it represented a lower number.

The time-to-failure for pipe samples less than 60 seconds implied that the rate of pressure to the pipe sample was high, and the pipe failed before 60 seconds; thus, the values of the burst pressure were less. Therefore, pipe samples with a time-to-failure of less than 60 seconds were considered outliers. However, the time-to-failure of 72 seconds is close to 70 seconds, showing more conservative data. The pipe samples with a time-to-failure of 72 seconds were not considered outliers. Therefore, in the data curation, the time-to-failure of pipe samples with less than 60 seconds was excluded from the data set, but 72 seconds were considered.

Table 5.4 shows the data set excluding pipe samples with abnormal pressure resistance and time-to-failure less than 60 seconds. Figure 5.11 shows the graphical representation of this data set.

Table 5.4 Data Set at 73° F Excluding Outliers

Sample #	Minimum Conditioning Time (hrs)	Outer Diameter, OD (in.)	Total Number of Test Runs	Sample Thickness (in.)	Burst Pressure (psi)	Burst Time (s)	Max Pressure (psi)	Max Pressure > Burst Pressure
11	16	7.90	4	0.228	306	72	306.2	No
10	16	7.89	4	0.249	409	66	409.0	No
56	16	7.88	3	0.310	534	69	534.5	No
49	16	7.90	3	0.388	550	72	550.4	No
27	16	7.85	4	0.507	825	63	824.9	No
60	16	7.86	4	0.532	810	60	909.0	Yes
48	16	7.89	7	0.618	925	60	924.8	No
33	16	7.85	2	0.631	1042	69	1042.4	No

The data set from Table 5.4 is represented as best fit linear and quadratic regression curves in Figure 5.11.

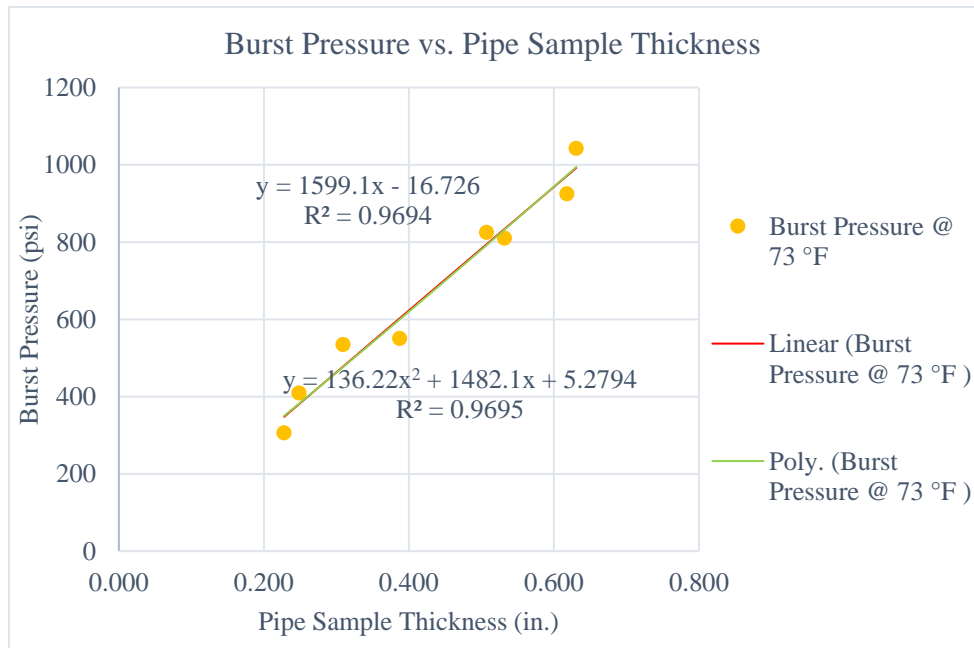


Figure 5.11 Burst Pressure vs. Pipe Thickness (after Data Curation)

Figure 5.11 shows the correlation between pipe thickness vs. burst pressure.

The linear regression equation is shown as below with $R^2= 0.9694$.

$$y = 1599.1x - 16.726 \quad 5.2$$

The quadratic regression equation is shown as below with $R^2= 0.9695$.

$$y = 136.22x^2 - 1482.1x + 5.2794 \quad 5.3$$


The R^2 for both liner and quadratic regressions is approximately 0.96; thus, both represent a higher degree of correlation between the pipe sample thickness and burst pressure.






Both linear and polynomial equations show approximately the same R^2 value of 0.96. Therefore, for simplicity and conservative liner design thickness, the approximate linear Equation 5.2 with R^2 value of 0.9694 can be used to estimate the burst pressure at any given thickness at a temperature of 73° F.





5.5.2 Pressure Integrity Test Results at 120° F Temperature

Table 5.5 below represents the results of the pressure integrity test conducted at a temperature of 120° F.

Table 5.5 Pressure Integrity Test Results at 120° F Temperature

Pressure Integrity Test Data @ 120° F Temperature							
Sample #	Sample thk (in.)	Burst Pressure (psi)	Failure Time (S)	Failure Mode	Any Special Material Behavior	Sample Failure Picture	Pre-test Visual Inspection
8	0.241	236.6	57	Elastic failure with burst near the seam line	Material behaved more elastic and failed with cracks.		No defects

Pressure Integrity Test Data @ 120° F Temperature							
Sample #	Sample thk (in.)	Burst Pressure (psi)	Failure Time (S)	Failure Mode	Any Special Material Behavior	Sample Failure Picture	Pre-test Visual Inspection
2	0.241	275.2	72	Elastic failure with burst near the seam line	Sample showed good pressure resistance at 0.241 in thickness. Good bonding between layers was observed.		Minor defects on seam line
44	0.267	74.2	33	Crack failure on seam line	Sample could not take pressure due to sample defects.		Defects on seam line. Gap intrusion of 0.054 to 0.125 in. (1.38 to 3.18 mm). Bulging at different points throughout the sample.
55	0.304	414.4	72	Elastic and catastrophic failure	Sample showed good pressure resistance. Good bonding between layers was observed. Minimal layers formation observed.		No defects
62	0.316	350	60	Elastic and catastrophic failure	Material took less pressure compared to #55. Good bonding between layers was observed. Minimal layers formation observed.		No defects
37	0.323	155	36	Crack failure on top end of pipe sample	Suspected that the sample had internal defects because sample showed less pressure resistance.		No visual defects, but pipe sample took less pressure and failed with crack.

Pressure Integrity Test Data @ 120° F Temperature							
Sample #	Sample thk (in.)	Burst Pressure (psi)	Failure Time (S)	Failure Mode	Any Special Material Behavior	Sample Failure Picture	Pre-test Visual Inspection
32	0.382	480.8	69	Elastic and catastrophic failure on seam line	Material showed good pressure resistance. Good bonding between layers was observed. Minimal layers formation observed.		No defects
46	0.39	434.3	72	Elastic and catastrophic failure on seam line	Material illustrated less pressure resistance compared to #32. Good bonding between layers was observed. Minimal layers formation observed.		No defects
20	0.456	455.7	63	Elastic and catastrophic failure on seam line	Sample showed less pressure resistance compared to #32 (0.382 in. thickness). May be due to defects on the seam line		Defects on the seam line and gap intrusion of 0.079 in. (2 mm)
39	0.539	557.7	60	Catastrophic failure on seam line	Sample demonstrated less pressure resistance compared to #26 at same thickness. Minor layer separation was observed at one end of the pipe sample. Suspected for internal defects		No visual defects






Pressure Integrity Test Data @ 120° F Temperature							
Sample #	Sample thk (in.)	Burst Pressure (psi)	Failure Time (S)	Failure Mode	Any Special Material Behavior	Sample Failure Picture	Pre-test Visual Inspection
26	0.539	639.7	72	Elastic and catastrophic failure on seam line	Good bonding between layers was observed. Minimal layers formation observed.		No defects
14	0.542	382.9	48	Cracks and fracture on seam line	Material showed less pressure resistance and fractured near the seam line. Less pressure resistance may be due to internal defects.		No visual defects
59	0.574	797.6	72	Elastic and catastrophic failure on seam line	Material demonstrated good pressure resistance. Good bonding between layers was observed. Minimal layers formation observed.		No defects
47	0.595	446	54	Cracks and fracture on seam line	Sample showed less pressure as compared to #59 because of defects on the seam line.		Sample was defective at the seam line. Major defects
57	0.614	819.5	66	Elastic and catastrophic failure on seam line	Sample could have taken more pressure at this thickness if the sample was not defective.		Minor defects on the seam line.

Table 5.5 includes the following information: sample number, sample thickness (in.), burst pressure (psi), failure time (seconds), failure mode of the pipe sample, any special material behavior observed, a picture of the pipe sample failure, and the pre-test visual inspection.

As illustrated by the pipe sample failure pictures shown in Table 5.5, the pipe samples failed at 120° F demonstrated an elastic and catastrophic mode of failure. These pipe samples failed due to deformation and they were shattered into fewer pieces compared to pipe samples tested at a temperature of 73° F. Additionally, the pipe samples showed elastic behavior and were deformed with crack formation. Thus, pipe samples demonstrated elastic and slightly brittle behavior to pressure resistance. Pipe samples #8, #2, #55, #62, #46, #20, #39, #26, #59, and #57, without defects showed an elastic and catastrophic failure. However, the pipe samples with defects failed under less pressure resistance and demonstrated crack failure with leaks. Pipe samples #44, #37, #14, and #47, with defects showed crack failure. The failure mode of these pipe samples was cracking, splitting, weeping, or leaking fluid from the pipe during the test.

The test results are summarized in Table 5.6 with burst pressure, time-to-failure, maximum pressure, and if the maximum pressure recorded was more than burst pressure. Multiple test runs were performed on some pipe samples so that the failure of the pipe samples was achieved between 60 and 70 seconds as per ASTM D1599.

Table 5.6 Summary of Pressure Integrity Test Results at 120° F

Sample #	Average Outer Diameter, D (in.)	Total Number of Test Runs	Average Thk t (in.)	Burst Pressure (psi)	Burst Time (s)	Max Pressure (psi)	Max Pressure > Burst Pressure
8	7.93	3	0.241	236.6	57*	285.5	Yes
2	7.88	2	0.241	275.2	72**	275.2	No
44	7.91	1	0.267	74.2	33*	74.2	No
55	7.86	2	0.304	414.4	72**	414.4	No
62	7.91	2	0.316	350	60	371.3	Yes
37	7.89	1	0.323	155	36*	155	No
32	7.84	3	0.382	480.8	69	480.8	No
46	7.89	2	0.39	434.3	72**	434.3	No

Sample #	Average Outer Diameter, D (in.)	Total Number of Test Runs	Average Thk t (in.)	Burst Pressure (psi)	Burst Time (s)	Max Pressure (psi)	Max Pressure > Burst Pressure
20	7.88	1	0.456	455.7	63	455.7	No
39	7.85	2	0.539	557.7	60	639.4	Yes
26	7.85	1	0.539	639.7	72**	639.7	No
14	7.86	1	0.542	382.9	48*	382.9	No
59	7.89	4	0.574	797.6	72**	797.6	No
47	7.88	1	0.595	446	54*	446	No
57	7.89	3	0.614	819.5	66	834.2	Yes

Note: *- if the time-to-failure < than 60 seconds and ** if the time-to-failure > than 70 seconds

Table 5.6 shows the burst pressure values of 15 samples. The time-to-failure of some pipe samples was between 60 and 70 seconds, some were less than 60 seconds, and some were more than 70 seconds. Figure 5.12 shows the graphical representation of Table 5.6 and represents the correlation between burst pressure and pipe sample thickness.

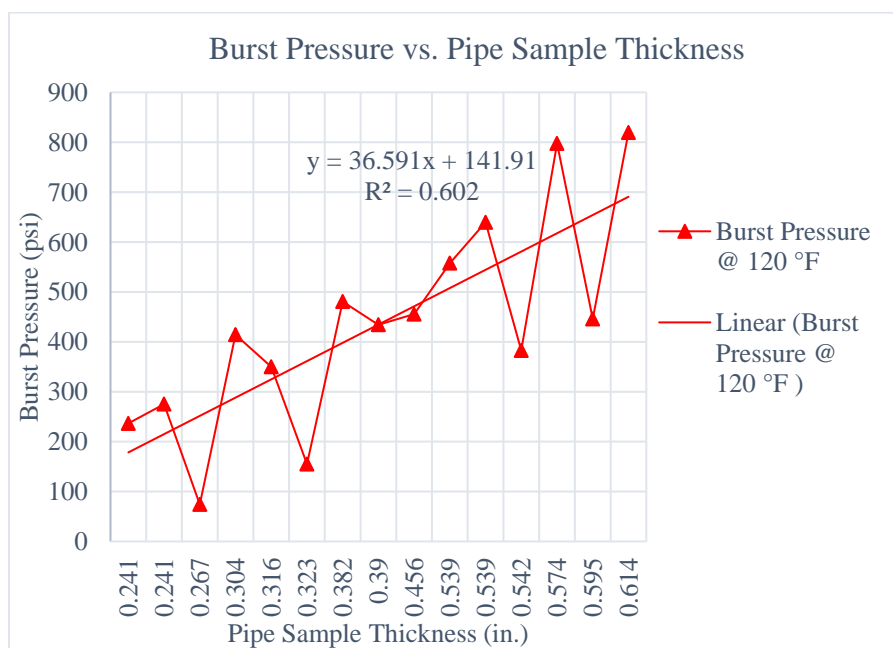


Figure 5.12 Burst Pressure vs. Pipe Thickness at 120° F

As depicted in Table 5.6 and Figure 5.12, some pressure resistance values were abnormal compared to the rest. The dips in the graph showed pipe samples with less pressure resistance.

This can be attributed to the presence of defects such as gap intrusions on the seam line or internal pipe defects that were not detected during visual inspection. These defects created weak points in the pipe samples and resulted in a reduced effective thickness compared to other regions of the pipe.

Data Curation (excluding underperformed pipe samples with defects and excluding time-to-failure less than 60 seconds)

The pipe samples with abnormal pressure resistance values were identified and the pre-test visual inspection of these samples was checked. In the pre-test visual inspection column of Table 5.5, samples #44 and #47 were found with major seam line defects and gap intrusions. From Tables 5.5 and 5.6, it is illustrated that samples #44 and #47 showed less resistance to pressure and failed with crack failure mode compared to other pipe samples.

No defects were found in the visual inspection of samples #37 and #14, but failed at a less pressure resistance; thus, it was implied that the sample could have internal defects. Hence, these four pipe samples were considered outliers and excluded from the data analysis.

In addition, the time-to-failure of pipe samples with less than 60 seconds were excluded from the data set, but 72 seconds was considered. Pipe sample #8 had a time-to-failure of less than 60 seconds and thus, it was considered outliers and excluded from the data set. Table 5.7 shows the data set of pipe samples after excluding outliers.

Table 5.7 Data Set Excluding Outliers at 120° F

Sample #	Average Outer Diameter, D (in.)	Total Number of Test Runs	Average Thickness t (in.)	Burst Pressure (psi)	Burst Time (s)	Max Pressure (psi)	Max Pressure > Burst Pressure
2	7.88	2	0.241	275.2	72	275.2	No
55	7.86	2	0.304	414.4	72	414.4	No
62	7.91	2	0.316	350	60	371.3	Yes
32	7.84	3	0.382	480.8	69	480.8	No
46	7.89	2	0.39	434.3	72	434.3	No
20	7.88	1	0.456	455.7	63	455.7	No
39	7.85	2	0.539	557.7	60	639.4	Yes

Sample #	Average Outer Diameter, D (in.)	Total Number of Test Runs	Average Thickness t (in.)	Burst Pressure (psi)	Burst Time (s)	Max Pressure (psi)	Max Pressure > Burst Pressure
26	7.85	1	0.539	639.7	72	639.7	No
59	7.89	4	0.574	797.6	72	797.6	No
57	7.89	3	0.614	819.5	66	834.2	Yes

The data set from Table 5.7 is represented as best fit linear and quadratic regression curves in Figure 5.13.

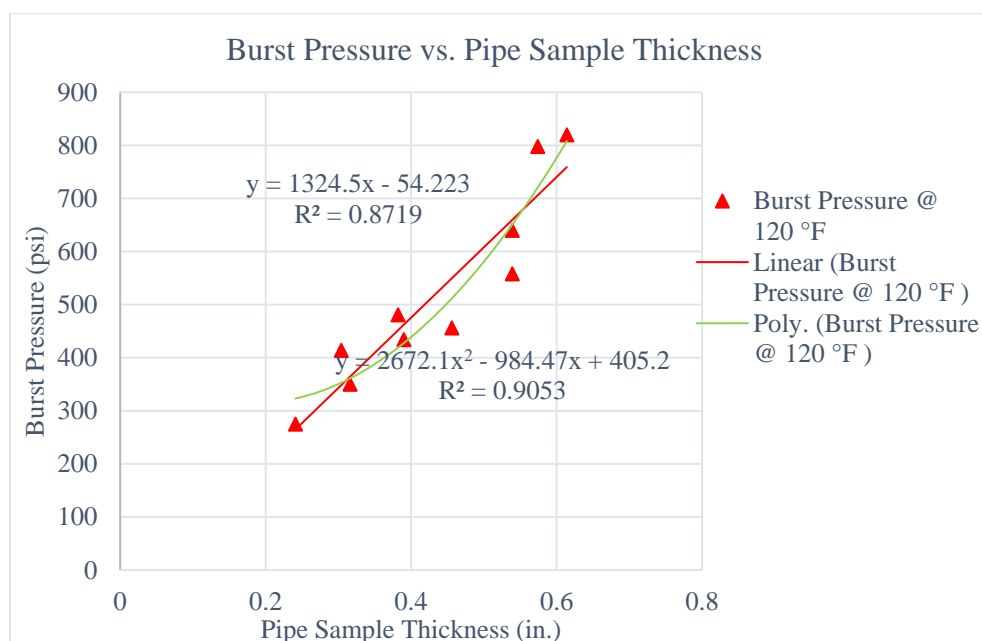


Figure 5.13 Burst Pressure vs. Pipe Thickness (After Data Curation)

Figure 5.13 shows the correlation between thickness vs. burst pressure.

The linear regression equation is shown as below with $R^2 = 0.8719$.

$$y = 1324.5x - 54.223 \quad 5.4$$

The quadratic regression equation is shown as below with $R^2 = 0.9053$.

$$y = 2672.1x^2 - 984.47x + 405.2 \quad 5.5$$

The R^2 for both linear and quadratic regressions is more than 0.87; thus, both represent a higher degree of correlation between the pipe sample thickness and burst pressure.

For simplicity and conservative liner design thickness for burst pressure, the approximate linear Equation 5.4 can be used to estimate the burst pressure at any given thickness at a temperature of 120° F.

5.5.3 Pressure Integrity Test Results at 150° F Temperature

The test at 150° F temperature was more challenging compared to 73° F and 120° F due to the elastic behavior of the material at elevated temperature. The pipe samples showed more bulging due material elasticity at this temperature, and the bulging areas were more noticeable for thinner pipe samples compared to thicker pipe samples. It was difficult to achieve the target pressure for a pipe sample at 150° F due to the bulging of the pipe samples, and occasionally the samples had to be taken out of the water bath to inspect the end caps and bolts. It was noticed that the bolts were loosened, and re-tightening of bolts for these samples was required to prevent the leakage at the end caps and to achieve the target pressure. While the samples were out of the water bath, the outer diameters of the bulged areas were recorded.

Figure 5.14 (a) shows the bulged area of the pipe sample #3 during the testing, and Figure 5.14 (b) shows the measurement of a bulged area of pipe sample #3.

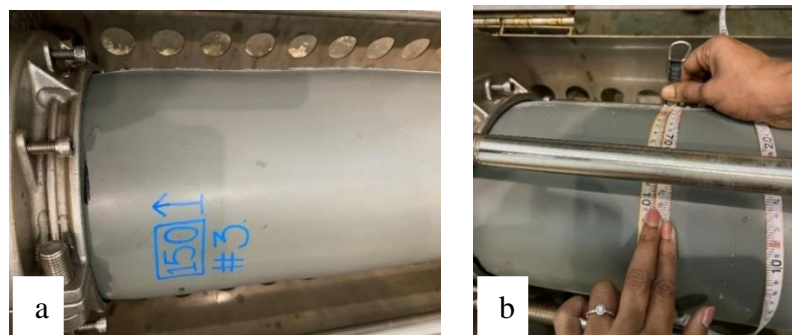

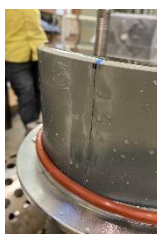






Figure 5.14 (a) Bulging of Pipe Samples (b) Measurement of Increase of OD

Sample # 3 was taken out from the water bath because the pressure was not increasing after the first test run. OD of this pipe sample was measured at two bulged points after test run 1. At one region of the pipe, the OD changed from 7.912 in. to 8.41 in., with a 6.3% increase in OD. At another region of the pipe, OD changed from 7.901 in. to 8.17 in., with a 3.26% increase in OD.





Table 5.8 below represents the results of the pressure integrity test conducted at a temperature of 150° F. The table includes the following information: sample number, sample thickness (in.), burst pressure (psi), failure time (seconds), failure mode of the pipe sample, any special material behavior observed, a picture of the pipe sample failure, and the pre-test visual inspection.

Table 5.8 Pressure Integrity Test Results at 150° F Temperature

Pressure Integrity Test Data @ 150° F Temperature							
Sample #	Sample Thk (in.)	Burst Pressure (psi)	Failure Time (S)	Failure Mode	Any Special Material Behavior	Sample Failure Picture	Pre-test Visual Inspection
5	0.207	116	72	Elastic failure with cracks and deformation on seam line.	Sample burst with longitudinal and minor transverse cracks at the seam line. Material showed elasticity with bulging observed at the failure points. An increase of 4.923 % in OD.		No defects
1	0.226	0	Not tested due to defects				Major gap intrusion on the seam line, thus leak at the end cap.

Pressure Integrity Test Data @ 150° F Temperature							
Sample #	Sample Thk (in.)	Burst Pressure (psi)	Failure Time (S)	Failure Mode	Any Special Material Behavior	Sample Failure Picture	Pre-test Visual Inspection
3	0.232	93	72	Crack Failure.	Sample bulged a lot in different areas. Sample failed due to a small crack generated close to the seam line.		No defects
23	0.316	121	63	Elastic failure with cracks and deformation on seam line.	Samp demonstrated less pressure resistance because of defects. A big bubble/ bulging was observed inside the pipe.		Bulging inside and outside of the pipe
53	0.329	256	72	Elastic failure with cracks and deformation on seam line.	Sample showed good pressure resistance. Good bonding between layers were observed.		No defects at the seam line, but bulging was observed at one point.
43	0.339	202	57	Elastic failure with cracks and deformation on seam line.	Sample took less pressure as compared to #53. Layer formation were observed.		No defects at the seam line, but bulging was observed in many areas externally. Inside of pipe, two big bulging spots were observed.

Pressure Integrity Test Data @ 150° F Temperature

Sample #	Sample Thk (in.)	Burst Pressure (psi)	Failure Time (S)	Failure Mode	Any Special Material Behavior	Sample Failure Picture	Pre-test Visual Inspection
30	0.401	267	72	Elastic failure with cracks and deformation, but not on seam line.	Elastic behavior and bulging observed near failure crack		No defects
22	0.402	338	81	Elastic failure with cracks and deformation on seam line.	Material showed elasticity and didn't fracture in pieces. Good bonding between layers.		No defects at the seam line. Minor bulging was observed at two points.
24	0.413	346	72	Elastic failure with cracks and deformation on seam line.	Material showed elasticity and didn't fracture in pieces. Good bonding between layers.		No defects at the seam line. Minor bulging was observed at two points.
12	0.461	380	72	Elastic failure with cracks and deformation on seam line.	Material showed elasticity and didn't fracture in pieces. Good bonding between layers.		No defects





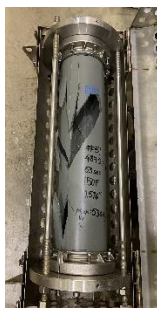
Pressure Integrity Test Data @ 150° F Temperature							
Sample #	Sample Thk (in.)	Burst Pressure (psi)	Failure Time (S)	Failure Mode	Any Special Material Behavior	Sample Failure Picture	Pre-test Visual Inspection
29	0.476	401	69	Elastic failure with cracks and deformation on seam line.	Material showed elasticity and didn't fracture in pieces. Good bonding between layers.		No defects
19	0.479	339	57	Elastic failure with cracks and deformation on seam line.	Sample took less pressure as compared to samples # 12 and 29.		No defects
13	0.509	370	63	Elastic failure with cracks and deformation on seam line.	Material showed elasticity and didn't fracture in pieces. Good bonding between layers.		No defects
50	0.567	506	72	Elastic failure with cracks and deformation on seam line.	Material showed elasticity and didn't fracture in pieces. Good bonding between layers. An increase of 4.15% in OD was observed.		No defects
51	0.576	439	63	Elastic failure with cracks and deformation on seam line. <i>But little catastrophic as well.</i>	Good bonding between layers. An increase of 3.67 % in OD was observed.		No defects

Table 5.8 shows the burst pressure values of 14 pipe samples because sample #1 could not be tested due to a major gap intrusion on the seam line that resulted in a leak in the installed end cap. As depicted in the pictures of the failure of the pipe sample shown in Table 5.8, it is observed that the pipe sample tested at 150° F demonstrated an elastic mode of failure. These pipe samples failed with deformation and cracks. The pipe samples tested at 150° F temperature showed more deformation and cracks compared to the pipe samples tested at 120° F. This implied that the material acted more elastic at a temperature of 150° F. Pipe samples #5, #23, #53, #43, #30, #22, #24, #12, #29, #19, #13, #50, and #51 showed elastic failure with deformation and cracks. Pipe sample #3 failed with deformation and a pin hole crack.

The test results are summarized in Table 5.9 with burst pressure, time-to-failure, maximum pressure, and if the maximum pressure recorded was more than burst pressure. Multiple test runs were performed on some pipe samples so that the failure of the pipe samples was achieved between 60 and 70 seconds.

Table 5.9 Summary of Pressure Integrity Test Results at 150° F

Sample #	Average Outer Diameter, D (in.)	Total Number of Test Runs	Average Sample Thickness, t (in.)	Burst Pressure (psi)	Burst Time (s)	Max Pressure (psi)	Max Pressure > Burst Pressure
5	7.9	4	0.207	116	72**	120.1	Yes
1	7.88	0	0.226	-	-	-	-
3	7.91	5	0.232	93	72**	118	Yes
23	7.91	1	0.316	121	63	121.4	No
53	7.9	2	0.329	256	72**	277.8	Yes
43	7.91	1	0.339	202	57*	201.7	No
30	7.84	3	0.401	267	72	292.3	Yes
22	7.88	1	0.402	338	81**	338	No
24	7.83	1	0.413	346	72**	345.7	No
12	7.88	1	0.461	380	72**	379.5	No
29	7.9	2	0.476	401	69	432.7	Yes

Sample #	Average Outer Diameter, D (in.)	Total Number of Test Runs	Average Sample Thickness, t (in.)	Burst Pressure (psi)	Burst Time (s)	Max Pressure (psi)	Max Pressure > Burst Pressure
19	7.87	2	0.479	339	57*	393.4	Yes
13	7.88	2	0.509	370	63	437.9	Yes
50	7.88	4	0.567	506	72**	506.2	No
51	7.81	5	0.576	439	63	536.6	Yes

Note: *- if the time-to-failure < than 60 seconds and ** if the time-to-failure > than 70 seconds

The time-to-failure of some pipe samples was between 60 and 70 seconds, some were less than 60 seconds, and some were more than 70 seconds. Figure 5.15 shows the graphical representation of Table 5.9 and represents the correlation between burst pressure and pipe sample thickness.

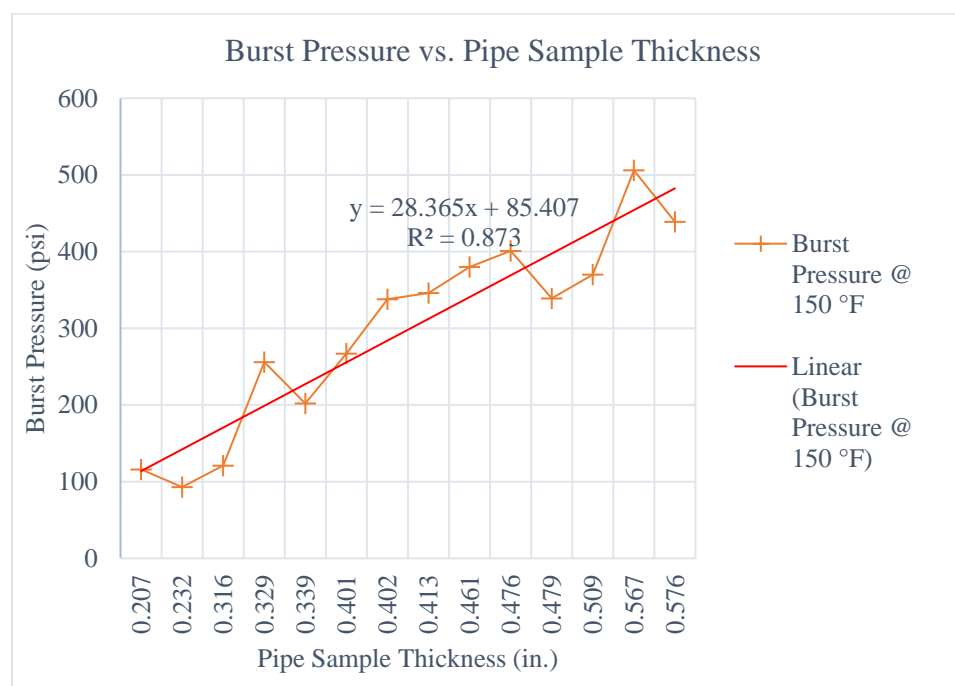


Figure 5.15 Burst Pressure vs. Pipe Thickness at 150° F

As depicted in Table 5.9 and Figure 5.15, some pressure resistance values were abnormal compared to the rest. The dips in the graph showed pipe samples with less pressure resistance.

Data Curation (excluding underperformed pipe samples with defects and excluding time-to-failure less than 60 seconds)

The pipe samples with abnormal pressure resistance values were identified and the pre-test visual inspection of these samples was checked. In the visual inspection column of Table 5.8, sample #43 was identified with two bulging spots inside the pipe, but the seam line showed no defects. This sample showed less pressure resistance and failed with crack failure.

No defects were found in the visual inspection of samples #3 and #19. From Table 5.8, it is depicted that samples #3 failed with a pin hole crack and #19 failed with crack failure mode; thus, it was implied that these samples could have internal defects. As a result, these three pipe samples were considered outliers and excluded from the data analysis.

The time-to-failure of pipe samples with less than 60 seconds was excluded from the data set, but 72 seconds was considered. Pipe sample #43 had a time-to-failure of less than 60 seconds and thus, it was considered outliers and excluded from the data set. The time-to-failure of sample #22 was more than 72 seconds, thus, it was also considered an outlier and excluded from the data analysis. Table 5.10 shows the data set excluding pipe samples with abnormal pressure resistance and time-to-failure less than 60 seconds. Figure 5.16 shows the graphical representation of this data set.

Table 5.10 Data Set Excluding Time-to-Failure Less than 60 seconds at 150 °F

Sample #	Average Outer Diameter, D (in.)	Total Number of Test Runs	Average Sample Thickness, t (in.)	Burst Pressure (psi)	Burst Time (s)	Max Pressure (psi)	Max Pressure > Burst Pressure
5	7.9	4	0.207	116	72	120.1	Yes
23	7.91	1	0.316	121	63	121.4	No
53	7.9	2	0.329	256	72	277.8	Yes
30	7.84	3	0.401	267	72	292.3	Yes
24	7.83	1	0.413	346	72	345.7	No
12	7.88	1	0.461	380	72	379.5	No

Sample #	Average Outer Diameter, D (in.)	Total Number of Test Runs	Average Sample Thickness, t (in.)	Burst Pressure (psi)	Burst Time (s)	Max Pressure (psi)	Max Pressure > Burst Pressure
29	7.9	2	0.476	401	69	432.7	Yes
13	7.88	2	0.509	370	63	437.9	Yes
50	7.88	4	0.567	506	72	506.2	No
51	7.81	5	0.576	439	63	536.6	Yes

The data set from Table 5.10 is represented as best fit linear and quadratic regression curves in Figure 5.16.

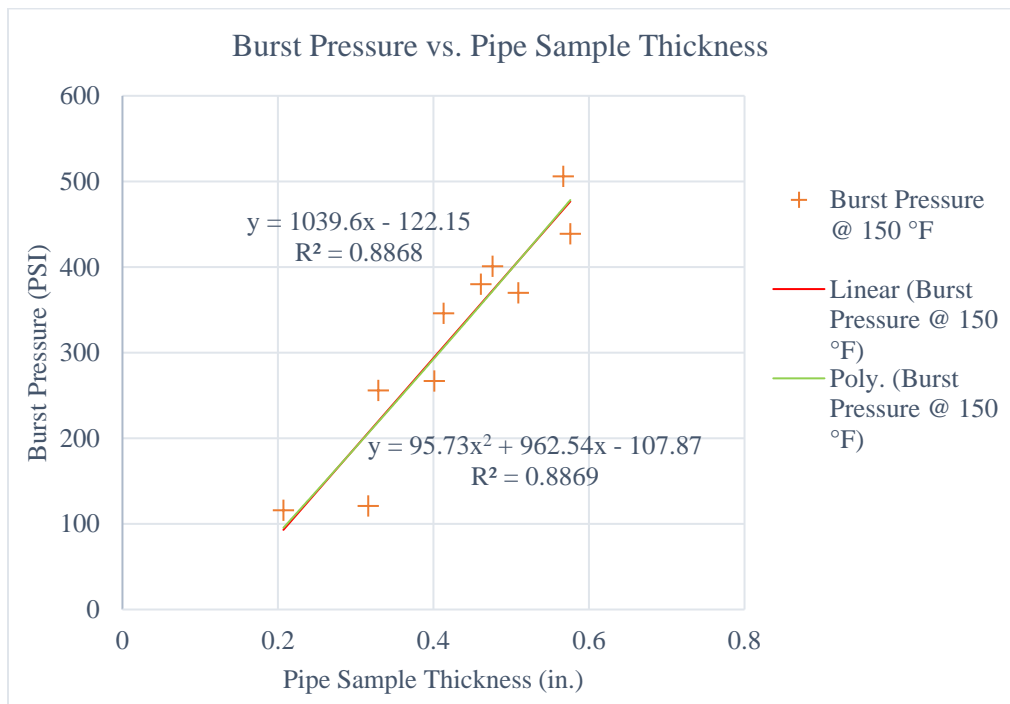


Figure 5.16 Burst Pressure vs. Pipe Thickness (After Data Curation)

Figure 5.16 shows the correlation between thickness vs. burst pressure.

The linear regression equation is shown as below with $R^2 = 0.8868$.

$$y = 1039.6x - 122.15 \quad 5.6$$

The quadratic regression equation is shown as below with $R^2 = 0.8869$.

$$y = 95.73x^2 + 962.54x - 107.87$$

5.7


The R^2 for both liner and quadratic regressions is approximately 0.88; thus, both represent a higher degree of correlation between the pipe sample thickness and burst pressure.





Since both the linear and polynomial equation show approximately same $R^2 = 0.88$, for simplicity and conservative liner design thickness for burst pressure, the approximate linear Equation 5.5 can be used to estimate the burst pressure at any given thickness at a temperature of 150° F.





5.5.4 Pressure Integrity Test Results at 41° F Temperature






Table 5.11 below represents the results of the pressure integrity test conducted at a temperature of 41° F. The table includes the following information: sample number, sample thickness (in.), burst pressure (psi), failure time (seconds), failure mode of the pipe sample, any special material behavior observed, a picture of the pipe sample failure, and the pre-test visual inspection.

Table 5.11 Pressure Integrity Test Results at 41° F Temperature

Pressure Integrity Test Data @ 41° F Temperature							
Sample #	Sample Thk (in.)	Burst Pressure (PSI)	Failure Time (S)	Failure Mode	Any Special Material Behavior	Sample Failure Picture	Pre-test Visual Inspection
25	0.248	-	-	-	-		Defective pipe sample. Hole on one end of seam. Could not test the pipe.

Pressure Integrity Test Data @ 41° F Temperature							
Sample #	Sample Thk (in.)	Burst Pressure (PSI)	Failure Time (S)	Failure Mode	Any Special Material Behavior	Sample Failure Picture	Pre-test Visual Inspection
6	0.252	-	-	-	-		Sample was oval at both ends, unable to install end caps. Could not test the pipe.
9	0.285	-	-	-	-		Sample was oval at both ends, unable to install end caps. Could not test the pipe.
15	0.298	195	60	Catastrophic failure with cracks other than seam line	Sample burst and cracks generated. Less catastrophic as compared to other samples.		No defects
54	0.33	387	57	Brittle catastrophic failure	Good bonding between layers		No defects

Pressure Integrity Test Data @ 41° F Temperature							
Sample #	Sample Thk (in.)	Burst Pressure (PSI)	Failure Time (S)	Failure Mode	Any Special Material Behavior	Sample Failure Picture	Pre-test Visual Inspection
34	0.362	318	45	Catastrophic failure, but with cracks	Sample showed less pressure resistance compared to Sample #54		Gap intrusion at different points on the seam line. Maximum gap intrusion was 0.197 in. (5 mm).
52	0.385	578	72	Brittle catastrophic failure	Sample showed good pressure resistance and good bonding between layers		No defects
36	0.414	528	63	Brittle catastrophic failure	Sample illustrated good pressure resistance, but less than sample #52 and good bonding between layers		No defects
18	0.425	423	51	Brittle catastrophic failure	Sample showed less pressure than samples #52 and # 36. Good bonding between layers		No defects

Pressure Integrity Test Data @ 41° F Temperature							
Sample #	Sample Thk (in.)	Burst Pressure (PSI)	Failure Time (S)	Failure Mode	Any Special Material Behavior	Sample Failure Picture	Pre-test Visual Inspection
38	0.429	261	42	Catastrophic failure, but with cracks	Material did not take good pressure. May be due to seam line and internal defects		Seam line defects at two points. Gap intrusion of 0.118 in. (3 mm).
7	0.508	377	57	Catastrophic failure, but with cracks	Sample failed at the seam line defects, seam line opened.		Defects at seam line.
21	0.52	707	69	Brittle catastrophic failure. Completely shattered pipe.	Sample showed good pressure resistance and good bonding between layers		No defects
61	0.568	799	72	Brittle catastrophic failure. Completely shattered pipe.	Sample showed good pressure resistance and good bonding between layers		No defects
42	0.631	55	15	Crack failure. Sample was defective	Due to defects, sample could not take pressure		Sample was defective. Sample had bulged area and a longitudinal crack inside of pipe


Pressure Integrity Test Data @ 41° F Temperature							
Sample #	Sample Thk (in.)	Burst Pressure (PSI)	Failure Time (S)	Failure Mode	Any Special Material Behavior	Sample Failure Picture	Pre-test Visual Inspection
58	0.642	623	66	Brittle catastrophic failure.	Sample showed less pressure resistance compared to samples #61 and #21		Very minor defects on seam line.

Table 5.11 shows the burst pressure values of 12 samples; sample #25 could not be tested due to a hole in the seam line at one end of the pipe sample. Samples #6 and #9 could not be tested because both ends were oval, so the end caps could not be properly installed.

As depicted in the pictures of pipe sample failure shown in Table 5.11, it was observed that the pipe samples that failed at 41° F demonstrated a more brittle catastrophic failure. These pipe samples were shattered into pieces, which implied brittleness of the pipe to pressure resistance. Pipe samples #54, #52, #36, #18, #21, #61, and #58 showed a more brittle catastrophic failure and were shattered into more pieces at the burst point. The pipe samples #15, #34, #38 and #7 showed brittle catastrophic failure, but to a lesser degree. Visual inspection of pipe samples #34, #38 and #7 showed seam line defects, thus a lesser degree of catastrophic mode failure was observed. Visual inspection of pipe samples #15 showed no defects, but a less catastrophic mode failure with cracks implied that the pipe sample could have internal defects. Sample #42 was defective with longitudinal, circumferential cracks and a bulging surface, therefore, it failed with a crack mode of failure.

The test results are summarized in Table 5.12 with burst pressure, time-to-failure, maximum pressure, and if the maximum pressure recorded was more than burst pressure. Multiple

test runs were performed on some pipe samples so that the failure of the pipe samples was achieved between 60 and 70 seconds.

Table 5.12 Summary of Pressure Integrity Test Results at 41° F

Sample #	Average Sample Outer Diameter, D (in.)	Total Number of Test Runs	Average Sample Thickness, t (in.)	Burst Pressure (psi)	Time-to-failure (s)	Max Pressure (psi)	Max Pressure > Burst Pressure
25	7.91	0	0.248	-	-	0	No
6	7.44	0	0.252	-	-	0	No
9	7.87	0	0.285	-	-	0	No
15	7.86	1	0.298	195	60	195	No
54	7.91	1	0.33	387	57*	386.6	No
34	7.9	4	0.362	318	45*	360.3	Yes
52	7.89	2	0.385	578	72**	577.5	No
36	7.89	2	0.414	528	63	533.2	Yes
18	7.87	1	0.425	423	51*	422.8	No
38	7.86	1	0.429	261	42*	260.6	No
7	7.84	1	0.508	377	57*	377.1	No
21	7.87	4	0.52	707	69	717.8	Yes
61	7.89	2	0.568	799	72**	798.7	No
42	7.89	1	0.631	55	15*	55	No
58	7.91	1	0.642	623	66	622.5	No

Note: *- if the time-to-failure < than 60 seconds and ** if the time-to-failure > than 70 seconds

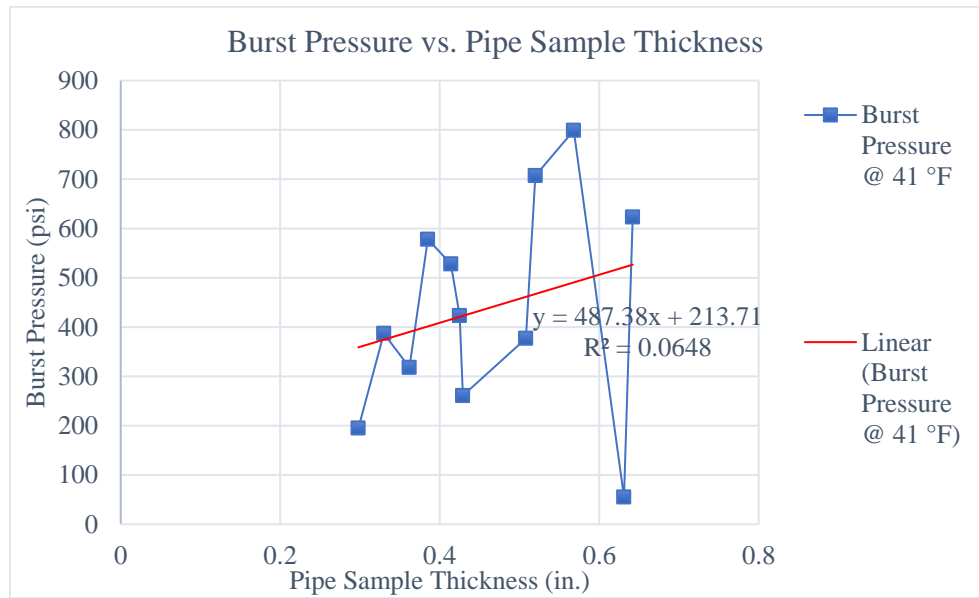


Figure 5.17 Burst Pressure vs. Pipe Thickness at 41° F

Table 5.12 shows the burst pressure values of 12 samples. The time-to-failure of certain pipe samples was between 60 and 70 seconds, while others were less than 60 seconds or more than 70 seconds. Figure 5.17 shows the graphical representation of Table 5.12 and represents the correlation between the burst pressure and pipe sample thickness.

As depicted in Table 5.12 and Figure 5.17, some pressure resistance values were abnormal compared to the rest. The dips in the graph showed pipe samples with less pressure resistance.

Data Curation (excluding underperformed pipe samples with defects and excluding time-to-failure less than 60 seconds)

The pipe samples with abnormal pressure resistance values were identified. In pre-test visual inspection, it was found that sample #42 was defective with longitudinal and circumferential cracks and a bulging surface, thus the pipe sample did not show pressure resistance at a thickness of 0.631 in. Therefore, sample #42 was considered as an outlier and excluded from the data analysis. The pressure resistance of sample #58 was less compared to other thinner pipe samples. Thus, sample #58 was also considered an outlier and excluded from the data analysis.

In the visual inspection column of Table 5.11, samples #34, #38 and #7 were found with major seam line defects and showed less resistance to pressure compared to pipe samples with similar of thicknesses. Therefore, these samples were considered outliers and excluded from data analysis. However, no defects were found in the visual inspection of samples #15. But from Table 5.11, it is depicted that sample #15 failed with a crack and a lesser degree of catastrophic failure mode; thus, it was implied that this sample could have internal defects and excluded from the data analysis. The time-to-failure for pipe samples less than 60 seconds was excluded from the data set, but 72 seconds was considered. Pipe samples #54 and #18 showed a time-to-failure of less than 60 seconds, and these were considered outliers and excluded from the data set.

Table 5.13 Data Set Excluding the Outliers at 41° F

Sample #	Outer Diameter, D (in.)	Total Number of Test Runs	Sample Thickness, t (in.)	Burst Pressure (psi)	Burst time (s)	Max Pressure (psi)	Max Pressure > Burst Pressure
52	7.89	2	0.385	578	72	577.5	No
36	7.89	2	0.414	528	63	533.2	Yes
21	7.87	4	0.52	707	69	717.8	Yes
61	7.89	2	0.568	799	72	798.7	No

The data set from Table 5.13 is represented as best fit linear and quadratic regression curves in Figure 5.18.

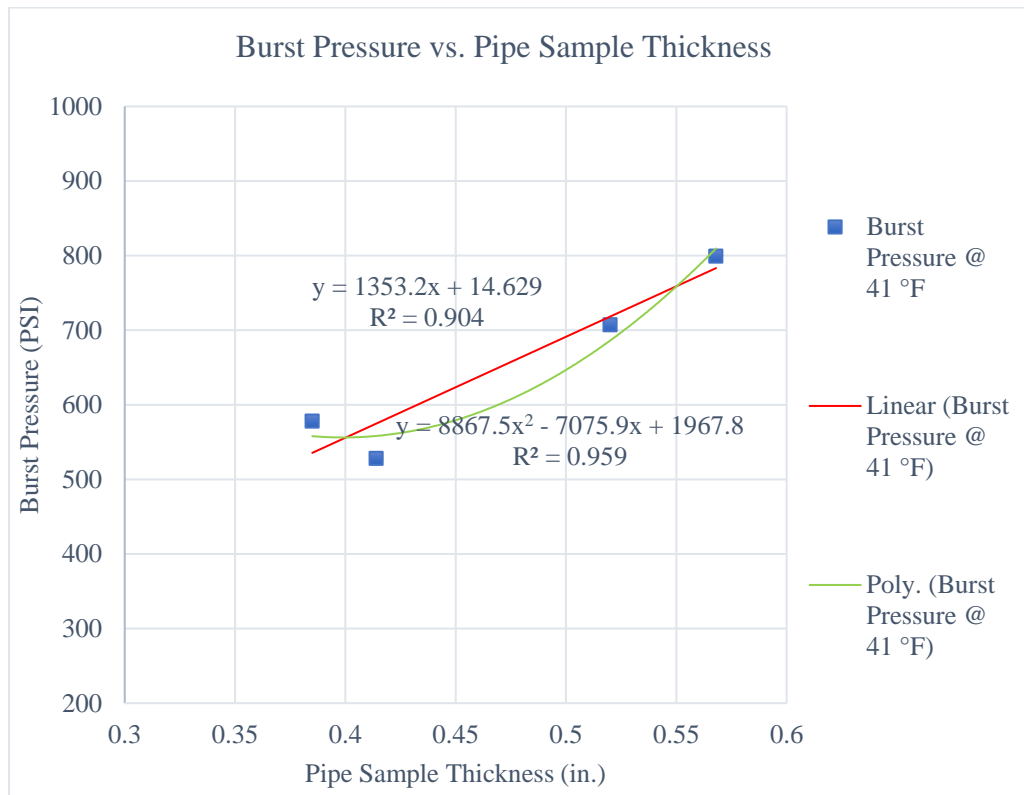


Figure 5.18 Burst Pressure vs. Pipe Thickness (After Data Curation)

Table 5.13 shows the data set that excludes pipe samples with abnormal pressure resistance and a failure time of less than 60 seconds. Figure 5.18 shows the graphical representation of this data set, and represent the correlation between thickness vs. burst pressure.

The linear regression equation is shown as below with $R^2= 0.904$.

$$y = 1353.2x + 14.629 \quad 5.8$$

The quadratic regression equation is shown as below with $R^2= 0.959$.

$$y = 8867.5x^2 - 7075.9x + 1967.8 \quad 5.9$$


The R^2 for both liner and quadratic regressions is approximately 0.90; thus, both represent a higher degree of correlation between the pipe sample thickness and burst pressure.


Since both the linear and polynomial equation show approximately same $R^2= 0.90$, for simplicity and conservative liner design thickness for the burst pressure, the approximate linear Equation 5.8 can be used to estimate the burst pressure at any given thickness at a temperature of 41° F.

5.5.5 Pipe Failure Mode Analysis

The pipe failure mode was analyzed for each pipe sample after the burst test. It was observed that the burst failure mode of pipe sample was different at room temperature, elevated temperature and low temperature. Table 5.14 represents the pipe failure modes observed in the experimental tests.

Table 5.14 Pipe Failure Modes

Failure Mode	Material Behavior	Failure Mode Picture
Catastrophic Failure	<ul style="list-style-type: none"> - Pipe was shattered into pieces, shows brittle fracture. - Material's brittle behavior to pressure resistance. - Pressure resistance was higher in such type of failures. - Observed at 73 °F and 41 °F temperature tests. 	





Failure Mode	Material Behavior	Failure Mode Picture
Elastic and Catastrophic Failure	<ul style="list-style-type: none"> - Pipes failed with cracks and few shattered pieces. - Material showed elasticity but also showed a slight brittle behavior to pressure resistance. - Pressure resistance was less in such type of failures. - Observed at 120 °F temperature test. 	
Ductile Failure	<ul style="list-style-type: none"> - Pipes responded more elastically and physically changed shape before ultimately splitting to a far less extent. Surface initiated cracks, pin hole leaks were observed. - Material showed more elastic behavior with high deformation. Ballooning of samples observed. Permanent deformation was observed. - Pressure resistance was very less in such type of failures. - Observed at 150 °F temperature test. 	

From Table 5.14, it is concluded that the pipe failure mode changed with the change in the test temperature. Pipe samples tested at low and ambient temperatures acted more stiffer and demonstrated maximum pressure resistance. Pipe samples failed with brittle fractures, illustrated an example of catastrophic failure. On the other hand, the stiffness of the polymer material decreases at elevated temperature. The material showed more deformation and cracks were generated during the pressure resistance at a high temperature. Thus, the sample showed a failure mechanism as ductile with deformation.

Another important failure characteristic observed was the formation of layers when inspecting the broken pieces from the samples. This characteristic was predominantly observed

during testing at temperatures of 73° F and 41° F. The formation of layers may be attributed to the curing behavior of the sprayed layers. The setting time between the sprayed layers to achieve the required thickness is relatively short, which can result in the previous sprayed layer setting before the second layer is applied. Additionally, the installation procedure could also contribute to layer formation. Furthermore, the presence of micro-bubbles was observed in the broken sample pieces.

Layer formation was not observed in the broken samples at elevated temperatures. This could be due to the fact that at high temperatures, the different layers formed tend to merge together since the polymers are softer and more flexible. As a result, no distinct layer formation was visible in the broken samples. Figure 5.19 shows the layer formation and micro-bubbles on the broken pieces of samples.

	
<p>Sample #33, Layers formation observed on broken pieces (Tested at 73° F)</p>	
	
<p>Sample #4, Layers formation observed on broken pieces (Tested at 73° F)</p>	<p>Sample #58, Layers formation observed on broken pieces (Tested at 41° F)</p>

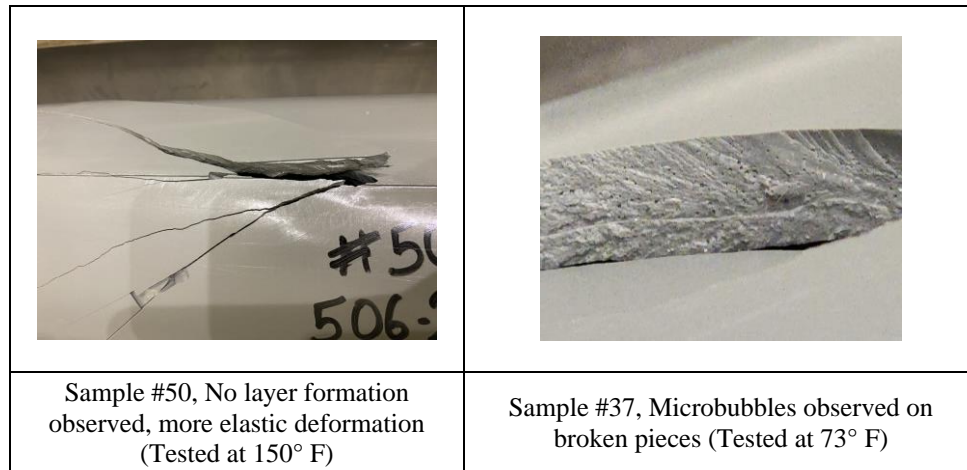


Figure 5.19 Pipe Failure Analysis

The formation of layers and the presence of microbubbles could potentially impact the strength of the material and its resistance to pressure.

5.5.6 Hoop Stress Calculations

Hoop stress is a tangential stress which acts along the pipe circumference, and it is generated due to internal pressure. Whereas the longitudinal stress acts in the axial direction of the pipe due to internal pressure. Hoop stress is twice the longitudinal stress. Hoop stress tends to increase the pipe diameter, whereas longitudinal stress tends to increase the pipe length. The hoop stresses induced by internal pressure are a critical factor that can lead to material rupture, especially in pressure pipes. If the hoop stresses exceed the material's ultimate tensile strength, they can result in the catastrophic failure of the pipe.

Burst pressure is the primary measure for estimating efficiency in the field of pressure pipes and vessels. Similarly, experimental tests were conducted on the polymeric SAPL liner material to establish a correlation between pipe thickness, burst pressure, hoop stress, and material performance. Furthermore, the influence of temperature on burst pressure and hoop stress was evaluated.

The hoop stress was calculated by using Barlow's equation as given below.

$$S = \frac{P \times (D - t)}{2 \times t} \quad 5.10$$

Where S= hoop stress, psi

P= internal pressure, psi

D= average outside diameter, in.

t = minimum pipe thickness, in.

The two types of end caps, without rods (called free ends) and with rods (called restrained ends), can be used to close the pipe ends. Free-end caps produce longitudinal, hoop, and radial stresses in the pipe due to internal pressure because the pipe can move both in the longitudinal and axial directions. However, the restrained end caps provide longitudinal support by the rods through connecting the two ends of the pipe and resist the thrust of the end. Thus, the pressure in the pipe can only produce the hoop and radial stresses.

In this pressure integrity test, the end caps used to test the pipe samples were restrained end caps. Due to the difference in the stresses produced in the pipe sample using the free-end caps and restrained end, the expected hoop stress in the pipe sample tested with free-end caps was approximately 11% less than the pipe sample tested with restrained end caps (as per ASTM D1599). Thus, the hoop stresses calculated for all pipe samples were reduced by 11% from the actual test results obtained.

5.5.6.1 Hoop Stress Calculations for 73° F Temperature

The hoop stresses were calculated based on the burst pressure values obtained from the pipe samples tested at 73° F, and Table 5.15 shows the hoop stress calculated for these pipe samples.

Table 5.15 Calculated Hoop Stress at 73° F Temperature

Sample #	Average Sample Outer Diameter, D (in.)	Average Sample Thickness, t (in.)	Burst Pressure (psi)	Burst Time (s)	*Hoop Stress (psi)
11	7.90	0.228	306	72	4,585
10	7.89	0.249	409	66	5,596
56	7.88	0.310	534	69	5,821
49	7.90	0.388	550	72	4,747
27	7.85	0.507	825	63	5,312
60	7.86	0.532	810	60	4,968
48	7.89	0.618	925	60	4,841
33	7.85	0.631	1042	69	5,308

**Hoop stress calculated reduced by 11% due to the use of restrained end caps in getting the burst pressure.*

As depicted in Table 5.15, pipe sample #56 with a thickness of 0.310 in. demonstrated a maximum hoop stress of 5,821 psi. This sample had no defects and the sample burst with a catastrophic failure, but not on the seam line. This sample showed good resistance to pressure. Therefore, this sample characterized a maximum value of the hoop stress at 73° F. The average value of the hoop stress is 5,147 psi.

5.5.6.2 Hoop Stress Calculations for 120° F Temperature

The hoop stresses were calculated based on the burst pressure values obtained from the pipe samples tested at 120° F, and Table 5.16 shows the hoop stress calculated for these pipe samples.

Table 5.16 Calculated Hoop Stress at 120° F Temperature

Sample #	Average Sample Outer Diameter, D (in.)	Average Sample Thickness, t (in.)	Burst Pressure (psi)	Burst Time (s)	*Hoop Stress (psi)
2	7.88	0.241	275	72	4,358
55	7.86	0.304	414	72	5,145

Sample #	Average Sample Outer Diameter, D (in.)	Average Sample Thickness, t (in.)	Burst Pressure (psi)	Burst Time (s)	*Hoop Stress (psi)
62	7.91	0.316	350	60	4,206
32	7.84	0.382	481	69	4,695
46	7.89	0.39	434	72	4,173
20	7.88	0.456	456	63	3,712
39	7.85	0.539	558	60	3,784
26	7.85	0.539	640	72	4,340
59	7.89	0.574	798	72	5,086
57	7.89	0.614	820	66	4,859

**Hoop stress calculated reduced by 11% due to the use of restrained end caps in getting the burst pressure.*

As depicted in Table 5.16, pipe sample #55 with a thickness of 0.304 in. demonstrated a maximum hoop stress of 5,145 psi. This sample had no defects, the sample failure mode was elastic and catastrophic and showed good resistance to pressure. Thus, this sample characterized a maximum value of the hoop stress at 120° F. The average value of the hoop stress is 4,436 psi.

5.5.6.3 Hoop Stress Calculations for 150 °F Temperature

The hoop stresses were calculated based on the burst pressure values obtained from the pipe samples tested at 150° F. Table 5.17 shows the hoop stress calculated for pipe samples tested at a temperature of 150° F.

Table 5.17 Calculated Hoop Stress at 150° F Temperature

Sample #	Average Sample Outer Diameter, D (in.)	Average Sample Thickness, t (in.)	Burst Pressure (psi)	Burst Time (s)	*Hoop Stress (psi)
5	7.9	0.207	116	72	2,156
23	7.91	0.316	121	63	1,454
53	7.9	0.329	256	72	2,946

Sample #	Average Sample Outer Diameter, D (in.)	Average Sample Thickness, t (in.)	Burst Pressure (psi)	Burst Time (s)	*Hoop Stress (psi)
30	7.84	0.401	267	72	2,477
24	7.83	0.413	346	72	3,107
12	7.88	0.461	380	72	3,058
29	7.9	0.476	401	69	3,127
13	7.88	0.509	370	63	2,679
50	7.88	0.567	506	72	3,263
51	7.81	0.576	439	63	2,757

**Hoop stress calculated reduced by 11% due to the use of restrained end caps in getting the burst pressure.*

As depicted in Table 5.17, pipe sample #50 with a thickness of 0.567 in. demonstrated a maximum hoop stress of 3,263 psi. This sample had no defects and the sample failure mode was elastic with deformation and cracks. Thus, this sample characterized a maximum value of the hoop stress at a temperature of 150° F. The average value of the hoop stress is 2,702 psi.

5.5.6.4 Hoop Stress Calculations for 41° F Temperature

The hoop stresses were calculated based on the burst pressure values obtained from the pipe samples tested at 41° F. Table 5.18 shows the hoop stress calculated for pipe samples tested at a temperature of 41° F.

Table 5.18 Calculated Hoop Stress at 41° F Temperature

Sample #	Average Sample Outer Dia, D (in.)	Average Sample Thk, t (in.)	Burst Pressure (psi)	Burst Time (s)	*Hoop Stress (psi)
52	7.89	0.385	578	72	5,634
36	7.89	0.414	528	63	4,767
21	7.87	0.52	707	69	4,997
61	7.89	0.568	799	72	5,150

**Hoop stress calculated reduced by 11% due to the use of restrained end caps in getting the burst pressure.*

As depicted in Table 5.18, the maximum hoop stress calculated is 5,634 psi for sample #52 with a thickness of 0.385 in. This sample had no defects, the sample burst with catastrophic failure, and good bonding between layers was observed. Thus, this sample represented a maximum value of the hoop stress at 41° F. The average value of the hoop stress at 41° F temperature is 5,137 psi.

5.5.7 Effect of Temperature on Burst Pressure and Hoop Stress

The burst pressure results for pipe samples of various thicknesses were compared at temperatures of 73° F, 120° F, 150° F, and 41° F. Figure 5.20 depicts the data points and trend lines illustrating the relationship between burst pressure and pipe thickness at these temperatures.

Figure 5.20 demonstrated that pipe samples show an increase in pressure resistance with an increase in pipe thickness. The trend for this increase in pressure is linear for all temperatures. The maximum burst pressure values were observed at a temperature of 73° F, and the minimum burst pressure values were observed at a temperature of 150° F. The second-highest burst pressure results were observed for a lower temperature of 41° F. The results for 41° F were slightly lower compared to 73° F. However, the performance of the material at lower temperatures should be greater than 73° F. The observed variation in the results may be due to a higher number of defects in the samples tested at 41° F temperature compared to the other samples. The third highest burst pressure results were observed at a temperature of 120° F.

Temperature changes have an impact on the tensile strength and Young's modulus of polymeric materials. Higher temperatures tend to increase the mobility of polymeric chains, leading to increased material deformation. Additionally, stresses induced in the material are more easily relaxed, resulting in decreased stiffness (Sapi and Bulter, 2020). A similar behavior was observed to the burst failure at elevated temperature; the material behaved less stiffer, and ultimately the strength of the material was compromised at higher temperatures.

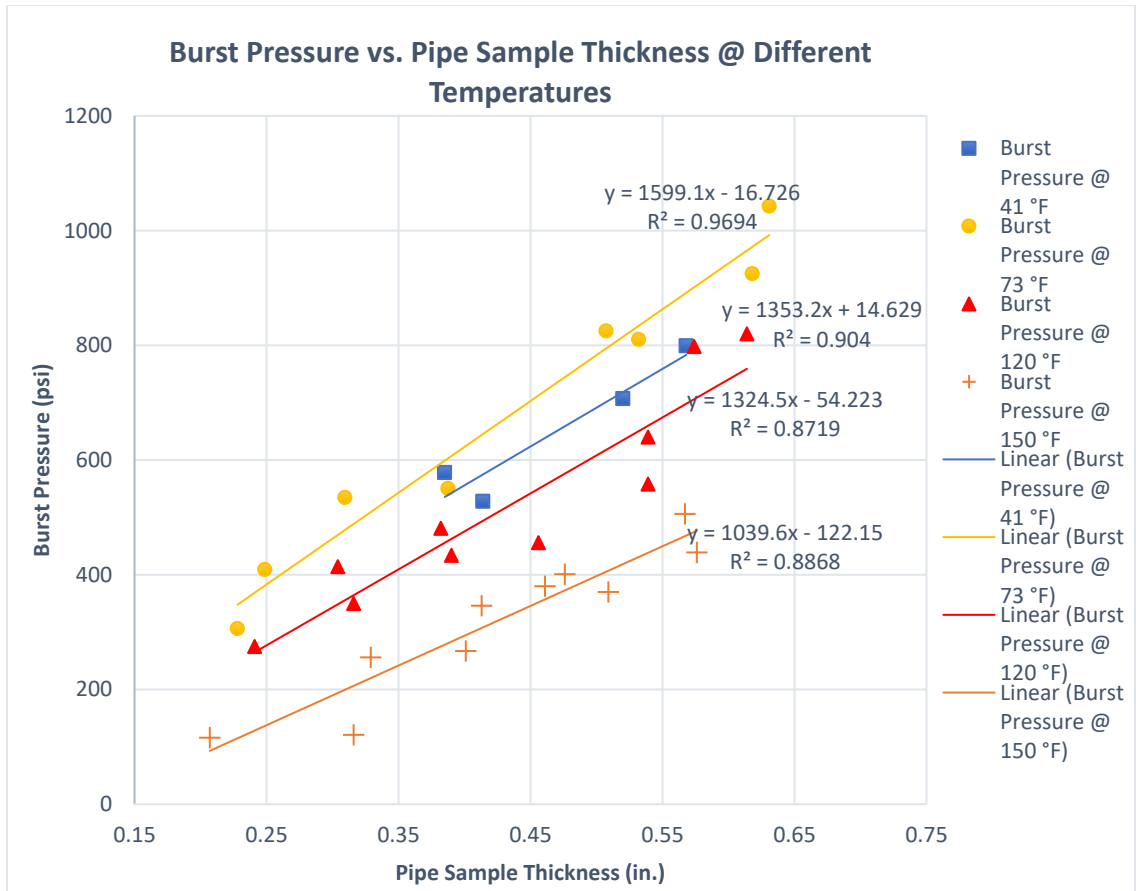


Figure 5.20 Burst Pressure vs. Pipe Sample Thickness Comparison at Different Temperatures

In Figure 5.20, it is illustrated that the performance of the material was higher at room temperature and lower temperature, the material acted more rigid and performed better against the pressure. The material performance at elevated temperature was less compared to that at room temperature and lower temperature. The rigidity of the material decreased at elevated temperature, and the material behaved more elastic with deformation. Temperature changes cause the material to expand or contract, leading to thermal stresses. These thermal stresses combined with the hoop stresses induced by internal pressure can influence the overall structural integrity of the system. Therefore, the hoop stresses generated at the higher temperature are both due to internal pressure

and temperature variations. As a result, the hoop stresses decreased with an increase in the temperature of the testing.

Table 5.19 shows the comparison of the average hoop stress for pipe samples tested at temperatures of 73° F, 120° F, 150° F and 41° F. The hoop stress values represented in the table below are more conservative, since the samples tested had some seam line defects. Additionally, when pipe samples were inspected after failure, some of the shattered pieces showed layer formation. Therefore, the bonding between the pipe samples layers was not strong, possibly resulting in a lower burst pressure value and, as a result, affect the hoop stresses.

Table 5.19 Average Hoop Stress at Different Temperatures

Temperature	Number of Samples (For calculation of average hoop stress)	Average Hoop Stress (psi)
73° F	8	5,147 psi
41° F	4	5,137 psi
120° F	10	4,436 psi
150° F	10	2,702 psi

Table 5.19 demonstrated that the maximum average hoop stress for the material was maximum at 73° F; thus, the material showed maximum resistance to pressure at this temperature. SAPL material performance was better at 73° F compared to the elevated and lower temperatures. The material's performance to the pressure resistance was minimum at the elevated temperature of 150° F because of the more elastic behavior, and the material experienced more deformation, which reduced the hoop stress. The hoop stresses at 41° F can be disregarded due to the limited number of pipe samples available for testing compared to the other temperature conditions.

Figure 5.21 shows the graphical representation of the hoop stress vs. temperature, and the correlation between hoop stress vs. temperature.

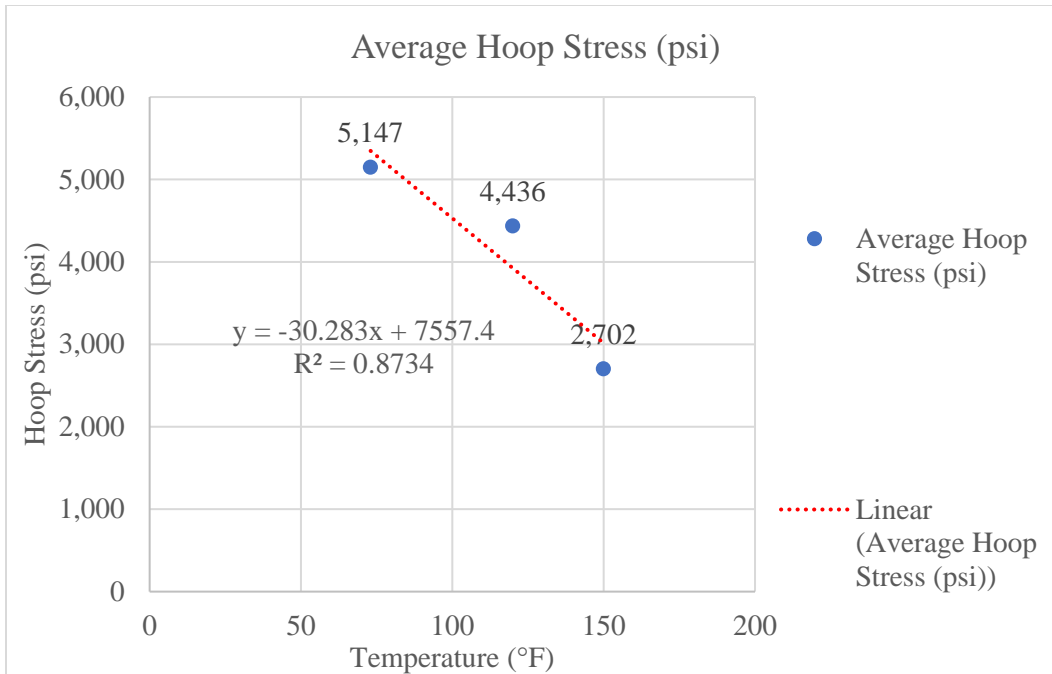


Figure 5.21 Hoop Stress vs. Temperature

The linear regression equation is shown as below with $R^2 = 0.8734$.

$$y = -30.283x + 7557.4 \quad 5.11$$

The R^2 for liner regression is approximately 0.87; thus, it represents a higher degree of correlation between hoop stress and temperature. The trend line represents that as the temperature goes up, the performance of the material goes down. Thus, the material represents a good resistance to pressure at room temperature as compared to elevated temperature.

Temperature has a significant impact on the liner structural integrity and it affects the pressure resistance of the pipe. Therefore, simply evaluating the hoop stress alone is insufficient when designing the liner for high-temperature applications. Thermal stresses generated at high temperature affects the material strength, and thus, the effect of temperature on material integrity should also be considered. High temperature can change the material at the microstructural level and can lead to internal damage of polymer materials, which in turn affects the structural capacity.

Consequently, it is concluded that the performance of the pipe samples was sensitive to temperature variations. The study further concluded that there exists an inverse relationship between burst pressure and temperature, as well as between hoop stress and temperature. This means that as the temperature increases, the burst pressure and hoop stress decrease.

5.5.8 Validation of AWWA Structural Design Equation

Accurate prediction of the burst pressure is crucial for engineering design and structural integrity assessment of pressure pipes; however, it is difficult to accurately predict the burst pressure. Predictive models based on various analytical and empirical equations have been developed to predict the burst pressure of pipes subject to internal pressure. These models quantify the maximum burst pressure as a function of pipe diameter, wall thickness, and material properties. Zhu and Leis (2012) conducted a comprehensive study on comparing the burst pressure output of the predictive models with five experimental burst tests, and the efficiency of the predictive models against the experimental data was evaluated. Similarly, in this study, the experimental data of the burst test was compared with the predicted burst pressure values using the AWWA design equation. The test data at 73° F, 120° F and 150° F were compared to validate the AWWA equation. However, the test data at 41° F was excluded from this comparison because the number of samples was not enough to perform a comparative analysis.

For designing the lining system as a fully structural component, the AWWA (2019) structural lining Classification system has provided a design equation for the Class IV, which is based on the Barlow formula. Most pressure pipes and vessels commonly use the Barlow equation to determine the burst pressure. The Equation 5.12 given below is the AWWA (2019) design equation for Class IV lining system.

$$t = \frac{D}{\left(\frac{2\sigma_{THL}}{PN}\right) + 1} \quad 5.12$$

Where D = inside diameter of host pipe, i.e., outer diameter of bare liner pipe

σ_{THL} = long-term tensile strength of the lining system (psi)

P = internal working pressure (psi)

N = design factor of safety

t = minimum recommended lining thickness at maximum allowable operating pressure (MAOP) (in.)

In this study, the safety factor was considered as 1, and the tensile strength of the liner was considered as short-term ultimate tensile strength (σ) for comparing the short-term burst results of the experimental test. Rearranging Equation 5.12 in terms of internal working pressure (Equation 5.13), is given below.

$$P = \frac{2\sigma t}{(D - t)} \quad 5.13$$

When using the above Equation 5.13 to calculate the predicted burst pressure values at different temperatures, the tensile strength of the material at each specific temperature was employed. The tensile strength of the material was determined through tensile coupon tests conducted at temperatures of 73° F, 120° F, and 150° F.

Table 5.20 Experimental Results vs. AWWA Analytical Design Calculations at 73° F

Sample #	Outer Diameter, OD (in.)	Sample Thickness, t (in.)	Burst Pressure, P (psi)	AWWA Predicted Burst Pressure, P1 (psi)
11	7.90	0.228	306	369
10	7.89	0.249	409	403
56	7.88	0.310	534	507
49	7.90	0.388	550	640
27	7.85	0.507	825	857
60	7.86	0.532	810	900
48	7.89	0.618	925	1,054

Sample #	Outer Diameter, OD (in.)	Sample Thickness, t (in.)	Burst Pressure, P (psi)	AWWA Predicted Burst Pressure, P1 (psi)
33	7.85	0.631	1042	1,084

Table 5.20 and Figure 5.22 present the comparison between experimental results at a temperature of 73° F and the predicted burst values obtained using the AWWA design Equation 5.13.

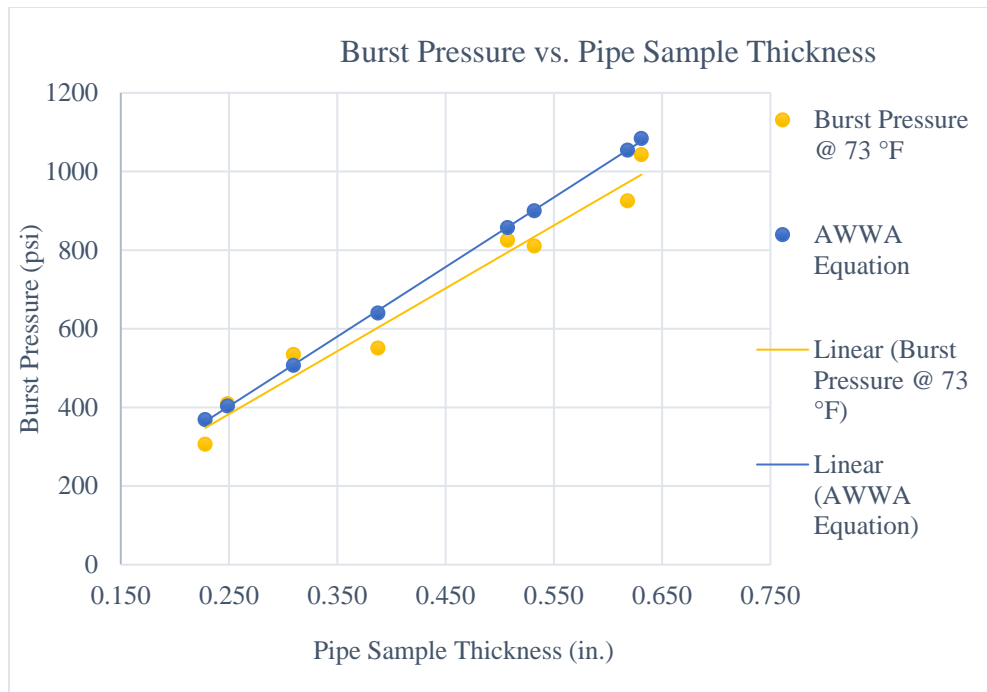


Figure 5.22 Experimental Test Results and AWWA Analytical Calculation at 73 °F

In Table 5.20, P1 represents the predicted burst pressure values calculated at a temperature of 73° F using Equation 5.13. Figure 5.22 shows that the predicted AWWA burst values are slightly higher than the experimental results at the same thickness.

Table 5.21 and Figure 5.23 present the comparison between experimental results at a temperature of 120° F and the predicted burst values obtained using the AWWA design Equation 5.13.

Table 5.21 Experimental Results vs. AWWA Analytical Design Calculations at 120° F

Sample #	Outer Diameter, OD (in.)	Sample Thickness, t (in.)	Burst Pressure, P (psi)	AWWA Predicted Burst Pressure, P2 (psi)
2	7.88	0.241	275	265
55	7.86	0.304	414	338
62	7.91	0.316	350	350
32	7.84	0.382	481	430
46	7.89	0.39	434	437
20	7.88	0.456	456	516
39	7.85	0.539	558	619
26	7.85	0.539	640	619
59	7.89	0.574	798	659
57	7.89	0.614	820	709

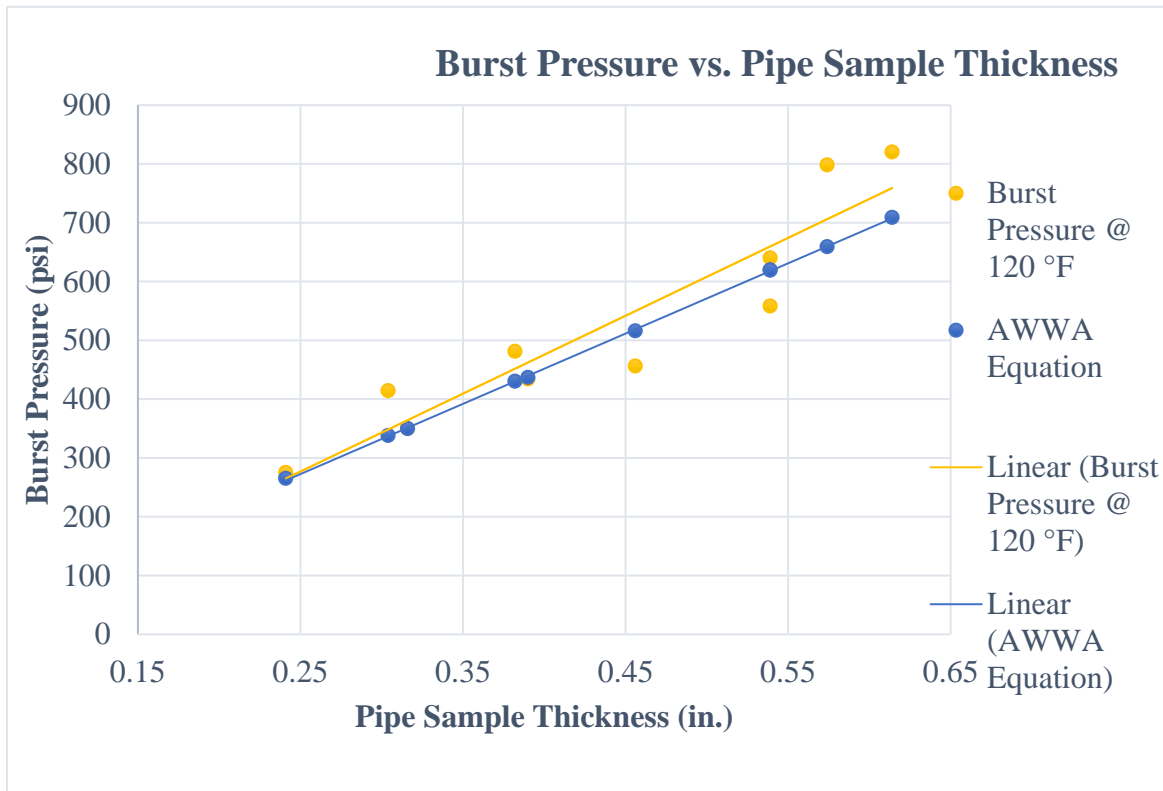


Figure 5.23 Experimental Test Results and AWWA Analytical Calculation at 120° F

In Table 5.21, P2 represents the predicted burst pressure values calculated at a temperature of 120° F using Equation 5.13. Figure 5.23 shows that the predicted AWWA burst values are lower

than the experimental results at the same thickness, which is in contrasts with the comparison results at 73° F, where the trend is opposite.

Table 5.22 and Figure 5.24 present the comparison between experimental results at a temperature of 150° F and the predicted burst values obtained using the AWWA design Equation 5.13.

Table 5.22 Experimental Results vs. AWWA Analytical Design Calculations at 150 °F

Sample #	Outer Diameter, OD (in.)	Sample Thickness, t (in.)	Burst Pressure, P (psi)	AWWA Predicted Burst Pressure, P3 (psi)
5	7.901	0.207	116	91
23	7.911	0.316	121	141
53	7.898	0.329	256	148
30	7.840	0.401	267	183
24	7.832	0.413	346	189
12	7.878	0.461	380	211
29	7.904	0.476	401	218
13	7.881	0.509	370	235
50	7.881	0.567	506	264
51	7.808	0.576	439	271

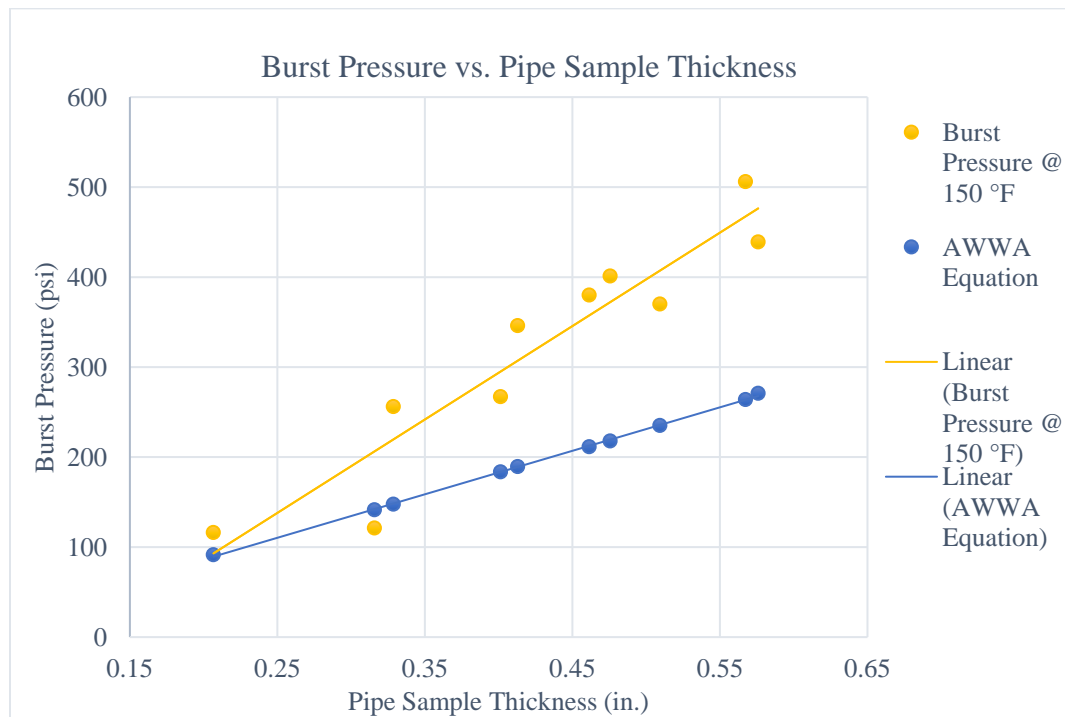


Figure 5.24 Experimental Test Results and AWWA Analytical Calculation at 150° F

In Table 5.22, P3 represents the predicted burst pressure values calculated at a temperature of 150° F using Equation 5.13. Figure 5.24 shows that the predicted AWWA burst values are lower than the experimental results at the same thickness. These results follow the same trend as observed in the comparison of the 120° F test.

Furthermore, the statistical analysis was used to compare the predicted burst values with experiment burst values. The predicted values were normalized by the corresponding experimental burst pressure data. Mean error (relative error) and standard deviations of the mean error were calculated for each set of data at 73° F, 120° F, and 150° F to compare the experimental data with the AWWA predicted burst values. The following Equations 5.14 and 5.15 were used to calculate the mean error and standard deviation (Zhu and Leis, 2012).

$$\text{Mean Error (ME)} = \frac{\sum \left(\frac{P_{i\text{cal}}}{P_{i\text{exp}}} - 1 \right)}{N} \quad 5.14$$

$$\text{Standard Deviation (SD)} = \sqrt{\frac{\sum \left(\frac{P_{i\text{cal}}}{P_{i\text{exp}}} - 1 - \text{ME} \right)^2}{N - 1}} \quad 5.15$$

Where $P_{i\text{cal}}$ =Calculated burst pressure using the AWWA equations for i -th samples, $P_{i\text{exp}}$ is the experiment burst pressure for i -th samples (at different temperatures), and N = total number of samples.

Table 5.23 represents experimental burst pressure, normalized predicted pressure values obtained by using AWWA Equation, ME and SD for the pipe samples tested at 73° F. Similarly, Tables 5.24 and 5.25 present the corresponding values for the pipe samples tested at temperatures of 120° F and 150° F, respectively.

Table 5.23 ME and SD for Test Dataset at 73° F

Sample #	11	10	56	49	27	60	48	33	Mean Error (%)	Standard Deviation (%)
Experiment P	306	409	534	550	825	810	925	1042		
Normalized P1	1.204	0.986	0.948	1.162	1.039	1.111	1.140	1.040	7.86	8.96

Table 5.24 ME and SD for Test Dataset at 120° F

Sample #	2	55	62	32	46	20	39	26	59	57	Mean Error (%)	Standard Deviation (%)
Experimental P	275	414	350	481	434	456	558	640	798	820		
Normalized P2	0.964	0.816	0.999	0.894	1.006	1.131	1.110	0.968	0.826	0.864	-4.21	10.93

Table 5.25 ME and SD for Test Dataset at 150° F

Sample #	5	30	24	12	29	13	50	51	Mean Error (%)	Standard Deviation (%)
Experimental P	116	267	346	380	401	370	506	439		
Normalized P3	0.787	0.577	0.687	0.547	0.556	0.543	0.635	0.521	-35.29	8.54

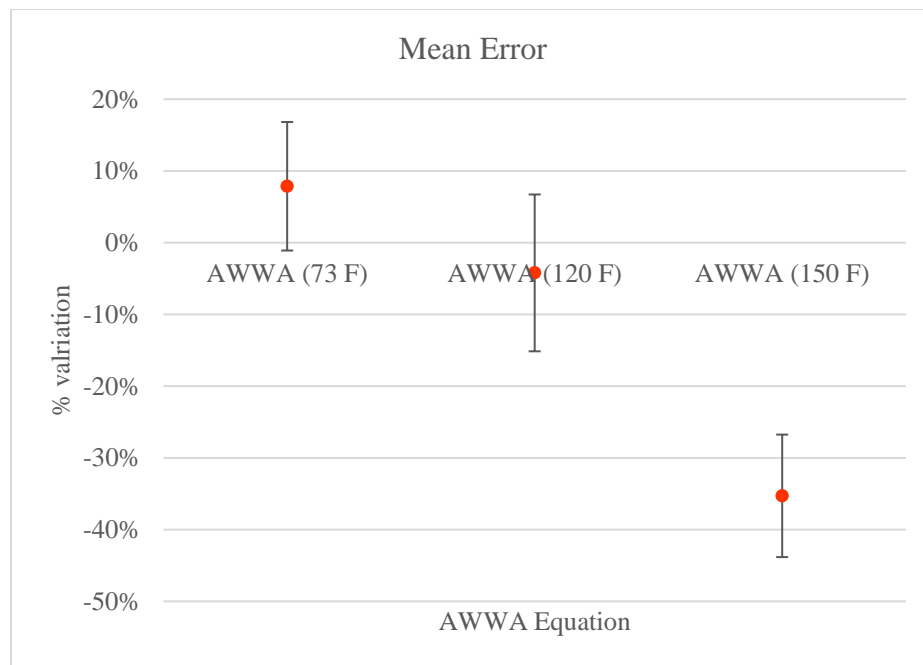


Figure 5.25 Mean Error and Standard Deviation of Predicted AWWA Burst Pressure

Figure 5.25 shows the mean error and standard deviation of the mean error for AWWA predicted burst values when compared with the experimental test results at 73° F, 120° F and 150° F. From Figure 5.25, it was concluded that the results predicted by using the AWWA design equation were 7.86% more than the experimental values at 73° F. On the other, the experimental test results at an elevated temperature showed that the predicted values by using the AWWA design equation were less than the experimental data. For temperatures of 120° F the predicted AWWA equation values were 4.21 % less than experimental values, and at 150° F, the predicted AWWA equation values were 35.29% less than experimental values. The standard deviation of the mean error for AWWA equation results at temperatures of 73° F, 120° F, and 150° F were approximately 8.96%, 10.93%, 8.54%, respectively.

If the AWWA equations predicted results exhibit a mean error close to zero and a smaller standard deviation, then this indicates that the experimental and predicted values were in agreement with each other. It was observed that the predicted values were in good agreement with the test results at a temperature of 73° F. However, the test results at elevated temperatures were not in good agreement with the predicted values of the AWWA equation. The equation underestimated the burst pressures, and thus, temperature has an impact on the burst pressure values. There are chances that the difference could be due to the use of the underestimated coupon tensile strength values obtained at elevated temperatures. Another reason could be that, at elevated temperatures, the performance of the material could vary when determining the tensile strength (in the uniaxial direction) in coupon testing and when the material experienced stress in the hoop direction.

Furthermore, the burst test results demonstrate a similar trend to the AWWA equation when analyzing the 73° F test data. This suggested that the SAPL material functioned as a stand-

alone pipe and exhibited the behavior expected of pressure pipes and vessels. Thus, the AWWA equation based on Barlow's equation can be employed to assess the pressure resistance of the liner material at 73° F. In addition, the SAPL material validates its suitability for structural applications in the rehabilitation process as a class IV.

However, AWWA equation recommended the use of factor of safety and creep factor for the material. The use of these factors is highly recommended when designing the liner thickness to ensure its structural integrity for Maximum Allowable Operating Pressure (MAOP).

5.6 Hydraulic Properties of Liner

The hydraulic flow test was designed to measure the friction factor of the lined pipe and then compare it with the friction factor of the bare new and corroded carbon steel pipes. In this study, one of the important characteristics considered in determining the friction factor was the high Reynolds number which resulted from a high flow rate. In addition, the test was aimed to measure the roughness profile of the liner and compare it with the roughness measured using an optical profilometer in the laboratory. In addition, the roughness of the liner was compared with corroded carbon steel pipes. In the end, the head loss was compared for bare pipe, lined and corroded pipes. In this section, the results of the hydraulic flow test are discussed.

5.6.1 Bare Pipe Test Results

The head loss (h_L) between the entrance and exit points, the mean velocity (v), Reynold's number (Re), friction factor (f), and relative roughness (ϵ/d) were calculated for each flow rate by using the following equations.

1. Head loss (h_L) was determined as the difference in pressure drop between two points (Entrance and Exit) at a distance L .

$$h_L(\text{ft}) = \text{Pressure at Exit point (ft)} - \text{Pressure at Entrance point (ft)} \quad 5.16$$

2. Mean Velocity

$$V \text{ (ft/s)} = \frac{Q}{A} \quad 5.17$$

3. Reynolds number (Re) for turbulent flow

$$Re = \frac{VD}{\nu} \quad 5.18$$

4. Friction factor was calculated by using Darcy-Weisbach equation.

$$h_L = f \frac{L V^2}{D 2g} \quad 5.19$$

5. Rearranging the equation in terms of friction factor (f) is given as below.

$$f = h_L \frac{D 2g}{L V^2} \quad 5.20$$

6. Relative roughness (ϵ/d) was calculated with Colebrook-White equation (Colebrook, 1939). In addition, Swamee-Jain equation (Swamee and Jain, 1976) was also used to calculate the relative roughness. These equations are given as below.

Colebrook-White Equation

$$\frac{1}{\sqrt{f}} = -2 \log \left(\frac{\epsilon}{3.7D} + \frac{2.51}{Re\sqrt{f}} \right) \quad 5.21$$

Where Re is the Reynolds number between $4000 \leq Re \leq 10^8$ and $0 \leq \epsilon \leq 0.5$

Swamee-Jain Equation

$$f = \frac{0.25}{\log \left(\frac{\epsilon}{3.7D} + \frac{5.74}{Re^{0.9}} \right)^2} \quad 5.22$$

$$f = \frac{1.325}{\ln \left(\frac{\epsilon}{3.7D} + \frac{5.74}{Re^{0.9}} \right)^2} \quad 5.23$$

Where, Re is the Reynolds number between $5000 \leq Re \leq 10^8$ and $10^{-6} \leq \epsilon \leq 10^{-2}$

Swamee-Jain equation is an approximation of the Colebrook-White equation and yields approximate values of friction factor within 1% results of the Colebrook-White equation (Streeter et al., 1998).

Rearranging the Colebrook-White equation in term of (ϵ/D) is as below.

$$\frac{\epsilon}{d} = 3.7 \left(\frac{1}{\sqrt{10\sqrt{f}}} - \frac{2.51}{\text{Re}\sqrt{f}} \right) \quad 5.24$$

Rearranging the Swamee-Jain equation in term of (ϵ/D) is as below.

$$\frac{\epsilon}{d} = 3.7 \left(e^{\sqrt{\frac{1.325}{f}}} - \frac{5.74}{\text{Re}^{0.9}} \right) \quad 5.25$$

Where,

h_L is the head loss between two points at distance, L (ft)

L is the length of test section between two points of pressure measurement (ft.)

Q is flow rate (ft^3/s)

A is pipe cross-sectional area (ft^2)

V is the fluid mean velocity (ft/s)

D is the pipe diameter (ft)

ν is the kinematic viscosity of water (ft^2/s)

(Note: The kinematic viscosity (ν) changes with the observed water temperature during each test run).

g is the gravitational acceleration ($32.174 \text{ ft}/\text{s}^2$)

f is the friction factor

ϵ/d is the relative roughness of pipe

The above mentioned parameters were calculated for each test run.

Figure 5.26 depicts the plotted relationship between the head loss and average flow rate for bare carbon steel pipe.

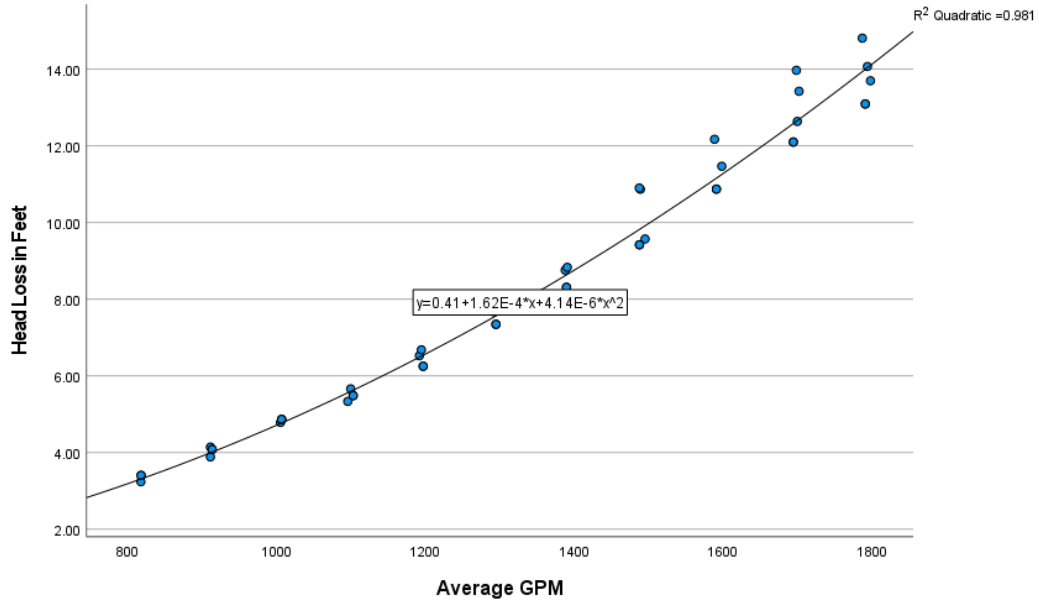


Figure 5.26 Bare Pipe Measured Head Loss vs. Flow Rate

A quadratic regression curve was fitted to the data points representing the relationship between flow rate and head loss to obtain the best fit. The approximate quadratic equation with $R^2 = 0.981$ obtained from regression curve is shown below.

$$y = 0.41 + 1.62 \times 10^{-4}x + 4.14 \times 10^{-6}x^2 \quad 5.26$$

The R^2 for the Equation 5.26 of head loss and average flow represents the higher degree of correlation between flow rate and head loss.

After the head loss calculation, the friction factor (f) and Reynolds (Re) numbers were calculated from the experimental data and plotted in Figure 5.26. It is depicted from Figure 5.26 that the friction factor decreases with the increase of Reynolds number, but not at a significant amount, confirming that flow regime experienced was transitional turbulence, aligning with the description provided in Moody's chart. The R^2 value for linear regression between Reynolds number and friction factor is 0.415 for as shown in Figure 5.27.

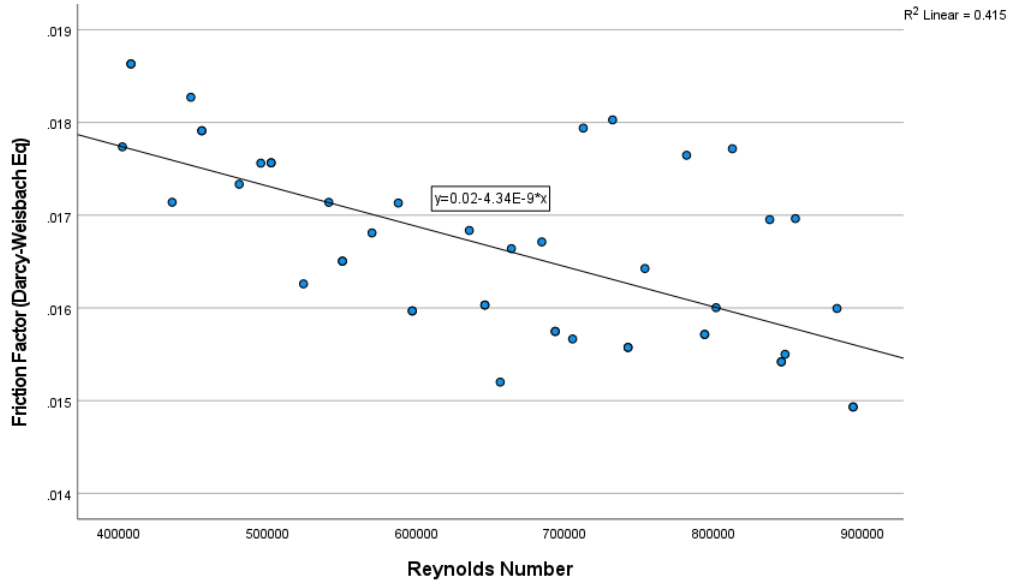


Figure 5.27 Bare Pipe Calculated Friction Factor vs. Reynolds number

The Darcy-Weisbach equation represented in the form of friction shows that the friction factor depends upon two main variables, velocity (v) and head loss (h_L).

$$f = h_L \frac{D}{L} \frac{2g}{V^2} \quad 5.27$$

Substituting the V in terms of Re is represented as below:

$$f = h_L \frac{1}{DL} \frac{2g}{v^2 Re^2} \quad 5.28$$

Thus, $f = f(V, D, L, h_L, v, g, Re)$

In this experiment, the values for D (diameter) and L (length) were kept constant. The values for v (kinematic viscosity) and g (acceleration due to gravity) were also considered constant. The kinematic viscosity (v) was considered constant because a drastic temperature variation was not observed during the test. The temperature variation was within the range of 4° F .

A multilinear regression was performed in which, the dependent variable (friction factor) was regressed on predicting variables of Reynolds number and head loss. The predicted values

from this regression line are represented in Figure 5.28. The R^2 value for multilinear regression is 0.79.

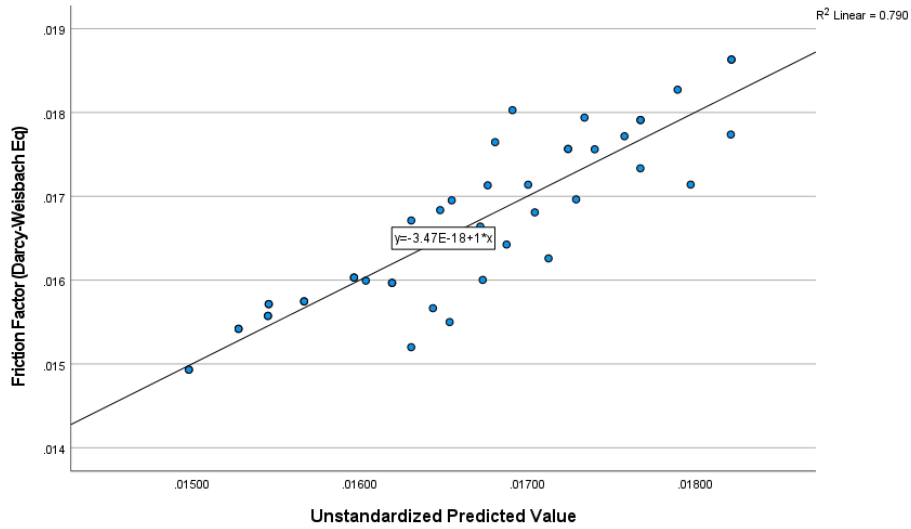


Figure 5.28 Bare Pipe Multiple Linear Regression Predicted Friction Factor vs. Calculated Friction Factor

The analysis of variance (ANOVA) and Coefficients results of dependent and independent variables for the bare pipe multi regression model generated from SPSS modelling software are shown below.

Regression

Descriptive Statistics			
	Mean	Std. Deviation	N
Friction Factor (Darcy's Weisbach Eq)	.01664	.001014	46
Reynold's Number	654534.2312	150589.94337	46
Head Loss in Feet	8.4022	3.50966	46

Model Summary^b

Model	R	R Square	Adjusted R Square	Std. Error of the Estimate	R Square Change	Change Statistics			
						F Change	df1	df2	Sig. F Change
1	.889 ^a	.790	.780	.000476	.790	80.831	2	43	<.001

a. Predictors: (Constant), Head Loss in Feet, Reynold's Number

b. Dependent Variable: Friction Factor (Darcy's Weisbach Eq)

ANOVA^a

Model		Sum of Squares	df	Mean Square	F	Sig.
1	Regression	.000	2	.000	80.831	<.001 ^b
	Residual	.000	43	.000		
	Total	.000	45			

a. Dependent Variable: Friction Factor (Darcy's Weisbach Eq)

b. Predictors: (Constant), Head Loss in Feet, Reynold's Number

Coefficients^a

Model		Unstandardized Coefficients		Standardized Coefficients	t	Sig.	95.0% Confidence Interval for B	
		B	Std. Error	Beta			Lower Bound	Upper Bound
1	(Constant)	.025	.001		36.089	<.001	.023	.026
	Reynold's Number	-2.309E-8	.000		-3.429	<.001	.000	.000
	Head Loss in Feet	.001	.000		2.851	<.001	.001	.001

a. Dependent Variable: Friction Factor (Darcy's Weisbach Eq)

Residuals Statistics^a

	Minimum	Maximum	Mean	Std. Deviation	N
Predicted Value	.01498	.01822	.01664	.000901	46
Residual	-.001108	.001116	.000000	.000465	46
Std. Predicted Value	-1.844	1.747	.000	1.000	46
Std. Residual	-2.329	2.347	.000	.978	46

a. Dependent Variable: Friction Factor (Darcy's Weisbach Eq)

The results show that the model has a value of $R^2 = 0.79$, with a significance value of P less than 0.001. The significance P value confirms that the result was acceptable. Also, the ANOVA value for P (significance) was less than 0.001, indicating that the regression was significant, and the dependent variables account for the friction factor. In addition, the coefficients results represent the individual P value for each variable were less than 0.001, which means these variables were significantly contributing the unique variance in predicting the dependent variable of friction factor.

The equation developed based on the multilinear regression result is given below.

$$f = 0.01 \times h_L \text{ (ft)} - 2.309 \times 10^{-8} \times Re + 0.025 \quad 5.29$$

The minimum and maximum friction factors observed by using the multi regression between friction factor, Reynolds number, and head loss in this experiment were 0.01498 at 8.9×10^5 Re, and 0.01822 at 4.0×10^5 Re. Thus, the average friction factor was 0.01664 within the range of Reynolds number between at 4.0×10^5 and 8.9×10^5 .

To understand the effect of roughness on the friction factor, the relative roughness (ϵ/D) was first calculated by using the Swamee-Jain and Colebrook-White equations. The relationship between the friction factor and relative roughness calculated with Swamee-Jain equation is plotted in Figure 5.29. This plotted data shows a strong quadratic correlation between the friction factor and the relative roughness with a R^2 of 0.968. Figure 5.29 shows that the friction factor increases with the increase of the relative roughness; thus, the experimental data confirms the Moody chart's turbulent transitional zone regime.

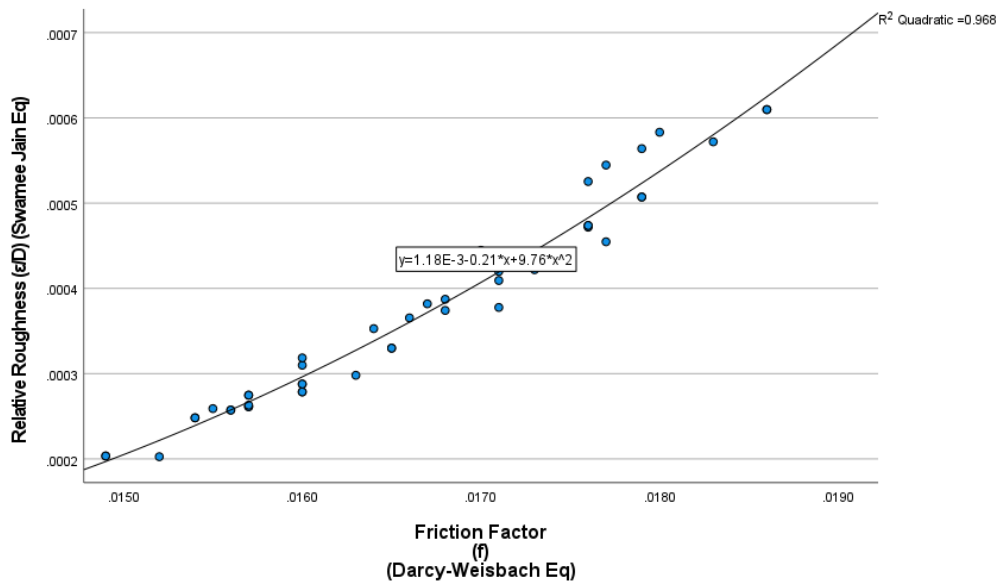


Figure 5.29 Bare Steel Pipe Friction Factor vs. Relative Roughness (Calculated with Swamee-Jain Equation)

The descriptive statistics shown below presents the regression results of the Relative Roughness vs. Friction Factor. The mean value of the relative roughness calculated was 0.000374.

The equation developed based on the regression results is as below.

$$\frac{\varepsilon}{D} = 1.18 \times 10^{-3} - 0.21 \times f + 9.76 \times f^2 \quad 5.30$$

Secondly, the relative roughness (ε/D) was calculated by performing the Colebrook-White equations. The relationship between the friction factor and relative roughness calculated with Colebrook-White equation is plotted in Figure 5.30. This plotted data shows a strong quadratic correlation between the friction factor and the relative roughness with a R^2 of 0.971 as compared to R^2 of 0.968 obtained by implementing Swamee-Jain equation. Figure 5.30 shows that the friction factor increases with the increase of the relative roughness; thus, the experimental data confirms the Moody chart's turbulent transitional zone regime.

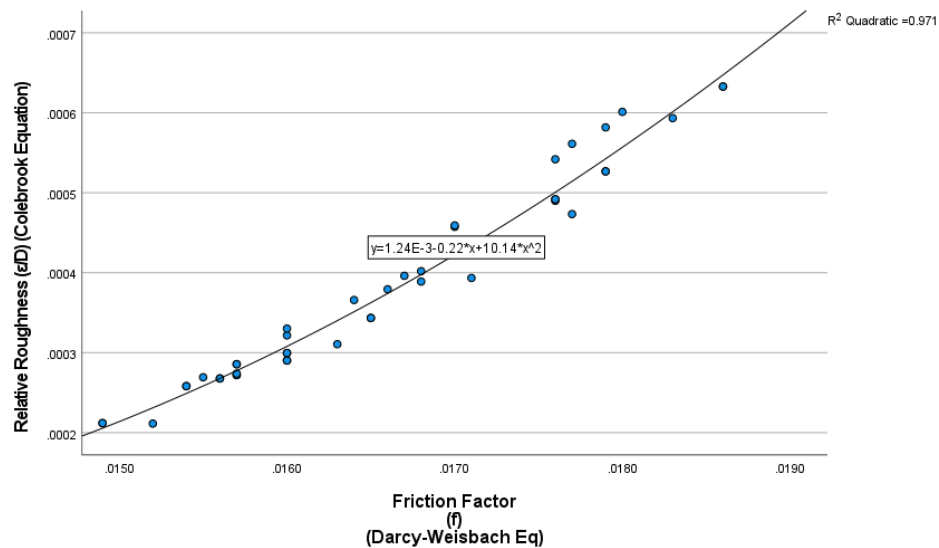


Figure 5.30 Bare Pipe Friction Factor vs. Relative Roughness
(Calculated with Colebrook-White Equation)

The descriptive statistics below show the regression results of the Relative Roughness vs. Friction Factor. The mean value of the relative roughness calculated was 0.000388.

The equation developed based on the regression results is as below.

$$\frac{\epsilon}{D} = 1.24 \times 10^{-3} - 0.22 \times f + 10.14 \times f^2 \quad 5.31$$

Thus, relative roughness calculated with Swamee-Jain was 0.00034, and with Colebrook-White equation was 0.00038, which were approximately equal. The values obtained from Swamee-Jain equation represent the relative roughness 4% less than the roughness values determined by Colebrook-White equation. Equivalent roughness (ϵ) determined with Swamee-Jain equation was 0.00262 in (0.052 mm). Equivalent roughness (ϵ) determined with Colebrook-White equation was 0.00230 in (0.058 mm). This measured equivalent roughness (ϵ) represents the carbon steel bare pipe roughness.

5.6.2 Lined Pipe Test Results

The data collected for the flow and head loss was used to calculate the velocity, Reynolds number, friction factor, and equivalent roughness. The flow rate vs. head loss were plotted in Figure 5.31.

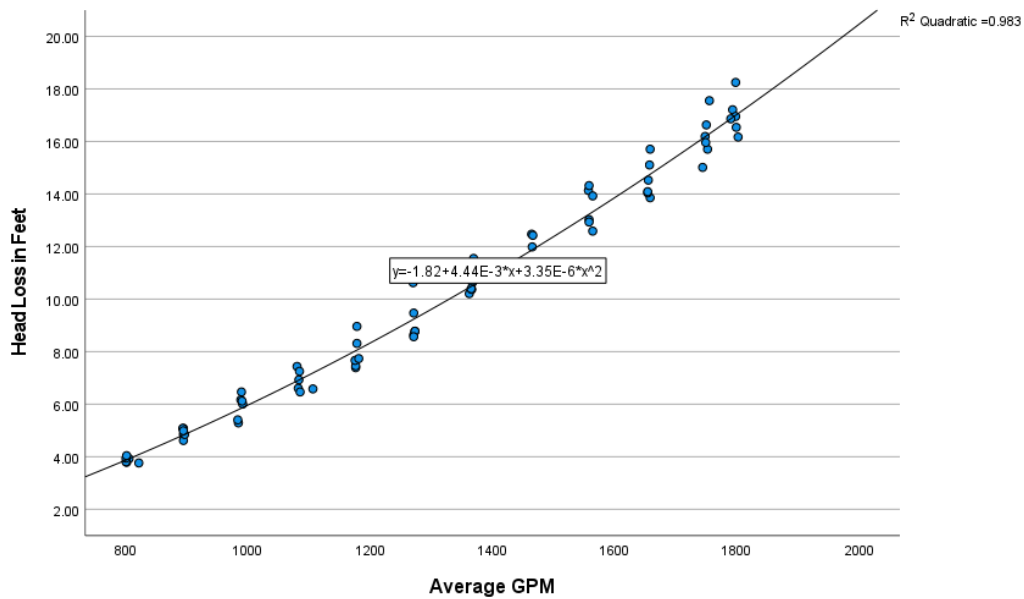


Figure 5.31 Lined Pipe Head Loss vs. Flow Rate

The best fit quadratic regression curve was fitted to the flow rate vs. head loss. The approximate quadratic equation can be used to estimate the head loss (h_L) at any given flow rate (Q) as represented in the following equation with $R^2=0.983$.

$$y = -1.82 + 4.44 \times 10^{-3}x + 3.35 \times 10^{-6}x^2 \quad 5.32$$

The R^2 for equation of head loss and average flow rate represents the higher degree of correlation for lined pipe similar to the bare pipe test.

Similar to the bare pipe test results, the calculated friction factor (f) and Reynolds number (Re) are plotted in Figure 5.32. A similar correlation of decreasing friction factor with increasing Reynolds number observed in bare pipe test was observed in lined pipe test. This confirms the transitional turbulence flow as described in the Moody's chart. The R^2 value for Reynolds number and friction factor was 0.468 for linear regression.

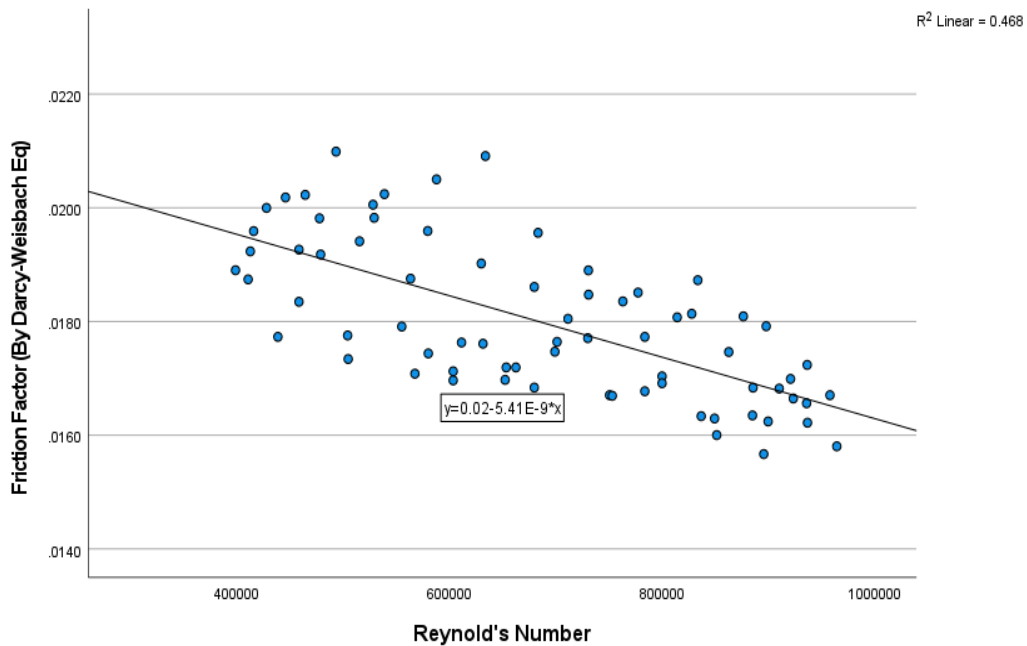


Figure 5.32 Lined Pipe Friction Factor vs. Reynolds number

As explained in the bare pipe test results, a similar multilinear regression applied in bare pipe was implemented to lined pipe test data.

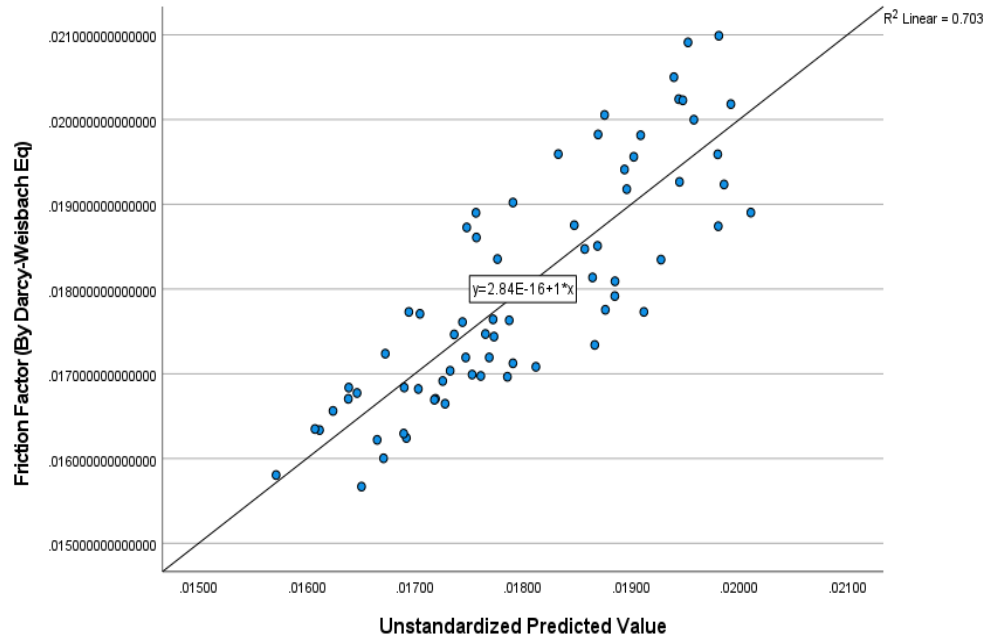


Figure 5.33 Lined Pipe Multi Regression
 Predicted Friction Factor vs. Calculated Friction Factor

The combined multilinear regression line between friction factor, Reynolds number, and head loss is represented in Figure 5.33, and the predicted values from this regression line are depicted in Figure 5.33. The R^2 value for multilinear regression has been improved to 0.703.

The detailed SPSS results for the multilinear regression with the ANOVA and Coefficients are shown as below.

Descriptive Statistics			
	Mean	Std. Deviation	N
Friction Factor (By Darcy Weisbach Eq)	.01799816745	.00133703935	72
Reynold's Number	684557.33396	169035.65598	72
Head Loss in Feet	10.198650000	4.3291344777	72

Model Summary ^b									
Model	R	R Square	Adjusted R Square	Std. Error of the Estimate	R Square Change	Change Statistics			
						F Change	df1	df2	Sig. F Change
1	.839 ^a	.703	.695	.00073872521	.703	81.792	2	69	<.001

a. Predictors: (Constant), Head Loss in Feet, Reynold's Number
 b. Dependent Variable: Friction Factor (By Darcy Weisbach Eq)

ANOVA^a

Model		Sum of Squares	df	Mean Square	F	Sig.
1	Regression	.000	2	.000	81.792	<.001 ^b
	Residual	.000	69	.000		
	Total	.000	71			

a. Dependent Variable: Friction Factor (By Darcy Weisbach Eq)
b. Predictors: (Constant), Head Loss in Feet, Reynold's Number

Coefficients^a

Model		Unstandardized Coefficients		Standardized Coefficients	t	Sig.	95.0% Confidence Interval for B	
		B	Std. Error	Beta			Lower Bound	Upper Bound
1	(Constant)	.027	.001		34.083	<.001	.025	.028
	Reynold's Number	-2.400E-8	.000	-3.035	-9.355	<.001	.000	.000
	Head Loss in Feet	.001	.000	2.400	7.399	<.001	.001	.001

a. Dependent Variable: Friction Factor (By Darcy Weisbach Eq)

Residuals Statistics^a

	Minimum	Maximum	Mean	Std. Deviation	N
Predicted Value	.01571694948	.02010799013	.01799816745	.00112130796	72
Residual	-.0013876890	.00138460856	.00000000000	.00072824631	72
Std. Predicted Value	-2.034	1.882	.000	1.000	72
Std. Residual	-1.878	1.874	.000	.986	72

a. Dependent Variable: Friction Factor (By Darcy Weisbach Eq)

The results show that the model has a value of R^2 equals to 0.703, with a significance value of P less than 0.01. The P value confirm that the result is acceptable. Also, the ANOVA value for P (significance) is less than 0.001, indicating that the regression is significant, and the dependent variables account for the friction factor. In addition, the coefficients results represent the individual P value for each variable is less than 0.001, which means these variables were significantly contributing the unique variance in predicting the dependent variable of friction factor.

The equation developed based on the multilinear regression results is given as below:

$$f = 0.01 \times h_L \text{ (ft)} - 2.40 \times 10^{-8} \times Re + 0.027 \quad 5.33$$

The minimum and maximum friction factor observed by using the liner regression between friction factor, Reynolds number and head loss in this experiment was 0.0157, and 0.0201 respectively. The mean value of the friction factor calculated was 0.0180.

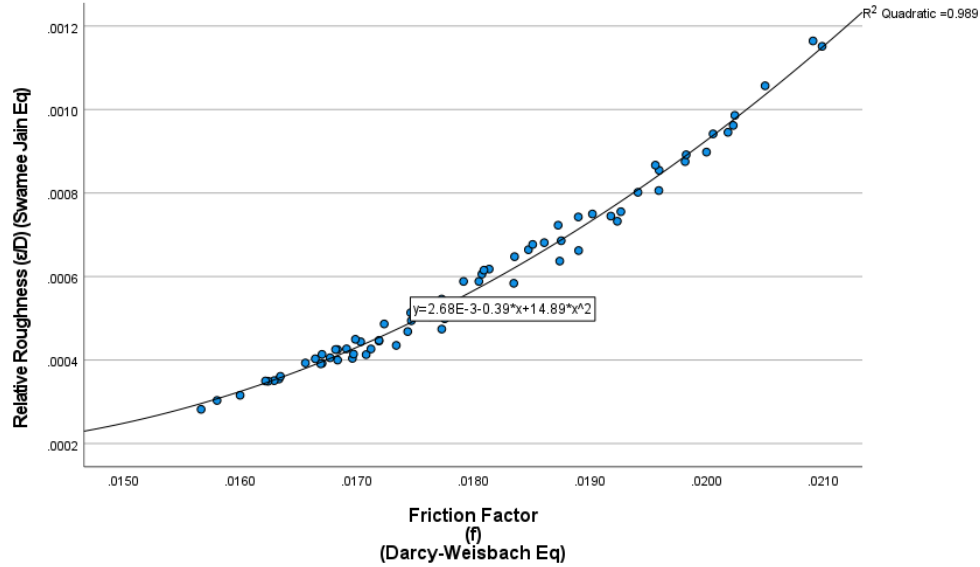


Figure 5.34 Friction Factor vs. Lined Pipe Relative Roughness (Calculated with Swamee-Jain Equation)

To understand the effect of roughness on the friction factor, the relative roughness (ϵ/D) was calculated by performing the Swamee-Jain and Colebrook-White equations. The relationship between the friction factor and relative roughness calculated with Swamee-Jain equation is plotted in Figure 5.34. This plotted data shows a strong quadratic correlation between the friction factor and the relative roughness with a R^2 of 0.989. Figure 5.34 shows that the friction factor increases with the increase of the relative roughness; thus, the experimental data confirms the Moody chart's turbulent transitional zone regime for the lined pipe.

The descriptive statistics below show the regression results of Relative Roughness vs. Friction Factor for lined pipe. The mean value of the relative roughness calculated was 0.000592. The equation developed based on the regression results as represented above is:

$$\frac{\epsilon}{D} = 2.68 \times 10^{-3} - 0.39 \times f + 14.89 \times f^2 \quad 5.34$$

The relative roughness (ϵ/D) for the lined pipe was calculated by performing the Colebrook-White equations as well. The relationship between the friction factor and relative

roughness calculated with Colebrook-White equation is plotted in Figure 5.35. This plotted data shows a strong quadratic correlation between the friction factor and the relative roughness with a R^2 of 0.991 as compared to R^2 of 0.989 obtained by implementing Swamee-Jain equation. Figure 5.35 shows that the friction factor increases with the increase of the relative roughness; thus, the experimental data confirms the Moody chart's turbulent transitional zone regime for lined pipe.

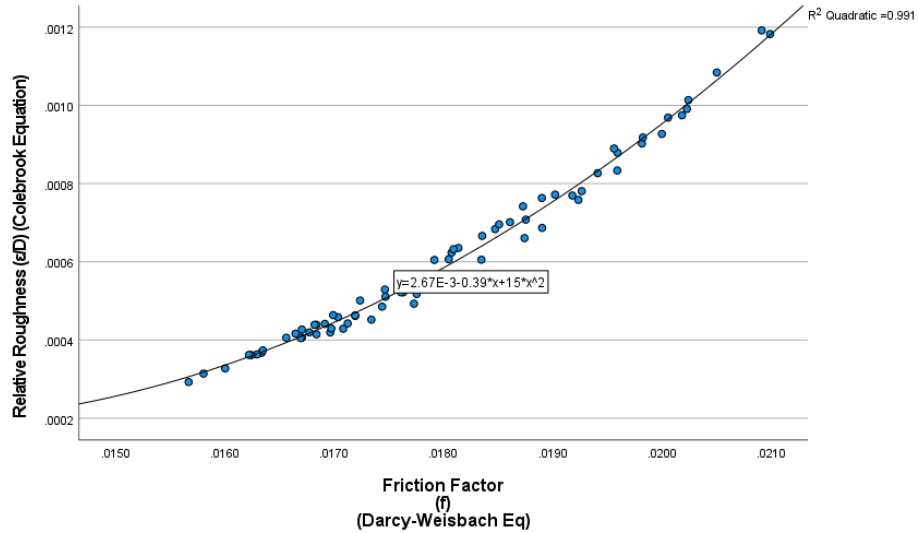


Figure 5.35 Friction Factor vs. Lined Pipe Relative Roughness (Calculated with Colebrook-White Equation)

The descriptive statistics below show the regression results of the relative roughness vs. friction factor. The mean value of the relative roughness calculated was 0.000611.

The equation developed based on the regression results is given below.

$$\frac{\varepsilon}{D} = 2.67 \times 10^{-3} - 0.39 \times f + 15 \times f^2 \quad 5.35$$

Thus, relative roughness calculated with Swamee-Jain was 0.000592, and with Colebrook-White equation was 0.000611, which were approximately equal. The values obtained from Swamee-Jain equation represent the relative roughness 3.1% less than the roughness values determined by Colebrook-White equation. Equivalent roughness (ε) determined with Swamee-Jain

equation was 0.003489 in (0.088 mm). Equivalent roughness (ϵ) determined with Colebrook-White equation was 0.0036 in (0.091 mm). The considered value of the lined pipe roughness was 0.0036 in. to compare it with bare pipe roughness values.

5.6.3 Field Measured Roughness of Lined Pipes

The roughness was measured on field with Mitutoyo portable surface roughness tester on the liner material that was coated inside the pipe diameter. The R_a , $R_{y_{max}}$, and R_z was measured with Mitutoyo surface tester in μin .

R_a is an arithmetic or average roughness, represents the average distance between peaks and valleys and the deviation from the mean line within a sampling length.

$R_{y_{max}}$ is the maximum height of the profile within a sampling length measured in y direction.

R_z is calculated by measuring five highest peaks and five deepest valleys obtained from five consecutive measuring length within a sampling length.

The probe tip radius was $5\ \mu\text{m}$, and the sampling length used for measuring the roughness was 0.1 in. The roughness was measured at the bottom of the pipe is as shown in Figure 5.36.



Figure 5.36 Roughness Measurement with Portable Surface Roughness Tester

Farshad and Pesacreta (2003) suggested that to measure the sand grain surface roughness, the measured peak-to-valley roughness, R_z gives a more realistic result as compared to arithmetic average roughness, R_a . In addition, R_z shows conservative roughness data, which could be considered for the liner measured roughness.

Adams and Grant (2012) proposed that profilometer roughness data cannot be directly applied to Moody's chart, which is commonly used for estimating the friction factor and determining head loss based on relative roughness. The Moody chart was developed using experimental data gathered from pipes with intentionally roughened surfaces coated with a layer of sand. As a result, the pipe wall roughness in the chart is based on the average diameter of the sand grains. Adams and Grant (2012) developed an algorithm to convert the measured surface roughness into equivalent sand-grain roughness. They suggested a conversion factor of 0.978 to convert the R_z roughness parameter to estimated sand-grain roughness (ϵ).

Table 5.26 below shows the measured R_a , $R_{y_{max}}$, R_z roughness readings at the bottom of the lined pipe.

Table 5.26 Measured Roughness Readings with Portable Surface Roughness Tester

R_a (μ in)	$R_{y_{max}}$ (μ in)	R_z (μ in)	R_a (in)	$R_{y_{max}}$ (in)	R_z (in)	Est. Equivalent Roughness*
53.15	67.86	267.86	0.000053	0.000068	0.00027	0.00026
19.33	25.21	132.63	0.000019	0.000025	0.00013	0.00013
55.95	73.06	351.66	0.000056	0.000073	0.00035	0.00034
35.92	48.28	296.97	0.000036	0.000048	0.00030	0.00029
28.06	38.22	206.47	0.000028	0.000038	0.00021	0.00020
18.34	28.14	173.20	0.000018	0.000028	0.00017	0.00017
18.97	25.9	132.74	0.000019	0.000026	0.00013	0.00013
52.02	73.7	306.31	0.000052	0.000074	0.00031	0.00030
15.09	19.32	106.69	0.000015	0.000019	0.00011	0.00010

*Estimated Equivalent Roughness= $R_z \times 0.978$ (Adams and Grant, 2012)

A conversion factor of 0.978 can be applied to the measured R_{zd} to determine the estimated equivalent roughness (Adams and Grant, 2012). From table 5.26, the highest value of the estimated equivalent roughness of 0.00034 in. was considered to represent the worst-case scenario.

5.6.4 Laboratory Measured Roughness of Lined Sample with Optical Profilometer

For a better comparison of liner friction factor, the liner roughness was also measured with optical profilometer in the laboratory. The measured roughness with profilometer can predict the extent of the improvement of the friction of liner when applied with 100% quality control. Figure 5.37 shows the KLA Tencor profilometer. Liner samples of less than 4 in. and thickness approximately 0.118-0.157 in. (3-4 mm) were tested with KLA Tencor optical profilometer. The instrument measured the root mean square roughness (R_{RMS} or S_q) which is square of the sum of the squares of the individual heights and depths from the average line. Also, the instrument measured the S_q which was same as R_z .

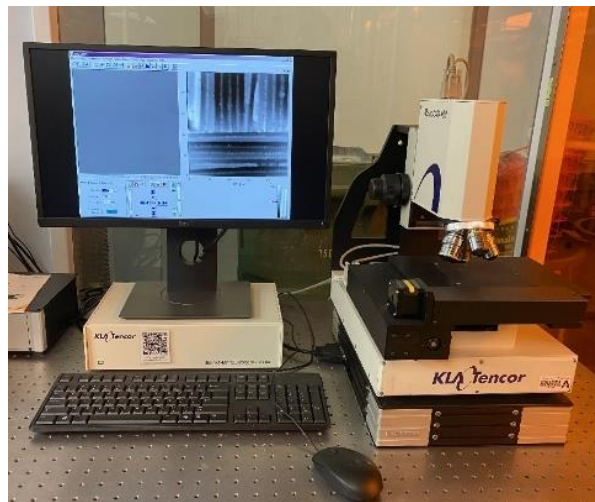


Figure 5.37 KLA Tencor Profilometer

Figure 5.38 shows the graph with surface characteristic values of sample 6. A 3D image of the roughness profile of the liner sample 6 is shown in Figure 5.39.

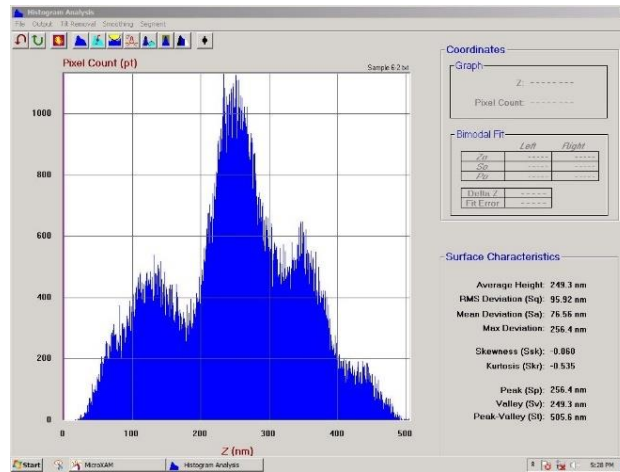


Figure 5.38 Sample 6 3D Roughness Profile

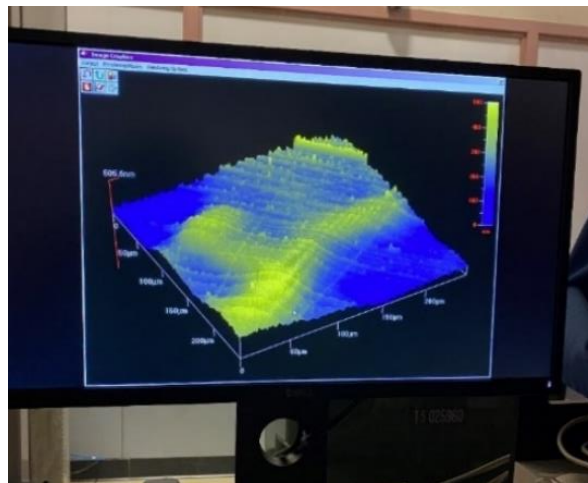


Figure 5.39 Sample 6 3D Image Roughness Characteristics

The roughness reading for five liner samples are shown in Table 5.27.

Table 5.27 Measures Liner Roughness with Optical Profilometer

Sample #	RMS Deviation (S_q) R_{RMS}		Peak-Valley (S_t) R_z		Estimated Equivalent Roughness	
	nm	in.	nm	in.		
Sample 2	L1	103.4	0.00000407	761.3	0.00003	0.000029
	L2	54.05	0.00000213	501.1	0.00002	0.000020
Sample 3	L1	87.23	0.00000343	628.4	0.00002	0.000020
	L2	109.2	0.00000430	889.2	0.00004	0.000039

Sample #		RMS Deviation (S_q) R_{RMS}	S_q	Peak-Valley (S_t) R_z	S_t	Estimated Equivalent Roughness
		nm	in.	nm	in.	in.
Sample 4	L1	50.93	0.00000201	357.2	0.00001	0.000010
	L2	195.8	0.00000771	838.7	0.00003	0.000029
Sample 5	L1	61.04	0.00000240	393.5	0.00002	0.000020
	L2	47.49	0.00000187	302.7	0.00001	0.000010
Sample 6	L1	43.66	0.00000172	360.3	0.00001	0.000010
	L2	95.92	0.00000378	505.6	0.00002	0.000020

*Estimated Equivalent Roughness= $R_z \times 0.978$ (Adams and Grant, 2012)

A conversion factor of 0.978 was applied to measured R_{zd} to determine the estimated equivalent roughness (Adams and Grant, 2012). Thus, the maximum estimated equivalent roughness after applying the conversion factor was 0.000039 in.

5.6.5 Comparison of Equivalent Estimated Roughness

The equivalent values of roughness were measured by using fluid flow experiment, KLA Tencor optical profilometer in laboratory, and by using the Portable Surface Roughness Tester with External Display, Marsurf Pocket Surf IV. These roughness values are represented in Table 5.28 as below.

Table 5.28 Comparison of Equivalent Estimated Roughness (ϵ)

Description	Flow Test	KLA Tencor optical profilometer	Portable Surface Roughness Tester
Estimated Equivalent Roughness	0.00408 in.	0.000039 in.	0.00034 in.

The equivalent roughness measured with three different methods showed different values, which was expected. The equivalent roughness measured with the flow test was more representative because it was obtained after performing the full-scale experimental method and assessment. This represents more ideal value because the liner installation might have some irregularities which can impact the roughness value.

However, the estimated roughness values by KLA Tencor optical profilometer reported the minimum value, even when it was calibrated with the conversion factor provided by Adam and Grant (2012). The roughness values obtained with KLA Tencor optical profilometer was based on a small square sample prepared in optimal environment and installation conditions. Whereas it is very difficult to achieve the same result of liner installation in the actual field application. Therefore, the values obtained by the optical profilometer cannot be considered as a representative roughness value in the pipeline industry for the liner application.

When considering the portable surface tester roughness values, the estimated roughness was lower than the flow test values because the roughness was measured at the bottom of the pipe. However, when inspecting the internal surface profile of the pipe, it was observed that the crown has more irregularities compared to bottom of the pipe. Thus, the estimated roughness values by the flow test were the most representative as compared to the other measured roughness values because it has considered all the effects of the liner installation on the internal pipe diameter in the actual field conditions.

However, the equivalent roughness obtained by flow test can be improved and may achieve comparable results to portable surface tester roughness values. These comparable results can be achieved in a condition that the liner profile at the top is similar to the bottom of pipe with minimal irregularities. Therefore, the equivalent roughness is highly depended on the liner application with proper quality control. In addition, when the liner application is considered for the large diameter pipes, the representative relative roughness (ϵ/D) would be improved at a larger scale.

5.6.6 Comparison of Lined Pipe Test Results with Bare and Corroded Pipes

Corrosion of pipes is a complex process, and evaluating the corrosion effect is difficult. Bain (1979) performed a study, evaluating the corrosion effect on the carbon steel raw piping

system used in Emergency Equipment Cooling Water (EECW) in a nuclear plant. This study considered approximately 50 pipe samples with different diameters from 9 different locations. These pipe samples were analyzed to determine the buildup chemical composition, average reduction in the internal pipe diameter, average wall reduction, and thinning. This study concluded that at the end of 40 years of plant life, carbon steel raw water piping system would experience an average reduction of 0.40 in. in the internal pipe diameter due to corrosion.

From Bain et al. (1979) corrosion study, the 6 in. diameter pipes with a service period of approximately 23 years were considered for calculating the head loss of the corroded pipes to be used in this study. The condition of these pipes was observed with a small amount of uniform buildup of iron and silicon oxide but with large tubercles (approximately 2 in. in height). The average reduction in internal diameter of these pipes was given as 0.133 in. These pipes were considered moderately corroded, so the absolute roughness was considered on the higher side of 0.0059-0.0394 in. (0.15-1 mm) (Neutrium, Thermal Engineering). Thus, the flow rate calculations for the corroded pipe were performed considering the average internal diameter reduction of 0.133 in. and roughness of 0.393 in. (1 mm).



Figure 5.40 Nuclear Service Water System Piping Tubercles Increased Pipe Roughness and Reduce Pipe Internal Diameter (Adapted from Onat et al., (2016))

However, the corrosion rate and subsequently, average internal diameter reduction will depend upon the fluid flowing through the pipe and its reaction with the host pipe. In addition, the

surrounding environmental conditions also impact the rate of corrosion. Other parameters of fluid properties such as velocity, temperature, hardness, total dissolved solids, pH level, alkalinity, and conductivity are major contributors to the corrosion rate (Alley, 2007). Figure 5.40 shows an example of the reduction in the internal diameter and roughness of a corroded pipe due to tubercles.

The bare, lined, and corroded pipe results were compared based on head loss vs. flow rate. Figure 5.41 shows that as the flow rate increases, the head loss increases for bare, lined, and corroded pipes. In addition, at higher flow rates, the difference in head loss between corroded pipe and lined pipes is increasing, but at a much higher rate.

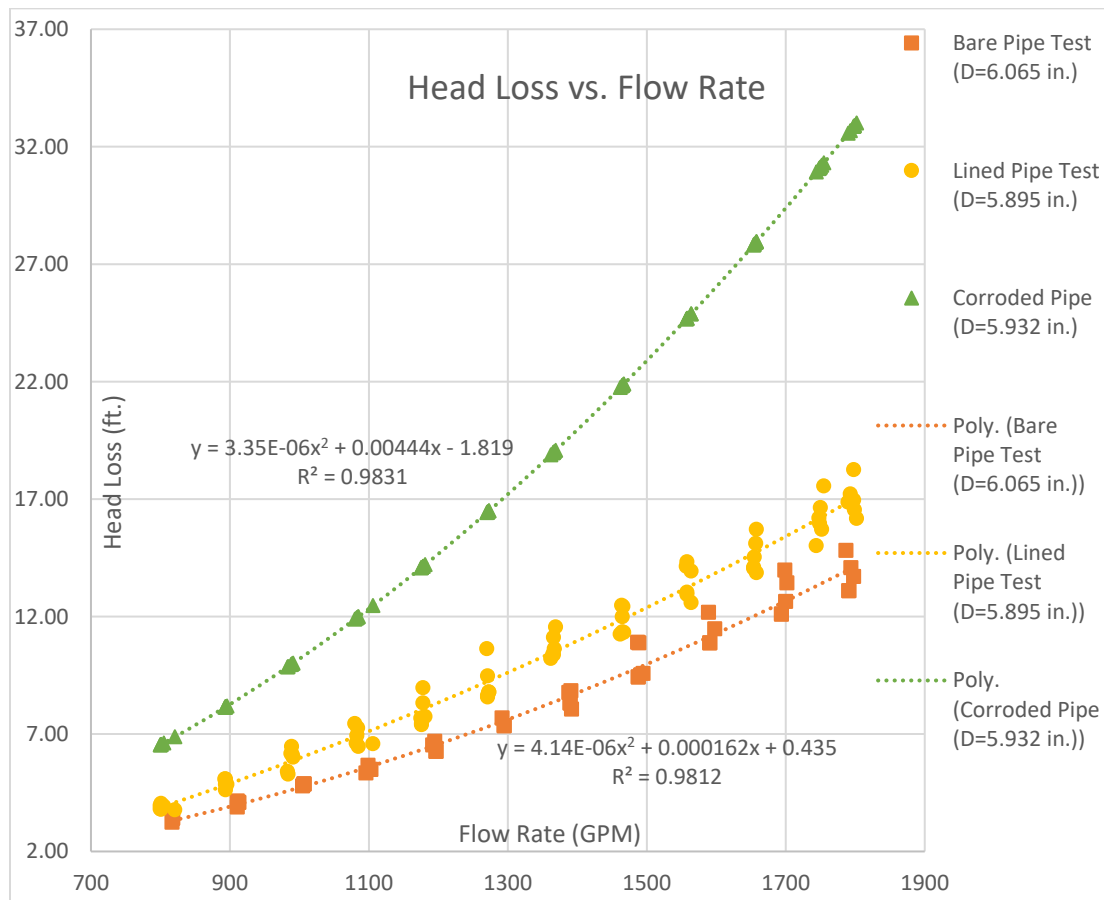


Figure 5.41 Head Loss Comparison for Bare, Lined and Corroded Pipes (at Different Flow Rate)

The head loss for the lined pipe was slightly more than the bare pipe. The increased head loss for the lined pipe is attributed to the reduced internal pipe diameter (ID) due to liner application. The following conclusions were made when comparing the head loss of the bare and lined pipes with a corroded pipe.

- Head loss of new carbon steel pipe was approximately 60.36 % less than moderately corroded pipe at 1800 GPM.
- Head loss of lined pipe was approximately 51.01 % less than moderately corroded pipe at 1800 GPM.

Thus, it was concluded that the application of liner on a moderately corroded pipe can reduce the head loss by approximately 51.01 %. This improvement in head loss would lead to an enhancement in flow performance. However, the efficiency of the lined pipes can be greatly improved when compared to highly corroded pipes. Therefore, liner application can effectively improve the head loss and, consequently, it can reduce the pumping requirement to maintain the flow.

Another important comparison was performed between the friction factors of the bare, lined, and corroded pipes at different Reynolds numbers. Figure 5.42 shows three regression lines, for bare, lined, and corroded pipes, following the trend of decreasing friction factor with the increase of Reynolds number and conforming to the transitional turbulence flow regime as described in Moody's chart.

The case scenario of a corroded pipe with absolute roughness of 0.03937 in. (Neutrium, Thermal Engineering) was used to calculate the friction factors at different flow rates, assuming the diameter reduction of 0.133 applied to the bare carbon steel pipe. The pipe reduction and absolute roughness were considered for moderately corroded pipes as described earlier.

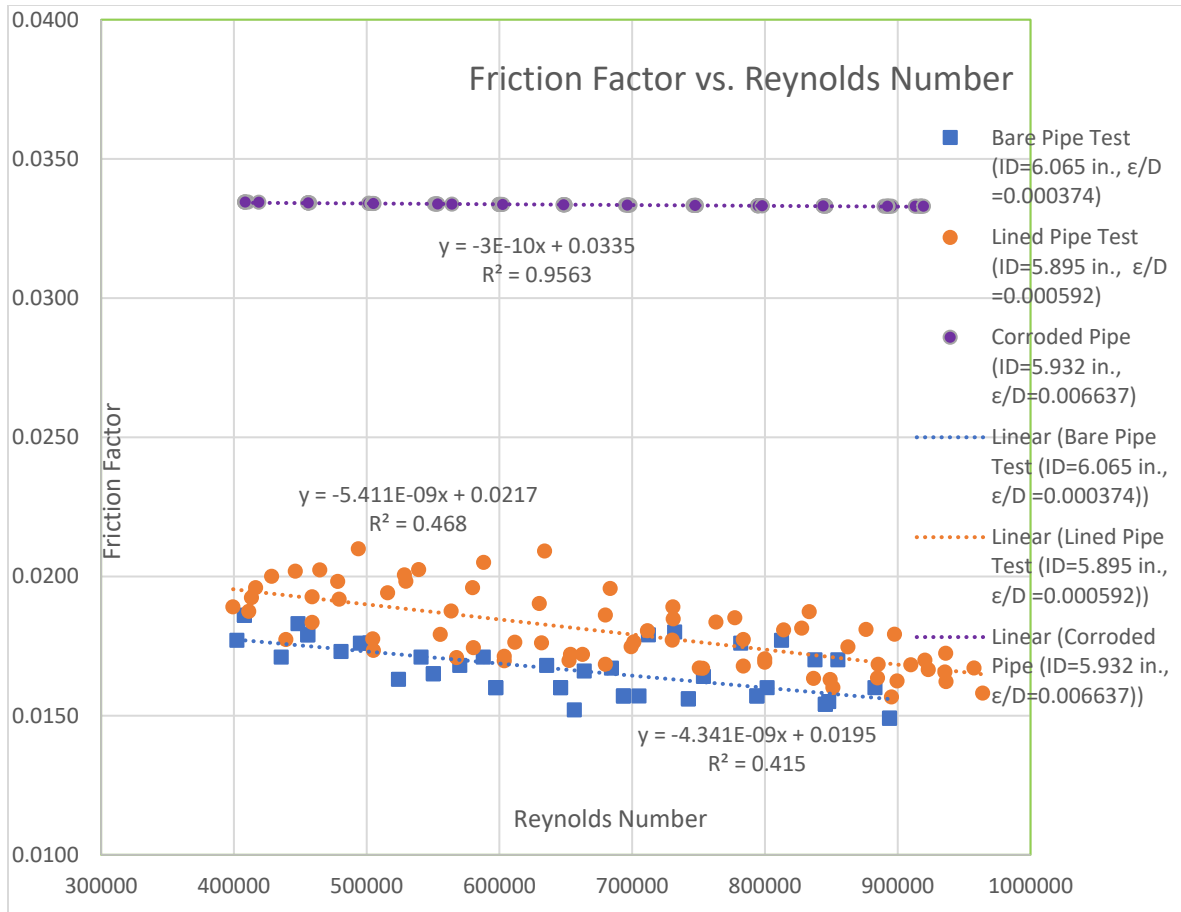


Figure 5.42 Friction Factor Comparison for Lined Pipe with Bare Pipe, and PVC Pipe

Figure 5.42 represents best-fit lines for friction factor vs. Reynolds number for lined, bare, and moderately corroded pipes. The corroded pipe results showed more friction factor as compared to bare and lined pipes. The average friction factor of corroded pipe was 0.0334 as compared to the friction factor of lined pipe 0.0180 and bare steel pipe 0.01664. When comparing the friction factor of the corroded pipe with the bare and lined pipes for a range of Reynolds numbers between 4×10^5 and 8.9×10^5 , the following observations were observed.

- The average friction factor of new carbon steel pipe was approximately 50.06 % less than moderately corroded pipe.
- The average friction factor of lined carbon steel pipe was approximately 45.86 % less than moderately corroded pipe.

5.7 Contribution to Body of Knowledge

This dissertation provided the test design methodologies and experimental test results to evaluate the polymeric SAPL lining system to classify its use as semi-structural (Class II) and fully structural (Class IV) in pipe rehabilitation. In addition, this study tested and evaluated the improvement in flow characteristics of the SAPL lined pipe compared to a moderately corroded pipe. Conducting tests on the SAPL lining system in large diameter pipes for hole-spanning, pressure integrity tests under extreme temperature conditions, and evaluating hydraulic flow in SAPL lined pipes within a turbulent flow regime contribute valuable data to the existing literature for SAPL practitioners. Lastly, this dissertation also studied the validation of the design equations for both semi-structural and fully structural lining system as recommended by AWWA (2019) structural classification system. The experimental test results suggested the need for modifications to these equations, in order to address the limitations within the design parameters and conditions.

5.8 Practical Applications

The test results of hole spanning and vacuum confirmed that the polymeric SAPL can be used as a pipe rehabilitation method when it is designed as semi-structural (Class II) lining system. The pressure integrity test results with temperature analysis can be used to design the SAPL lining system as fully structural (Class IV) in industrial high-pressure application pipes, especially under extreme temperature conditions. The test data obtained from this research on friction factor and roughness for SAPL material can be used to perform the hydraulic flow design and analysis.

5.9 Chapter Summary

This chapter presented the results of the structural and hydraulic testing and evaluation of the SAPL application in pressure pipes. Comprehensive test results and evaluation were

represented in different sections, including material testing, short-term hole spanning test, pressure integrity test, and hydraulic flow test. The material testing provided the mechanical properties of the material. The thickness of the liner design and the structural ability of the SAPL to bridge the corrosion holes of 0.5, 1, and 2 in. in a 30 in. diameter host pipe were presented in this chapter. Furthermore, the SAPL liner was designed as fully structural for 60 pipe samples of 8 in. diameter with different thicknesses, were tested at different temperatures. Lastly, it was important to test the hydraulic flow analysis of the liner. The hydraulic flow testing for bare carbon steel pipe of 6 in. diameter with and without SAPL was tested. The results were compared with corroded pipes to predict the percentage improvement of head loss for the corroded pipe by applying SAPL.

Chapter 6 Conclusions and Recommendations for Future

Research Studies

6.1 Conclusions

This dissertation conducted extensive experimental full-scale laboratory tests and provided detailed test methodologies to evaluate the structural and hydraulic properties of polymeric SAPL material in pressure pipes application. The polymeric SAPL material was tested as semi-structural and fully structural in pressure pipes. In addition, the hydraulic properties of the liner were also tested and evaluated to determine the head loss and flow improvement by applying polymeric SAPL to the host pipe.

The conclusions for this study have been divided into four sections such as 1) Short-term hole spanning internal hydrostatic pressure test, 2) Vacuum test, 3) Pressure integrity test, and 4) Hydraulic flow properties of the liner.

6.1.1 Short-term Hole Spanning Test

This test was designed to determine the capacity of polymeric pure polyurea liner to bridge the corrosion holes of 0.5, 1, and 2 in. in the host pipe. The pure polyurea material was used as a semi-structural SAPL liner to bridge these corrosion holes. The test results showed that the liner thickness designed using the modified AWWA Eq 3.2 demonstrated the ability to withstand the required pressure resistance of approximately 500 psi. The liner exhibited satisfactory performance at the hole spanning, and showed no indications of liner failure or bulging. Therefore, the modified design equation of AWWA (2019) structural classification of the lining system for class II to design the liner thickness showed acceptable criteria. However, multiple tests need to be done to

justify the results and to validate the change in the equation for using the tensile strength instead of flexural strength.

In addition, the maximum strain value obtained at 485 psi pressure for 2 in. hole spanning was approximately 6,200 $\mu\epsilon$, equal to 0.62% of strain. The percentage strain obtained was less than 5%, a recommended long-term performance strain of buried high density polyethylene pipes (HDPE) (Janson, 1981; Peggs et al., 2005). The material showed good resistance properties for high pressure values.

When comparing the stress vs. strain graphs obtained from the strain gauge used on the 2 in. hole spanning with the stress vs. strain graph of the coupon tensile test conducted on the same material, it was concluded that the material showed lower stress and deformation as compared to the coupon test stress and strain values obtained. The observed differences in stresses and deformations can be due to the variations in temperature during the two experiments. The coupon material testing conducted in the laboratory was performed at 73° F, whereas the hole-spanning experiment performed at an approximate ambient temperature of 54° F, with the water temperature in the test setup at 50° F. The elastomeric properties of the liner material show different behaviors at different temperatures, with the material behaving stiffer at lower temperatures compared to higher temperatures. Thus, the performance of polymeric material depends upon the temperature. Therefore, while designing the liner material application for elevated temperatures, a necessary design factor for temperature effect should be considered.

6.1.2 Vacuum Pressure Test

When designing the lining system as Class II, the liner material should have a minimal ring stiffness, which depends on the adhesive strength of the liner. The ring stiffness of the polymeric SAPL installed in the previous hole spanning test was tested by performing a vacuum test, in which

a vacuum pressure of 24.6 in. of Hg was achieved. No cracks, failures, or delamination of the liner from the host pipe were observed during the test. The test results demonstrated a strong bonding strength between the liner and the host pipe.

Therefore, the test results concluded that the polymeric lining system has minimal ring stiffness, which is required for Class II liner design to prevent any collapse in case of depressurizing the pipe. The short-term hole spanning, and vacuum pressure test results concluded that the liner designed as per AWWA Class II sufficiently resisted the internal hydrostatic pressure and vacuum load. When designing the lining system as Class II, the liner material should have a minimal ring stiffness, which depends upon the adhesive strength of the liner.

6.1.3 Pressure Integrity Test

Pressure integrity test was aimed to test the liner capabilities as a fully structural component, assuming that there is no support from the host pipe. The pipe samples were casted with hybrid polyurea SAPL material with different thicknesses, and these pipe samples were tested at temperatures of 73° F, 120° F, 150° F and 41° F. Testing the polymeric material at different thicknesses and temperatures was important to determine their effects on material performance.

6.1.3.1 Burst Pressure at Different Temperatures

It was concluded that the burst pressure values changed with a change in the test temperatures. Normally these values decreased at elevated temperatures, but higher at room and lower temperatures. In addition, it was noted that under hydrostatic pressure the performance was linearly decreased with an increase in temperature. Higher temperature has an impact on the tensile strength and tensile modulus, and thus, it degrades the material performance.

On the other side, polymeric material acted more rigid and showed higher tensile strength at ambient and lower temperatures and subsequently, pressure resistance was higher in comparison to elevated temperatures. At elevated temperatures, the mobility of the polymeric chains increases, leading to material deformation, and plasticity. Temperature changes cause the material to expand or contract, resulting in thermal stresses. At elevated temperatures, the thermal stresses combined with the hoop stresses induced by internal pressure can influence the overall structural integrity of the system. The burst test results concluded that material behaved less stiff at higher temperatures, and ultimately the strength of the material was compromised.

In addition, the AWWA design equation for Class IV is based on the tensile material properties, diameter, and working pressure. However, the equation does not specify the requirement of using material properties at a desired temperature of application. It is important to note that when the liner system is designed for different temperatures, the material properties at that desired temperature should be consideration while using the AWWA Class IV design equation.

It was also concluded that when considering the tensile strength of material at the required test temperature in the Equation 5.3, to predict the burst pressure, the equation worked well up to temperature of 120° F. The predicted results by using Equation 5.3 showed conformance with experimental results. However, at 150° F, even when using the tensile strength of the material at that elevated temperature, the Equation 5.3 exhibited significant inconsistencies. This significant variation could be due to testing the material above its recommended temperature limit of 134° F, which is considered 30° F below the glass transition temperature of 164° F of the material. Thus, it is recommended to evaluate the non-linearity of the Equation 5.3 closer to and beyond the material's glass transition temperature.

6.1.3.2 Failure Modes at Different Temperatures

Different pipe failure modes were observed at different temperatures, which confirmed that material behavior changes with a temperature change. It was concluded that pipe sample at ambient and lower temperatures acted more brittle and experienced a catastrophic failure. However, the pipe samples tested at a temperature of 120° F exhibited elastic and catastrophic failure modes. The material at this temperature showed elasticity but also showed a slight brittle behavior compared to pipe samples tested at ambient and lower temperatures.

On the other hand, the pipe samples tested at 150° F temperature demonstrated ductile failure, in which the material responded more elastically and physically changed its shape before ultimately splitting to a far less extent. In this type of failure, the pipe surfaces were initiated with cracks, and sometimes pin hole leaks were observed. Additionally, ballooning of samples and permanent deformation was observed. Therefore, it was concluded that the pressure, along with the temperature, affects the failure modes of the pipe samples.

6.1.3.3 Layer Formation

The broken pieces of the pipe samples revealed a common failure characteristic: the formation of layers. This was especially noticeable when the pipe samples were tested at temperatures of 73° F and 41° F. The formation of layers may be attributed to the curing behavior of the sprayed layers. The setting time between the sprayed layers was relatively short, which could result in setting of the previous sprayed layer before the next layer was applied. The problem of layer formation was mostly observed in pipe samples with higher thicknesses. Additionally, the installation procedure could also contribute to layer formation. Furthermore, the presence of microbubbles was observed in the broken sample pieces.

At elevated temperatures, no layer formation was seen in the broken samples. This could be because the polymers become softer and more flexible at high temperatures, causing the layers to merge together. The presence of layers and microbubbles could have an effect on the strength of the material and its ability to withstand pressure. It was concluded that the layer formation and microbubbles created weak internal areas along the wall thickness, leading to decreased burst pressure and hoop stress values.

6.1.3.4 Defects in Pipe Samples

The results obtained for burst pressure and hoop stress were based on testing the pipe samples casted by spraying the liner material on a circular pipe mold made with two semi-arch-shaped halves. The point of connection of these two semi-arches created a seam on some of the pipe sample. These pipe samples were observed with major seam defects and gap intrusions, however, some of the pipe samples were inspected with no seam line defects. The gap intrusions reduced the effective pipe thickness for testing, and created weak joints which led to burst failure points at the seam. It was observed that majority of the samples failed at the seam line. Thus, it was concluded that the presence of seam lines in the tested samples contributed significantly to the failures. Therefore, it was suggested that obtaining data from samples without seam lines could produce more representative results.

The material performance and failure mode changed with the temperature variation, thus, the combined effects of internal pressure and temperature must be taken into account when designing the SAPL for pressure pipes at varied temperature applications, to ensure structural integrity. During the SAPL application, the setting time between layers must be considered to avoid layer formation which can impact the material strength and performance.

6.1.4 Hydraulic Properties Test

Full-scale laboratory tests were conducted to determine the head loss, friction factor, and equivalent roughness of carbon steel pipe (new condition), and a pipe lined with SAPL polyurea hybrid material. The Darcy-Weisbach equation was used to calculate the friction factor, and Swamee-Jain and Colebrook-White equations were used to determine the roughness characteristics of the pipe with and without the liner. One of the important requirements of the test was to measure the head loss at high Reynolds number, i.e., completely turbulent flow regime, which is typically encountered in high pressure pipelines. The flow capacity, friction factor, and roughness of the bare, lined, and corroded pipes were compared to evaluate the improvement in the flow characteristics of lined pipe.

The head loss of the lined pipe closely resembles that of the new carbon steel pipe, with the latter exhibiting slightly less head loss. The head loss depends on pipe condition, diameter, and dimension ratio (DR). Thus, it is concluded that when considering a realistic scenario of a corroded pipe that is renewed with the SAPL material, the result is a potential reduction in the head loss of the lined pipe compared to the corroded pipe.

6.1.4.1 Comparison of Friction Factor

Friction factor was compared between bare and lined carbon steel pipe at different Reynolds number in the turbulent flow regime. The test results plotted for friction factor vs. Reynolds number followed the turbulent flow regime and confirming the Moody's chart. The friction factor depends upon the Reynolds number and the equivalent roughness.

- For bare pipe, the minimum value of friction factor was 0.01498 at 8.9×10^5 Reynolds number, and the maximum value of friction factor was 0.01822 at $4.0 \times$

10^5 . Thus, the average friction factor was 0.01664 within the range of Reynolds number between 4.0×10^5 and 8.9×10^5 .

- For lined pipe, the minimum value of friction factor was 0.01572 at 8.9×10^5 Reynolds number, and the maximum value of friction factor was 0.02010 at 4.0×10^5 . Thus, the average friction factor was 0.01800 within the range of Reynolds number between 4.9×10^5 and 8.9×10^5 .

When comparing the average friction factor of a new carbon steel pipe with a moderately corroded pipe, it was approximately 50.06 % less than a moderately corroded pipe. On the other hand, when comparing the average friction factor of a lined carbon steel pipe with a moderately corroded pipe, it was approximately 45.86 % less than a moderately corroded pipe.

6.1.4.2 Comparison of Roughness

Relative roughness was compared for both bare and lined pipe.

- The average relative roughness of bare carbon steel pipe calculated by Swamee-Jain equation was 0.000374; thus, the estimated equivalent roughness (ϵ) was 0.00227 in. (0.058 mm). Whereas the average relative roughness of bare carbon steel pipe calculated by Colebrook-White equation was 0.000388; thus, the estimated equivalent roughness (ϵ) was 0.00236 in. (0.060 mm). Both values of equivalent roughness were corresponding to carbon steel pipe values of absolute roughness of 0.02-0.050 mm (Neutrium, Thermal Engineering).
- The average relative roughness of lined carbon steel pipe calculated by Swamee-Jain equation was 0.000592; thus, the estimated equivalent roughness (ϵ) was 0.003489 in. (0.088 mm). Whereas the average relative roughness of lined carbon

steel pipe calculated by Colebrook-White equation was 0.000611, thus, the estimated equivalent roughness (ϵ) was 0.00360 in. (0.091 mm).

When these values were compared with carbon steel pipe (moderately corroded) having an absolute roughness of 0.15-1.00 mm (Neutrium, Thermal Engineering), an improvement in the roughness profile of the corroded pipe is predicted when lined with the liner material. Furthermore, the value of (ϵ/D) will improve with large diameter pipes, significantly reducing the friction factor and head loss.

Additionally, when a corroded carbon steel pipe is lined with the liner material, the value of equivalent roughness (ϵ) is constant over time, which is more acceptable. Thus, the liner application can ensure continued acceptable hydraulic performance of the piping system. In contrast, the value of (ϵ) for corroded pipe will increase over time.

6.1.4.3 Reduction of Head Loss

The lined pipe performance was compared with the corroded pipe to determine the reduction in head loss. The internal diameter reduction of corroded pipe was used from the available literature data provided by Bain (1979), and available roughness of moderately corroded pipe was used (Neutrium, Thermal Engineering). The comparison results concluded that applying liner on a moderately corroded pipe could reduce the head loss by approximately 51.01%.

6.2 Recommendations

6.2.1 Short-term Hole Spanning Test

The thickness of the liner depends upon the hole, host pipe diameter, and the strength of the liner material. In this study, only three pipe samples were tested of larger diameter and performing test on these large diameters was expensive. Thus, it is recommended that a greater

number of samples with different diameter, and holes sizes should be tested in the future study to predict the more precise evaluation of the effect of holes on the designed liner thickness of the SAPL lines pipes. Furthermore, Finite Element Modelling (FEM) can be performed in the future studies to understand the liner performance for different holes, pipe diameters and liner material properties.

In this study, the liner was designed as a Class II semi-structural and bonded to the host pipe; however, for future study, the liner can be designed as Class II semi-structural and non-bonded to the host pipe. Thus, the liner application can be tested if future deterioration of the pipe can change the condition of the pipe from partially deteriorated to fully deteriorated.

Additionally, it was concluded that temperature played an important role on the material performance of the polymeric liner material. Thus, a detailed study should be performed considering the temperature effect on the designing and performance of the liner for the hole spanning of the lined pipes.

6.2.2 Vacuum Pressure Test

In this study, a vacuum test was performed on the liner material which was completely adhesive to the host pipe. It is recommended that future testing should be performed on the Class II liner non-bonded to the host pipe to determine the ring stiffness of the SAPL liner system.

6.2.3 Pressure Integrity Test

The study conducted on evaluating the structural capability of liner when designed as Class IV by performing testing on 60 numbers of pipe samples with one diameter size of 8 in., having different thicknesses, at different temperatures. It is recommended that liner material should be tested as Class IV by conducting testing on different diameters of pipe with different thickness and

temperatures to evaluate the performance of material at different diameter, and subsequently, a relationship can be evaluated for the change in diameter and hoop stresses.

For the validation of AWWA design equation at elevated temperatures, more research testing and evaluation is needed to analyze the thermal stresses affect and liner design thickness. It is recommended that more testing should be performed to quantify the effect of thermal stresses on the burst pressure and hoop stresses, which can later be incorporate in the AWWA recommended design equations.

6.2.4 Hydraulic Flow Test

In this experimental test setup, only one diameter size was tested with and without liner. Different diameter sizes of pipe with and without liner should be tested for future study to prove the expected improvement of the friction factor and head loss for larger pipe diameters. The test can be performed in the laminar flow also in order to compare the friction factor and head loss in this flow regime.

The liner application with proper quality control is an essential factor in achieving the improved values of equivalent roughness (ϵ), friction factor (f), and head loss (h_L). Thus, liner installation procedure with quality control and assurance can also be studied in future studies.

References

- Adams, T., Grant, C., & Watson, H. (2012). A simple algorithm to relate measured surface roughness to equivalent sand-grain roughness. *International Journal of Mechanical Engineering and Mechatronics*, 1(2), 66-71.
- Allouche, E.N., Bainbridge, K., Moore, I.D., 2005. Laboratory examination of a cured-in- place pipe liner for portable water distribution pipes. Paper no. D03-04, NODIG, Orlando, Florida.
- American Water Works Association. (2008). “AWWA C222 Standard For Polyurethane Coatings for the Interior and Exterior of Steel Water Pipe And Fittings.” American Water Works Association, Denver, Co.
- American Water Works Association. (2019). *Structural Classification of Lining Systems*.
- Ampiah, N., Fam, A., Moore, I.D., 2010. Effect of wrinkles on the circumferential strength of a cast-in-place composite polymer liner used in retrofitting pressure pipes. *J. Mater. Civ. Eng. (ASCE)* 22, 1304–1314.
- ASCE. (2017). *Report card for America’s infrastructure*. Reston, VA: ASCE.
- ASCE. (2021). *Report card for America’s infrastructure*. Reston, VA: ASCE.
- ASTM F1216. (2009). *Standard Practice for Rehabilitation of Existing Pipelines and Conduits by the Inversion and Curing of a Resin-Impregnated Tube 12*. ASTM International.
- ASTM F1743. (2017). *Rehabilitation of Existing Pipelines and Conduits by Pulled-in- Place Installation of Cured-in-Place Thermosetting Resin Pipe (CIPP)*. ASTM International.
- ASTM (2015). *Standard test methods for tensile properties of plastics. ASTM D638. Annual book of ASTM Standards*.

- ASTM (2017). Standard Test Method for Shear Strength of Plastics by Punch Tool. ASTM D732. Annual book of ASTM Standards.
- ASTM (2017). Standard test methods for flexural properties of unreinforced and reinforced plastics and electrical insulating materials. ASTM D790.
- Awe, O. (2017). Testing of Innovative Pipe Renewal Liners for Renovation of Potable Water Distribution Pipelines (Master's thesis, University of Waterloo).
- AWWA (American Water Works Association). 2004. AWWA Manual M11 Steel Pipe: A Guide For Design And Installation, Fifth Edition.
- AWWA (American Water Works Association). 2009. AWWA Manual M41 Ductile-Iron Pipe and Fittings.
- Saegrov, S., J. F. Melo Baptista, P. Conroy, R. K. Herz, P. LeGauffre, G. Moss, J. E. Oddevald, B. Rajani and M. Schiatti (1999). "Rehabilitation of water networks: Survey of research needs and on-going efforts." *Urban Water* 1(1): 15-22.
- Bain, S.W. (1979) Corrosion in Carbon Steel Raw Water Piping, Tennessee Valley Authority, September, 1979 <https://www.nrc.gov/docs/ML2132/ML21323A101.pdf>
- Barber, M. E., Bakeer, R. M., Sever, V. F., & Boyd, G. R. (2005). Effect of close-fit sliplining on the hydraulic capacity of a pressurized pipeline. *Tunnelling and underground space technology*, 20(1), 23-31.
- Barton, N. A., Farewell, T. S., Hallett, S. H., & Acland, T. F. (2019). Improving pipe failure predictions: Factors affecting pipe failure in drinking water networks. *Water research*, 164, 114926.
- Boxall, J. B., A. O'Hagan, S. Pooladsaz, A. J. Saul and D. M. Unwin (2007). "Estimation of burst rates in water distribution mains." *Water Management* 160: 73-82.

- Cetinel, H. (2012). The artificial neural network based prediction of friction properties of Al₂O₃-TiO₂ coatings. *Industrial Lubrication and Tribology*.
- Chukin, V., Andrianov, A., and Orlov, V.(2014). “The Steel Pipe Corrosion in Drinking Water Distribution Systems and its Rehabilitation Techniques.” International No-Dig 2014 32nd International Conference and Exhibition, Madrid.
- Colebrook, C. F. (1939). Turbulent flow in pipes with a particular reference to the transition region between smooth and rough pipe laws. <http://dx.doi.org/10.1680/ijoti.1939.13150>.
- Curran, P. and Cain, A. (2016). Make the right choice for metal coating for the right application. Accessed on Jun 5, 2023.
- da Costa Mattos, H. S., Paim, L. M., & Reis, J. M. L. (2012). Analysis of burst tests and long-term hydrostatic tests in produced water pipelines. *Engineering Failure Analysis*, 22, 128-140.
- Darabnoush Tehrani, A. (2020). Development of a Structural Design Methodology for Cementitious Sprayed Applied Pipe Linings in Gravity Storm Water Conveyance Conduits. The University of Texas at Arlington.
- Davidovits, J. (2015). *Geopolymer Chemistry and Applications*. J. Davidovits.–Saint-Quentin, France.
- Davies, J., Clarke, B., Whiter, J., and Cunningham, R. (2001). Factors influencing the structural deterioration and collapse of rigid sewer pipes. *Urban Water*, 73-89.
- Elliot, G.A. 1922. The Use of Steel Pipe in Water Works. *Jour. AWWA*, 9(11):839

- Ellison, D., F. Sever, P. Oram, W. Lovins, A. Romer, S. J. Duranceau and G. Bell (2010). Global review of spray-on structural lining technologies. Denver, U.S.A., Water Research Foundation.
- EPA. (2004). "Report to congress: Impacts and control of CSOs and SSOs." Accessed June 05, 2023. <http://www.Ep.gov/nrmrl>.
- EPA. (2007). "Innovation and research for water infrastructure for the 21st century." Accessed April 2018. <http://www.Ep.gov/nrmrl>.
- EPA. (2012). "Performance Evaluation of Innovative Water Main Rehabilitation Cure-in-Place Lining Product in Cleveland, Ohio". Accessed June 07, 2023. <https://nepis.epa.gov/Exe/ZyPDF.cgi/P100DZL3.PDF?Dockey=P100DZL3.PDF>
- Farshad, F. F., & Pesacreta, T. C. (2003). Coated pipe interior surface roughness as measured by three scanning probe instruments. *Anti-Corrosion Methods and Materials*.
- Fu, G., Shannon, B., Azoor, R., Deo, R., & Kodikara, J. (2022). Equations for gap-spanning design of underground cast iron pipes lined with thermosetting polymeric liners. *Tunnelling and Underground Space Technology*, 119, 104234.
- Guo, X., Wang, T., Yang, K., Fu, H., Guo, Y., & Li, J. (2020). Estimation of equivalent sand-grain roughness for coated water supply pipes. *Journal of Pipeline Systems Engineering and Practice*, 11(1), 04019054.
- Ha, S. K., Lee, H. K., & Kang, I. S. (2016). Structural behavior and performance of water pipes rehabilitated with a fast-setting polyurea-urethane lining. *Tunnelling and Underground Space Technology*, 52, 192-201.

Harries, K. A., Sweriduk, M., & Warren, D. (2014). Performance of spray-applied epoxy lining system subject to infiltration. *Tunnelling and underground space technology*, 43, 389-397.

<https://neutrium.net/fluid-flow/absolute-roughness-of-pipe-material/> Accessed May 25, 2023.

<https://www.xometry.com/resources/materials/what-is-polymer/>, Accessed on Jun 5, 2023.

Janson, L.E., (1981). *Proceedings of the International Conference on Underground Plastic Pipe*, ASCE, New York, NY, USA.

Jeong, H. S., Baik, H.-S., and Abraham, D. M. (2005). An ordered probit model approach for developing Markov chain-based deterioration model for wastewater infrastructure systems. *ASCE Pipelines*, 649-661.

Jibreen, A., Najafi, M., Kaushal, V., Kaur, K., Arjun, M., & Shir Khanloo, S. Investigation of Factors Affecting Remaining Useful Life of Prestressed Concrete Cylinder Pipes. In *Pipelines 2023* (pp. 286-295).

Jun, H. J., Park, J. K., & Bae, C. H. (2020). Factors affecting steel water-transmission pipe failure and pipe-failure mechanisms. *Journal of Environmental Engineering*, 146(6), 04020034.

Kaur, K., Ghalambor, S., Najafi, M., & Jibreen, A., (2022a). Evaluation of a Hybrid Polyurea Spray Applied Pipe Lining for Structural Pipe Rehabilitation. In *Proceedings of the North American Society for Trenchless Technology NASTT's 2022 No-Dig Show*, Minneapolis, MN, USA, 10–14 April 2022.

Kaur, K., Ghalambor, S., Najafi, M., Jibreen, A., & Arjun, M. (2022b). Testing and Evaluation of a Hybrid Polyurea Spray Applied Pipe Lining for Structural Applications. In *Proceedings of the ASCE Pipeline Conference*, Indianapolis, IN, USA, 31 July–03.

- Kaur, K., Ghalambor, S., Najafi, M., & Diego, C., (2023a). Review of Classification and Certification Requirements for Polymeric Spray Applied Pipe Lining for Gravity and Pressure Pipes. In Proceedings of the North American Society for Trenchless Technology NASTT's 2023 No-Dig Show, Portland, OR, USA, April 30– May 04, 2022.
- Kaur, K., Ghalambor, S., Najafi, M., & Karthikeyan, L., Shirkhanloo, S.(2023b). Short-term Hole Spanning Testing and Evaluation for Spray Applied Pipe Lining. In Proceedings of the ASCE Pipeline Conference, San Antonio, TX, USA, 12 August–16 August 2023.
- Kirmeyer, G. J., W. Richards, and C. Dery Smith. 1994. Assessment of water distribution systems and associated research needs. Denver: American Water Works Association.
- Kohankar Kouchesfehni, Z. (2020). “Development of a Structural Design Methodology for Polymeric Spray Applied Pipe Linings.” The University of Texas at Arlington.
- Kohankar Kouchesfehni, Z., Darabnoush Tehrani, A., Najafi, M., Syar, J. E., and Ed Kampbell, P. E. (2019). “Adding Additional Reinforcement to Improve the Structural Performance of Spray Applied Pipe Lining Rehabilitation Technology: A Review.” *Pipelines 2019: Multidisciplinary Topics, Utility Engineering, and Surveying*, ASCE, Nashville.
- Kouchesfehni, Z. K., Tehrani, A. D., and Najafi, M. (2021). “Culvert renewal with cementitious-geopolymer spray-applied pipe lining: Field data collection and assessment.” *Journal of Pipeline Systems Engineering and Practice*, 12(3), ASCE.
- Li, Z., Tang, Y., Tang, F., Chen, Y., & Chen, G. (2018). Elastic buckling of thin-walled polyhedral pipe liners encased in a circular pipe under uniform external pressure. *Thin-Walled Structures*, 123, 214-221.

- Loganathan, K. (2021). "Development of a Model to Prioritize Inspection and Condition Assessment of Gravity Sanitary Sewer Systems." Dissertation, University of Texas at Arlington, Arlington, TX, U.S.
- Loganathan, K., Najafi, M., & Kumar Maduri, P. (2022). Development of a Model to Prioritize Inspection and Condition Assessment of Gravity Sanitary Sewer Systems. In *Pipelines 2022* (pp. 1-9).
- Loganathan, K., Najafi, M., Kumar Maduri, P., & Kaur, K. (2023). Condition Prediction of Sanitary Sewer Pipe Dataset with Imbalanced Classification. In *Proceedings of the ASCE Pipeline Conference, San Antonio, TX, USA, 12 August–16 August 2023*.
- Lubini, A. T., & Fuamba, M. (2011). Modeling of the deterioration timeline of sewer systems. *Canadian Journal of Civil Engineering*, 38(12), 1381-1390.
- Misiunas, D. (2005). Failure monitoring and asset condition assessment in water supply systems. Sweden: Lund University.
- Moore, I. (2021). Response of a polymer liner passing across a pressure pipeline joint opening under axial ground movements. *Computers and Geotechnics*, 139, 104429.
- Motlagh, S. G., Jain, A., & Najafi, M. (2013). Comparison of spray-on linings for water pipeline renewal applications. In *Pipelines 2013: Pipelines and Trenchless Construction and Renewals—A Global Perspective* (pp. 1113-1125).
- Najafi, M. and Gokhale, S. (2022). *Trenchless Technology*. McGraw Hill Education.
- NASSCO. (2023). "Pipe Rehabilitation." <https://www.nassco.org/trenchless-technology/rehabilitation/pipe-rehabilitation/> Accessed on June 11, 2023.
- NASSCO. (2023). "Pipe Rehabilitation." <https://www.nassco.org/trenchless-technology/rehabilitation/pipe-rehabilitation/> Accessed on June 11, 2023.

- Onat, E. A., Walters, T. W., Mobley, D. M., & Mead, J. J. (2016, June). Hydraulic Model Calibration of a Nuclear Plant Service Water System. In *ASME Power Conference* (Vol. 50213, p. V001T11A002). American Society of Mechanical Engineers.
- Park, Y., Abolmaali, A., Kim, Y. H., and Ghahremannejad, M. (2016). "Compressive strength of fly ash-based geopolymer concrete with crumb rubber partially replacing sand." *Construction and Building Materials*, Elsevier Ltd, 118(2016), 43–51.
- Peggs, I. D., Schmucker, B., & Carey, P. (2005). Assessment of maximum allowable strains in polyethylene and polypropylene geomembranes. In *Waste containment and remediation* (pp. 1-16).
- Rajani, B. and Y. Kleiner (2001). "Comprehensive review of structural deterioration of water mains: physically based models." *Urban Water* 3(3): 151-164.
- Rajani, B. and Y. Kleiner (2002). "Towards Pro-active Rehabilitation Planning of Water Supply Systems." *International Conference on Computer Rehabilitation of Water Networks-CARE-W*, Dresden, Germany.
- Royer, J., and Iseley, T. (2017). "Laboratory testing and analysis of geopolymer pipe-lining technology for rehabilitation of sewer & storm water conduits, part II - CMP culvert analysis." *NASTT's No-Dig Show and ISTT's 35th International No-Dig*, 1–10.
- Rueda, F., Marquez, A., Otegui, J. L., & Frontini, P. M. (2016). Buckling collapse of HDPE liners: Experimental set-up and FEM simulations. *Thin-Walled Structures*, 109, 103-112.
- Salman, A. A. (2018). *An Investigation of Water Pipeline Renewal Practices* (Master's Thesis). University of Texas at Arlington.
- Sápi, Z., & Butler, R. (2020). Properties of cryogenic and low temperature composite materials—A review. *Cryogenics*, 111, 103190.

Shannon, B. and Azoor, R. (2020). Smart Linings for Pipe and Infrastructure Report. Monash University.

Singh, A., and Adachi, S. (2011). Bathtub curves and pipe prioritization based on failure rate Built Environment: Project Asset Management, 105-122.

Skipworth, P., M. Engelhardt, A. Cashman, D. Savic, A. Saul and G. Walters (2002). Whole Life Costing for Water Distribution Network Management. London, Thomas Telford.

Streeter V. L., Wylie B. E., Bedford K. W. (1998) Fluid Mechanics, WCB McGraw-Hill, New York.

Swamee, P. K., & Jain, A. K. (1976). Explicit equations for pipe-flow problems. Journal of the hydraulics division, 102(5), 657-664.

U.S. Environmental Protection Agency (USEPA), 2005. Drinking Water Infrastructure Needs Survey and Assessment-Third Report to Congress. Office of Water, Office of Ground Water and Drinking Water, Drinking Water Protection Division (EPA 816-R-05-001).

Walski, T. M. and A. Pelliccia (1982). "Economic analysis of water main breaks." Journal American Water Works Association 74(3): 140-147.

Wang, C.-W., Z.-G. Niu, H. Jia and H.-W. Zhang (2010). "An assessment model of water pipe condition using Bayesian inference." Journal of Zhejiang University: Science A 11(7):495-504.

Water Infrastructure Networks. April 2001. "Clean & Safe Water for the 21st Century." Accessed November 2021.

WRF Report 4326 (2018). Advanced condition assessment and failure prediction technologies for optimal management of critical water supply pipes. J. Kodikara. Denver, CO, USA, Water Research Foundation: 1–307.

- Xometry. (2023). "Polymers: Definition, Properties, Types, and Applications,"
- Yan, J. (2006). Risk Assessment of Condition Intrusion into Water Distribution System. PhD, Loughborough University.
- Zhao, Q. (1999). Finite element simulation of creep buckling of CIPP liners under external pressure. Louisiana Tech University.
- Zhou, Y. (2018). Deterioration and Optimal Rehabilitation Modelling for Urban Water Distribution Systems (1st ed.). CRC Press.
<https://doi.org.ezproxy.uta.edu/10.1201/9780429451799>
- Zhu, X. K., & Leis, B. N. (2012). Evaluation of burst pressure prediction models for line pipes. International Journal of Pressure Vessels and Piping, 89, 85-97.